Biennial Report

Zweijahresbericht 2020/2021

Leibniz Association

TROPOS

Leibniz Institute for Tropospheric Research

Leibniz Institute for
Tropospheric Research

Leibniz
Association

Imprint

Published by
TROPOS
Leibniz Institute for Tropospheric Research
Leibniz-Institut für Troposphärenforschung e.V. Leipzig
Member of the Leibniz Association

Permoserstraße 15
04318 Leipzig
Germany

Phone: ++49 (341) 2717-7060
Fax: ++49 (341) 2717-99-7060
Email: info@tropos.de
Internet: http://www.tropos.de

Copy editors
Katja Schmieder, Caroline Damm, Konstanze Kunze,
Kerstin Müller, Beate Richter, Tilo Arnhold (Photographer)

Editorial board
Andres Macke, Hartmut Herrmann, Ina Tegen, Mira Pöhlker,
Ulla Wandinger, Frank Stratmann, Kathrin Niehuus

Photo and illustration credits © TROPOS / as described
in the captions
p. 1: top - Ronny Engelmann / TROPOS
middle - Gregory Tran / AWIPEV
bottom - Christian Pilz / TROPOS
p. 33: top - Patric Seifert / TROPO
middle - Olaf Straub / TROPOS
bottom - Edson Silva Delgado, Etfilmes / OSCM
p. 143: top - Liina Tõnisson / TROPOS
middle - Ronny Engelmann / TROPOS
bottom - DWD

Table of contents

Table of contents

Introduction / Einleitung

Overview / Übersicht

Introduction

Since 1992 the Leibniz Institute for Tropospheric Research (TROPOS) is located in the “Research Park Leipzig/Permoserstraße” close to the Helmholtz Centre for Environmental Research, the Leibniz-Institute for Surface Modification and other research establishments and related businesses. Its name

Fig. / Abb. 1: TROPOS main building. / TROPOS-Hauptgebäude. (Photo: Patric Seifert / TROPOS)

identifies TROPOS as a member of the Leibniz Association. The institute is funded by the federal and state governments with a basic budget of approx. 10,3 million euros, approx. 9,6 million euros per year are raised in third-party funds. TROPOS employs a total of 160 people, 117 of whom are scientists (as at December 2021).

Over the years a well-defined and globally unique research profile of TROPOS emerged. With a focus on the physical and chemical interactions between atmospheric small airborne particles (aerosol particles) and cloud particles. Despite their minute absolute amount, aerosol and cloud particles are essential parts of the atmosphere because they control the

Fig. / Abb. 2: The new TROPOS chemistry laboratory. / Des neue TROPOS-Chemielaborgebäudes. (Photo: Tilo Arnhold / TROPOS)

Einleitung

Im Wissenschaftspark Leipzig/Permoserstraße befindet sich seit 1992 das Leibniz-Institut für Troposphärenforschung e. V. (TROPOS) in Nachbarschaft zum Helmholtz-Zentrum für Umweltforschung, zum Leibniz-Institut für Oberflächenmodifizierung sowie weiteren Einrichtungen. Sein Name weist es als Mitglied der Wissenschaftsgemeinschaft Gottfried Wilhelm Leibniz aus.

Das Institut wird von Bund und Ländern mit einem jährlichen Grundetat von ca. 10,3 Millionen Euro gefördert, ca. 9,6 Millionen pro Jahr werden an Drittmitteln eingeworben.

Am TROPOS sind insgesamt 160 Mitarbeitende beschäftigt, davon 117 Wissenschaftlerinnen und Wissenschaftler (Stichtag 31.12.2021). Gegründet wurde das TROPOS zur Erforschung physikalischer und chemischer Prozesse in der belasteten Troposphäre.

Das TROPOS hat ein klares und weltweit einzigartiges Forschungsprofil herausgebildet, in dessen Mittelpunkt heute die physikalischen und

Fig. / Abb. 3: TROPOS cloud laboratory. / TROPOS-Wolkenlabor. (Photo: Tilo Arnhold / TROPOS)

chemischen Wechselwirkungen zwischen atmosphärischen Schwebeteilchen (Aerosolpartikeln) und Wolkenpartikeln stehen. Trotz geringster absoluter Mengen sind diese Partikel wesentliche Bestandteile der Atmosphäre, weil sie den Energie-, Wasser- und Spurenstoffhaushalt des Erdsystems beeinflussen. Menschliche Aktivitäten können die Eigenschaften dieser hochdispersen Systeme verändern und damit sowohl direkt als auch indirekt auf den Menschen in den Bereichen Gesundheit und Klima zurückwirken.

Zur Klärung dieser wichtigen Beziehungen müssen die physiko-chemischen Prozesse von Aerosol- und Wolkenbildung und die Wirkungen auf Gesundheit und Klima zu einem erheblichen Teil noch erforscht werden. Besondere Herausforderungen

Fig. / Abb. 4: TROPOS lidar crew in reversed order of their planned mission onboard MOSAiC. / TROPOS-Lidar-Crew in umgekehrter Reihenfolge ihres geplanten Einsatzes bei MOSAiC (Ronny Engelmann, Hannes Griesche, Martin Radenz, Karsten Hanbuch, Julian Hofer, Dietrich Althausen). (Photo: Tilo Arnhold / TROPOS)

budgets of energy, water and trace substances of the Earth System. Human activities can change these highly disperse systems and thus directly as well as indirectly feedback on human beings in terms of health and climate.

For the understanding of these strong connections the physico-chemical processes of aerosol and cloud formation and the impacts on health and climate still need to be investigated to a large extent. Particular challenges here are the analysis of the very small samples and the complex behaviour of tropospheric multiphase systems, in which individual processes seldom can clearly be distinguished. In climate research this limitation is reflected in much larger uncertainties in predicted anthropogenic aerosol and cloud effects in comparison to the greenhouse effects of gases.

To gain significant advances in our process understanding of the tropospheric multiphase system and to improve the application of this process understanding in the prediction of human impacts in this system –coordinated field studies, laboratory and model studies for the investigation of aerosol particles and clouds are developed and performed. These three approaches provide a framework for the overall process understanding of atmospheric multiphase systems.

The long-term measurements, to a large extend initiated by TROPOS, increasingly enable the identification of trends in regional and large-scale aerosol distribution.

Field experiments

Field experiments elucidate the atmospheric life cycle of aerosol and cloud particles and related hierbei sind die Analyse der beteiligten kleinsten Stoffmengen und das komplexe Verhalten atmosphärischer Mehrphasensysteme, deren Einzelprozesse in der Atmosphäre nicht klar getrennt beobachtet werden können. Beim gegenwärtigen Stand zum globalen Klimawandel spiegelt sich diese Komplexität in den sehr viel größeren Unsicherheiten in allen zu Aerosol- und Wolkenwirkung veröffentlichten Zahlen im Vergleich zum Kenntnisstand der Auswirkungen von Treibhausgasen wider.

Um einen signifikanten Zuwachs im Prozessverständnis troposphärischer Mehrphasenprozesse zu erreichen und dessen Anwendung auf die Vorhersage der Folgen menschlicher Eingriffe zu verbessern, werden am TROPOS aufeinander abgestimmte Feld-, Labor und Modellstudien zur Untersuchung von Aerosolpartikeln und Wolken entwickelt und durchgeführt, welche den Rahmen für ein umfassendes Prozessverständnis atmosphärischer Multiphasensysteme bilden. Die vom TROPOS maßgeblich initiierten Langzeitmessungen erlauben mehr und mehr auch die Erfassung von Trends in der regionalen und großräumigen Aerosolverteilung und deren Auswirkung auf Wolken und Klima.

Feldexperimente

Die Feldexperimente des Instituts dienen der Aufklärung des atmosphärischen Kreislaufs der Aerosol- und Wolkenpartikel und der damit verbundenen Prozesse. Die Komplexität des Aerosol-Wolken-Systems wird dabei unter anderem dadurch bestimmt, dass in der Atmosphäre Partikel und Tropfen auftreten, deren Durchmesser sich vom Nano- bis zum Mikrometerbereich um mehr als sechs Größenordnungen

Fig. / Abb. 5: Aurora borealis during the MOSAiC expedition at 87° 28‘ North in the morning of 22 January 2020. / Polarlicht während der MOSAiC-Expedition am Morgen des 22. Januar 2020. Hannes Griesche (TROPOS, links) und Dean Howard (University of Colorado Boulder, rechts) auf der Eisscholle. (Photo: Hannes Griesche, TROPOS)

processes. The complexity of the aerosol-cloud-system is reflected in the fact that atmospheric aerosols and cloud particle exist with diameter from nano- to micrometre spanning more than six orders of magnitude. Furthermore, the cloud- and ice-forming properties of aerosols interact with a regionally and globally changing Earth system. As a result of the diversity of microphysical, chemical and meteorological processes that occur, there is still a lack of quantitative understanding regarding the importance of aerosol-cloud interactions in the global climate system.

This uncertainty already begins with particle sources, which are TROPOS research subjects as well. The combustion of fossil and renewable fuels is a significant aerosol source. Measurements of the institute at many urban and rural background stations show that emissions of particles and their precursor gases are followed by strong physical and chemical transformations that need to be investigated with high-resolution sensors in order to identify the underlying processes.

Also, the conurbation Leipzig and the background station Melpitz is in the focus of investigations on air pollution with emphasis on aerosol particles, often conducted in collaboration with national and international institutions. Despite wide-ranging legal regulations, air pollution still exists in Germany and Europe with its consequences for morbidity and mortality of the population. The Melpitz research station is more and more applied to specific measurement campaigns to combine the high-resolution physical-chemical characterization on the ground with other in-situ and remote sensing measurements of the entire column (“Melpitz-Column”).

Fig. / Abb. 6: : At TAME-BC, three Leibniz institutes have been looking for solutions to reduce the health burden of air pollution with soot in the Southeast Asian megacity of Manila (Philippines). / Bei TAME-BC haben drei Leibniz-Institute nach Lösungen gesucht, um die Gesundheitsbelastung durch Luftverschmutzung mit Ruß in der südostasiatischen Megacity Manila zu senken (Philippinen). (Photo: Leizel Madueño / TROPOS)

Fig. / Abb. 7: The regional background station Melpitz (40km north-east of Leipzig) is being further expanded within the framework of ACTRIS. / Die regionale Hintergrund-Station Melpitz (40km nordöstlich von Leipzig) wird im Rahmnen von ACTRIS weiter ausgebaut. (Photo: Olaf Straub / TROPOS)

unterscheiden. Außerdem stehen die wolken- und eisbildenden Eigenschaften der Aerosole in Wechselwirkung mit einem sich regional und global ändernden Erdsystem. Als Folge der Vielfalt der auftretenden mikrophysikalischen, chemischen und meteorologischen Prozesse mangelt es nach wie vor an quantitativem Verständnis hinsichtlich der Bedeutung von Aerosol-Wolkenwechselwirkungen im globalen Klimasystem.

Diese Unsicherheit beginnt schon bei den Partikelquellen, die ebenfalls Forschungsgegenstand am TROPOS sind. Die Verbrennung fossiler und nachwachsender Brennstoffe zur Energieerzeugung und im Verkehr ist eine maßgebliche Aerosolquelle. Messungen des Instituts an vielen urbanen Messstellen und kontinentalen Hintergrundstationen zeigen, dass den Emissionen von Partikeln und deren Vorläufern vielfältige physikalische und chemische Umwandlungen folgen, die mit hoher zeitlicher Auflösung analysiert werden müssen, um die beteiligten Prozesse aufzuklären.

Auch der Ballungsraum Leipzig mit der Hintergrundstation Melpitz steht hier immer wieder im Interesse für Untersuchungen zur Luftverschmutzung mit dem Schwerpunkt auf Partikeln, die oft in nationalen und internationalen Kooperationen durchgeführt werden. Trotz sehr weitgehender gesetzlicher Regelungen existiert in Deutschland und Europa immer noch Luftverschmutzung mit ihren Folgen für Morbidität und Mortalität der Bevölkerung. Die Forschungsstation Melpitz wird zunehmend für fokussierte Messkampagnen genutzt, auch um die physikalisch-chemisch hoch aufgelöste in-situ Charakterisierung am Boden mit in-situ- und Fernerkundungsmessungen der gesamten Säule zu kombinieren („Melpitz-Säule“).

Fig. / Abb. 8: RV Polarstern at the end of the polar night during the MOSAiC expedition in the Central Arctic. / Die Polarstern am Ende der Polarnacht während der MOSAiC-Expedition in der zentralen Arktis. (Photo: Hannes Griesche / TROPOS)

The strongest polluted regions over North America, Europe, Asia with priority on China, Africa, the Indian subcontinent, and South America are far from being sufficiently characterized in terms of aerosol burdens and ensuing climate effects. Subsequently the institute focuses its participation in international field campaigns and dedicated long-term studies in Asia, South America and the Mediterranean area. But also, the marine troposphere over the clean southern and the polluted northern Atlantic is observed by long-term measurements for a better understanding aerosol cloud interaction.

Investigations on mineral dust and marine aerosol particles and its impact on the radiation budget, cloud formation processes and the atmospheric ice nucleation remain a core component of the institute's research. To this end, investigations in the

Fig. / Abb. 9: The FDS15 is a measuring device that comes in a small box the length of a tetra-pack and can be attached to light poles, among other things. / Das FDS15 ist ein Messgerät, das in einem kleinen Kästchen von der Länge eines Tetra-Packs steckt und u.a. an Laternenmasten angebracht werden kann. (Photo: Dr. Födisch Umweltmesstechnik AG)

Die am stärksten belasteten Regionen über Nordamerika, Europa, Asien mit dem Schwerpunkt China, Afrika, über dem indischen Subkontinent und Südamerika sind bei weitem noch nicht hinreichend bezüglich ihrer Aerosolbelastungen und den daraus resultierenden Klimawirkungen untersucht. Auf diese Regionen konzentrieren sich daher in internationaler Zusammenarbeit die Feldexperimente des TROPOS, u. a. in Form von Messkampagnen und Langzeitmessungen in Asien, Südamerika und dem mediterranen Bereich. Aber auch die maritime Troposphäre über dem sauberen südlichen und dem belasteten nördlichen Atlantik wird langfristig vermessen, um Aerosol-Wolken-Wechselwirkungen besser zu verstehen.

Untersuchungen zum Mineralstaub und marinen Aerosolpartikeln und deren Wirkungen auf den Strahlungshaushalt, die Wolkenbildung und die atmosphärische Eisbildung bleiben ein Kernbestandteil der Arbeiten am TROPOS. Durch die Nutzung eines kommerziellen Verkehrsflugzeuges der Lufthansa werden im Rahmen der Europäischen Forschungsinfrastruktur IAGOS auch Aerosolverteilungen in der oberen Troposphäre auf regelmäßig beflogenen interkontinentalen Routen gemessen und analysiert.

Am TROPOS werden verschiedene bodengebundene Fernerkundungsverfahren gekoppelt, um so zu einem synergetischen Bild der vertikalen Verteilung von Aerosolen und Hydrometeoren sowie deren Prozessierung zu gelangen.

Auf kleineren Skalen werden Untersuchungen zur Partikelbildung und Wechselwirkung zwischen Aerosolpartikeln und Wolken und der Einfluss turbulenter Mischungsprozesse auf die Wolkenentwicklung mit Hilfe der hubschraubergetragenen Messplattform ACTOS durchgeführt. Zusätzlich werden Bergstationen zu Prozessstudien genutzt, die sich dem

Fig. / Abb. 10: DACAPO-PESO field experiment on clouds and precipitation under clean air conditions: LACROS measured for three years in Punta Arena (Chile) in the southern hemisphere. / DACAPO-PESO-Feldexperiment zu Wolken und Niederschlag unter Reinluftbedingungen: Drei Jahre hat LACROS in Punta Arena (Chile) in der Südhemisphäre gemessen. (Photo: Martin Radenz / TROPOS)

Central Asian and the Mediterranean region will be intensified.

In the framework of the European infrastructure IAGOS the aerosol distribution in the upper troposphere is measured and analysed using a commercial Lufthansa aircraft operated on frequent intercontinental routes.

At TROPOS different ground-based remote sensing methods are coupled in order to achieve a synergetic picture of the vertical distribution of aerosols and hydrometeors as well as their processing.

On smaller scales, investigations concerning new particle formation, the interactions between aerosol particles and clouds, and the influences of turbulent mixing processes on cloud development are carried out with help of the helicopter-borne measurement platform ACTOS. In addition, process studies are conducted at suitable locations such as mountain observatories to investigate particle nucleation, particle processing through clouds, and the influence of aerosols particles on the development and freezing of clouds.

TROPOS leads several regional, national and European measurement networks to monitor atmospheric aerosols and cloudiness. In the framework of the Global Atmospheric Watch (GAW) programme of the WMO TROPOS hosts the World Calibration Centre for physical in-situ aerosol measurement (WCCAP) to assure high quality standards at national and international observatories.

Further on TROPOS is primary responsible for the development and operation of the European and national measurement network for the observation of aerosols, clouds and trace gases (ACTRIS) to ensure, besides process understanding, a basis for the long-term characterisation of short-lived climate components.

Verständnis von Einzelprozessen, wie der Partikelneubildung, der physiko-chemischen Veränderung der Aerosolpartikel beim Wolkendurchgang und dem Einfluss von Aerosolpartikeln auf die Entwicklung und das Gefrieren von Wolken widmen.

TROPOS ist maßgeblich an regionalen, nationalen und Europäischen Messnetzen zur Erfassung des atmosphärischen Aerosols und der Bewölkung beteiligt. Das Institut betreibt im Rahmen des Global Atmospheric Watch (GAW) Programmes der WMO das Weltkalibrierzentrum für physikalische Aerosolmessungen (WCCAP) mit dem Ziel der Qualitätssicherung von in-situ Messungen an nationalen und internationalen Messstationen.

TROPOS ist weiterhin federführend an der Entwicklung und dem Betrieb der vernetzten europäischen und nationalen Forschungsinfrastruktur zur

Fig. / Abb. 11: MetPVNet measurement campaign in Allgäu: Analyses of the influence of aerosols on the yield of photovoltaic systems contribute to making the energy transition more secure. / MetPVNet-Messkampagne im Allgäu: Analysen zum Einfluss von Aerosolen auf den Ertrag von Photovoltaik-Anlagen helfen, die Energiewende sicherer zu machen. (Photo: Jonas Witthuhn / TROPOS)

Fig. / Abb. 12: Following the successful MOSAiC expedition, the BELUGA tethered balloon was deployed in Ny-Ålesund on Svalbard at the end of 2020. TROPOS and the University of Leipzig took measurements in the polar night for the first time. / Nach der erfolgreichen MOSAiC-Expedition kam der BELUGA-Fesselballon Ende 2020 in Ny-Ålesund auf Spitzbergen zum Einsatz. TROPOS und Universität Leipzig haben dabei erstmals in der Polarnacht gemessen. (Photo: André Ehrlich, Universität Leipzig)

Field campaigns are supported and complemented by analyses based on meteorological satellites. In particular, satellite products are used to study the spatiotemporal development of clouds and their radiative forcing, as well as the transport paths of aerosols.

Laboratory experiments

Laboratory experiments cover the development of a large number of methods to characterize atmospheric particles in ground-based or airborne field measurement campaigns. This work includes for example the improvement of aerosol size spectrometers as well as collection systems for the physical and chemical characterization of cloud droplets and the interstitial aerosol – that means those aerosol particles that are suspended in the gas phase inside the cloud along with the cloud particles.

Optical measurement techniques are developed and applied to determine the extinction coefficient of aerosol particles. Multi-wavelength lidar systems and a wind lidar are further developed in the laboratory and applied in the field to determine aerosol properties, aerosol fluxes and meteorological parameters such as temperature, relative humidity and wind. The amount of black carbon and mineral aerosol components in the aerosol samples are quantified with spectral absorption measurements.

Research at the Leipzig Aerosol Cloud Simulator LACIS addresses the activation of cloud droplets and primarily the heterogeneous formation of ice under realistic turbulent surrounding conditions. These

Erfassung von Aerosolen, Wolken und Spurengasen (ACTRIS) beteiligt, um die Prozesse der kurzlebigen Klimakomponenten auf allen relevanten Skalen zu untersuchen und zu verstehen.

Feldexperimente werden durch Analysen, basierend auf meteorologischen Satelliten, unterstützt und erweitert. Insbesondere werden mit Satellitenprodukten die raumzeitliche Entwicklung von Wolken und deren Strahlungsantrieb untersucht, ebenso wie die Transportwege von Aerosolen.

Laborexperimente

In Laborexperimenten werden zahlreiche Messmethoden entwickelt, die zur Partikelcharakterisierung in boden- und luftgestützten Feldmesskampagnen eingesetzt werden. Diese Arbeiten beinhalten z. B. die Weiterentwicklung von Aerosolgrößenspektrometern sowie Sammelsysteme zur physikalischen und chemischen Charakterisierung von Wolkentröpfchen und dem interstitiellen Aerosol, also denjenigen Aerosolpartikeln, die innerhalb von Wolken neben den Wolkenpartikeln selbst in der Gasphase suspendiert sind.

Optische Messmethoden werden zur Bestimmung des Extinktionskoeffizienten von Partikeln entwickelt und angewendet. Mehrwellenlängenlidare und ein Windlidar werden zur Bestimmung von Aerosoleigenschaften, Aerosolflüssen und meteorologischen Parametern wie Temperatur, Feuchte und Wind im Labor weiterentwickelt und im Feld eingesetzt. Die Anteile „schwarzen Kohlenstoffs“ und mineralischer Aerosolkomponenten in Aerosolproben werden durch spektrale Absorptionsmessungen bestimmt.

Am Feuchtluftwindkanal LACIS-T werden die Aktivierung von Wolkentröpfchen und die heterogene

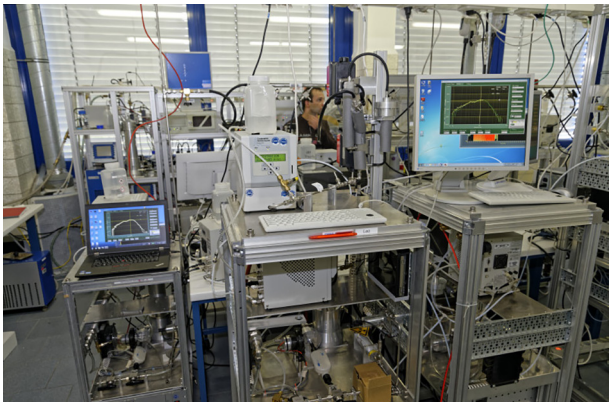

Fig. / Abb. 13: World Calibration Centre for Aerosol Physics (WCCAP), which TROPOS operates in Leipzig on behalf of the World Meteorological Organisation (WMO). / Weltkalibrierzentrum für aerosolphysikalische Feinstaubmessungen (WCCAP), das TROPOS im Auftrag der Weltorganisation für Meteorologie (WMO) in Leipzig betreibt. (Photo: Tilo Arnhold / TROPOS)

investigations aim at a better understanding of the underlying fundamental processes, the identification of critical and controlling parameters, and the development of parameterizations to characterize droplet and ice formation processes for applications in dynamical models.

Gas phase reactions of various radicals are being investigated in flow reactors. The interactions of trace gases with particles and oxidative conditions are the working topic at the aerosol chamber ACD-C. These reactions are important for ozone and particle formation caused by anthropogenic or biogenic volatile hydrocarbons. The generated particles are also investigated with regard to hygroscopic growth and cloud droplet activation behaviour. In single drop experiments, investigations on phase transfer parameters of trace gases and radicals are being conducted. The determination of phase transfer parameters and reactive uptake coefficients hereby is being extended to previously not considered chemical species and complex surfaces.

In the field of liquid phase mechanisms reactions of primarily radical oxidants are investigated with time-resolved optical detection techniques. These reactions proceed within haze particles, fog and cloud droplets as well as in deliquescent aerosol particles. For the understanding of the oxidation of organic trace gases in the tropospheric multiphase system, a large number of reactions with various radicals are being studied as well as reactions of halogenated oxidants. The latter species are of interest for the emission of reactive halogen compounds from sea salt particles, the so-called halogen activation.

The liquid phase laboratory for the investigation of tropospheric liquid phase processes is an

Fig. / Abb. 14: Parallel to the studies of the water in the clouds, analyses are also taking place in the ocean: Sebastian Zeppenfeld in the fjord near Fjord in Ny-Ålesund. / Parallel zu den Untersuchungen des Wassers in den Wolken finden auch Untersuchungen im Meer statt: Sebastian Zeppenfeld am Fjord in Ny-Ålesund. (Photo: Sebastian Zeppenfeld / TROPOS)

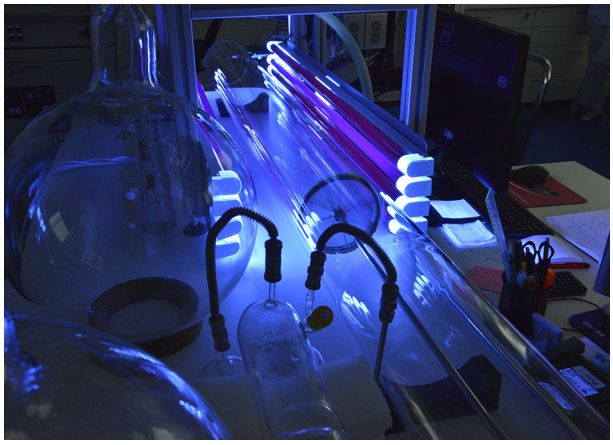

Fig. / Abb. 15: The team succeeded in laboratory experiments using a special flow apparatus at TROPOS in Leipzig, which allows interference-free investigations of gas phase reactions at atmospheric pressure. / Dem Team gelangen Laborexperimente mittels einer speziellen Strömungsapparatur am TROPOS, welche störungsfreie Untersuchungen von Gasphasenreaktionen bei Atmosphärendruck zulässt. (Photo: Tilo Arnhold / TROPOS)

Eisbildung unter realitätsnahen turbulenten Umgebungsbedingungen erforscht. Ziele dieser Untersuchungen sind die Erlangung eines besseren Prozessverständnisses auf fundamentaler Ebene, die Identifikation kritischer und kontrollierender Parameter und die Entwicklung geeigneter Parametrisierungen zur Beschreibung von Tröpfchen- und Eisbildung in dynamischen Modellen.

Gasphasenreaktionen verschiedener Radikale werden in Strömungsreaktoren untersucht. Die Wechselwirkungen von Spurengasen mit Partikel und oxidativen Bedingungen sind das Arbeitsthema bei der Aerosolkammer ACD-C. Diese Prozesse sind von Interesse für die Ozon- und Partikelbildung, verursacht durch anthropogene oder biogene flüchtige Kohlenwasserstoffe. Die erzeugten Partikel werden auch hinsichtlich ihres Feuchtewachstums- und Aktivierungsverhaltens untersucht.

In Einzeltropfenexperimenten werden Untersuchungen bzgl. der Phasentransferparameter für Spurengase und Radikale durchgeführt. Die Bestimmung von Phasentransferparametern und reaktiven Aufnahmekoeffizienten wird dabei auf bisher nicht betrachtete chemische Spezies und komplexe Oberflächen ausgeweitet.

Im Bereich von Flüssigphasenmechanismen werden Reaktionen von vorwiegend radikalischen Oxidantien mit zeitaufgelösten optischen Nachweistechniken untersucht. Diese Reaktionen laufen in den Tröpfchen von Wolken, Regen und Nebel sowie in wässrigen Aerosolpartikeln ab. Hier werden zum Verständnis der Oxidation organischer Spurengase im troposphärischen Mehrphasensystem eine Vielzahl

important centre for this research area. The process studies result in the improvement of chemical mechanisms, which can be applied to the self-developed model mechanism CAPRAM and then increasingly also in higher-scale models.

In the field of analytic measurement technology laboratory experiments are dedicated to improve and test methods for the chemical characterization of organic aerosol components. These methods are mostly based on mass spectrometric processes, which are deployed in various coupling techniques. In the field of sampling techniques, the "Atmospheric Chemistry Department" closely collaborates with the "Experimental Aerosol and Cloud Microphysics Department" on the development of the specific segregation of aerosol particles of a distinct size and their chemical analysis and also on the development of inlet systems and reactors.

Modeling

For the description of complex atmospheric processes, model systems of varying dimensions, complexity, and scales are developed, tested and applied, also in combination with data from field and satellite measurements. The model investigations are intended to describe the cycles, interactions and phase transfers between aerosol particles, gases and clouds, as well as the direct and indirect influences of aerosol particles on the radiation budget.

Chemistry-transport modelling is realized with the three-dimensional modelling system COSMO-MUSCAT that has been developed at TROPOS. Its appropriateness for the simulation of particle and gas distribution on regional scale was demonstrated in international model-intercomparison studies and

von Reaktionen verschiedener Radikale sowie Reaktionen von halogenhaltigen Oxidantien untersucht. Letztere Spezies sind von Interesse bei der Freisetzung von Halogenverbindungen aus maritimen Seesalzpartikeln, der so genannten Halogenaktivierung.

Das Flüssigphasen-Laserlabor zur Untersuchung der troposphärischen Flüssigphasenprozesse ist ein wichtiges Zentrum dieses Forschungsbereiches. Aus den Prozessuntersuchungen resultieren Verbesserungen chemischer Mechanismen, die in der Modellierung mit dem eigenen Mechanismus CAPRAM und dann zunehmend auch in höherskaligen Modellen angewendet werden.

In der analytischen Messtechnik werden in Laborexperimenten Verfahren zur besseren chemischen Charakterisierung der organischen Bestandteile von Aerosolpartikeln entwickelt und getestet. Diese Techniken beruhen zumeist auf massenspektrometrischen Verfahren, die in verschiedenen Kopplungstechniken eingesetzt werden. Im Bereich der Probenahmetechniken gibt es auch hier eine enge Kooperation mit der Abteilung „Experimentelle Aerosol- und Wolkenmikrophysik" zur Entwicklung einer gezielten Abscheidung von Partikeln bestimmter Größe und deren chemischer Analyse aber auch zur Entwicklung von Einlasssystemen und Reaktoren.

Modellierung

Zur Beschreibung der komplexen atmosphärischen Vorgänge werden Modellsysteme verschiedener Dimension, Komplexität und Skalenbereiche entwickelt, überprüft und angewendet, auch in Kombination mit Daten aus Feldmessungen und aus satellitengestützten Fernerkundungen. Die

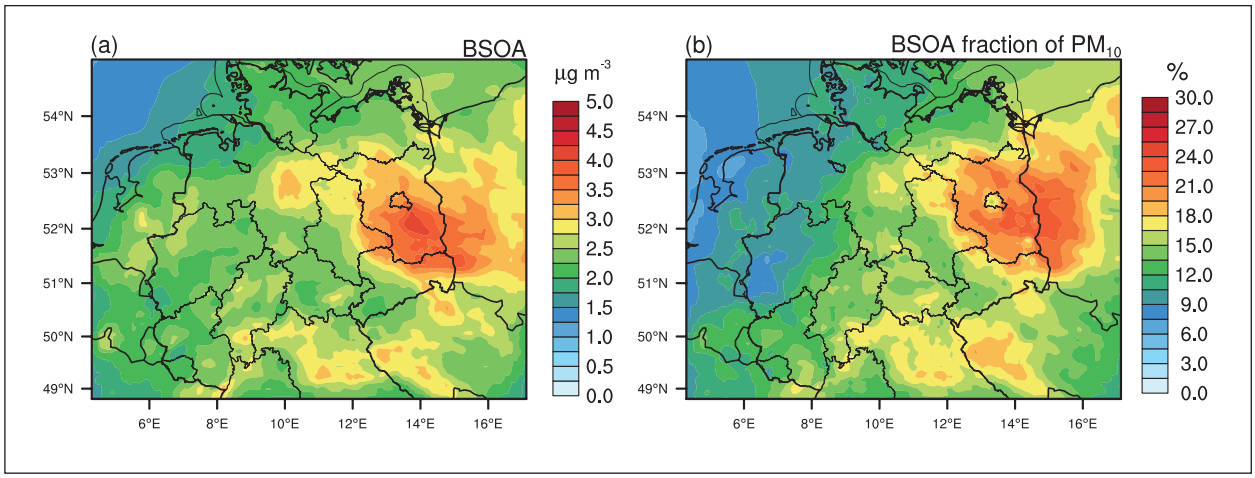

Fig. / Abb. 16: Mean biogenic SOA mass concentration [µg/m³] and the corresponding PM_{10} fraction [%] in Germany for May 2014 modelled by COSMO-MUSCAT. / Mittlere biogene SOA-Massenkonzentration [µg/m³] und der entsprechende PM_{10}-Anteil [%] in Deutschland für Mai 2014, modelliert mit COSMO-MUSCAT.

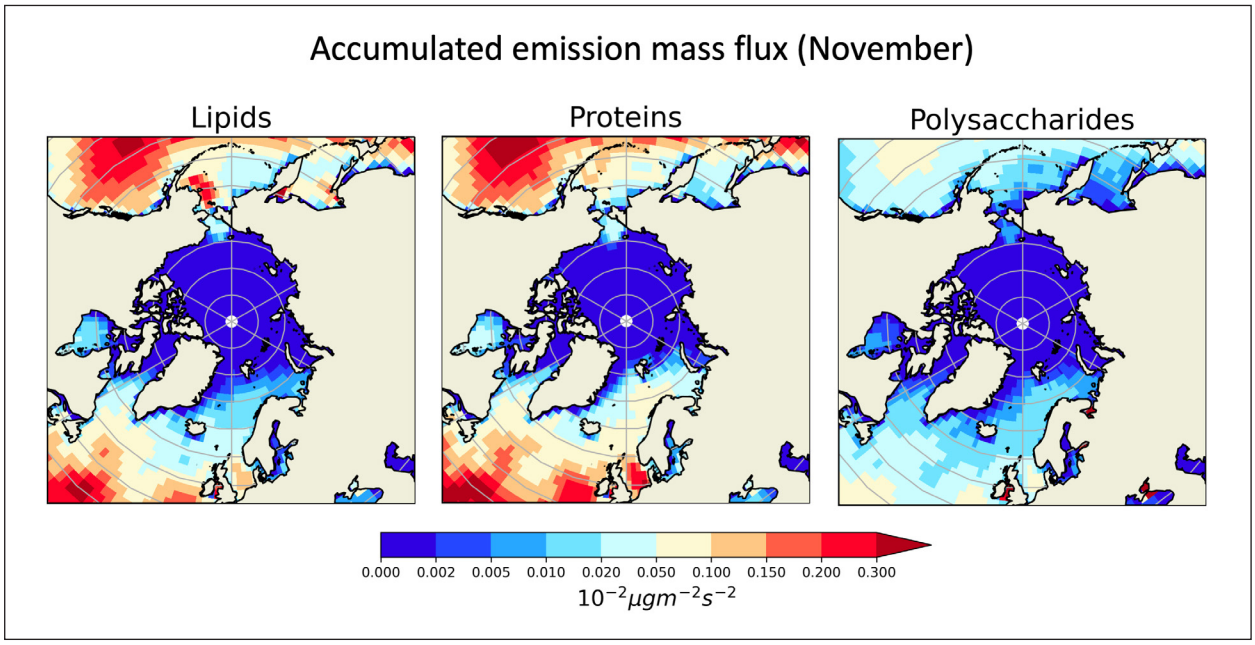

Fig. / Abb. 17: Marine Primary Organic Aerosol (MPOA) emissions computed by the aerosol-climate model ICON-HAM using the OCEANFILMS parameterization from Susannah Burrows (PNNL). A particular interest is in marine sugars, which are thought to have ice-nucleating properties and thus are relevant to climate and precipitation formation. / Marine primäre organische Aerosole (MPOA), berechnet mit dem Aerosol-Klimamodell ICON-HAM unter Verwendung der OCEANFILMS-Parametrisierung von Susannah Burrows (PNNL). Ein besonderes Interesse besteht an marinen Zuckern, von denen angenommen wird, dass sie eisbildende Eigenschaften haben und daher für das Klima und die Niederschlagsbildung relevant sind.

in applications on air quality issues. Several projects simulate the dynamics of primary and secondary particles and investigate their interaction with radiation and clouds. For further studies an additional "urbanized" version of COSMO-MUSCAT is being developed using a horizontal grid resolution up to a few 100 m.

On the other hand, by transferring the results of the higher-resolution model studies into the aerosol scheme of the global aerosol climate model ECHAM-HAM, direct consideration of the model parameterisation developed on high-resolution scales will be possible in climate studies on direct and indirect aerosol effects. One research focus is the investigation of control factors and effects of natural aerosols such as mineral dust, marine aerosol, smoke particles from forest fires or organic aerosol from plant emissions.

Besides this, one- and two-dimensional process models were also developed and will be developed further. SPECS (SPECtral bin cloud microphysicS) can be used for the description of cloud processes.

It allows an explicit and very precise calculation of the processes condensation, collision or freezing, and can be used as a box model as well as for case studies coupled with the regional COSMO model. One focus for the study of aerosol-cloud processes is the investigation of the role of dust particles for heterogeneous ice formation processes in clouds.

Modelluntersuchungen sollen der Beschreibung von Kreisläufen, Wechselwirkungen und Phasenübergängen zwischen Aerosolpartikeln, Gasen und Wolken, sowie der direkten und indirekten Einflüsse von Aerosolpartikeln auf den Strahlungshaushalt dienen.

Regionale Chemie-Transportmodellierung wird durch das am TROPOS entwickelte 3D-Modellsystem COSMO-MUSCAT realisiert. Seine Eignung zur Simulation des Ausbreitungsverhaltens von Partikeln und Gasen auf regionaler Skala wurde in mehreren internationalen Modellvergleichen und bei der Bearbeitung von Fragen zur Luftqualität gezeigt. In mehreren Projekten wird die Dynamik primärer und sekundärer Aerosolpartikel simuliert und deren Wechselwirkung mit Strahlung und Wolken untersucht. Für weitere Anwendungsmöglichkeiten insbesondere Luftqualitätsstudien wurde zusätzlich eine „urbanisierte" Version von COSMO-MUSCAT entwickelt, die eine horizontale Gitterauflösung bis zu wenigen 100 m nutzt. Andererseits werden durch Übertragung der Ergebnisse der höheraufgelösten Modellstudien in das Aerosolschema des globalen Aerosol-Klimamodells ECHAM-HAM eine direkte Berücksichtigung der auf hochaufgelösten Skalen entwickelten Modellparametrisierung in Klimastudien zu direkten und indirekten Aerosoleffekten möglich. Ein Forschungsschwerpunkt ist die Untersuchung von Kontrollfaktoren und Effekten natürlicher Aerosole wie

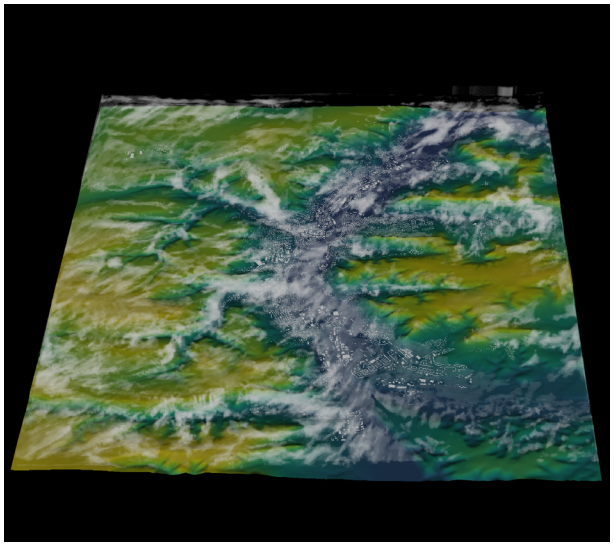

Fig. / Abb. 18: Topography and buildings in the Saale Valley near Jena as well as cloud cover, simulated with the new microscale urban model CAIRDIO with 40 m grid spacings. CAIRDIO is used for the dynamic downscaling of regional air quality simulations. / Topographie und Bebauung im Saaletal bei Jena sowie Bewölkung, simuliert mit dem neuen mikroskaligen Stadtmodell CAIRDIO mit 40 m Gitterweite. CAIRDIO wird für das dynamische Downscaling von regionalen Luftqualitätssimulationen genutzt.

SPACCIM (SPectral Aerosol Cloud Chemistry Interaction Model) is a parcel model, which combines the size-resolved description of microphysics with a complex multiphase chemistry. The process modelling studies are realized in connection with field studies and laboratory experiments.

Besides the dynamic/microphysical/chemical modelling at TROPOS also radiation transport models are developed and applied. These models are used to generate remote sensing algorithms for the improved understanding of the solar and thermal radiation effect of aerosols and clouds.

Mineralstaub, marines Aerosol, Rauchpartikel aus Waldbränden oder organischem Aerosol aus Pflanzenemissionen.

Daneben wurden und werden ein- und zweidimensionale Prozessmodelle weiterentwickelt. SPECS (SPECtral bin cloud microphysicS) dient zur Beschreibung von Wolkenprozessen. Es erlaubt eine explizite und sehr genaue Berechnung der Prozesse Kondensation, Kollision oder Gefrieren, und kann als Boxmodell sowie auch für Fallstudien gekoppelt mit dem regionalen COSMO Modell verwendet werden. Ein Schwerpunkt für die Untersuchung von Aerosol-Wolkenprozessen ist die Untersuchung der Rolle von Staubpartikeln für heterogene Eisbildungsprozesse in Wolken. SPACCIM (SPectral Aerosol Cloud Chemistry Interaction Model) ist ein Paketmodell zur gekoppelten größenaufgelösten Beschreibung von Mikrophysik und Mehrphasenchemie. Die Prozessmodellierungen werden im Zusammenhang mit Feldstudien sowie mit Laborexperimenten durchgeführt.

Neben der dynamischen/mikrophyskalischen/chemischen Modellierung werden am TROPOS auch Strahlungstransportmodelle entwickelt und betrieben, um Fernerkundungsalgorithmen zu entwerfen und den solaren und thermischen Strahlungseffekt von Aerosolen und Wolken besser zu verstehen.

Overview of the individual contributions

This biennial report presents selected work of TROPOS in the period 2020 to 2021 in four long and 20 short contributions. As in previous years, a broad spectrum of field, laboratory and modelling work is presented, which investigates fundamental and novel physical and chemical mechanisms in the aerosol and their interactions with clouds, but also opens up new fields such as the recording of atmospheric dynamics from satellite measurements of the aerosol. TROPOS' expertise in conducting long-term campaigns and increasingly networked research has again made it possible to record spectacular and climatically relevant major events such as the global spread of forest fire aerosol and to better understand the associated processes. Large-scale and regional studies of air quality are also becoming more complex and are increasingly taking into account the social, political and health context.

Long contributions

Air pollutants continue to be one of, if not the greatest health burden in urban areas. Especially there, numerous surfaces (windows, building walls, roofs) offer the possibility for deposits of organic dirt films ("urban grime"), which in turn are subject to heterogeneous chemical processes. To what extent this leads to sinks or sources of urban air pollution depends on the nature of the heterogeneous and multiphase reactions on the surfaces. Using extensive sample collections in controlled laboratory experiments, **Mothes and Herrmann** have now identified novel reaction pathways that allow a better understanding of the photoreactive behaviour of urban dirt films in particular and thus contribute to the understanding of the urban aerosol process chain.

In addition to such fundamental studies on chemical aerosol processing, the recording of the small-scale spatial and temporal distribution of size-resolved aerosol in urban areas is also fundamental information for assessing air quality and its effects, especially for the medical sector and for social and political decision-makers. A transdisciplinary framework suitable for this purpose has been developed by **Madueño et al.** for the Metro-Manila region as an example of a rapidly growing megacity. This work contributes to an assessment of the causes and health consequences of urban soot emissions and thus enables the development of solutions.

While anthropogenic emissions dominate the aerosol composition in urban areas, one of the most important processes for the large-scale distribution of aerosol is the condensation of biogenic precursor

Übersicht der Einzelbeiträge

Der vorliegende Zweijahresbericht stellt in vier Lang- und 20 Kurzbeiträgen ausgewählte Arbeiten des TROPOS im Zeitraum 2020 bis 2021 vor. Wie auch in den Vorjahren liegt ein breites Spektrum von Feld-, Labor-, und Modellierungsarbeiten vor, die sowohl fundamentale und neuartige physikalische und chemische Mechanismen im Aerosol und deren Wechselwirkungen mit Wolken untersuchen, aber auch neue Felder erschließen wie etwa die Erfassung der atmosphärischen Dynamik aus Satellitenmessungen des Aerosols. Die Expertise des TROPOS, langfristige Kampagnen durchzuführen und zunehmend vernetzt zu forschen hat es wieder ermöglicht, spektakuläre und klimatisch relevante Großereignisse wie die globale Ausbreitung des Waldbrandaerosols zu erfassen und die zugehörigen Prozesse besser zu verstehen. Auch großräumige und regionale Studien zur Luftqualität werden komplexer und berücksichtigen mehr und mehr das gesellschaftliche, politische und gesundheitliche Umfeld.

Langbeiträge

Luftschadstoffe sind weiterhin eine, wenn nicht die größte Gesundheitsbelastung im urbanen Raum. Gerade dort bieten zahlreiche Oberflächen (Fenster, Gebäudewände, Dächer) die Möglichkeit zu Ablagerungen von organischen Schmutzfilmen („urban grime"), die wiederum Gegenstand heterogener chemischer Prozesse sind. Inwieweit dies zu Senken oder Quellen der urbanen Luftverschmutzung führt, hängt von der Art der heterogenen und Multiphasen-Reaktionen an den Oberflächen ab. **Mothes und Herrmann** haben nun anhand von umfangreichen Probesammlungen in kontrollierten Laborexperimenten neuartige Reaktionswege identifiziert, die insbesondere das photoreaktive Verhalten von urbanen Schmutzfilmen besser verstehen lassen und so einen Beitrag zum Verständnis der Prozesskette des urbanen Aerosols leisten.

Neben solchen grundlegenden Studien zur chemischen Aerosolprozessierung ist im urbanen Raum auch die Erfassung der kleinskaligen räumlichen und zeitlichen Verteilung des größenaufgelösten Aerosols eine fundamentale Information zur Bewertung der Luftqualität und ihren Auswirkungen, insbesondere für den medizinischen Bereich und für soziale und politische Entscheidungsträger. Einen hierfür geeigneten transdisziplinären Rahmen haben **Madueño et al.** für die Region Metro-Manila als Beispiel für eine schnell wachsende Megastadt entwickelt. Diese Arbeiten tragen zu einer Bewertung der Ursachen und der gesundheitlichen Folgen von

gases from vegetation into aerosol particles. This formation of secondary organic aerosol (SOA) is very complex due to the large number of precursor compounds and atmospheric reaction pathways. **Wolke et al.** have created a model environment based on three-dimensional coupled physical/chemical process parameterizations, with which it is now possible to investigate the influence of meteorology, land use and vegetation types on SOA formation in detail.

Certainly, the most spectacular measurement campaign of TROPOS in the reporting period was the participation in the international ice drift expedition MOSAiC on board the German research icebreaker Polarstern as well as accompanying field campaigns in Greenland and Svalbard to study the Arctic climate system. **Engelmann et al.** report on the extensive TROPOS measurements on board Polarstern, which were carried out continuously throughout the five cruise legs. An unexpected highlight was the large-scale detection of Siberian Forest fire aerosol in the central Arctic up to the middle stratosphere and the clear indication of associated cirrus formation in the upper troposphere and ozone depletion in the polar stratosphere.

Short contributions

Global activities

In addition to extensive observations and model studies in an alarmingly rapidly changing Arctic and a Northern Hemisphere that continues to be heavily anthropogenically polluted, TROPOS has also focused in recent years on the Southern Hemisphere as a region that is still little researched and also as a less heavily polluted contrast to the Northern Hemisphere. However, it is also evident here that the more marine and less continental southern hemisphere is not spared aerosol pollution on a hemispheric scale. The five studies presented in the following section are also examples of the TROPOS strategy of investigating distinct atmospheric processes together with field observations, laboratory studies and modelling work in order to gain a deeper understanding of the complex multiphase system.

The three-year operation of the TROPOS Supersite LACROS in Punta Arenas has produced the longest continuous lidar and radar time series in the mid-latitudes of the southern hemisphere, detailing, among other things, the long-range transport and dynamics of the massive wildfires in Australia in 2019/2020. **Ohneiser et al.** were able to detect the presence of smoke layers up to the middle stratosphere for more than two years in remote Punta Arenas. The simultaneous decrease in the southern

städtischen Rußemissionen bei und ermöglichen so die Entwicklung von Lösungswegen.

Während anthropogene Emissionen die Aerosolzusammensetzung im urbanen Raum dominieren, ist einer der wichtigsten Prozesse zur großräumigen Verteilung des Aerosols die Kondensation biogener Vorläufergase aus der Vegetation zu Aerosolpartikeln. Diese Bildung von Sekundärem Organischem Aerosol (SOA) ist aufgrund der Vielzahl der Vorläuferverbindungen und der atmosphärischen Reaktionspfade sehr komplex. **Wolke et al**. haben eine Modellumgebung auf der Basis dreidimensionaler gekoppelter physikalischer/chemischer Prozessparametrisierungen geschaffen, mit der es nun möglich ist, den Einfluss von Meteorologie, Landnutzung und Vegetationstypen auf die SOA-Bildung im Detail zu untersuchen.

Die sicher spektakulärste Messkampagne des TROPOS im Berichtszeitraum war die Teilnahme an der internationalen Eis-Drift-Expedition MOSAiC an Bord des deutschen Forschungseisbrechers Polarstern sowie begleitender Feldkampagnen in Grönland und Spitzbergen zur Untersuchung des arktischen Klimasystems. **Engelmann et al.** berichten von den umfangreichen TROPOS-Messungen an Bord der Polarstern, die kontinuierlich während der gesamten fünf Fahrtabschnitte durchgeführt wurden. Ein unerwartetes Highlight war die großflächige Erfassung von sibirischem Waldbrandaerosol in der zentralen Arktis bis in die mittlere Stratosphäre und der deutliche Hinweis auf damit verbundene Zirrusbildung in der oberen Troposphäre und Ozonabbau in der polaren Stratosphäre.

Kurzbeiträge

Globale Aktivitäten

Neben umfangreichen Beobachtungen und Modellstudien in einer sich beunruhigend schnell verändernden Arktis und einer weiterhin stark anthropogen belasteten Nordhemisphäre hat TROPOS in den letzten Jahren auch die Südhemisphäre als noch wenig erforschte Region und auch als weniger stark belasteten Kontrast zur Nordhemisphäre in den Fokus genommen. Allerdings zeigt sich auch hier, dass die stärker marin und weniger kontinental geprägte Südhemisphäre auch nicht von Aerosolbelastungen hemisphärischen Ausmaßes verschont bleibt. Die im folgenden Abschnitt dargestellten fünf Arbeiten sind auch Beispiele für die Strategie des TROPOS, bestimme atmosphärische Prozesse gemeinsam mit Feldbeobachtung, Labor-Studien und Modellierungsarbeiten zu untersuchen, um zu einem tieferen Verständnis des komplexen Multiphasensystems zu gelangen.

Mit dem dreijährigen Betrieb der TROPOS-Supersite LACROS in Punta Arenas wurde die längste

hemispheric ozone layer indicates smoke-induced ozone depletion and urgently calls for further international research in this field.

With the help of the global aerosol-climate model ECHAM-HAM and the above-mentioned lidar measurements in Punta Arenas, **Heinold et al.** were able to demonstrate how the still poorly understood mechanism of pyroconvection transported the Australian forest fire aerosol far into the stratosphere, where it led to dispersion throughout the entire mid-latitudes of the southern hemisphere and thus influenced hemispheric warming rates and radiation balances comparable to a large volcanic eruption. Associated effects on the dynamics of the southern hemisphere are subject to further research.

The polar regions of the Southern Hemisphere are also not shielded from climate change, and here too the role of ocean-aerosol-cloud interactions, for example, in accelerating warming is still largely unclear. Thanks to the excellent cooperation with the AWI at the unique Neumayer III research station, **Henning et al.** were able to measure complete annual cycles of Antarctic cloud condensation (CCN) and ice nucleation particle (INP) concentrations for the first time. In addition to distinct annual cycles of CCN concentration and hygroscopicity, a consistently very low INP concentration was observed. The low number of available INP fits the observation that supercooled water clouds dominate in the high latitudes of the southern hemisphere and the recognition allows the improvement of cloud parameterisations in climate models.

This is also confirmed by the aforementioned long-term lidar and radar measurements of TROPOS at Punta Arenas. Here, in a long-term comparison with results of comparable ground-based aerosol and cloud remote sensing in Leipzig and Limassol (Cyprus), **Radenz et al.** were able to show that ice formation in supercooled water clouds is less frequent in the free and undisturbed southern hemisphere than over the northern hemisphere under similar meteorological conditions. On the other hand, these differences almost disappear as soon as local continental INP sources influence cloud formation.

The frequency and distribution of INPs in the upper troposphere and lower stratosphere is still largely unresolved, as direct measurements have not been possible so far. **Grawe et al.** have now developed a method to collect INPs in filter samples from the aircraft and later examine them in the laboratory for their temperature-dependent ice nucleation capacity. Initial applications on the German research aircraft HALO were successful and were able to demonstrate, for example, the transport of ground-level INPs by high-range convection.

durchgehende Lidar- und Radar-Zeitserie in den mittleren Breiten der Südhemisphäre erstellt, die unter anderem den Ferntransport und die Dynamik der gewaltigen Waldbrände in Australien in 2019/2020 im Detail erfasst hat. **Ohneiser et al.** konnten im entfernten Punta Arenas die Präsenz der Rauchschichten bis in die mittlere Stratosphäre über mehr als zwei Jahre nachweisen. Die gleichzeitige Abnahme der südhemisphärischen Ozonschicht weist auf einen rauchinduzierten Ozonabbau hin und verlangt dringend weitere internationale Forschung auf diesem Gebiet.

Mithilfe des globalen Aerosol-Klima-Modells ECHAM-HAM und den oben genannten Lidarmessungen in Punta Arenas konnten **Heinold et al.** nachweisen, wie der noch wenig erforschte Mechanismus der Pyrokonvektion das australische Waldbrandaerosol bis weit in die Stratosphäre transportierte, dort zu einer Ausbreitung in die gesamten mittleren Breiten der Südhemisphäre führte und so hemisphärisch Erwärmungsraten und Strahlungsbilanzen vergleichbar zu einem großen Vulkanausbruch beeinflusst hat. Damit verbundene Auswirkungen auf die Dynamik der Südhemisphäre sind Gegenstand weitere Forschung.

Auch die Polarregionen der Südhemisphäre sind vor dem Klimawandel nicht gefeit und auch hier ist die Rolle von Ozean-Aerosol-Wolken-Wechselwirkungen z.B. für eine Beschleunigung der Erwärmung noch weitgehend unklar. Durch die hervorragende Zusammenarbeit mit dem AWI an der einzigartigen Forschungsstation Neumayer III konnten **Henning et al.** erstmalig komplette Jahresgänge der antarktischen Wolkenkondensations- (CCN) und Eisnukleationskeimkonzentrationen (INP) messen. Neben ausgeprägten Jahresgängen der CCN-Konzentration und -Hygroskopizität zeigte sich eine durchgehend sehr niedrige INP-Konzentration. Die geringe Anzahl verfügbarer INP passt zur Beobachtung das unterkühlte Wasserwolken in den hohen Breiten der Südhemisphäre dominieren und die Berücksichtigung erlaubt die Verbesserung von Wolkenparametrisierungen in Klimamodellen.

Dies bestätigen auch die bereits genannten Langzeit-Lidar- und Radar-Messungen des TROPOS auf Punta Arenas. Hier konnten **Radenz et al.** in einem langjährigen Vergleich mit Ergebnissen vergleichbarer bodengebundener Aerosol- und Wolkenfernerkundung in Leipzig und Limassol (Zypern) zeigen, dass Eisbildung in unterkühlten Wasserwolken in der freien und ungestörten Südhemisphäre weniger häufig ist als über der Nordhemisphäre bei ähnlichen meteorologischen Bedingungen. Auf der anderen Seite verschwinden diese Unterschiede nahezu, sobald lokale kontinentale INP-Quellen die Wolkenbildung beeinflussen.

Die Häufigkeit und Verteilung von INPs in der oberen Troposphäre und unteren Stratosphäre ist

Ultimately, on the global scale, satellite data and model studies enable us to understand the hemispheric differences in the ice formation of global cloud cover. Here, in particular, stronger dust-induced heterogeneous freezing of supercooled water clouds is expected due to the stronger mineral dust sources in the northern hemisphere. On the basis of three satellite-based multi-year data sets, **Villanueva et al.** were able to demonstrate that the regions of higher freezing frequencies correspond globally with those of higher mineral dust concentrations.

Aerosol-cloud-radiation interaction

Since we are still far from being able to sufficiently resolve aerosol and cloud physical and chemical processes on a global scale in modelling, regional modelling studies continue to be an important tool for process understanding of the aerosol-cloud system. In particular, these studies can accompany previous and current field campaigns and place them into a larger context, as well as provide hints for future campaign designs.

For example, a change in cloud condensation and ice nucleation nuclei does not have a 1:1 effect on ice and precipitation formation, but is a complex non-linear interaction between primary ice formation and crystal growth in an environment of differently sized supercooled cloud droplets, as **Schrödner et al.** were able to show with the help of the spectrally resolved cloud microphysical model COSMO-SPECS. In contrast to models with simplified microphysics parameterisations, a significantly better agreement with observed cloud and precipitation formation was also found.

The cloud-resolving German community model ICON-LEM is also being co-developed at TROPOS and used for aerosol-cloud process studies on the regional scale. An interesting application, especially in anthropogenically polluted areas, is the investigation of the effect of absorbing aerosol, e.g. soot, on the energy balance, stability and cloud formation. Here **Senf et al.** show, using the example of the HOPE measurement campaign, how absorbing aerosol in a high-pressure situation over Germany increases the solar heating of the atmosphere near the ground by 1 K per day and reduces the solar radiation on the ground by 4 W m^{-2} on average. Due to the resulting reduced relative humidity in the boundary layer, the cloud cover is reduced by about 1% and the amount of cloud water by about 5%.

The fact that aerosols have a significant influence on the Earth's radiation balance has been known qualitatively for years. However, high-quality and representative measurements are needed to estimate the effect. Also, for applications in photovoltaics, **Witthuhn et al**. combined several years of data from the DWD's

noch weitgehend ungeklärt, da direkte Messungen bislang nicht möglich waren. **Grawe et al.** haben nun ein Verfahren entwickelt, vom Flugzeug aus INP in Filterproben zu sammeln und später im Labor auf ihre temperaturabhängige Eiskeimfähigkeit zu untersuchen. Erste Anwendungen auf dem deutschen Forschungsflugzeug HALO waren erfolgreich und konnten z.B. den Transport von bodennahen INPs durch hochreichende Konvektion nachweisen.

Auf der globalen Skala schließlich ermöglichen Satellitendaten und Modellstudien, die hemisphärischen Unterschiede in der Eisbildung der globalen Bewölkung zu verstehen. Hier ist insbesondere aufgrund der stärkeren Mineralstaubquellen in der Nordhemisphäre ein stärkeres staubinduziertes heterogenes Gefrieren unterkühlter Wasserwolken zu erwarten. Auf der Basis dreier satellitengestützter mehrjähriger Datensätzen konnten **Villanueva et al.** nachweisen, dass die Regionen höherer Vereisungshäufigkeiten global mit denen höherer Mineralstaub-Konzentration übereinstimmen.

Aerosol-Wolken-Strahlung-Wechselwirkung

Da wir noch weit davon entfernt sind, aerosol- und wolkenphysikalische und -chemische Prozesse auf globaler Skala im Modell hinreichend aufzulösen, bilden regionale Modellstudien weiterhin ein wichtiges Werkzeug zum Prozessverständnis des Aerosol-Wolken-Systems. Insbesondere können diese Studien frühere und aktuelle Feldkampagnen begleiten und in einen größeren Kontext stellen, oder auch Hinweise für zukünftige Kampagnengestaltungen geben.

So wirkt sich eine Änderung der Wolkenkondensations- und Eisnukleationskeime nicht 1:1 auf die Eis- und Niederschlagsbildung aus, sondern ist ein komplexes nicht-lineares Zusammenspiel zwischen primärer Eisbildung und Kristallwachstum in einer Umgebung unterschiedlich großer unterkühlter Wolkentropfen, wie **Schrödner et al.** mit Hilfe des spektral aufgelösten wolkenmikrophysikalischen Modells COSMO-SPECS zeigen konnten. Im Gegensatz zu Modellen mit vereinfachten Mikrophysik-Parametrisierungen wurde so auch eine deutlich bessere Übereinstimmung mit beobachteter Wolken- und Niederschlagsbildung gefunden.

Auch das wolkenauflösende deutsche Gemeinschaftsmodell ICON-LEM wird am TROPOS mit entwickelt und für Aerosol-Wolken-Prozess-Studien auf der regionalen Skala genutzt. Eine interessante Anwendung gerade im anthropogen belasteten Raum ist die Untersuchung des Effektes von absorbierendem Aerosol, z.B. Ruß, auf Energiehaushalt, Stabilität und Wolkenbildung. Hier zeigen **Senf et al.** am Beispiel der HOPE-Messkampagne, wie absorbierendes Aerosol in einer Hochdrucklage über Deutschland die solare

ground radiation network with satellite measurements and thus showed that aerosols over Germany lead to a cooling of the earth's surface by 10.6 Wm^{-2} and to a warming of the atmosphere by 4.1 Wm^{-2}. In particular, the absorption behavior of the aerosols plays a decisive role here.

Fundamental processes

Many fundamental processes of aerosol formation, oxidation in aerosol and cloud particles as well as ice formation are still not sufficiently understood and their investigations still lead to surprising results.

One example is the emission of biogenic substances from the ocean, which enters the atmosphere as aerosol via accumulation on the microscopically thin ocean surface and through spray effects and can thus contribute to cloud and ice formation. Using samples from Antarctic waters, **Zeppenfeld et al.** have shown that the chemical composition in the marine aerosol indicates bacterial degradation processes, thus confirming aerosol particles as a habitat for bacteria.

The formation of secondary organic aerosol in the atmospheric liquid phase is another poorly understood process. Here, **Schaefer et al.** are investigating the so-called process of photosensitisation and were able to identify novel reaction pathways for SOA formation in the laboratory using laser light excitation and liquid chromatography. The photosensitizers can either be primarily emitted organic compounds, but they can also be formed secondarily in the atmosphere. Photosensitizers can be drivers of oxidation processes in aerosol particles and cloud droplets in addition to the classical radicals OH, SO_4- and NO_3 and the non-radical oxidants ozone and H_2O_2.

Parallel to the above-mentioned work for the particle phase, a new substance group could be identified in the gas phase as further oxidants in laboratory experiments: the so-called hydrotrioxides, ROOOH, of which up to 10 million tons are produced annually from OH-initiated oxidation of isoprene. **Berndt et al.** present reaction pathways and detection methods of this novel strongly oxidizing substance class in the atmosphere.

The fact that there are occasionally more ice particles than ice nuclei in the same volume in the atmosphere is explained by so-called secondary ice formation processes. The best-known of these mechanisms, the Hallet-Mossop process, was investigated experimentally by **Hartmann et al.** using a newly developed setup at TROPOS. They found a significantly lower ice formation rate than previously assumed, which presumably lessens the importance of the Hallet-Mossop process for the formation of ice crystal size distributions in the atmosphere.

Heizung der bodennahen Atmosphäre um 1 K pro Tag erhöht und die solare Einstrahlung am Boden um 4 W m^2 im Mittel verringert. Aufgrund der dadurch reduzierten relativen Luftfeuchte in der Grenzschicht wird der Wolkenbedeckungsgrad um ca. 1% und die Wolkenwassermenge um ca. 5% reduziert."

Das Aerosole die Strahlungsbilanz der Erde maßgeblich beeinflussen, ist seit Jahren qualitativ bekannt. Allerdings benötigt man zur Abschätzung der Wirkung hochwertige und repräsentative Messungen. Auch für Anwendungen in der Photovoltaik haben **Witthuhn et al.** mehrjährige Daten des Boden-Strahlungs-Netzwerks des DWD mit Satellitenmessungen kombiniert und so gezeigt, dass Aerosole über Deutschland zu einer Abkühlung am Erdboden um 10.6 Wm^{-2} und zu einer Erwärmung der Atmosphäre um 4.1 Wm^{-2} führen. Insbesondere das Absorptionsverhalten der Aerosole spielt hierbei eine entscheidende Rolle.

Fundamentale Prozesse

Nach wie vor sind viele fundamentale Prozesse der Aerosolbildung, der Oxidation im Aerosol und in Wolkenpartikeln sowie der Eisbildung nicht hinreichend verstanden und deren Untersuchungen führen immer noch zu überraschenden Ergebnissen.

Ein Beispiel ist die Emission von biogenen Substanzen aus dem Ozean, die über Anreicherung an der mikroskopisch dünnen Meeresoberfläche und durch Sprüheffekte als Aerosol in die Atmosphäre gerät und so zu Wolken- und Eisbildung beitragen kann. **Zeppenfeld et al.** haben anhand von Proben aus antarktischen Gewässern gezeigt, dass die chemische Zusammensetzung im marinen Aerosol auf bakterielle Abbauprozesse hinweist, , also Aerosolpartikel als Lebensraum für Bakterien bestätigt.

Die Bildung von sekundärem organischem Aerosol in der atmosphärischen Flüssigphase ist ein weiterer wenig verstandener Prozess. Hier gehen **Schaefer et al.** dem sogenannten Prozess der Photosensibilisierung nach und konnten im Labor durch Laserlichtanregung und Flüssigkeitschromatographie neuartige Reaktionswege zur SOA-Bildung identifizieren. Die Photosensibilisatoren können entweder primär emittierte organische Verbindungen sein, sie können aber auch sekundär in der Atmosphäre gebildet werden. Photosensibilsatoren können in Aerosolpartikeln und Wolkentropfen neben dem klassischen Radikalen OH, SO_4^- und NO_3 sowie den nichtradikalischen Oxidantien Ozon und H_2O_2 zu den Treibern von Oxidationsprozesen gehören.

Paralle zu den o.a. Arbeiten für die Partikelphase konnte in der Gasphase eine neue Substanzgruppe als weitere Oxidationsmittel in Laborexperimenten identifiziert werden: die sogenannten Hydrotrioxide, ROOOH, von denen jährlich bis 10 Millionen Tonnen

Dynamics

Active remote sensing of the aerosol with lidar technology has long been used at TROPOS to determine the vertical wind via the Doppler effect. The novel wind satellite AEOLUS also uses this effect to determine the zonal wind at different heights. To validate the AELUS wind products, **Bley et al.** combined wind data from the Google Loon stratospheric balloons with modelled wind fields in an extensive study and thus quantified systematic and random errors.

Another AEOLUS validation campaign took place in Cape Verde in summer and autumn 2021. **Baars et al.** report on the TROPOS ground-based lidar measurements and their integration with aircraft measurements. In addition to the wind profiles, the aerosol products from AEOLUS were also investigated. Overall, a good agreement with AEOLUS was found within the instrument inaccuracies and, incidentally, the aerosol of the La Palma volcanic eruptions was measured.

Air quality

The pollutant level in the air at a given location at a given time is the result of complex emission, transport, ageing and mixing processes and can only be recorded and understood with extensive measurement networks, laboratory studies and models. Here, TROPOS is involved in the entire spectrum of local and networked measurements and modelling activities.

An example of this overall concept is presented by **Poulain et al.** in which TROPOS, with the participation of all departments and with international partners for the Central European region, combined anthropogenic sources for an overall picture of pollutant load and thus also made a significant contribution to the validation of the TROPOS chemical transport modelling.

Anthropogenic sources include not only emissions from combustion mechanisms in industry, traffic or heating with point sources, but also locally and on a large scale from agricultural activities. Especially for agricultural dust, **Faust et al.** have created a model environment with which it is possible to couple turbulent chaotic transports of dust emissions from the boundary layer with a dynamic atmospheric model in order to provide realistic dust dispersion scenarios for given weather situations.

A similar approach is taken by **D. van Pinxteren** et al. to understand the distribution of ozone as an important secondary air pollutant in Saxony, as well as its long-term concentration trends. Here, machine learning techniques and dynamic modelling are combined to evaluate extensive station measurements

aus OH-initiierter Oxidation von Isopren entstehen. **Berndt et al.** stellen Reaktionswege und Nachweismethoden dieser neuartigen stark oxidierenden Substanzklasse in der Atmosphäre vor.

Das in der Atmosphäre gelegentlich mehr Eisartikel als Eiskeime im gleichen Volumen vorhanden sind, wird durch sogenannte sekundäre Eisbildungsprozesse erklärt. Den bekanntesten dieser Mechanismen, den Hallet-Mossop-Prozess haben **Hartmann et al.** mit einem neu am TROPOS entwickelten Aufbau experimentell untersucht. Dabei stellte sich eine deutlich geringere Eisbildungsrate als bislang vermutet heraus, was vermutlich die Bedeutung des Hallet-Mossop-Prozesses für die Bildung von Eiskristallgrößenverteilungen in der Atmosphäre schmälert.

Dynamik

Die aktive Fernerkundung des Aerosols mit Lidartechnik wird schon lange am TROPOS auch über den Dopplereffekt zur Bestimmung des Vertikalwindes genutzt. Der neuartige Windsatellit AEOLUS nutzt diesen Effekt ebenfalls zur Bestimmung des zonalen Windes in verschiedenen Höhen. Zur Validierung der AELUS-Windprodukte haben **Bley et al.** in einer umfangreichen Studie Winddaten der Google Loon Stratosphärenballone mit modellierten Windfeldern kombiniert und so systematische und zufällige Fehler quantifiziert.

Eine weitere AEOLUS-Validierungskampagne fand im Sommer und Herbst 2021 auf den Kapverden statt. **Baars et al.** berichten von den bodengebundenen Lidarmessungen des TROPOS und deren Einbettung in Flugzeugmessungen. Dabei wurden neben den Windprofilen auch die Aerosolprodukte von AEOLUS untersucht. Insgesamt wurde eine gute Übereinstimmung mit AEOLUS im Rahmen der Instrumentenungenauigkeiten gefunden und nebenbei auch das Aerosol der La Palma Vulkan-Eruptionen vermessen.

Luftqualität

Die Schadstoffbelastung in der Luft an einem bestimmten Ort zu einer bestimmten Zeit ist das Ergebnis komplexer Emissions-, Transport-, Alterungs- und Mischungsprozesse und kann nur mit umfangreichen Messnetzen, Laborstudien und Modellen erfasst und verstanden werden. TROPOS ist hier am gesamten Spektrum von lokalen und vernetzten Messungen und Modellierungsaktivitäten beteiligt.

Ein Beispiel für dieses Gesamtkonzept wird von **Poulain et al.** vorgestellt, in dem TROPOS unter Beteiligung aller Abteilungen und mit internationalen Partnern für den zentral-europäischen Raum anthropogene Quellen für ein Gesamtbild der Schadstoffbelastung zu einem Gesamtbild zusammengeführt und so auch ein wesentlicher Beitrag zur Validierung

of ground-level ozone and to investigate the influences of precursor gases and particles as well as weather conditions on ozone formation. This should make it possible to specifically understand and evaluate the influence of certain environmental factors on local ozone pollution.

Especially in the boundary layer and there in heterogeneous urban areas, spatial and temporal distributions of aerosol are highly variable due to the proximity to local sources and the local dynamics of the boundary layer. More and more measurement drones are now making it possible to capture this variability. **Düsing et al.** have succeeded in recording a large number of aerosol parameters at high resolution by drone through clever instrument miniaturisation. This lays the foundation for future swarm measurements of small-scale aerosol dispersion processes in urban areas or in the vicinity of strong emission sources such as motorways or industrial plants.

Ultimately, the health-damaging effect of air pollutants, especially soot, depends on the physical and chemical uptake in the respiratory tract. For this purpose, a mobile system for determining the aerosol concentration in the inhaled and exhaled air was developed at TROPOS, which, together with soot concentration measurements of the ambient air, allows the determination of soot deposition in the respiratory tract. **Madueño et al.** present the system and the results of two measurement campaigns of different extreme conditions (high mountains, tropical city). Together with other health parameters such as pulse and heart rate, health burdens caused by air pollutants can thus be better understood.

der Chemie-Transport-Modellierung des TROPOS geleistet wurde.

Anthropogene Quellen umfassen nicht nur Emissionen durch Verbrennungsmechanismen in Industrie, Verkehr oder Heizung mit punktfürmigen Quellen,, sondern lokal und großräumig auch durch landwirtschaftliche Aktivitäten. Speziell für Agrarstaub haben **Faust et al.** eine Modellumgebung geschaffen, mit der es gelingt, turbulente chaotische Transporte von Staubemissionen aus der Grenzschicht mit einem dynamischen Atmosphärenmodell zu koppeln, um so für vorgegebene Wettersituation realistische Staubausbreitungsszenarien zur Verfügung zu stellen.

Einen ähnlichen Ansatz verfolgen **D. van Pinxteren et al.**, um die Verteilung von Ozon als wichtigem sekundären Luftschadstoff in Sachsen, sowie seine langfristigen Konzentrationstrends zu verstehen. Hier werden Machine-Learning-Techniken und dynamische Modellierung kombiniert, um umfangreiche Stationsmessungen des bodennahen Ozons auszuwerten und die Einflüsse von Vorläufergasen und Partikeln sowie der Wetterlage in die Ozon-Entstehung zu untersuchen. Damit soll es möglich werden, gezielt den Einfluss bestimmter Umweltfaktoren auf die lokale Ozonbelastung zu verstehen und zu bewerten.

Insbesondere in der Grenzschicht und dort im heterogenen urbanen Raum sind räumliche und zeitliche Verteilungen des Aerosols aufgrund der Nähe zu lokalen Quellen und der lokalen Dynamik der Grenzschicht hochvariabel. Diese Variabilität zu erfassen ermöglichen nun mehr und mehr Messdrohnen. Hier ist es **Düsing et al.** durch geschickte Instrumenten-Miniaturisierung gelungen, eine Vielzahl von Aerosolparametern hochaufgelöst per Drohne zu erfassen. Damit ist der Grundstein gelegt für zukünftige Schwarmmessungen zu kleinskaligen Aerosol-Ausbreitungsprozessen im städtischen Raum oder in der Nähe von starken Emissionsquellen wie Autobahnen oder Industrieanlagen.

Letztlich hängt die gesundheitsschädigende Wirkung von Luftschadstoffen, insbesondere von Ruß, von der physikalischen und chemischen Aufnahme in den Atemwegen ab. Hierzu wurde am TROPOS ein mobiles System zur Bestimmung der Aerosolkonzentration in der ein- und ausgeatmeten Luft entwickelt, das zusammen mit Rußkonzentrationsmessungen der Umgebungsluft die Bestimmung der Rußdeposition in den Atemwegen erlaubt. **Madueño et al.** stellen das System und die Ergebnisse zweier Messkampagnen unterschiedlicher extremer Bedingungen (Hochgebirge, tropische Großstadt) vor. Zusammen mit weiteren Gesundheitsparametern wie Puls und Herzfrequenz lassen sich gesundheitliche Belastungen durch Luftschadstoffe so besser verstehen.

Transfer in science and society – overview / Transfer in Wissenschaft und Gesellschaft – Überblick

Transfer in science and society – overview

Knowledge transfer and public visibility

On account of the application oriented fundamental research of the Institute, its scientific knowledge is mainly transferred through scientific publications and conference contributions (see list, p. 145).

During the reporting period the following **conferences with TROPOS contribution** are highlighted:

The conference "Future GUAN" (German Ultrafine Aerosol Network) on 9 and 10 March 2020 brought together researchers to discuss the future of the ultra-fine dust network. The partners involved are carrying out important pioneering work in data collection and quality assurance.

The Collaborative Research Centre "Arctic Climate Change (AC)³" under the leadership of Leipzig University entered its second funding period in 2020. The research network will continue its successful work for another four years and is funded by the German Research Foundation (DFG) with 14.5 million euros. The network includes the universities in Bremen, Cologne and Leipzig as well as the Alfred Wegener Institute, Helmholtz Centre for Polar and Marine Research (AWI) and TROPOS. The aim is to investigate the dramatic climate change in the Arctic in order to improve the reliability of models and enable more precise predictions of further warming in the Arctic. The kick-off meeting for the 2nd phase of the network in Cologne (8 to 10 October 2020) with over 100 participants had to take place mainly virtually due to the Corona pandemic. Two TROPOS

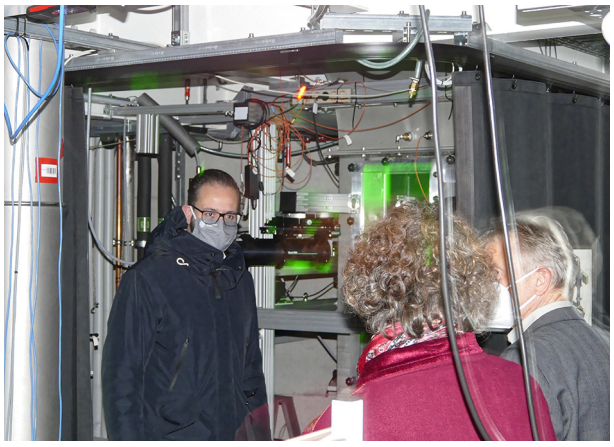

Fig. / Abb. 1: In 2020, Saxony's Science Minister Sebastian Gemkow informed himself about the excellence plans of the University of Leipzig and also visited the TROPOS cloud laboratory. / Sachsens Wissenschaftsminister Sebastian Gemkow informierte sich 2020 über die Exzellenzpläne der Uni Leipzig und besuchte dazu auch das TROPOS-Wolkenlabor. (Photo: Tilo Arnhold / TROPOS)

Transfer in Wissenschaft und Gesellschaft – Überblick

Wissenstransfer und Außenwirkung

TROPOS-Forschung für Fachpublikum. Auf Grund der Ausrichtung des Institutes auf anwendungsorientierte Grundlagenforschung erfolgt die Verwertung der wissenschaftlichen Ergebnisse hauptsächlich in Fachpublikationen und Konferenzbeiträgen (siehe Liste, S. 145).

Aus den **wissenschaftlichen Tagungen**, an deren TROPOS beteiligt war, stechen im Berichtszeitraum folgende heraus:

Die Tagung „Future GUAN" (09.-10.03.20) brachte Forschende des German Ultrafine Aerosol Network (GUAN) zusammen, um über die Zukunft des Ultrafeinstaub-Netzwerkes zu diskutieren. Die am Netzwerk beteiligten Partner leisten dabei wichtige Pionierarbeit in der Datenerhebung und Qualitätssicherung.

Der Sonderforschungsbereich „Arktische Klimaänderung (AC)³" unter der Federführung der Universität Leipzig ging 2020 in die zweite Förderperiode. Der Forschungsverbund setzt damit seine erfolgreiche Arbeit für vier weitere Jahre fort und wird von der Deutschen Forschungsgemeinschaft (DFG) mit 14,5 Millionen Euro gefördert. Zum Verbund gehören die Universitäten in Bremen, Köln und Leipzig sowie das Alfred-Wegener-Institut, Helmholtz-Zentrum für Polar- und Meeresforschung (AWI) und TROPOS. Ziel ist es, den dramatischen Klimawandel in der Arktis zu untersuchen, um die Verlässlichkeit von Modellen zu verbessern und genauere Vorhersagen zur weiteren Erwärmung in der Arktis zu ermöglichen. Das Auftaktreffen für die 2. Phase des Verbunds in Köln (08.-10.10.2020) mit über 100 Teilnehmenden musste wegen der Corona-Pandemie überwiegend virtuell stattfinden. Im wissenschaftlichen Leitungsteam sind mit Prof. Andreas Macke und Prof. Ina Tegen zwei Forschende von TROPOS vertreten.

Zu einem wichtigen Austauchforum hat sich die jährlich stattfindende ACTRIS-Week entwickelt. 2020 trafen sich über 300 Teilnehmende online (26. - 28.10.2020). Ziel der virtuellen Konferenz war es, sich in der ACTRIS-Community auszutauschen und eine Plattform für technische Diskussionen innerhalb der In-situ- und Fernerkundungs-Gemeinschaft, der thematischen Zentren und des Datenzentrums zu bieten.

Ausgewählte Themen und Aktivitäten für Politik und Gesellschaft. Die Forschungsergebnisse des TROPOS dienen auch als ein Beitrag zur

researchers, Prof. Andreas Macke and Prof. Ina Tegen, are members of the scientific management team.

The annual ACTRIS Week has become an important exchange forum. In 2020, over 300 participants met online (26 to 28 October 2020). The aim of the virtual conference was to exchange ideas within the ACTRIS community and to provide a platform for technical discussions within the in situ and remote sensing community, the Topical Centers and the Data Center.

Selected topics and activities for policy and society. Results from TROPOS research contributes to **policy advice in the environmental sector**. For example, for the Land of Saxony or the Federal Environmental Agency (UBA), practise-oriented investigations regarding the behaviour and the future development of air pollutants in the atmosphere are conducted. In the framework of projects in collaboration with the Environmental Agency and the Saxon State Office for the Environment, Agriculture and Geology (LfULG) measurement data of fine and ultrafine particles are collected, evaluated and provided for further interpretation of the concentration and chemical composition of these particles.

In 2020, the BMBF project WTimpact, which investigated collaborative knowledge development as a transfer instrument, was successfully completed. A total of four institutes of the Leibniz Association were investigating new methods of knowledge transfer. Within the project part "Air in Leipzig" Leipzig residents were able to measure particulate matter and soot in the city. For TROPOS, the pilot project provided important impulses and experience in the area of knowledge transfer.

Since 2021, the DUSTRISK project has been investigating the health effects of mineral dust, which can cause or aggravate respiratory diseases such as asthma or pneumonia. In the interdisciplinary project, these aspects are investigated in combination with adhering microbes. Field studies, laboratory investigations as well as modelling studies will be carried out in collaboration with partners from the Leibniz institutes DSMZ, FZB, IUF and TROPOS as well as from Cape Verde, including hospitals, universities and public health institutes. DUSTRISK is funded by the Leibniz "Cooperative Excellence" competition.

Ultrafine dust as a potential health hazard is being investigated in the project "Ultrafine dust pollution from airports in Berlin" (ULTRAFLEB) until the end of 2024 on behalf of the Federal Environment Agency. For this purpose, stationary and mobile field measurements of ultrafine particles (UFP) and various other quantities in the area surrounding Berlin Brandenburg BER Airport are being carried out with

Fig. / Abb. 2: Meeting of the Saxon Leibniz Institutes with the Saxon Minister of Science Sebastian Gemkow on 02.07.20 at the IPF in Dresden. / Treffen der Sächsischen Leibniz-Institute mit dem Sächsischem Wissenschaftsminister Sebastian Gemkow am 02.07.20 am IPF in Dresden. (Photo: Oliver Killig / SMWK)

Politikberatung im Umweltbereich. So werden u.a. für das Land Sachsen oder das Umweltbundesamt (UBA) praxisrelevante Untersuchungen zum Verhalten und zur künftigen Entwicklung von Schadstoffen in der Atmosphäre durchgeführt. Außerdem werden im Rahmen von Auftragsprojekten für das UBA und das Sächsische Landesamt für Umwelt und Geologie (LfULG) über längere Zeiträume Messdaten zu den Konzentrationen feiner und ultrafeiner Aerosolpartikel sowie zur chemischen Partikelzusammensetzung in der Atmosphäre erhoben, wissenschaftlich ausgewertet und zur weiteren Nutzung zur Verfügung gestellt.

2020 wurde das BMBF-Projekt WTimpact erfolgreich abgeschlossen, dass die kollaborative Wissensentwicklung als ein Transferinstrument untersuchte. Insgesamt untersuchen vier Institute der Leibniz-Gemeinschaft neue Methoden des Wissenstransfers auf diese Art. Leipzigerinnen und Leipziger konnten bei „Luft in Leipzig" selbst mobil Feinstaub und Ruß in der Stadt messen. Für TROPOS brachte das Pilotprojekt wichtige Impulse und Erfahrungen im Bereich Wissenstransfer.

Das Projekt DUSTRISK untersucht seit 2021 die Gesundheitsauswirkungen von Mineralstaub, der Atemwegserkrankungen wie Asthma oder Lungenentzündung verursachen oder verschlimmern kann. Im interdisziplinären Projekt werden diese Aspekte in Kombination mit anhaftenden Mikroben untersucht. Feldstudien, Laboruntersuchungen sowie Modellierungsstudien werden in Zusammenarbeit mit Partnern der Leibniz-Institute DSMZ, FZB, IUF und TROPOS sowie der Kapverden durchgeführt, darunter Krankenhäuser, Universitäten und öffentliche Gesundheitsinstitute. DUSTRISK wird durch den Leibniz-Wettbewerb „Kooperative Exzellenz" gefördert.

the TROPOS aerosol container, as well as model calculations. In addition to the TROPOS aerosol group, the following intitutions are also involved in the project: TNO, TU Braunschweig, TU Berlin, IVU Umwelt GmbH, Ingenieurbüro Janicke GbR and BER Airport. Important cooperation partners are also the Brandenburg State Office for the Environment (LfU) and the Berlin Brandenburg Air Study (BEAR) - a health study started in 2020 by the Charité-Universitätsmedizin Berlin and the University Hospital Düsseldorf.

Mobile measurements by TROPOS took place in Dresden-Neustadt in summer 2021 on behalf of the state agency LfULG to investigate the so-called "Friday/Saturday evening effect". The study was motivated by the observation of increased concentrations of soot as well as ultrafine and fine dust particles in the summer half-year on weekends in the evening, which are higher than during the rest of the week. Among other things, open fires and charcoal grills are suspected as possible sources. With the TROPOS measuring backpacks, an increase was mostly observed in the vicinity of allotment gardens and parks as well as street gastronomy. The results therefore support the thesis that the emissions originate from leisure activities (barbecues, fire bowls, etc.), which are strongly influenced by weather and holidays.

In addition to the fields of climate and air quality, the TROPOS expertise on aerosols in connection with the COVID 19 pandemic was asked for political advice in the years 2020 and 2021:

On 29 June 2020, TROPOS researchers explained in a statement, that reduced emissions during the COVID-19 Lockdown do not automatically lead to lower immissions, as various complex factors

Fig. / Abb. 3: Saxony's Science Minister Sebastian Gemkow and University Rector Beate Schücking together with the Leipzig participants of the MOSAiC expedition. / Sachsens Wissenschaftsminister Sebastian Gemkow und Uni-Rektorin Beate Schücking zusammen mit den Leipziger Teilnehmenden der MOSAiC-Expedition. (Photo: Tilo Arnhold / TROPOS)

Ultrafeinstaub als potenzielle Gesundheitsgefahr untersucht das Projekt „Ultrafeinstaubbelastung durch Flughäfen in Berlin" (ULTRAFLEB) bis Ende 2024 im Auftrag des Umweltbundesamtes. Dazu finden stationäre und mobile Feldmessungen von Ultrafeinpartikeln (UFP) und verschiedener anderer Größen im Umfeld des Flughafens Berlin Brandenburg BER mit dem Aerosolcontainer des TROPOS sowie Modellrechnungen statt. Am Projekt sind neben der TROPOS-Aerosolgruppe ebenfalls beteiligt: TNO, TU Braunschweig, TU Berlin, IVU Umwelt GmbH, Ingenieurbüro Janicke GbR und der BER-Flughafen. Wichtige Kooperationspartner sind außerdem das Landesamt für Umwelt (LfU) Brandenburg und die Berlin Brandenburg Air Study (BEAR) - eine im Jahr 2020 begonnene Gesundheitsstudie der Charité-Universitätsmedizin Berlin und des Universitätsklinikums Düsseldorf.

Mobile Messungen des TROPOS fanden im Sommer 2021 im Auftrag des LfULG in Dresden-Neustadt statt, um den sogenannten „Freitag-/Samstagabendeffekt" zu untersuchen. Anlass war die Beobachtung, dass die Konzentrationen von Ruß sowie ultrafeinen und feinen Staubpartikeln im Sommerhalbjahr an Wochenenden abends im Vergleich zur restlichen Woche immer wieder ansteigen. Als mögliche Quellen werden unter anderem offene Feuer und Holzkohlegrills vermutet. Mit den TROPOS-Messrucksäcken wurde ein Anstieg meist in der Umgebung von Kleingärten und Parkanlagen sowie von Straßen-Gastronomie beobachtet. Die Ergebnisse stützen daher die These, dass die Emissionen aus Freizeitaktivitäten (Grills, Feuerschalen, etc.) stammen, die stark von Wetter und Feiertagen geprägt sind.

Neben den Feldern Klima und Luftqualität war 2020/21 in der Politikberatung auch die TROPOS-Expertise zu Aerosolen im Zusammenhang mit der COVID-19-Pandemie gefragt:

In einem Statement zum Corona-Lockdown klärten Forschende des TROPOS am 29.06.20 darüber auf, dass reduzierte Emissionen während des COVID-19-Lockdowns nicht automatisch zu geringeren Immissionen führen, da verschiedene komplexe Einflussfaktoren auf Schadstoffkonzentrationen in der Luft wirken. Dass wetterbedingt die Schadstoffkonzentrationen trotz Lockdown nicht zurückgegangen war, hatte eine öffentliche Diskussion über das Konzept der Luftreinhaltung und der Grenzwerte entfacht.

Das Übertragungsrisiko von SARS-CoV-2 über Aerosole könnte deutlich gesenkt werden, wenn mehr gegen Viren in der Innenraumluft getan würde. Der Arbeitsausschuss Feinstäube (AAF) hat daher am 08.12.20 eine Stellungnahme mit Empfehlungen wie Masken, Lüften und Luftreinigung vorgelegt. Der Arbeitsausschuss vereint Expertinnen und Experten

Fig. / Abb. 4: "Book a Scientist" on 10 November 2020 - with Christian Pilz from TROPOS, among others. / „Book a Scientist" am 10. November 2020 - u.a. mit Christian Pilz vom TROPOS. (Quelle: Leibniz-Gemeinschaft)

influence pollutant concentrations in the air. The fact that weather-related pollutant concentrations had not decreased despite the lockdown, had initiated a public discussion about the concept of air pollution control and limit values.

The risk of spreading SARS-CoV-2 via aerosols can be significantly reduced if more was done against viruses in indoor air. The Working Committee on Fine Dusts (AAF) therefore presented a statement on 8 December 2020 with recommendations for measures like masks, ventilation and air purification. The working committee brings together experts from engineering, chemistry, physics, biology, meteorology and medicine who are organized in the professional societies ProcessNet (DECHEMA/ VDI-GVC), Gesellschaft Deutscher Chemiker (GDCh) and VDI/DIN-Kommission Reinhaltung der Luft (KRdL). The chairman is Prof. Hartmut Herrmann from TROPOS.

Also in December 2020, the position paper on the role of aerosol particles in SARS-CoV-2 infections was published (9 December 2020). The Society for Aerosol Research (GAeF), with the support of more than 185 international experts, has compiled the current state of knowledge and recommendations for protection against the virus. The paper explains, among other things, why face visors or cutting discs can do little against the spread, but FFP2 masks can do a lot. Among the authors is Dr. Birgit Wehner of TROPOS, who is Secretary General of GAeF and the European Aerosol Assembly (EAA). Among the signatories are also many TROPOS researchers.

The workshop "Aerosol & SARS-CoV-2" on 17 March 2021 was one of the first interdisciplinary events where representatives of aerosol research, medicine, virology and ventilation technology exchanged ideas. The event was held under the patronage of Prof. Dr. Lothar Wieler, President of the aus Ingenieurswissenschaften, Chemie, Physik, Biologie, Meteorologie und Medizin, die in den Fachgesellschaften ProcessNet (DECHEMA/ VDI-GVC), Gesellschaft Deutscher Chemiker (GDCh) und VDI/ DIN-Kommission Reinhaltung der Luft (KRdL) organisiert sind. Vorsitzender ist Prof. Hartmut Herrmann vom TROPOS.

Ebenfalls im Dezember 2020 erschien das Positionspapier zur Rolle von Aerosolpartikeln beim SARS-CoV-2-Infektionsgeschehen (09.12.20). Die Gesellschaft für Aerosolforschung (GAeF) hat mit Unterstützung von mehr als 185 internationalen Expertinnen und Experten den aktuellen Wissensstand und Empfehlungen zum Schutz vor dem Virus zusammengetragen. Das Papier erläuterte u.a. weshalb Gesichtsvisiere oder Trennscheiben wenig gegen die Ausbreitung, FFP2-Masken aber viel leisten können. Zu den Autoren gehört Dr. Birgit Wehner vom TROPOS, die Generalsekretärin der GAeF und der European Aerosol Assembly (EAA) ist. Unter den Unterzeichnenden sind auch weitere TROPOS-Forschende.

Der Workshop „Aerosol & SARS-CoV-2" am 17.03.21 war einer der ersten interdisziplinären Veranstaltungen, bei denen sich Aerosolforschung, Medizin, Virologie und Lüftungstechnik austauschten. Die Veranstaltung stand unter der Schirmherrschaft von Prof. Dr. Lothar Wieler, dem Präsidenten des Robert-Koch-Instituts. TROPOS-Aerosolexpertin Dr. Birgit Wehner war als Generalsekretärin der GAeF intensiv eingebunden und moderierte die Session „Ansteckungsweg Aerosol".

Am 11.04.21 haben sich Aerosolforschende in einen offenen Brief an die Politik gewendet: Die Forschenden betonten, dass Corona-Infektionen überwiegend im Innenraum stattfinden und die Maßnahmen zur Eindämmung der Pandemie vor allem dort ansetzen sollten. Zur Infektionsvermeidung empfehlen sie Punkte wie Lüften, Masken und Luftfilter. Zu den Unterzeichnenden gehört u.a. Dr. Birgit Wehner, Generalsekretärin der Gesellschaft für Aerosolforschung (GAeF) und Aerosol-Forscherin am TROPOS.

Im Bereich der Luftreinhaltung trägt TROPOS zur Politikberatung auch durch eigene Forschungsergebnisse bei, die z.B. in der Richtliniendiskussion oder bei der Erstellung von Luftreinhalteplänen verwendet werden:

Am 13. Januar 2021 fand eine öffentliche Anhörung im Ausschuss für Umwelt, Natur und nukleare Sicherheit des Deutschen Bundestages zu Kraftwerksemissionen statt. Die Neufassung der Verordnung über Großfeuerungs-, Gasturbinen- und Verbrennungsmotoranlagen betrifft etwa 580 Kraftwerke und ähnliche Anlagen in Deutschland. Prof. Hartmut

Transfer in science and society – overview / Transfer in Wissenschaft und Gesellschaft – Überblick

Fig. / Abb. 5: A small backpack enabled citizens at Luft-Leipzig to measure particulate matter and soot in their city themselves. / Ein kleiner Rucksack ermöglichte Bürger:innen bei Luft-Leipzig, Feinstaub und Ruß in ihrer Stadt selber zu messen. (Photo: Liina Tõnisson / TROPOS)

Robert Koch Institute. TROPOS aerosol expert Dr. Birgit Wehner was intensively involved as Secretary General of the GAeF and moderated the session "Infection Pathway Aerosol".

On 11 April 2021, aerosol researchers addressed an open letter to politicians: The researchers emphasized that Corona infections predominantly take place indoors and that the measures to mitigate the pandemic should primarily start there. To prevent infection, they recommend items such as ventilation, masks and air filters. Among the signatories is Dr. Birgit Wehner, Secretary General of the Society for Aerosol Research (GAeF) and aerosol researcher at TROPOS.

In the field of air pollution control, TROPOS also contributes to policy advice through its own research results, which are used, for example, in the discussion of guidelines or in the preparation of air pollution management plans:

On 13 January 2021, a public hearing on power plant emissions was held in the Committee for Environment, Nature and Nuclear Safety of the German Bundestag. The new version of the Ordinance on Large Combustion Plants, Gas Turbine Plants and Herrmann vom TROPOS nahm an der Anhörung als Sachverständiger teil und brachte so seine Expertise in Sachen Atmosphärenchemie und Luftqualität ein.

2020 nahmen 89 Mitgliederinnen und Mitglieder des Bundestags an „Leibniz im Bundestag" teil, um sich mit Fachleuten auszutauschen. Am 25. Mai sprachen dabei Ulli Nissen (SPD) mit Prof. Hartmut Herrmann und Ralph Lenkert (Die Linke) mit Dr. Dominik van Pinxteren über Fragen der Luftqualität. Beide MdBs sind im Umweltausschuss des Bundestags aktiv.

Das 6. LfULG-Statuskolloquium „Luftqualität in Sachsen" fand am 30.09.21 online statt: Dieses Jahr u.a. mit Vorträgen von Dr. Jens Voigtländer zu mobilen Messungen in Leipzig und Dresden sowie Dr. Dominik van Pinxteren zu Luftschadstoff bodennahes Ozon.

Die Weltgesundheitsorganisation WHO hat am 22.09.21 ihre neuen Leitlinien zur Luftqualität veröffentlicht und senkt darin ihre Empfehlungen für die Belastungen mit Feinstaub und Stickstoffdioxid zum Teil massiv ab. Das Science Media Center (SMC) hat dazu ein umfangreiches Dossier für die Medien erstellt und 14 internationale Expertinnen und Experten um Stellungnahme gebeten – darunter auch Prof. Hartmut Herrmann und Prof. Alfred Wiedensohler vom TROPOS. Beide kommentieren die neuen WHO-Leitlinien als lange erwarteten und wichtigen Schritt, verweisen aber auch darauf, dass ein Richtwert für Benzo(a)pyren (Indikator für Holz-Verbrennung) und Grenzwerte für schwarzen beziehungsweise elementaren Kohlenstoff (BC/EC) als gesundheitsrelevanten Teil von Feinstaub $PM_{2.5}$ fehlen.

TROPOS-Forschung für die breite Öffentlichkeit. TROPOS steht im Dialog mit der Öffentlichkeit – u.a. auch über Printmedien sowie Hör- und Fernsehfunk. 2020/21 wurden 24 Pressemitteilungen herausgegeben. Dazu kamen online veröffentlichte Kurzmitteilungen und Pressemitteilungen von Partnerinstitutionen mit TROPOS-Erwähnung (11) sowie Statements (6). Daraus resultierten im Jahr 2020 über 255 Medienveröffentlichungen (soweit bekannt). Im Jahr 2021 waren es 145 Veröffentlichungen (soweit bekannt).

Besonders hervorzuheben sind zahlreiche Zeitungs-, Radio- und Fernsehbeiträge zur Erwärmung der Arktis: Die Teilnahme an der einjährigen MOSAiC-Expedition mit TROPOS-Beteiligung fand ein vielfältiges Echo von der Lokalausgabe der BILD-Zeitung über Podcasts bis hin zu einer 90minütigen Fernsehdokumentation zur Primetime der ARD. Mehrere Zeitungen widmeten zudem ganze Seiten einzelnen Expeditionsteilnehmern des TROPOS, um über diese ausgewöhnliche Fahrt in der zentralen Arktis zu berichten. Die zunehmende

Combustion Engine Plants affects about 580 power plants and similar facilities in Germany. Prof. Hartmut Herrmann from TROPOS participated in the hearing as an expert and thus contributed his expertise in atmospheric chemistry and air quality.
In 2020, 89 members of the Bundestag took part in the exchange forum "Leibniz in the Bundestag" to exchange views with experts. On 25 May, Ulli Nissen (SPD) spoke with Prof. Hartmut Herrmann and Ralph Lenkert (Die Linke) with Dr. Dominik van Pinxteren about air quality issues. Both minister presidents are working in the Environment Committee of the Bundestag.

The 6th LfULG status colloquium "Air Quality in Saxony" was an online event on 30 September 2021 with the following TROPOS contributions: Dr. Jens Voigtländer presented results of mobile measurements in Leipzig and Dresden and Dr. Dominik van Pinxteren spoke about ground-level ozone as an air pollutant.
On 22 September 2021, the World Health Organisation (WHO) published its new guidelines on air quality, in some cases massively lowering its recommendations on limit values for the exposure of particulate matter and nitrogen dioxide. The Science Media Center (SMC) has prepared a comprehensive media dossier, where 14 international experts had been asked to comment - among them Prof. Hartmut Herrmann and Prof. Alfred Wiedensohler from TROPOS. Both expressed, that the new WHO guidelines are a long-awaited and important step, but also point out that a benchmark for benzo(a)pyrene (indicator for wood combustion) and limit values for black or elemental carbon (BC/EC) as a health-relevant part of $PM_{2.5}$ are missing.

TROPOS research results for the public at large. TROPOS seeks dialogue with the public using print media, radio and TV. In 2020 and 2021, 24 press releases were published. In addition, there were short news releases online and press releases from partner institutions (11) as well as TROPOS statements (6). This resulted in over 255 media publications in 2020 (as far as known). In 2021, there were 145 publications (as far as known).

Particularly noteworthy are numerous newspaper, radio and television reports on the warming of the Arctic: the participation in the one-year MOSAiC expedition with TROPOS participation found a diverse echo from the local edition of the BILD newspaper to podcasts and a 90-minute prime-time television documentary on the German TV channel ARD. Several newspapers also dedicated entire pages to individual TROPOS expedition participants to report on this extraordinary journey in the central Arctic.

Klimaerwärmung mit starken Waldbränden führte zu neuen Beobachtungen wie Rauch aus Kalifornien über Leipzig oder Rauch aus Australien über Südamerika und diversen Medienberichten über die TROPOS-Lidar-Gruppe. Über deren These, Waldbrände könnten der Ozonschicht schaden, berichtete im November 2021 das SCIENCE-Magazin. Aerosol-Forschende von TROPOS waren gefragte Interviewpartner zu Fragen rund um die luftgetragene Ausbreitung des Corona-Erregers in Innenräumen und den Schutz davor mit FFP2-Masken oder Raumluftfiltern. Weltweite Beachtung in den Medien fand eine Forschungsarbeit von Dr. Ajit Ahlewat und Prof. Alfred Wiedensohler, die den Zusammenhang zwischen der relativen Luftfeuchte in Innenräumen und dem Infektionsrisiko durch den Corona-Virus SARS-CoV-2 untersucht hatte. Bundesweit berichtet wurde auch über eine Jahrhundertdürre im Mittelalter sowie zu Feinstaub und Saharastaub.

Das Internetangebot tropos.de richtet sich neben Forschenden zugleich an die breite Öffentlichkeit. Die Rubrik „Entdecken" hat daher zum Ziel, die Forschung leicht verständlich zu erläutern. So informiert z.B. die Webseite „Der Klimawandel geht weiter - Was wir heute übers Klima wissen" über den Klimawandel. Zum ersten internationalen „Tag der sauberen Luft für einen blauen Himmel" am 07.09.20 entstand eine Webseite, die die TROPOS-Forschung zur Luftqualität zusammenfasst. 2021 stand der Welttag der Meteorologie unter das Motto „Der Ozean, unser Klima und Wetter". Dazu entstand ein Überblick wie Leipziger Forschende zum Verstehen des Klimas auf den Ozeanen beitragen.

Bedingt durch die Pandemie mussten viele Messkampagnen ausfallen und damit auch die Berichte im Kampagnen-Blog.

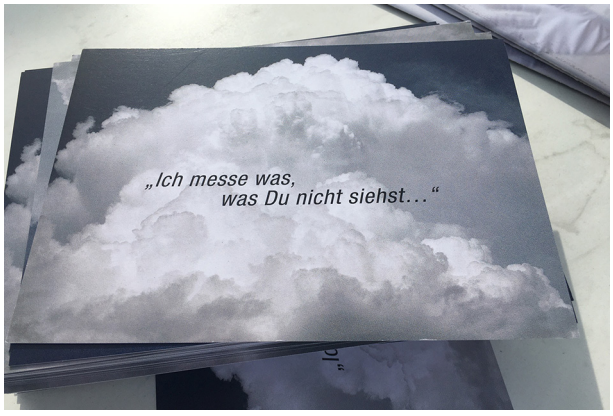

Fig. / Abb. 6: Postcards from "Luft Leipzig" (Air Leipzig), with which Leipzig residents could measure the air quality in their city themselves as part of the WTimpact knowledge transfer project. / Postkarten von "Luft Leipzig", mit dem Leipziger:innen im Rahmen des Wissenstransferprojekts WTimpact die Luftqualität in ihrer Stadt selber messen konnten. (Photo: Liina Tõnisson / TROPOS)

Transfer in science and society – overview / Transfer in Wissenschaft und Gesellschaft – Überblick

The increasing climate warming with strong forest fires led to new observations such as smoke from California over Leipzig or smoke from Australia over South America and various media reports about the TROPOS lidar group. Their thesis that forest fires could damage the ozone layer was reported in the SCIENCE magazine in November 2021. Aerosol researchers from TROPOS were sought-after interview partners on questions about the airborne spread of the Corona virus indoors and protection against it with FFP2 masks or indoor air filters. A research paper by Dr. Ajit Ahlewat and Prof. Alfred Wiedensohler, which investigated the connection between the relative humidity in indoor rooms and the risk of infection by the corona virus SARS-CoV-2, received worldwide media attention. Nationwide reports were also given on a drought of the century in the Middle Ages and on fine dust and Saharan dust.

The tropos.de website addresses not only researchers, but also the general public. The "Discover" section therefore aims to explain research in an easily understandable way. For example, the website "Climate change continues - What we know about the climate today" provides information about climate change. For the first international "Clean Air Day for Blue Skies" on 7 September 2020, a website was created that summarizes TROPOS research on air quality. In 2021, the theme of the World Meteorology Day was "The ocean, our climate and weather". For this purpose, an overview was created of how Leipzig researchers contribute to the understanding of the oceans' climate.

Due to the pandemic, many measurement campaigns had to be cancelled and with them the reports in the campaign blog.

Fig. / Abb. 7: „Polarzeit": Ronny Engelmann reported on the MOSAiC expedition in the Arctic at the Leipzig Museum of Natural History on 20 April 2020. / Polarzeit: Ronny Engelmann berichtete am 20.02.20 im Naturkundemuseum Leipzig über die MOSAiC-Expedition in der Arktis. (Photo: Tilo Arnhold / TROPOS)

Mit den Twitter-Kanälen „@TROPOS_de" & „@TROPOS_eu" ist das Institut auch in den sozialen Medien auf deutsch bzw. englisch aktiv. Der deutschsprachige Kanal richtet sich primär an die breite Öffentlichkeit in Deutschland; der englischsprachige dient auch der Vernetzung innerhalb der wissenschaftlichen Community. Ca. 970 bzw. 810 Personen und Institutionen haben den Kanal abonniert („Follower"). Damit konnte die Anzahl im Vergleich zum vorigen Zeitraum etwa verdoppelt werden.

Veranstaltungen. Die gesellschaftliche Diskussion um die Folgen des Klimawandels und das gestiegene Interesse an Informationen aus erster Hand führte zu deutlich mehr Anfragen nach Expertinnen und Experten für Veranstaltungen zum Thema Klima:

Die zweite Klimakonferenz Sächsischer Schüler*innen fand am 29.02.20 in Dresden statt. Rund 600 Schüler:innen haben dabei gemeinsam mit Ministerpräsident Kretschmer und mehreren Vertretenden der Staatsministerien über die Klimapolitik in Sachsen diskutiert. Dr. Heike Wex vom TROPOS war bei der Veranstaltung dabei. Außerdem informierte ein Poster über den sächsischen Beitrag zur Arktis-Expedition MOSAiC.

In der Veranstaltungsreihe „Book a Scientist" der Leibniz-Gemeinschaft beantworten Leibniz-Forschende in 25-minütigen Einzelgesprächen Fragen zu Themen, die das alltägliche Leben berühren. Vom TROPOS berichteten Christian Pilz am 10.11.20 über „Welche Rolle spielt Feinstaub bei der Erwärmung der Arktis?" und Sebastian Zeppenfeld am 18.03.21 über „Alles andere als salzig: Wie aus Zucker Wolken über den Ozeanen werden".

Den Klimawandel in der Arktis erklärten den Jüngsten auch Robert Wagner, Hannes Griesche und Markus Hartmann am 21.10.20 im Rahmen der Kinder-Uni der Universität Leipzig. Die Veranstaltung „Ich glaub mein Eis schmilzt! Chaos in der arktischen Klimaküche" fand wie viele andere online statt. Ebenfalls online erschienen ist die YouTube-Serie des DKK zu „Klima und Corona". Am 29.10.20 erschien dort ein Statement von Prof. Hartmut Herrmann über „Gute Luft und Klimaschutz / 2 Seiten, 1 Medaille". In einer Hybridveranstaltung der Seniorenakademie der Universität Leipzig berichtete Dr. Denise Assmann über „Mobile Rucksackmessungen – ein Projekt in Leipzig mit Bürgerbeteiligung" zum Thema Luftqualität.

Die Corona-Pandemie spiegelte sich auch in den Veranstaltungsthemen wider: Großen Zuspruch fand das Webinar „Dicke Luft im Klassenzimmer - Luftqualität & Infektionsschutz in der Schule". Am 14.4.21 und am 1.7.21 informierten Forschende,

With the twitter channels "@TROPOS_de" & "@TROPOS_eu", the Institute is also active in the social media in German and English. The German-language channel is primarily aimed at the general public in Germany; the English-language channel is also used for networking within the scientific community. Approximately 970 and 810 people and institutions respectively have subscribed to the channel ("followers"). This means that the number has roughly doubled compared to the previous period.

Events. The societal discussion about the consequences of climate change and the increased interest in first-hand information led to significantly more requests for experts in events on the climate topics:

The second Climate Conference of Saxon Pupils took place on 29 February 2020 in Dresden. Around 600 students discussed climate policy in Saxony with minister president Kretschmer and several representatives of the state ministries. Dr. Heike Wex from TROPOS was present at the event. In addition, a poster provided information about Saxony's contribution to the Arctic expedition MOSAiC.

In the Leibniz Association's event series "Book a Scientist", Leibniz researchers answer questions in 25-minute one-on-one talks on topics that are relevant to everyday life. From TROPOS, Christian Pilz reported on "What role does fine dust play in the warming of the Arctic?" on 10 November 2020 and Sebastian Zeppenfeld on "Anything but salty: How sugar becomes clouds over the oceans" on 18 March 2021.

As part of the Children's University at the University of Leipzig, Robert Wagner, Hannes Griesche and Markus Hartmann explained climate change in the Arctic to the youngest students on 21 October 2020. The event "I think my ice is melting! Chaos in the Arctic Climate Kitchen" took place online, like also the DKK YouTube series on "Climate and Corona". On 29 October 2020, a statement by Prof. Hartmut Herrmann on "Clean air and climate protection" appeared there. In a hybrid event of the Seniors Academy of the University of Leipzig, Dr. Denise Assmann reported on the air quality topic "Mobile backpack measurements - a project in Leipzig with citizen participation".

The Corona pandemic was also reflected in the topics of public events: The webinar "Thick Air in the Classroom - Air Quality & Infection Protection in Schools" was very well-attended. On 14 April 2021 and 1 July 2021, researchers provided information on how pupils and teachers could be better protected during the Corona pandemic through the consistent implementation of ventilation concepts. In addition to

Fig. / Abb. 8: MesSBAR project meeting at TROPOS on 30 January 2020. Since September 2019, a flexible drone-based measurement system has been developed, tested and applied in the „MesSBAR" project. / MesSBAR-Projekttreffen am TROPOS am 30.01.20. Seit September 2019 wird im Projekt „MesSBAR" ein flexibel einsetzbares drohnengestütztes Messsystem entwickelt, erprobt und angewendet. (Photo: Tilo Arnhold / TROPOS)

wie Schüler:innen und Lehrende durch die konsequente Umsetzung wissenschaftlich fundierter Lüftungskonzepte besser in der Corona-Pandemie geschützt werden könnten. An den Online-Veranstaltungen war neben Vertretende von S4F Leipzig, der HTWK Leipzig und der ITG Dresden auch Prof. Hartmut Herrmann vom TROPOS aktiv beteiligt. Praktische Tipps gegen Corona-Infektionen über Aerosole war auch das Anliegen einer Gesprächsrunde am 06.07.21 der Reihe „achatec am Dienstag" der Deutschen Akademie der Technikwissenschaften: Zum Thema „Aerosole erforschen und Luftqualität verbessern" sprach unter anderem Dr. Birgit Wehner vom TROPOS.

„Leipzig liest extra", die Sonderausgabe der Leipziger Buchmesse 2021, fand pandemiebedingt überwiegend digital statt. Der renommierte Klimaforscher Michael E. Mann las dabei aus seinem neuen Buch „The new climate war" (dt. Titel „Propagandaschlacht ums Klima"). Ergänzt wurde die Lesung durch eine Gesprächsrunde & Diskussion zum Buch. Diese Veranstaltung fand an zwei Abenden am 27. und 28. Mai auf Englisch bzw. Deutsch statt. Klima war auch ein Thema der Langen Nacht der Wissenschaften Leipzig, die am 16.07.21 nur online stattfinden konnte. TROPOS beteiligte sich daran mit Präsentationen über die arktische Klima-Verstärkung und Luftqualität sowie Experimenten für Kinder. Auf der 1. Tauchaer Klimakonferenz (24.-25.9.21) gab Heike Wex vom TROPOS einen Impulsvortrag zum Klimawandel.

Außerdem ist TROPOS an den Öffentlichkeitsaktionen des Deutschen Klimakonsortiums (DKK), des Klimanavigators und der Leibniz-Gemeinschaft aktiv beteiligt.

Fig. / Abb. 9: TROPOS has been honoured for the fourth time with the "berufundfamilie" certificate for its family-friendly working and study conditions. / TROPOS ist zum vierten Mal mit dem Zertifikat „berufundfamilie" für seine familiengerechte Arbeits- und Studienbedingungen geehrt worden. (Photo: Tilo Arnhold / TROPOS)

representatives from S4F Leipzig, HTWK Leipzig and ITG Dresden, Prof. Hartmut Herrmann from TROPOS was also actively involved in the online events. Practical advice against Corona infections via aerosols was also the concern of a discussion panel on 6 July 2021 in the series "achatec on Tuesday" of the German Academy of Science and Engineering: Dr. Birgit Wehner from TROPOS, among others, spoke on the topic of "Researching aerosols and improving air quality".

"Leipzig liest extra" (Leipzig reads), the special edition of the Leipzig Book Fair 2021, took place mainly digitally due to the pandemic. The renowned climate researcher Michael E. Mann read from his new book "The new climate war". The reading was complemented by a roundtable discussion. This event took place on two evenings on 27 and 28 May in English and German respectively. Climate was also a topic of the "Long Night of Sciences Leipzig", which could only take place online on 16 July 2021. TROPOS participated with presentations on Arctic climate amplification and air quality as well as experiments for children. At the 1st Taucha Climate Conference (24 to 25 September 2021), Heike Wex from TROPOS gave an impulse lecture on climate change.

In addition, TROPOS is actively involved in the publicity campaigns of the German Climate Consortium (DKK), the Climate Navigator and the Leibniz Association.

Equal opportunities and promotion of young researchers

Gender equality is implemented as a guiding principle at TROPOS. The Institute thus fulfils the equality standards of the Leibniz Association. A key instrument in this is the Equality Opportunity Plan; its

Chancengleichheit und Nachwuchsförderung

Gleichstellung ist am TROPOS als Leitprinzip implementiert. Das Institut erfüllt damit die Gleichstellungsstandards der Leibniz-Gemeinschaft. Ein wesentliches Instrument dabei ist der Gleichstellungsplan, dessen Umsetzung die Chancengleichheit für Menschen aller Geschlechter am TROPOS fördern und nachhaltig sichern soll. Im August 2022 wurde ein für die nächsten vier Jahre geltender Gleichstellungsplan aufgestellt. Er enthält schwerpunktmäßig Maßnahmen zur absolut diskriminierungsfreien Zusammenarbeit am Institut vom Einstellungsverfahren bis zur weiteren Erhöhung des Anteils von Frauen im Post-Doc-Bereich, in Festanstellungen, wissenschaftlichen Führungspositionen und Gremien. TROPOS orientiert sich in den Zielvorgaben für die Erhöhung des Frauenanteils am Kaskadenmodell der Leibniz-Gemeinschaft, wobei ein an die momentane institutsspezifische Stellensituation angepasstes Stufenmodell definiert wurde.

Zum 10.12.20 wurde das Zertifikat zum Audit berufundfamilie nach erfolgreich durchlaufenem Dialogverfahren bestätigt. Damit erhält das Zertifikat, das als Qualitätssiegel für eine strategisch angelegte familien- und lebensphasenbewusste Personalpolitik gilt, seinen dauerhaften Charakter.

Nachwuchsförderung. TROPOS fördert aktiv den wissenschaftlichen Nachwuchs in der Bachelor- und Masterausbildung, während der Promotionsvorhaben und darüber hinaus. Das Institut ist eng in die Entwicklung und in die Durchführung der neuen Bachelor- und Masterstudiengänge an der Universität Leipzig eingebunden und ist für 12 Module verantwortlich.

Hochqualifizierte Mitarbeiterinnen und Mitarbeiter beteiligen sich als gemeinsame Berufungen an der Lehre der Universität Leipzig. Neben Studierenden der Meteorologie werden am TROPOS auch Chemie- und Physikstudierende ausgebildet (siehe Liste, S. 168).

Das Institut bietet jungen Wissenschaftlerinnen und Wissenschaftlern individuell abgestimmte und von einem Betreuungsteam begleitete Realisierung ihrer Promotionen im Rahmen der strukturierten Promovendenausbildung. Mitarbeitende des TROPOS halten Kurse an den Universitäten von Jena, Peking, Jinan und Shanghai, Helsinki und Stockholm und bei internationalen Sommerschulen, Ausbildungskursen und -netzwerken (siehe Liste, S. 166).

Die im Juli 2012 gegründete Leibniz-Graduiertenschule zu „Wolken, Aerosolen und Strahlung" hat die Promovendenausbildung am TROPOS gemeinsam mit der Universität Leipzig auf eine solide Grundlage

intention is to promote and sustainably secure equal opportunities for people of all genders at TROPOS. In August 2022, the current Gender Equality Plan was drawn up for the next four years. It focuses on measures for absolutely non-discriminatory collaboration at the Institute, from the recruitment process to further increasing the proportion of women in post-doc positions, permanent positions, scientific leadership positions and committees. TROPOS follows the cascade model of the Leibniz Association in the targets for increasing the proportion of women, whereby a level model was defined that is adapted to the current situation of positions at the Institute. The work and family audit (berufundfamilie) certificate was confirmed on 10 December 2020 after a successful dialogue procedure. This gives a permanent character to this certifi- cate, which is regarded as a quality label for a strategically designed family- and life-phase-conscious human resources policy.

Promotion of young researchers. TROPOS actively promotes young researchers in the bachelor and master education at the Leipzig University as well as during and after doctoral research projects. The institute is involved in the development and implementation of the new bachelor and master programmes and is exclusively responsible for 12 modules.

Highly qualified scientists of the Institute contribute to teaching activities in cooperation with the Leipzig University as joint appointments. In addition to meteorology students also chemistry and physics students are trained at TROPOS (see list, p. 168).

The institute offers young researchers an individualized realization of their dissertation projects supported by the supervision committee in the framework of a structured doctoral training programme. TROPOS scientists give lectures at the universities of Jena, Beijing, Jinan, and Shanghai, Helsinki and Stockholm, in international summer and winter schools, training courses and networks (see list, p. 166).

The 2012 founded Leipzig Graduate School on "Aerosols, Clouds and Radiation" provided together with the University Leipzig a solid basis for the doctoral training at TROPOS and combines the expertise of both partners within the coupled research fields "aerosols, clouds, and radiation". By now the Graduate School has 50 members and is located in the Research Academy Leipzig (RAL).

Create future. TROPOS supports the path to natural science studies by showing career perspectives in the field of atmospheric research. Pupils learn about research work in a playful way and get to talk to researchers from the MINT field. As part of the

gestellt und bündelt die gemeinsame Expertise in den gekoppelten Bereichen „Aerosole-Wolken-Strahlung". Sie ist mit aktuell 50 Mitgliedern in der „Research Academy Leipzig" (RAL) verortet.

Zukunft schaffen. TROPOS unterstützt den Weg zum naturwissenschaftlichen Studium, indem berufliche Perspektiven im Bereich der Atmosphärenforschung aufgezeigt werden. Schülerinnen und Schüler lernen die Forschungsarbeit auf spielerische Art kennen und kommen mit Forschenden aus dem MINT-Bereich ins Gespräch. Im Rahmen der MINT-Initiative, die zum Ziel hat, Jugendliche für einen Beruf in den Fächern Mathematik, Informatik, Naturwissenschaften und Technik zu begeistern, beteiligt sich TROPOS auch am Girls' Day, dem Zukunftstag. 2021 konnten sich an diesem Tag interessierte Schülerinnen bei einem Online-Programm interaktiv über die Forschungsarbeit und Ausbildungsmöglichkeiten informieren. Mit weiteren Online-Angeboten für die „Kinderuni" Leipzig, „Jugend forscht" wurde versucht, fehlende Präsenzangebote während der Pandemie zu kompensieren.

Im Februar 2020 war es noch möglich, an der Schülerklimakonferenz Sachsens mitzuwirken; die diesjährige Teilnahme ist geplant.

TROPOS wird auch in den nächsten Jahren mindestens einen Lehrlingsausbildungsplatz aus Haushaltsmitteln finanzieren.

Bedeutende Kooperationen und Vernetzung in der Forschung

Zahlreiche bisher gewachsene Vernetzungen innerhalb der Leibniz-Gemeinschaft, mit Universitäten, mit Max-Planck-Instituten, mit Instituten der Helmholtz-Gemeinschaft sowie auf internationaler

Fig. / Abb. 10: Conversion of the Lufthansa Airbus A350-900 for IAGOS-CARIBIC. / Umbau des Lufthansa-Airbus A350-900 für IAGOS-CARIBIC. (Photos: Torsten Gehrlein, KIT; Montage: Peter Braesicke, KIT; https://www.kit.edu/kit/28770.php)

MINT initiative, which aims to inspire young people to pursue a career in the subjects of mathematics, computer science, natural sciences and technology, TROPOS also participates in Girls' Day, a future day for female students.

In 2021, interested pupils were able to inform themselves interactively about the research work and training opportunities during an online programme on this day. With further online events for the "Kinderuni" (university for children) Leipzig and "Jugend forscht" (youth science competition), an attempt was made to compensate for the lack of face-to-face events during the pandemic.

In February 2020, it was still possible to participate in Saxony's student climate conference; this year's participation is planned.

TROPOS will continue to finance at least one apprenticeship training place from budget funds in the coming years.

Cooperation and networking

Numerous grown networks within the Leibniz Association, with universities, with Max Planck Institutes, with institutes of the Helmholtz Society, and collaborations at the international level demonstrate the actual level of TROPOS networking in the field of interdisciplinary aerosol and cloud research. Similar alike TROPOS is networked on the European and global level and actively develops research programmes (see list, p. 181). Technological developments at TROPOS lead to international standards in the experimental direct and indirect acquisition of aerosols and hydrometeors from ground up to the high atmosphere as well as in model-based descriptions of the complex multiphase system.

In the framework of the Leibniz competition funds cooperation is extended among the Leibniz Association and with university institutes. The Institute is associated with numerous international institutions through cooperation agreements (see list, p. 181).

TROPOS plays a leading role in the European research infrastructure network ACTRIS (Aerosols, Clouds, and Trace gases Research InfraStructure Network).

In August 2021, the Federal Ministry of Education and Research (BMBF) announced the funding of the German contribution develpment with a total of 86 million euros over the next eight years. The German part is coordinated by TROPOS. At the European level, more than 120 institutions in over 20 countries are already involved.

In 2019, the ERATOSTHENES Centre of Excellence (ECoE) was founded to become a leading digital innovation centre (DIH) for Earth observation

Ebene zeigen den derzeitigen Stand der Vernetzung des TROPOS in der interdisziplinären Aerosol- und Wolkenforschung. Ähnlich ist TROPOS auf der europäischen und weltweiten Ebene vernetzt und entwickelt hier aktiv Forschungsprogramme (siehe Liste, S. 181).

Technologische Entwicklungen am TROPOS führen zu internationalen Standards in der experimentellen direkten und indirekten Erfassung von Aerosolen und Hydrometeoren vom Boden bis zur hohen Atmosphäre sowie in der Modellierung des komplexen Multiphasensystems.

Im Rahmen des Wettbewerbsfonds der Leibniz-Gemeinschaft werden die Kooperationsmöglichkeiten innerhalb der Leibniz-Gemeinschaft und mit Universitätsinstituten ausgebaut. Durch Kooperationsvereinbarungen ist das Institut mit zahlreichen internationalen Einrichtungen verbunden (siehe Liste, S. 181).

TROPOS spielt eine führende Rolle im Netzwerk der europäischen Forschungsinfrastruktur ACTRIS (Aerosols, Clouds, and Trace gases Research InfraStructure Network). Im August 2021 gab das Bundesministerium für Bildung und Forschung (BMBF) bekannt, dass es den Aufbau des deutschen Beitrags in den kommenden acht Jahren mit insgesamt 86 Millionen Euro fördert. Koordiniert wird der deutsche Teil durch das Leibniz-Institut für Troposphärenforschung (TROPOS) in Leipzig. Auf europäischer Ebene sind bereits mehr als 120 Institutionen in über 20 Ländern beteiligt.

2019 wurde das Fernerkundungszentrum ERATOSTHENES Centre of Excellence (ECoE) gegründet, dass in den nächsten sieben Jahren zu einem führenden digitalen Innovationszentrum (DIH) für Erdbeobachtung und Geodaten werden soll, um den globalen Wandel in Klima, Bodennutzung und den damit verbundenen gesellschaftlichen Herausforderungen im östlichen Mittelmeer aus dem All und vom Boden aus besser untersuchen zu können. Im September 2020 wurde ein am TROPOS aufgebautes Polly-XT-Lidargerät in Limassol aufgestellt, welches das ECoE mit ACTRIS und Pollynet verbindet.

Ausgebaut werden soll die Zusammenarbeit mit dem Deutschen Wetterdienst (DWD), um Meteorologie und Klimaforschung in Deutschland zu stärken. Ein entsprechender Kooperationsvertrag wurde am 22.01.21 per Videokonferenz unterzeichnet.

Der Lufthansa-Airbus „Erfurt" wird künftig ein 1,6 Tonnen schweres Forschungslabor, den sogenannten CARIBIC-Messcontainer, im Gepäckraum transportieren und wichtige Klimadaten liefern. Dazu wurde die Linienmaschine in Malta umgebaut. Die Abkürzung CARIBIC steht für „Civil Aircraft for the Regular Investigation of the atmosphere Based on an Instrument Container". Das Labor ist vergleichbar mit einem

and geodata over the next seven years The goal is to better study global change in climate, land use and the associated societal challenges in the eastern Mediterranean from space and from the ground. In September 2020, a Polly-XT lidar set up at TROPOS was deployed in Limassol, linking ECoE to ACTRIS and Pollynet.

The cooperation with the German Weather Service (DWD) is to be expanded in order to strengthen meteorology and climate research in Germany. A cooperation agreement to this effect was signed via video conference on 22 January 2021.

In the coming years, the Lufthansa Airbus "Erfurt" will transport a 1.6-ton research laboratory, the so-called CARIBIC measuring container, in the cargo hold and provide important climate data. For this purpose, the airliner was converted in Malta. The abbreviation CARIBIC stands for "Civil Aircraft for the Regular Investigation of the atmosphere Based on an Instrument Container". The laboratory is comparable to a large research aircraft. TROPOS contributed to the design of a new inlet system.

In 2021 TROPOS was also involved in the CIrrus-HL mission with the HALO research aircraft of the German Aerospace Centre. The Hera4HALO filter collector developed at the institute was part of the extensive cloud measurement instrumentation on 25 measurement flights from Central Europe to the Arctic. The focus was on aviation, atmospheric research and climate-friendly flying.

TROPOS was part of the MOSAiC expedition for the first annual exploration of the Arctic from autumn 2019 to autumn 2020. Results from the three MOSAiC teams Atmosphere (ATMOS), Physical Oceanography (OCEAN) and Snow and Sea Ice (ICE) were presented in three review articles in February 2022.

TROPOS participates in the new Leibniz research network Integrated Earth System Research (iESF) via a cooperation agreement, which aims to gain action-relevant knowledge for society about people in the Earth system. Above all, the ecological capacities of the Earth system are to be determined and sustainable development paths derived from them.

TROPOS continues to be actively involved in the Leibniz research network "Infections'21" and in the research network "CrisEn" (Environmental Crisis - Crisis Environments), which emerged from the research network "Crises of a Globalized World".

großen Forschungsflugzeug. TROPOS hat am Design eines neuen Einlasssystems mitgearbeitet.

Auch an der Mission CIrrus-HL mit dem Forschungsflugzeug HALO des Deutschen Zentrums für Luft- und Raumfahrt war TROPOS 2021 beteiligt. Der am Institut entwickelte Filtersammler Hera4HALO war Teil der umfangreicher Wolkenmessinstrumentierung auf 25 Messflügen von Mitteleuropa bis in die Arktis. Schwerpunkte waren die Themen Luftfahrt, Atmosphärenforschung und klimafreundliches Fliegen.

TROPOS war Teil der MOSAiC-Expedition zur erstmaligen Erforschung der Arktis im Jahresverlauf von Herbst 2019 bis Herbst 2020. Ergebnisse der drei MOSAiC-Teams Atmosphäre (ATMOS), Physikalische Ozeanographie (OCEAN) sowie Schnee und Meereis (ICE) wurden in drei Übersichtsartikeln im Februar 2022 vorgestellt.

TROPOS beteiligt sich per Kooperationsvertrag an dem neuen Leibniz-Forschungsnetzwerk Integrierte Erdsystemforschung (iESF), das für die Gesellschaft handlungsrelevante Erkenntnisse über die Menschen im Erdsystem gewinnen will. Vor allem die ökologischen Tragfähigkeiten des Erdsystems sollen bestimmt und daraus nachhaltige Entwicklungspfade abgeleitet werden.

Am Leibniz-Forschungsverbund „Infections'21" ist TROPOS weiterhin aktiv beteiligt; ebenso am Forschungsnetzwerk „CrisEn" (Environmental Crisis - Crisis Environments), dass aus dem Forschungsverbund „Krisen einer globalisierten Welt" entstanden ist.

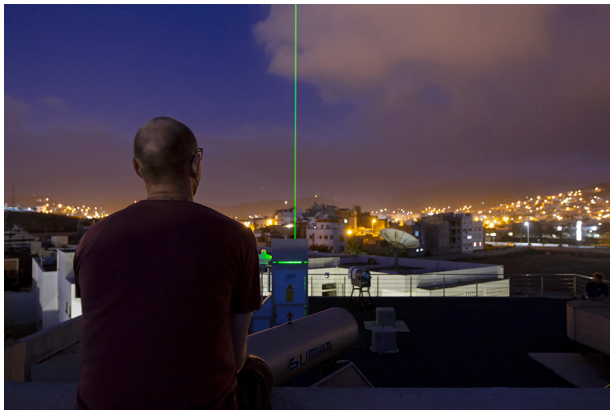

Fig. / Abb. 11: A TROPOS lidar analysed the dust over Mindelo on Cabo Verde in summer 2021, providing important data for the „Aeolus Tropical Atlantic Campaign" of ESA's Aeolus wind satellite. / Ein TROPOS-Lidar untersuchte im Sommer 2021 den Staub über Mindelo auf Cabo Verde und lieferte damit wichtige Daten für die „Aeolus Tropical Atlantic Campaign" des ESA-Windsatelliten Aeolus. (Photo: Edson Silva Delgado, Etfilmes / OSCM)

Facts and figures / Zahlen und Fakten

160 / 64 female

Employees

78 / 20 female

Scientists

39 / 19 female

Doctoral candidates

2020 / 2021

7 / 11

Doctoral theses

2 / 1

Master of Science

7 / 3

Bachelor of Sciences

21 Mio €

Budget in total

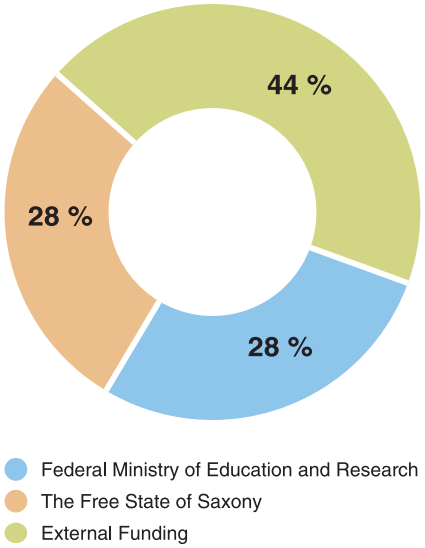

2020 / 2021

116 / 105

Publications (peer-reviewed)

261 / 197

Reviews

5 / 9

Scientific events

2020 / 2021

6 / 5

National campaigns

28 / 23

International campaigns

5 / 6

Long-term measurements

2020 / 2021

38 / 40

National cooperations

63 / 65

International cooperations

26 / 27

General cooperations

2020 / 2021

5 / 15

Public events

10 / 14

Press releases

255 / 144

Media publications

Articles

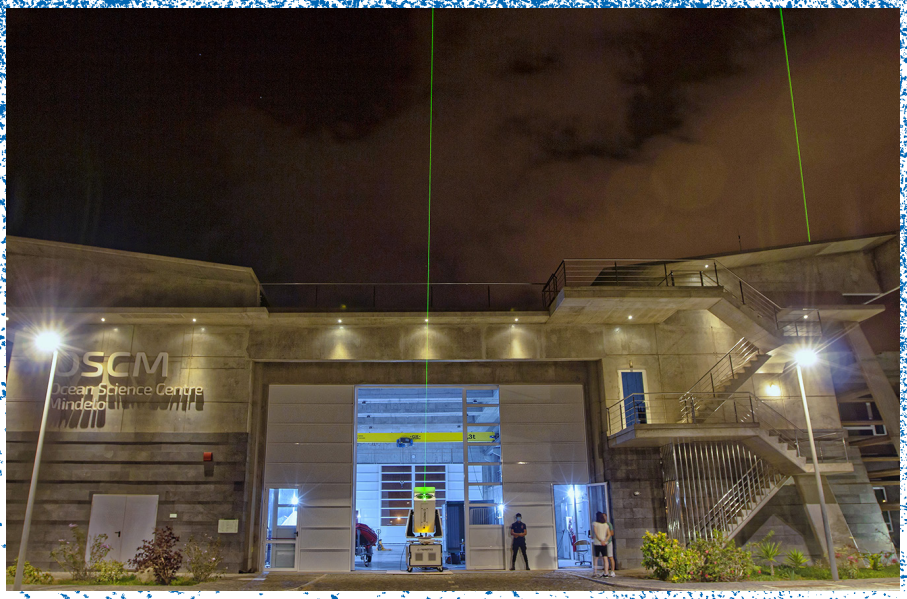

Urban Grime Photochemistry

Falk Mothes, Hartmut Herrmann

Die Verbesserung städtischer Luftqualität ist ein wichtiges Anliegen, das das Interesse am Verständnis der wichtigsten chemischen Prozesse und Wege von Luftschadstoffen wie zum Beispiel den Stickoxiden (NO_x), Ozon (O_3) und verschiedenen flüchtigen organischen Verbindungen (VOCs) verstärkt. Neben der Gasphasenchemie sind heterogene und mehrphasige Reaktionen bei der Wechselwirkung von Gasen mit städtischen Oberflächen (z. B. Fenster, Gebäudewände, Dächer, Bürgersteige, Straßen usw.) Prozesse, die das Verhalten von Luftschadstoffen beeinflussen könnten. Es ist bekannt, dass sich auf Oberflächen, wenn sie eine gewisse Zeit lang der Atmosphäre ausgesetzt sind, ein so genannter urbaner Schmutzfilm („urban grime“) aus anorganischen und organischen Bestandteilen bildet. Das Wissen über die Wechselwirkung dieses neuen Umweltkompartiments mit Luftschadstoffen unter Sonneneinstrahlung ist jedoch noch begrenzt. Daher kombiniert die vorliegende Studie intensive Laborexperimente zur Charakterisierung des photoreaktiven Verhaltens von im städtischen Raum gesammelten Realproben, mit dem Ziel der Bewertung, ob dieser Oberflächenfilm als Senke oder sogar als Quelle für Luftschadstoffe fungiert.

Introduction

Air pollution in Europe has been reduced in the past decades by a variety of legislative measures. However, at present still a significant negative impact on ecosystems and human health exists [*EEA*, 2021]. Hence, especially in cities, the improvement of air quality is still a major concern. Despite the successful reduction of direct emissions of air pollutants, traffic related air pollution becomes more and more important. Nitrogen oxides (NO_x=NO+NO_2) and volatile organic compounds (VOCs) play an important role, since they can contribute to the formation of the most problematic secondary pollutants ozone (O_3) and particulate matter (PM), with associated health and climate effects [*Finlayson-Pitts and Pitts*, 2000; *SOER*, 2015]. This still growing concern about air quality, especially in urban areas, strengthens the interest in understanding the most relevant chemical processes and pathways of these air pollutants [*von Schneidemesser et al.*, 2015].

Besides gas phase chemistry, also heterogeneous and multiphase processes, based on the interaction with, e.g., mineral dust (components) or urban surfaces are potentially affecting the fate of air pollutants [*George et al.*, 2015]. Especially in urban areas, there are many impervious surfaces, such as windows, rooftops, sidewalks, roads and other surfaces which can interact with ambient air, illustrated in Fig. 1.

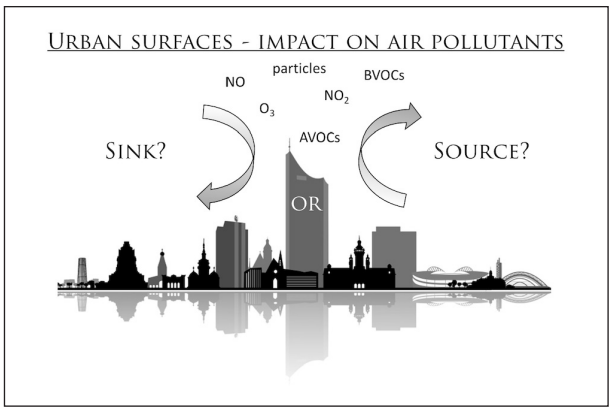

Fig.1: Scheme on the interaction of air pollutants with urban surfaces (BVOCs: biogenic volatile organic compounds; AVOCs: anthropogenic volatile organic compounds).

When such surfaces are exposed to the atmosphere for a certain time, a so called “urban grime” film develops. This was reported for the first time by *Law and Diamond* [1998]. The authors mentioned that the organic film develops via direct condensation of semi-volatile chemicals and/or via the deposition of secondary organic aerosol (SOA) and can potentially act as a separate environmental compartment.

Following research studies [*Lam et al.*, 2005; *Q-T Liu et al.*, 2003a; *Simpson et al.*, 2006] on the analysis of the urban grime chemical composition demonstrated a mixture of nitrate, sulfate, carbonate and ammonium, sodium, calcium as inorganic anions and cations, respectively, and of no more than 25% organics. However, studies have been dominated by the analysis of the organic fraction and proved the existence of fatty acids, long chain aliphatic compounds, polycyclic aromatic hydrocarbons (PAHs), polychlorinated biphenyls (PCBs), polybrominated biphenyls (PBBs) and polybrominated diphenyl ethers (PBDEs) at trace levels within the grime [*Butt et al.*, 2004; *Diamond et al.*, 2000; *Gingrich et al.*, 2001; *Lam et al.*, 2005; *Liu et al.*, 2003a; *Simpson et al.*, 2006; *Wu et al.*, 2008]. The presence of such "toxicologically active" compound classes like PAHs and PCBs emphasizes the importance of a complete understanding of the partitioning and reactive environment provided by the urban grime potentially impacting human health [*Cheruiyot et al.*, 2015; *Kameda*, 2011]. To name one example: It is discussed that these urban films enhance the particle capture efficiency of the surface and the sorption of gas phase chemicals to the surface and thereby serve as a reservoir for semi-volatile hydrophobic organic compounds [*Butt et al.*, 2004; *Liu et al.*, 2003b]. Multimedia models of chemical dynamics in an urban area, treating the grime with a surface area-to-volume ratio of 10^6-10^7, suggested that re-activation of organic compounds from surface films could occur by re-volatilization, wash-off, and photoinduced reactions [*Diamond et al.*, 2001; *Kwamena et al.*, 2007]. Therefore, the urban grime film can be expected to act as a new urban environmental compartment with a potential wide impact on its surrounding air and aquatic ecosystems. However, only a small number of laboratory studies exist to proof this hypothesis in detail. For example, studies exist on merely proxies for urban grime, like 1- octanol [*Handley et al.*, 2007], a 1:1 mixture of Apiezon N grease and glyceryl trioleate [*Baergen and Donaldson*, 2013], pyrene [*Ammar et al.*, 2010; *Brigante et al.*, 2008], fluoranthene [*Cazoir et al.*, 2014], humic acid [*Stemmler et al.*, 2006] and several partially oxidized aromatics [*George et al.*, 2005], trying to understand the photoactive nature of many of the organic compounds identified in the real samples. The main results of these studies were a photoenhanced uptake of air pollutants like NO_2 [*Ammar et al.*, 2010; *George et al.*, 2005] and HNO_3 [*Handley et al.*, 2007] on the organic surfaces and the demonstration of a photoinduced production of gas phase nitrous acid (HONO), depending on the chemical composition (nitrate content) of the organic film [*Baergen and Donaldson*, 2013; *George et al.*, 2005] that potentially explains observed daytime HONO results in different field studies [*Ma et al.*, 2013; *Michoud et al.*, 2014; *Spataro et al.*, 2013; *Wong et al.*, 2013; *Wong et al.*, 2012]. Additionally, such a heterogeneous photochemical source of HONO in the urban environment is of major research interest, because of the known toxicity of HONO and the formation of hydroxyl radicals due to daytime HONO photolysis [*Gligorovski*, 2016; *Wall and Harris*, 2017]. In summary, re-volatilization, wash off or photoinduced reaction products resulting from urban grime will impact the interaction/processes of NO_x with VOCs (and therefore also the secondary formation of O_3) and its corresponding environmental problems and health hazards [*Guerreiro et al.*, 2014; *Skalska et al.*, 2010; *von Schneidemesser et al.*, 2015].

Nevertheless, to date scientific knowledge regarding the chemistry, especially the photochemical processes occurring within real urban grime samples and its surface, respectively, is very limited. Only a few studies investigated the chemistry occurring on real urban grime film samples. The group of D. J. Donaldson demonstrated a photochemical renoxification of nitric acid due to nitrate photolysis at the surface of a proxy (1:1 mixture of Apiezon N grease and glyceryl trioleate) and real urban grime samples using an in situ technique [*Baergen and Donaldson*, 2013]. A follow up laboratory study on photochemical and oxidative processing of field collected urban grime samples showed that besides a deposition of air pollutants like NO_x as a net loss from the atmosphere, the illumination of the surface resulted likewise in the formation of gas phase NO_x depending on the relative humidity [*Baergen and Donaldson*, 2016]. These results have been confirmed by a recent study performed on real urban grime samples collected in Guangzhou, China [*J Liu et al.*, 2019]. Additionally, there exists field measurements reporting on the physical and chemical characterization [*Grant et al.*, 2019; *Kroptavich et al.*, 2020] as well as on the chemistry taking place associated with urban grime surfaces. The latter study, was already performed by TROPOS in Leipzig, 2014 and determined a relation between urban grime chemical composition (inorganic and organic) and particle composition indicating for example again a possible mechanism for the recycling of the nitrate anion to reactive nitrogen species [*Baergen et al.*, 2015; *Styler et al.*, 2018].

Therefore, based on these results the present study aims at a more detailed understanding of the photoreactivity of urban grime at impervious surfaces by small scale laboratory and aerosol chamber experiments to investigate if urban grime surface films could potentially act as a sink or even as a source of air pollutants (see Fig. 1).

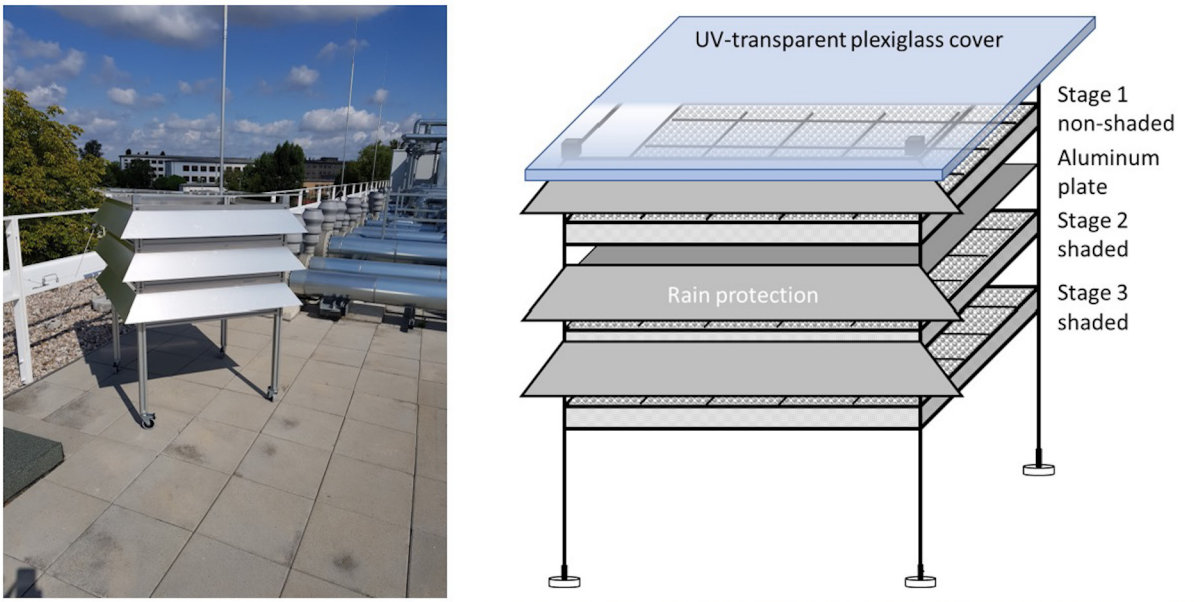

Fig. 2: Overview of the custom built 3-stage passive sampling device for real urban grime surface film sampling.

Sample collection and experimental setup

Sampling of the real urban grime surface films was performed on soda lime glass beads (3 mm in diameter) that were placed in a custom built 3-stage passive sampling device as shown in Fig. 2.

Each stage consists of 25 fields that are filled with approximately 85 g of glass beads (dimension chosen to be applicable for the small scale photoreactor experiments), resulting in one monolayer of glass beads laying on a wired mesh to let the air passively pass through the stage. The top of the sampling device was made out of a UV-transparent plexiglass plate protecting the upper stage from rain but not from the (UV-part of the) sunlight. Therefore, these samples are later on called “non-shaded” samples. In contrast to that, the two lower stages were blocked from the sunlight by an aluminium plate between the first and the second stage. These samples are called “shaded” glass beads. Additional aluminium plates at the sides of the sampler protect the samples from rain. All samples were collected on the roof of the TROPOS ACD laboratory building representing urban background conditions. A sampling period was always 12 weeks and provided in total 75 samples at 85 g of glass beads for further experiments in the laboratory.

Small scale photoreactor experiments have been performed by using a horizontal bed flow photoreactor. A schematic overview of the experimental setup is given in Fig. 3, a detailed description can be found in *Mothes et al.* [2018].

Briefly, the photoreactor itself is made out of Teflon and can be filled with approximately 85 g of glass beads, representing one monolayer inside the photoreactor. The reactor is airtight closed on top via a quartz glass plate and an additional

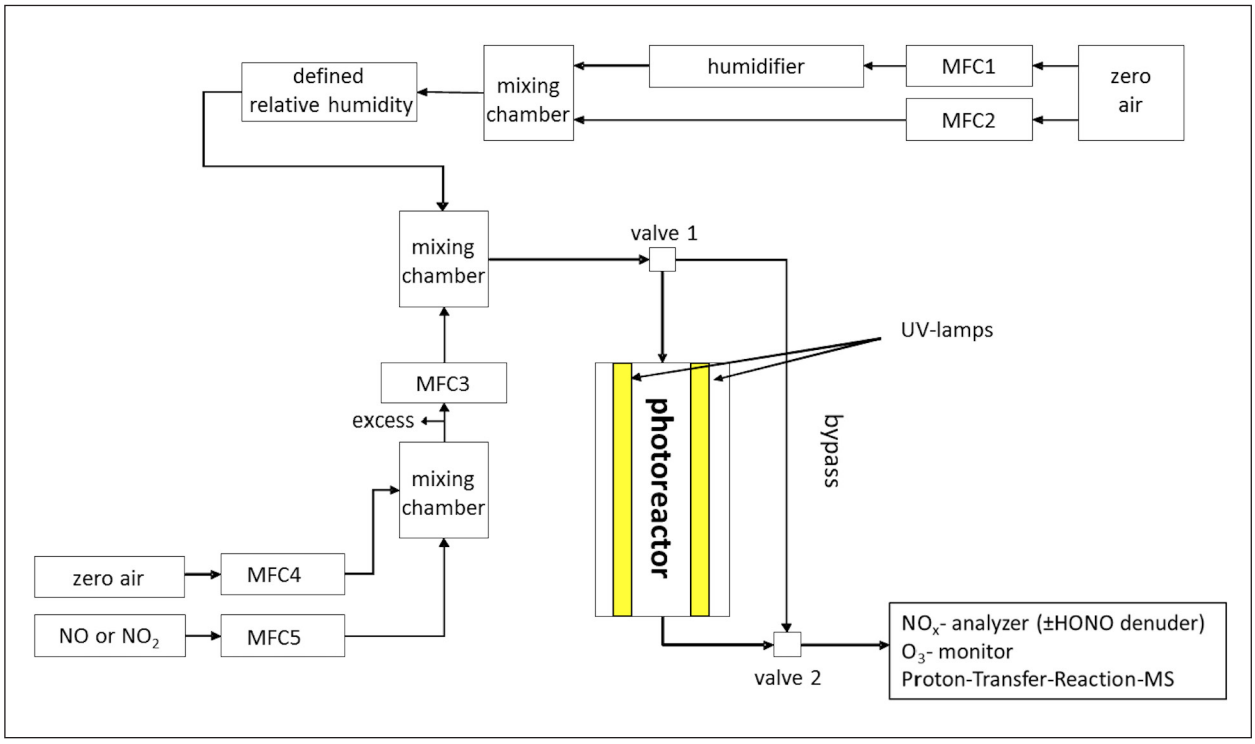

Fig. 3: Overview of the experimental setup for the small scale photoreactor experiments on urban grime (MFC: mass flow controller).

cover with 2 UV-lamps can be placed above the reactor to simulate the UV-part of the sunlight. The setup allows to perform the experiments either with clean compressed air or by adding selected target compounds to the air stream, all under controllable relative humidities. Standard experimental conditions are: flow rate 4 L min^{-1}, relative humidity (RH) 70% and light intensity 21 W m^{-2} (range 300-400 nm). For gas phase analysis, an O_3-monitor, a NO_x-analyser (± HONO denuder), a CAPS NO_2 system and a Proton-Transfer-Reaction- mass spectrometer (PTR-MS) are connected to the exit of the photoreactor. To determine the chemical composition dedicated samples are analyzed by using ion chromatography (IC) adopted from *Baergen et al.* [2015] and optimized regarding extraction efficiency and Curie-Point-Pyrolysis gas chromatography (CPP-GC-MS) adopted from *Styler et al.* [2018]. All data are evaluated under consideration of experiments using "blank glass beads" without urban grime.

Clean air experiments on real urban grime surface films

Small scale photoreactor experiments using clean compressed air have been performed to investigate if real urban grime surface films act as a potential source for air pollutants. Therefore, the mixing ratio of O_3, NO_x, HONO and the VOCs were monitored continuously during the bypass (no contact with the samples), in the dark and under irradiation of the samples with UV-light.

For the applied standard experimental conditions (cf. experimental section), the formation of O_3 and NO were negligible small, below 1 ppb. The results observed for nitrogen dioxide (NO_2) are shown in Fig. 4.

NO_2 mixing ratios were measured either with a common NO_x-analyser based on chemiluminescence (called ThermoNO2, solid lines) as well as with cavity attenuated phase shift technique (CAPSNO2, dotted lines). This approach, in combination with an additional HONO denuder (sodium carbonate filled glass tube), that was inserted into the sampling line of the ThermoNO2 for a certain time of the experiment (highlighted in orange), enabled the separation of the observed results into real NO_2 and HONO. As can be seen in Fig. 4, only a small NO_2-signal (small peak after switching from bypass to the reactor) was measured for UV-OFF using the ThermoNO2, but not by the CAPSNO2, indicating the presence of HONO instead of NO_2 in the dark. However, values were below 1 ppb, close to the error of the instrument. In contrast to that, the NO_2-signal significantly increases if the UV-light was switched on, up to values of 7 ppb measured by the ThermoNO2 for the shaded samples, followed by a decreasing trend until they reached a kind of steady state condition about 2 hours after starting the irradiation. Two important differences become clear during UV-ON. First, the

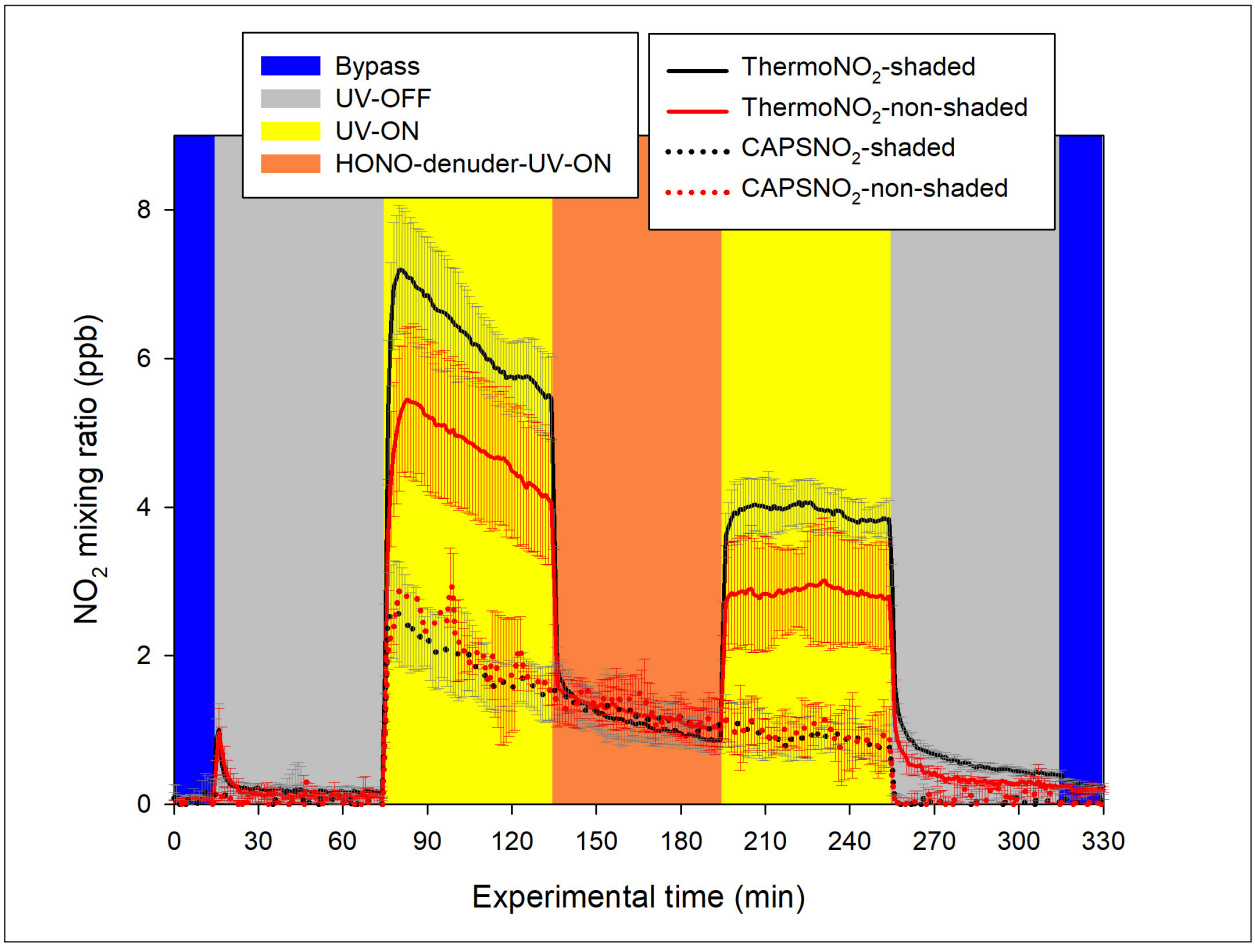

Fig. 4: NO_2 mixing ratio during clean air photoreactor experiments.

Tab. 1: NO_2 and HONO formation rates under steady state conditions in dependence on the sample type.

	NO_2 formation rate (molecules cm^{-2} s^{-1})	HONO formation rate (molecules cm^{-2} s^{-1})
Non-shaded glass beads	(2.3±0.6) ×10^9	(3±1) ×10^9
Shaded glass beads	(2.6±0.6) ×10^9	(8±1) ×10^9

NO_2-signal behaviour of the ThermoNO2 and the CAPSNO2 for both, the phases with and without the HONO denuder clearly proofs the photochemical formation of NO_2 and HONO and second, this formation is dependent on the sample type, shaded vs. non-shaded samples. Therefore, NO_2 and HONO formation rates (average values and corresponding 1σ standard deviations) were calculated for the steady state conditions (experimental time 195-255 min) and are summarized in Tab. 1.

In general, the observed formation rates for both, NO_2 and HONO are in the range of 10^9 molecules cm^{-2} s^{-1} during UV-ON, with 2.5 times higher HONO formation rates compared to NO_2, on shaded glass beads. As can be seen from Tab. 1, while the formation of NO_2 is independent on the sampling conditions, the HONO formation is clearly higher for shaded compared to non-shaded samples, indicating potentially different source mechanisms.

In addition to the observed formation of nitrogen oxides, also a release of organics under dark conditions and a clear proof of photochemically induced formation of organics was shown for both sample types, with highest for shaded samples (data not shown). According to the mass to charge ratio it is assumed that these compounds are most likely short-chain organics like acetaldehyde, acetone, propanal, acetic acid and butanal.

Following these experiments, it was the aim to investigate if the observed product formations are dependent on the experimental conditions, meaning the relative humidity and the light intensity. The relative humidity has been varied in the range of <1% and 95%. The resulting impact on the formation rates of NO_2, HONO and some selected mass to charge ratios is presented in Fig. 5.

A clear impact of RH on all compounds is observed, with in general higher values with increasing humidity. It is important to note, that almost

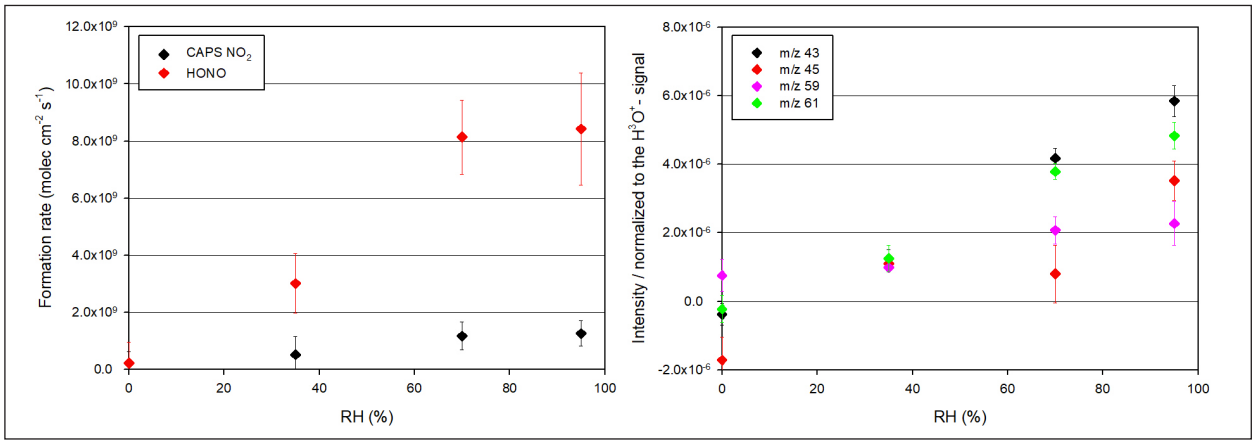

Fig. 5: Product formation from shaded urban grime film samples under irradiation in dependence on RH; left: formation rate of NO_2 and HONO, right: signal intensities for selected m/z.

no formation occurs for experiments under dry conditions (<1% RH), indicating that humidity is important regarding the formation mechanism. Formation rates of NO_2 and HONO as well as most of the signal intensities for the selected VOCs increase up to 70% RH, but show no further impact for values higher than 70% RH, demonstrating a levelling off effect under these conditions.

Furthermore, the light intensity was varied in a range of 5-48 W m^{-2} (300-400 nm). As expected for a photochemically driven reactivity, a clear impact on the light intensity is observed (data not shown), with in general higher values of compound formation with increasing light intensity. For most of the compounds mentioned before, a clear signal increase occurs up to approximately 20 W m^{-2}, but no further impact is shown with increasing light intensity, indicating a surface saturation effect. One additional set of experiments under variation of the light source proved, that the UV-part of the light source is responsible for the observed product formation.

To investigate in detail possible mechanisms for the observed product formation, a certain set of real urban grime film samples have been extracted before and after the small scale photoreactor experiments and analysed for their chemical composition. The results of the inorganic composition are presented in Fig. 6 as the difference of "after minus before" the photoreactor experiments for non-shaded compared to the shaded samples.

In general, negative values indicate a consumption of compounds due to the small scale photoreactor experiments. A clear decrease is observed for nitrate and sulfate, for both shaded and non-shaded glass beads. Highest consumption occurs for nitrate and the shaded glass beads, that corresponds well to the observed highest NO_2 and HONO formation rates for this type of samples and the fact that in literature the photolysis of nitrate is a discussed source of nitrogen oxides in the atmosphere [*Baergen and Donaldson*, 2013; 2016; *Baergen et al.*, 2015; *Ma et al.*, 2013]. Since the difference is not significant, this experimental approach was repeated using another set of samples enabling a higher number of samples. Based on that, if was decided to perform the detailed analysis of the organic fraction of the urban grime samples only for the extended set of samples. However, the detailed data analysis is currently in progress and could not be part of the present report.

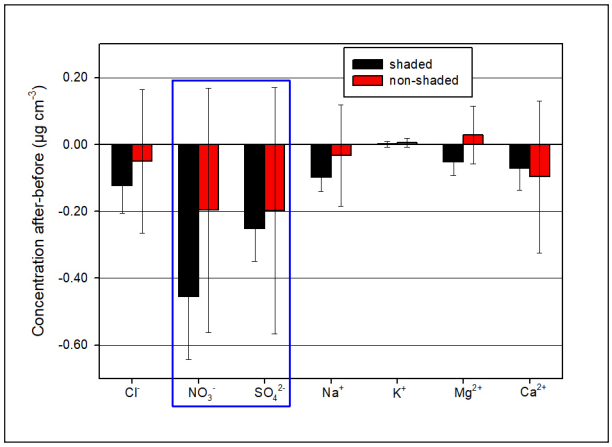

Fig. 6: Inorganic composition of urban grime film samples "after-before" the photoreactor experiments in dependence on the sampling conditions.

Interaction of target pollutants with real urban grime surface films

The uptake of both NO_2 and O_3 at a variety of atmospheric surfaces, including humic substances, mineral dust, and soot, has been shown to exhibit a light enhancement [*D'Anna et al.*, 2009; *Ndour et al.*, 2009; *Zelenay et al.*, 2011]. Given that urban grime

is a complex mixture, these pathways would also be expected to operate on its surface. In order to test this hypothesis, real urban grime samples have been exposed to different urban air pollutants, dependent on the experimental conditions and changes in the gas-phase concentrations were continuously monitored. Up to now photoreactor experiments are done for the nitrogen oxides NO and NO_2. Since the data analysis is currently in progress, only some preliminary results will be discussed.

The uptake of NO was investigated by adding 45 ppb of NO to the gas flow in contact with the urban grime surface film. The NO-signal during these experiments was not changing either when switching from the bypass to the reactor in the dark nor under irradiation of the urban grime, demonstrating no impact of the urban grime on the uptake behavior of NO on such coated surfaces (data not shown). In addition to that, the impact of varying additional NO on the formation rates of NO_2 and HONO under steady state conditions (UV-ON) was investigated and the results are shown in Fig. 7.

In general, negative values show a slightly negative impact of NO-addition on the formation of NO_2 and HONO for the tested shaded glass beads. However, under consideration of the 1σ standard deviation, the results in Fig. 7 show no significant impact of the quantity of added NO on the product formation rates interacting with the urban grime surface films in the range of 45-187 ppb NO. In conclusion, there is no atmospheric relevant interaction process of NO and the urban grime surface film, either in direction towards the films nor the formation of observed reaction products.

Besides NO, BTR-experiments with urban grime samples under addition of NO_2 as target compound

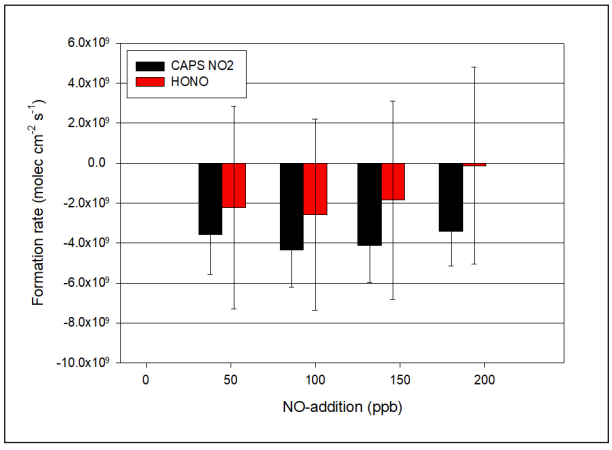

Fig. 7: Formation rates of NO_2 and HONO under steady state conditions (UV-ON) in dependence on the additional amount of NO for shaded glass beads, plotted as the difference of results w/ NO minus w/o additional NO (bypass values considered).

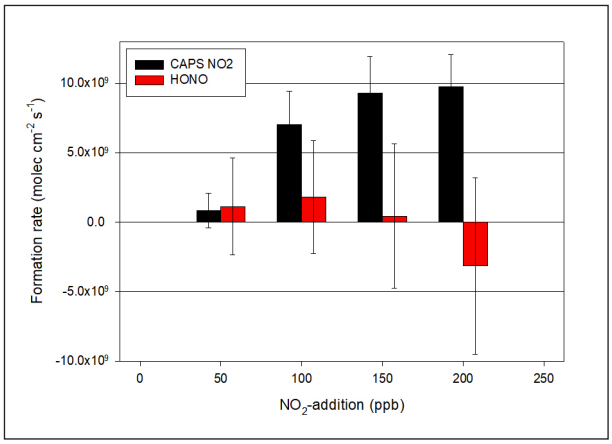

Fig. 8: Formation rates of NO_2 and HONO under steady state conditions (UV-ON) in dependence on the additional amount of NO_2 for shaded glass beads, plotted as the difference of results w/ NO_2 minus w/o additional NO_2 ($J(NO_2)$ and bypass values considered).

have been performed. Following the structure of Fig. 7 the impact of varying additional NO_2 on the formation rates of NO_2 and HONO under steady state conditions (UV-ON) are shown in Fig. 8.

The calculated formation rates for NO_2 and HONO are, with the exception of the result for HONO under addition of 200 pbb NO_2, positive. This indicates, in contrast to the addition of NO, no general negative impact of added NO_2 as air pollutant on the product formation from urban grime samples under irradiation. While the addition of about 50 ppb NO_2 impacts both products similarly with only slightly increased formed NO_2 and HONO (formation rates approx. 1.0×10^9 molecules cm^{-2} s^{-1}) the further increase up to 200 ppb of additional NO_2 results in different trends of product formation. The increase of added NO_2 leads to higher amounts of formed NO_2 levelling off at about 1.0×10^{10} molecules cm^{-2} s^{-1}. In contrast, the obtained values for HONO decreased down to even negative values. Although, these dependencies are not significant under consideration of the 1σ standard deviation, they are again indicators for different formation mechanisms of NO_2 and HONO during the irradiation of the urban grime films. In addition to these sets of experiments, currently ongoing data evaluation on the impact of the relative humidity in cross combination with additional NO and NO_2 will gain more insights on photochemical urban grime product formation.

Furthermore, it is planned to investigate the reactivity of the urban grime towards O_3 and some selected VOCs like toluene, acetaldehyde, isoprene, alpha-pinene as representatives of anthropogenic and biogenic emitted VOCs with different chemical properties.

Summary and outlook

The improvement of urban air quality is still a major concern that fosters the interest in understanding the most relevant chemical processes and pathways of air pollutants, especially regarding heterogeneous and multiphase reactions when gases interact with urban surfaces (e.g., windows, building walls, rooftops, sidewalks, roads, etc.) that could affect the fate of air pollutants. The presented study, therefore, combined real urban grime sampling with laboratory and modelling studies to characterize the photoreactive behavior of urban grime at impervious surfaces.

A custom built 3-stage passive sampling device enables the sampling of the real urban grime surface film on pure soda lime glass beads (3 mm in diameter) within a sampling time of 3 months. Small lab scale photoreactor experiments have been performed to investigate whether urban grime is potentially acting as a sink or a source for air pollutants. This used experimental approach provided for the first-time comprehensive data on the kinetics (product formation rates, uptake coefficients, deposition velocities, etc.) for different air pollutants (e.g., HONO, NO_2) and gave some preliminary insights into reaction mechanisms and potential secondary product formation. Clean air photoreactor experiments clearly proved the formation of NO_2 and HONO with formation rates in the range of 10^9 molecules cm^{-2} s^{-1} during UV-ON, with 2.5 times higher HONO formation rates compared to NO_2, on glass beads that were protected from the sunlight during sampling. Also, a release of organics under dark conditions and a clear proof of photochemically induced formation of short chain organics was shown for both sample types, with highest for shaded samples. All observed formation rates are depending on the experimental conditions, like RH, light intensity and sampling type. Preliminary results on the interaction of NO and NO_2 with real urban grime surface films indicated different interaction processes resulting in either increased or decreased formation rates of NO_2 and HONO, up to one order of magnitude.

The additional analysis of the urban grime chemical composition by IC and CPP-GC-MS before and after these photoreactivity experiments extended the results to a multiphase chemical data set which will further be applied in a modelling module. The planned modelling will finally provide useful insights into the overall lifetimes and fates of air pollutants associated with urban grime.

Overall, the ongoing urban grime studies at TROPOS ACD will for the first time give a comprehensive answer to the question how urban grime as a new environmental compartment in urban areas will impact air quality with its associated health effects.

References

Ammar, R., M. E. Monge, C. George, and B. D'Anna (2010), Photoenhanced NO_2 Loss on Simulated Urban Grime, *ChemPhysChem*, *11*(18), 3956-3961, https://doi.org/10.1002/cphc.201000540.

Baergen, A. M., and D. J. Donaldson (2013), Photochemical Renoxification of Nitric Acid on Real Urban Grime, *Environ. Sci. Technol.*, *47*(2), 815-820, https://doi.org/10.1021/es3037862.

Baergen, A. M., and D. J. Donaldson (2016), Y Formation of reactive nitrogen oxides from urban grime photochemistry, *Atmos. Chem. Phys.*, *16*(10), 6355-6363, https://doi.org/10.5194/acp-16-6355-2016.

Baergen, A. M., S. A. Styler, D. van Pinxteren, K. Muller, H. Herrmann, and D. J. Donaldson (2015), Chemistry of Urban Grime: Inorganic Ion Composition of Grime vs Particles in Leipzig, Germany, *Environ. Sci. Technol.*, *49*(21), 12688-12696, https://doi.org/10.1021/acs.est.5b03054.

Brigante, M., D. Cazoir, B. D'Anna, C. George, and D. J. Donaldson (2008), Photoenhanced Uptake of NO_2 by Pyrene Solid Films, *J. Phys. Chem. A*, *112*(39), 9503-9508, https://doi.org/10.1021/jp802324g.

Butt, C. M., M. L. Diamond, J. Truong, M. G. Ikonomou, and A. F. H. ter Schure (2004), Spatial Distribution of Polybrominated Diphenyl Ethers in Southern Ontario As Measured in Indoor and Outdoor Window Organic Films, *Environ. Sci. Technol.*, *38*(3), 724-731, https://doi.org/10.1021/es034670r.

Cazoir, D., M. Brigante, R. Ammar, B. D'Anna, and C. George (2014), Heterogeneous photochemistry of gaseous NO_2 on solid fluoranthene films: A source of gaseous nitrous acid (HONO) in the urban environment, *J. Photoch. Photobio. A*, *273*, 23-28, https://doi.org/10.1016/j.jphotochem.2013.07.016.

Cheruiyot, N. K., W. J. Lee, J. K. Mwangi, L. C. Wang, N. H. Lin, Y. C. Lin, J. J. Cao, R. J. Zhang, and G. P. Chang-Chien (2015), An Overview: Polycyclic Aromatic Hydrocarbon Emissions from the Stationary and Mobile Sources and in the Ambient Air, *Aerosol Air Qual. Res.*, *15*(7), 2730-2762, https://doi.org/10.4209/aaqr.2015.11.0627.

D'Anna, B., A. Jammoul, C. George, K. Stemmler, S. Fahrni, M. Ammann, and A. Wisthaler (2009), Light-induced ozone depletion by humic acid films and submicron aerosol particles, *J. Geophys. Res. - Atmos.*, *114*(D12301), https://doi.org/10.1029/2008JD011237.

Diamond, M. L., D. A. Priemer, and N. L. Law (2001), Developing a multimedia model of chemical dynamics in an urban area, *Chemosphere*, *44*(7), 1655-1667, https://doi.org/10.1016/S0045-6535(00)00509-9.

Diamond, M. L., S. E. Gingrich, K. Fertuck, B. E. McCarry, G. A. Stern, B. Billeck, B. Grift, D. Brooker, and T. D. Yager (2000), Evidence for Organic Film on an Impervious Urban Surface: Characterization and Potential Teratogenic Effects, *Environ. Sci. Technol.*, *34*(14), 2900-2908, https://doi.org/10.1021/es9906406.

EEA (2021), Air quality in Europe 2021. Report no. 15/2021.

Finlayson-Pitts, B. J., and J. N. Pitts (2000), *Chemistry of the Upper and Lower Atmosphere*.

George, C., R. S. Strekowski, J. Kleffmann, K. Stemmler, and M. Ammann (2005), Photoenhanced uptake of gaseous NO_2 on solid-organic compounds: a photochemical source of HONO?, *Faraday Discuss.*, *130*, 195-210, https://doi.org/10.1039/b417888m.

George, C., M. Ammann, B. D'Anna, D. J. Donaldson, and S. A. Nizkorodov (2015), Heterogeneous Photochemistry in the Atmosphere, *Chem. Rev.*, *115*(10), 4218-4258, https://doi.org/10.1021/cr500648z.

Gingrich, S. E., M. L. Diamond, G. A. Stern, and B. E. McCarry (2001), Atmospherically Derived Organic Surface Films along an Urban-Rural Gradient, *Environ. Sci.Technol.*, *35*(20), 4031-4037, https://doi.org/10.1021/es010699o.

Gligorovski, S. (2016), Nitrous acid (HONO): An emerging indoor pollutant, *J. Photoch. Photobio. A*, *314*, 1-5, https://doi.org/10.1016/j.jphotochem.2015.06.008.

Grant, J. S., Z. Zhu, C. R. Anderton, and S. K. Shaw (2019), Physical and Chemical Morphology of Passively Sampled Environmental Films, *ACS Earth Space Chem.*, *3*(2), 305-313, https://doi.org/10.1021/acsearthspacechem.8b00158.

Guerreiro, C. B. B., V. Foltescu, and F. de Leeuw (2014), Air quality status and trends in Europe, *Atmos. Environ.*, *98*, 376-384, https://doi.org/10.1016/j.atmosenv.2014.09.017.

Handley, S. R., D. Clifford, and D. J. Donaldson (2007), Photochemical Loss of Nitric Acid on Organic Films: a Possible Recycling Mechanism for NO_x, *Environ. Sci.Technol.*, *41*(11), 3898-3903, https://doi.org/10.1021/es062044z.

Kameda, T. (2011), Atmospheric Chemistry of Polycyclic Aromatic Hydrocarbons and Related Compounds, *J. Health Sci.*, *57*(6), 504-511, https://doi.org/10.1248/jhs.57.504.

Kroptavich, C. R., S. Zhou, S. F. Kowal, and T. F. Kahan (2020), Physical and Chemical Characterization of Urban Grime Sampled from Two Cities, *ACS Earth Space Chem.*, *4*(10), 1813-1822, https://doi.org/10.1016/j.conbuildmat.2020.Oc00192.

Kwamena, N.-O. A., J. P. Clarke, T. F. Kahan, M. L. Diamond, and D. J. Donaldson (2007), Assessing the importance of heterogeneous reactions of polycyclic aromatic hydrocarbons in the urban atmosphere using the Multimedia Urban Model, *Atmos. Environ.*, *41*(1), 37-50, https://doi.org/10.1016/j.atmosenv.2006.08.016.

Lam, B., M. L. Diamond, A. J. Simpson, P. A. Makar, J. Truong, and N. A. Hernandez-Martinez (2005), Chemical composition of surface films on glass windows and implications for atmospheric chemistry, *Atmos. Environ.*, *39*(35), 6578-6586, https://doi.org/10.1016/j.atmosenv.2005.07.057.

Law, N. L., and M. L. Diamond (1998), The role of organic films and the effect on hydrophobic organic compounds in urban areas: An hypothesis, *Chemosphere*, *36*(12), 2607-2620, https://doi.org/10.1016/s0045-6535(97)10222-3.

Liu, J., S. Li, M. Mekic, H. Jiang, W. Zhou, G. Loisel, W. Song, X. Wang, and S. Gligorovski (2019), Photoenhanced Uptake of NO2 and HONO Formation on Real Urban Grime, *Environ. Sci.Technol. Lett.*, Ahead of Print, https://doi.org/10.1021/acs.estlett.9b00308.

Liu, Q.-T., R. Chen, B. E. McCarry, M. L. Diamond, and B. Bahavar (2003a), Characterization of Polar Organic Compounds in the Organic Film on Indoor and Outdoor Glass Windows, *Environ. Sci. Technol.*, *37*(11), 2340-2349, https://doi.org/10.1021/es020848i.

Liu, Q.-T., M. L. Diamond, S. E. Gingrich, J. M. Ondov, P. Maciejczyk, and G. A. Stern (2003b), Accumulation of metals, trace elements and semi-volatile organic compounds on exterior window surfaces in Baltimore, *Environ. Pollut.*, *122*(1), 51-61, https://doi.org/10.1016/S0269-7491(02)00286-5.

Ma, J. Z., Y. C. Liu, C. Han, Q. X. Ma, C. Liu, and H. He (2013), Review of heterogeneous photochemical reactions of NO_y on aerosol - A possible daytime source of nitrous acid (HONO) in the atmosphere, *J. Environ. Sci. (China)*, *25*(2), 326-334, https://doi.org/10.1016/s1001-0742(12)60093-x.

Michoud, V., A. Colomb, A. Borbon, K. Miet, M. Beekmann, M. Camredon, B. Aumont, S. Perrier, P. Zapf, G. Siour, W. Ait-Helal, C. Afif, A. Kukui, M. Furger, J. C. Dupont, M. Haeffelin, and J. F. Doussin (2014), Study of the unknown HONO daytime source at a European suburban site during the MEGAPOLI summer and winter field campaigns, *Atmos. Chem. Phys.*, *14*(6), 2805-2822, https://doi.org/10.5194/acp-14-2805-2014.

Mothes, F., S. Ifang, M. Gallus, B. Golly, A. Boréave, R. Kurtenbach, J. Kleffmann, C. George, and H. Herrmann (2018), Bed flow photoreactor experiments to assess the photocatalytic nitrogen oxides abatement under simulated atmospheric conditions, *Appl. Catal. B - Environ.*, *231*, 161-172, https://doi.org/10.1016/j.apcatb.2018.03.010.

Ndour, M., M. Nicolas, B. D'Anna, O. Ka, and C. George (2009), Photoreactivity of NO_2 on mineral dusts originating from different locations of the Sahara desert, *Phys. Chem. Chem. Phys.*, *11*(9), 1312-1319, https://doi.org/10.1039/B806441E.

Simpson, A. J., B. Lam, M. L. Diamond, D. J. Donaldson, B. A. Lefebvre, A. Q. Moser, A. J. Williams, N. I. Larin, and M. P. Kvasha (2006), Assessing the organic composition of urban surface films using nuclear magnetic resonance spectroscopy, *Chemosphere*, *63*(1), 142-152, https://doi.org/10.1016/j.chemosphere.2005.07.013.

Skalska, K., J. S. Miller, and S. Ledakowicz (2010), Trends in NO_x abatement: A review, *Sci.Total Environ.*, *408*(19), 3976-3989, https://doi.org/10.1016/j.scitotenv.2010.06.001.

SOER (2015), The European environment - state and outlook 2015 > European briefings > Air pollution.

Spataro, F., A. Ianniello, G. Esposito, I. Allegrini, T. Zhu, and M. Hu (2013), Occurrence of atmospheric nitrous acid in the urban area of Beijing (China), *Sci.Total Environ.*, *447*, 210-224, https://doi.org/10.1016/j.scitotenv.2012.12.065.

Stemmler, K., M. Ammann, C. Donders, J. Kleffmann, and C. George (2006), Photosensitized reduction of nitrogen dioxide on humic acid as a source of nitrous acid, *Nature*, *440*(7081), 195-198, https://doi.org/10.1038/nature04603.

Styler, S. A., A. M. Baergen, D. J. Donaldson, and H. Herrmann (2018), Organic Composition, Chemistry, and Photochemistry of Urban Film in Leipzig, Germany, *ACS Earth Space Chem.*, *2*(9), 935-945, https://doi.org/10.1021/acsearthspacechem.8b00087.

von Schneidemesser, E., P. S. Monks, J. D. Allan, L. Bruhwiler, P. Forster, D. Fowler, A. Lauer, W. T. Morgan, P. Paasonen, M. Righi, K. Sindelarova, and M. A. Sutton (2015), Chemistry and the Linkages between Air Quality and Climate Change, *Chem. Rev.*, *115*(10), 3856-3897, https://doi.org/10.1021/acs.chemrev.5b00089.

Wall, K. J., and G. W. Harris (2017), Uptake of nitrogen dioxide (NO2) on acidic aqueous humic acid (HA) solutions as a missing daytime nitrous acid (HONO) surface source, *J. Atmos. Chem.*, *74*(3), 283-321, https://doi.org/10.1007/s10874-016-9342-8.

Wong, K. W., C. Tsai, B. Lefer, N. Grossberg, and J. Stutz (2013), Modeling of daytime HONO vertical gradients during SHARP 2009, *Atmos. Chem. Phys.*, *13*(7), 3587-3601, https://doi.org/10.5194/acp-13-3587-2013.

Wong, K. W., C. Tsai, B. Lefer, C. Haman, N. Grossberg, W. H. Brune, X. Ren, W. Luke, and J. Stutz (2012), Daytime HONO vertical gradients during SHARP 2009 in Houston, TX, *Atmos. Chem. Phys.*, *12*(2), 635-652, https://doi.org/10.5194/acp-12-635-2012.

Wu, R. W., T. Harner, and M. L. Diamond (2008), Evolution rates and PCB content of surface films that develop on impervious urban surfaces, *Atmos. Environ.*, *42*(24), 6131-6143, https://doi.org/10.1016/j.atmosenv.2008.01.066.

Zelenay, V., M. E. Monge, B. D'Anna, C. George, S. A. Styler, T. Huthwelker, and M. Ammann (2011), Increased steady state uptake of ozone on soot due to UV/Vis radiation, *J. Geophys. Res. - Atmos.*, *116*(D11301), https://doi.org/10.1029/2010JD015500.

Funding

German Research Foundation (Deutsche Forschungsgemeinschaft (DFG) - Project number 415705351).

Transdisciplinary research setup in solving air pollution: First look at the Environmental Pillar of TAME-BC

Leizel Madueño, Simonas Kecorius, Liina Tõnisson, Alfred Wiedensohler, Mira Pöhlker

Schlechte Luftqualität ist ein großes Umweltrisiko für die menschliche Gesundheit, insbesondere in Entwicklungsregionen, in denen es an Informationen über die physikalischen und chemischen Eigenschaften von Luftschadstoffen mangelt. Das von TROPOS koordinierte Projekt TAME-BC (Transdisciplinary Approach to Mitigate Emissions of Black Carbon) bot einen transdisziplinären Rahmen für die Entwicklung einer nachhaltigen Lösung zur Verringerung der BC-Emissionen in der Metropolregion Manila. Dieser Artikel gibt einen Überblick über das Projekt und seine vorläufigen Ergebnisse.

Introduction

In recent years, ambient particulate matter (PM) has been recognized as one of the top ten most significant environmental risks to health, which caused about seven million premature deaths worldwide per year (citation needed). In the year 2050, two-thirds of the World's population, more than 6.5 billion people, will be living in towns and cities [*Floater et al.,* 2014]. Asia is foreseen to accommodate over half of the planet's population in numerous megacities with more than 10 million inhabitants. Many studies have already owed the decline of air quality to emissions from the unsustainable transportation sector. Finding solutions to this threat poses a significant challenge to practitioners and policymakers alike. The benefits of transdisciplinary research on solution-oriented development may pave the way to solve local problems sustainably.

Over the last decades, TROPOS has participated and led numerous intensive measurement campaigns focusing on urban air quality, e.g., PAPILA 2018, CARE 2017 [*Costabile et al.,* 2017], MACE 2015 [*Kecorius et al.*, 2015]. The expertise of TROPOS combined with experts from social and health sciences provided a transformational approach in solving air pollution issues through the transdisciplinary project TAME-BC (Transdisciplinary Approach to Mitigate Emissions of Black Carbon). The concept of the TAME-BC project is briefly described here; for a more in-depth discussion, please refer to *Tõnisson et al.* [2020]. This article presents an overview of the experimental measurements and the first results of TAME-BC.

Motivation of TAME-BC: Aerosol Characterization in Metro Manila, Philippines

The cooperation between research institutes, universities, and non-governmental organizations in Metro Manila (called ResCueAir) and TROPOS started in 2014, resulting in an intensive measurement campaign in Metro Manila. The Manila Aerosol Characterization Experiment (MACE 2015) was conducted to characterize air pollution in three locations in the megacity. An aerosol measurement container was brought from Germany to the Philippines equipped with state-of-the-art aerosol instrumentation to measure air pollution levels at the urban background and roadside level in Metro Manila (Fig. 1). The measurements focused on the physical-chemical properties of particulate pollution, with specific attention on black carbon (BC) particles.

One of the prominent observations from MACE2015 is that the emission from the transport sector dominates urban air quality in Metro Manila. Alarmingly, the urban air of Metro Manila is comprised of high concentrations of both ultrafine (<100 nm) and equivalent BC particles [*Kecorius et al.,* 2017]. The equivalent BC concentration level at the roadside

Fig. 1: Map of Metro Manila with the approximate locations of the intensive measurement campaigns during TAME-BC (red triangle) and MACE 2015 (black cross) using state-of-the-art aerosol measurement instrumentation.

measurement location was precariously high, up to 50 times higher than in European or North American urban areas [*Madueño et al.,* 2019a]. The complementary mobile measurements confirmed that the equivalent BC is significantly high along the roads and in areas with very high transport activities [*Alas et al.,* 2018]. In terms of vehicular emission contribution at street level, the most commonly used Public Utility Jeepneys (PUJs) contributed up to 94% of the overall equivalent BC emissions [*Kecorius et al.,* 2017; *Madueño et al.,* 2019a]. Alarmingly, Metro Manila city dwellers' time in transit traffic is up to 2.2 times longer than in Europe, America, Korea, or China [*Kecorius et al.,* 2018], which conveys those commuters have a prolonged time of exposure to extreme levels of vehicular emissions. These findings back in 2015 gave rise to the TAME-BC project, launched in 2019, which focused on the PUJs as the mode of transport that necessitates a sustainable transformation.

From Transfer to Knowledge Co-Production: TAME-BC Framework

There is limited knowledge on the characterization of air pollutants in rapidly urbanizing countries. The impact of air pollution on public health and the challenge to find a sustainable solution that considers the dynamics of socio-political institutional frameworks is mainly unknown. To help set up an applicable transdisciplinary framework in addressing air pollution, the TAME-BC was launched in the Philippines, where experts in different scientific fields from Germany (Leibniz Institute for Tropospheric Research; Leibniz Institute for Environmental Medicine; German Development Institute) and the Philippines (Clean Air Asia; Manila and Quezon City Local Government; ResCue Air; Lung Center of the Philippines; Department of Transportation; Jeepney Driver Association; Manila North Port) acted together to tackle the worsening urban air pollution in Metro Manila. The research setup of TAME-BC is an innovative package of technological, socio-political, and health interventions for decision-makers to mitigate BC emissions. The TAME-BC presents a novel approach that integrates the environmental, social, and health sciences to address the perennial air pollution problem in Metro Manila (Fig. 2). One of the overarching goals of TAME-BC was to investigate and evaluate the dynamically evolving policies, rules, norms, and values that determine the current state of air quality in Metro Manila. In brief, TAME-BC is structured around four pillars that act as a foundation of the project. Each pillar is spearheaded by different German institutions working together with Philippine institutions and stakeholders to achieve the following specific goals:

- Pillar 1 (Environmental):
  assesses BC pollution levels and adaptation strategies in the transport sector;
- Pillar 2 (Social):
  understanding the institutional environment of air quality regulations, including the local and national governance structures in the Philippines;
- Pillar 3 (Health):
  assessment and current state of human exposure to BC and related potential health effects;

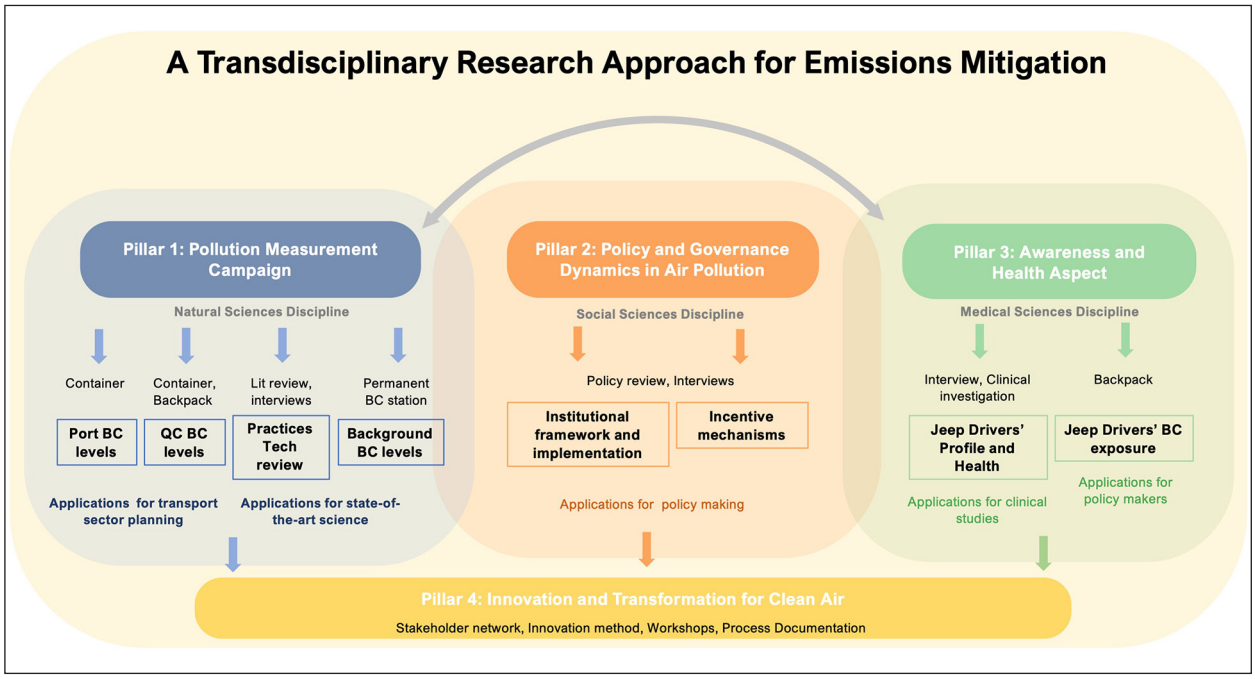

Fig. 2: Visualization of a novel approach for sustainability research in the context of air quality management.

- Pillar 4 (Stakeholder):
  analyze the institutional workings of the air-pollution-related innovation system to effectively integrate the knowledge obtained from the findings into sustainable solutions.

TROPOS acted as the lead German institution for the environmental pillar and functioned as the overall project coordinator for TAME-BC.

Environmental Pillar of TAME-BC Framework

During the definition phase of the project, the environmental pillar of TAME-BC was focused on the assessment of air pollution levels and physical-chemical aerosol properties in Manila North Port (December 2019 to January 2020) to assess the contribution of freight service of the port to Metro Manila air pollution budget, and in Quezon City (East Avenue, January to February 2020) to assess the emission contribution from source points, as well as tracing the interaction between BC particles and personal exposure.

The aerosol instrumentation used in the TAME-BC measurement campaign includes:

- mobility and aerodynamic particle size spectrometers (MPSS and APS), to measure the aerosol particle size distribution;
- absorption photometers, such as the aethalometer (AE31) and the multiple angle absorption photometer (MAAP) to measure the absorption coefficient;
- a volatility-tandem differential mobility analyzer (V-TDMA), to measure volatility properties;
- an aerosol chemical speciation monitor (ACSM) to measure the chemical composition of aerosol particles;
- an automated weather station was used to monitor basic meteorological parameters (e.g., wind speed, direction, temperature, relative humidity, etc.).

Aside from the custom-made state-of-the-art measurement container, which stayed in a single location for a set time, a complimentary cutting edge portable aerosol backpack was developed to investigate BC exposure concentrations along the streets and in different locations that require mobility. The instrumentation inside the backpack includes an optical particle size spectrometer (OPSS) and a micro-aethalometer (AE51, MA200). On top of the planned measurements during TAME-BC, a complementary experiment focused on the in-situ respiratory tract deposition of BC particles using the TROPOS-built measurement platform, MERDOC [Measuring Real-world Deposition Of black Carbon particles, *Madueño et al.*, 2019b] was conducted. Moreover, investigation of indoor-outdoor particle number size distributions of generic and refractory particles (using TROPOS-type MPSS system combined with a thermodenuder) was measured in 4 households across Metro Manila to determine indoor-outdoor air quality relation, pollutant infiltration ratios, and indoor respiratory tract deposition of particulates.

Fig. 3: Measurement site in Manila North Port. The red triangle marks TROPOS measurement container location. Letters A-D indicates wind sector used in data analysis (Sector A - North to Northeast winds; Sector B – Northeast to Southerly winds; Sector C – Southerly to Northwest winds; and Sector D – Northwest to North winds).

Contribution of Port activities to Air Pollution in Manila City

On the first leg of the TAME-BC measurement campaign, the aerosol measurement container was placed in Manila North Port (14.60N, 120.96E, Fig. 3) in the vicinity of North Port Passenger Terminal Complex, Manila, Philippines, to investigate the contribution of port freight emission to the overall air pollution budget of the area. The initial observation on the measurement site showed intensive port activities, which involve running fork trucks, ship cranes, and heavy-duty vehicles (mainly powered by diesel engines) inside and outside the port yard vicinity. From the first look at the results, we found an average total particle number concentration (N_{CN}; integrated in a size range from 10 to 800 nm; ± one standard deviation) of $5.2 \times 10^4 \pm 2.4 \times 10^4$ particles cm^{-3}, with ultrafine particles (<100 nm) contributing to an average of 90% to the total PNC (Fig. 4, Left panel). In contrast, the average background N_{CN} was $2.5 \times 10^4 \pm 7.5 \times 10^3$ particles cm^{-3}. The total N_{CN} had a pronounced diurnal variation, with increased concentrations between 05:00 to 07:00 and 10:00 to 14:00 local time. While the general diurnal trend of number fraction (NF) of externally mixed refractory particles (EMPR) can be seen on particles larger than 35 nm in diameter being more volatile during the midday hours (Fig. 4, Right panel). This indicates a photochemical production of secondary organic aerosol, which is

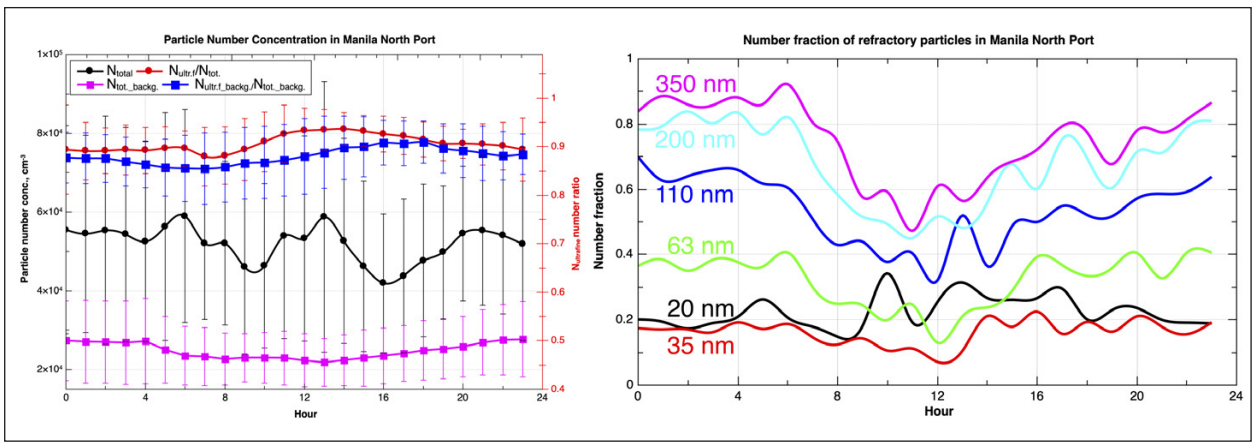

Fig. 4: Diurnal trend of particle number concentration (Left panel): total particle number concentration inside the port (black), calculated background particle number concentration (pink) using the method presented in Kecorius et al. [2017], and the ratio of ultrafine to total and background particle number concentration (red and blue, respectively); and diurnal trend of size segregated number fraction of refractory particles in Manila North Port (Right panel).

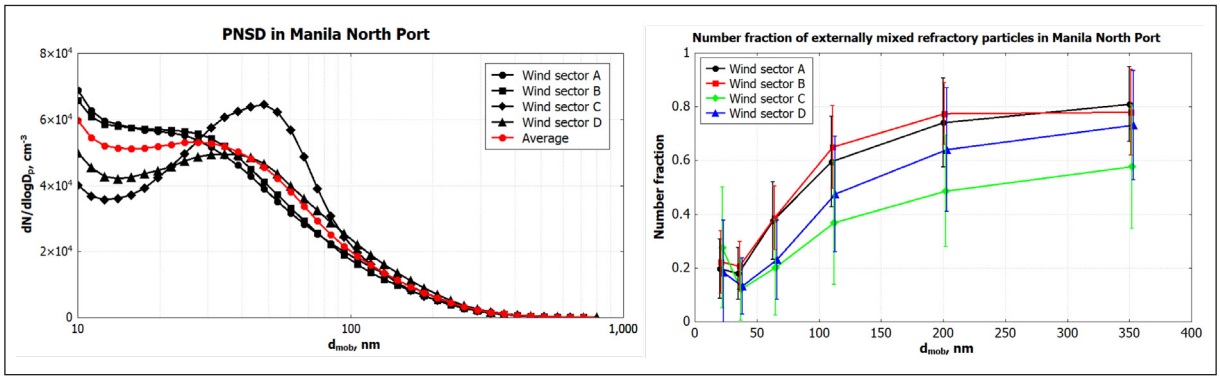

Fig. 5: Average particle number size distribution and number fraction of externally mixed refractory particles segregated by wind sector in Manila North Port.

more volatile than other externally mixed species (e.g., BC). Both the particle number concentration and NF of EMPR were relatively invariant during weekdays; the general driving cause of high variability was observed due to local sources of particulate pollution (e.g., running fork trucks).

The high-resolution continuous measurements of N_{CN} were used to retrieve the background concentration using the running minimum method presented by *Kecorius et al.* [2017]. Additionally, segregation of pollution sources by wind sectors was done to estimate the contribution of activities from inside and outside the port vicinity. The measurement data were separated between different wind sectors, where wind sectors C and D were preliminarily set as the fingerprint of port pollution (see Fig. 3). The analysis revealed that the average background N_{CN} from winds prevailing from sectors A-B and C-D was $2.6 \times 10^4 \pm 8.7 \times 10^3$ and $2.3 \times 10^4 \pm 7.5 \times 10^3$ particles cm^{-3}, respectively (Fig. 5). Interestingly, background N_{CN} associated with wind sectors A and B is by 3000 cm^{-3} higher than sectors C-D, suggesting that background N_{CN} inside Manila North Port is somewhat lower than surrounding landmass. Despite this, it can be estimated that the N_{CN} inside the port area increases by two folds due to locally present pollution sources and pollution transported downwind from the main road. In terms of NF of EMRP, the aerosol particles from wind sectors A-B were less volatile than those from C-D, indicating direct vehicular emission contribution to port pollution. The size segregated average NF of EMRP resided mainly in the size range between 110 – 350 nm (Fig. 5). We have initially observed that in Manila North Port, the NF of EMRP increased up to 80% with increasing particle diameter. On the other hand, these values became as low as approx. 20% for particles smaller than 63 nm. The most volatile particles were those of 35 nm in diameter.

Contribution of Road activities to Air Pollution in Quezon City

On the second leg of the TAME-BC measurement campaign, the aerosol measurements were

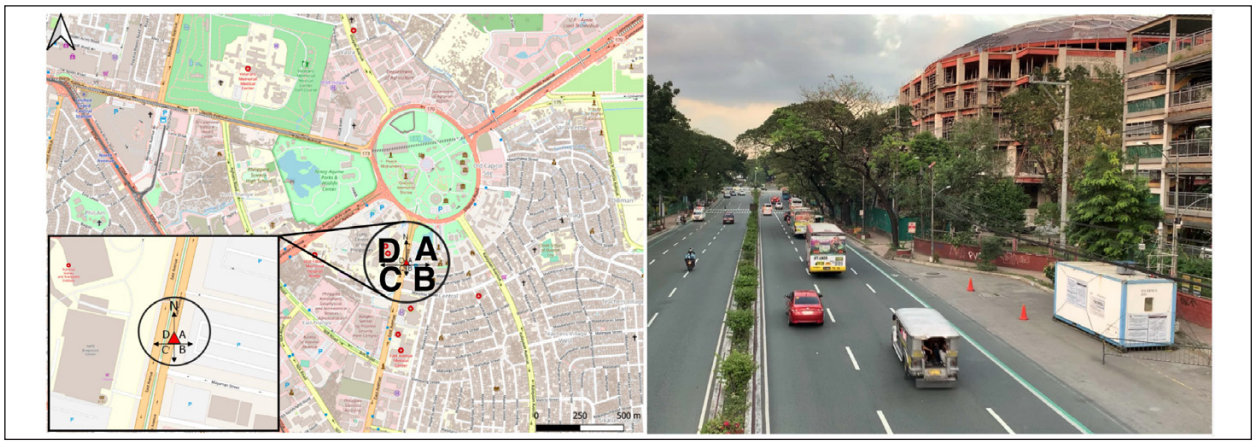

Fig. 6: Measurement site in East Avenue, Quezon City. The red triangle marks TROPOS measurement container location. Letters A-D indicates the wind sector used in data analysis (Sector A - North to Northeast winds; Sector B – Northeast to Southerly winds; Sector C – Southerly to Northwest winds; and Sector D – Northwest to North winds).

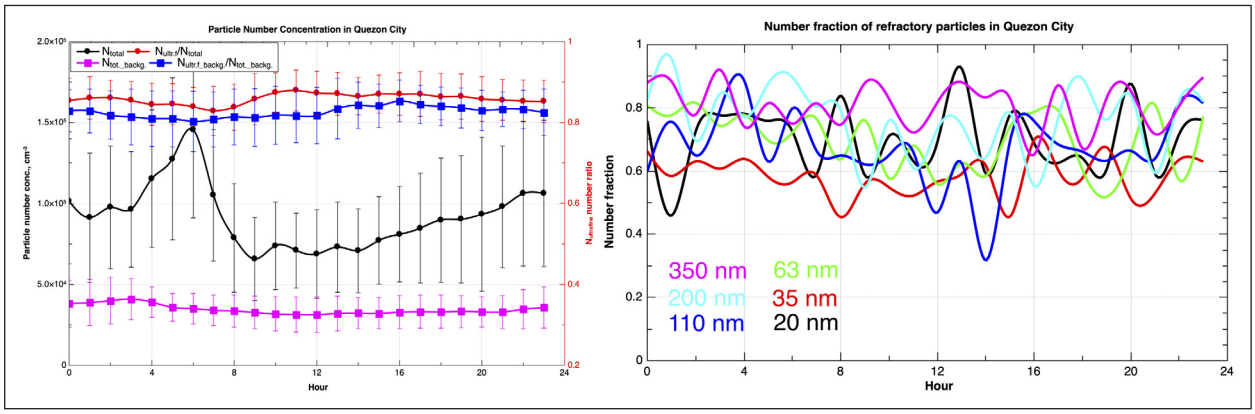

Fig. 7: Diurnal trend of particle number concentration (Left panel): total particle number concentration on the streetside (black), calculated background particle number concentration (pink), and the ratio of ultrafine to total and background particle number concentration (red and blue, respectively); and diurnal trend of size segregated number fraction of refractory particles in Quezon City (Right panel).

performed on East Avenue (street site) in Quezon City (14.6N, 121.0E, Fig. 6). East Avenue is composed of six lanes, where the measurement container was placed on one of the emergency bays along the road. From general visual observations, East Avenue during the day was shared mainly by light-duty and public utility vehicles (PUJs, buses). A five-story parking building was situated to the East of the measurement container, which possibly obstructed the free flow of eastern winds. The surrounding buildings and high dense trees created a street-canyon-like condition, trapping pollutants emitted from passing vehicles. The initial results showed an average total N_{CN} of $9.2 \times 10^4 \pm 4.2 \times 10^4$ cm^{-3}, with ultrafine particles on average contributing 85% to total particle number while the average background N_{CN} concentration was $3.5 \times 10^4 \pm 1.1 \times 10^4$ cm^{-3} (Fig. 7, Left panel). A distinct peak of total N_{CN} on streetside was observed during 06:00 local time, signifying the immense contribution of road traffic emissions during morning rush hours.

The ultrafine refractory particles in Quezon City were found to be more abundant than in Manila North Port (Fig. 7, Right panel). There was no observed diurnal variation of NF of EMRP in Quezon City. This can be attributed to different vehicular fleets and measurement site proximity to direct emissions. Furthermore, the NF of EMRP in Quezon city is less volatile than in Manila North Port, which conveys a higher concentration of externally mixed refractory particles (e.g., BC).

Similar to the preliminary analysis of pollution sources in Manila North Port, the measurement data were segregated into different wind sectors. Sectors C and D were identified as the apparent contribution from vehicle emissions along East Avenue (Fig. 6). The average PNSD measured in Quezon City is shown in Fig. 8 (Left panel). Wind sectors A-B and C-D exhibit similar PNSD shapes consisting of intense Aitken mode and weak Accumulation mode particles, indicating the same pollution source independent to wind direction. However, sectors C-D

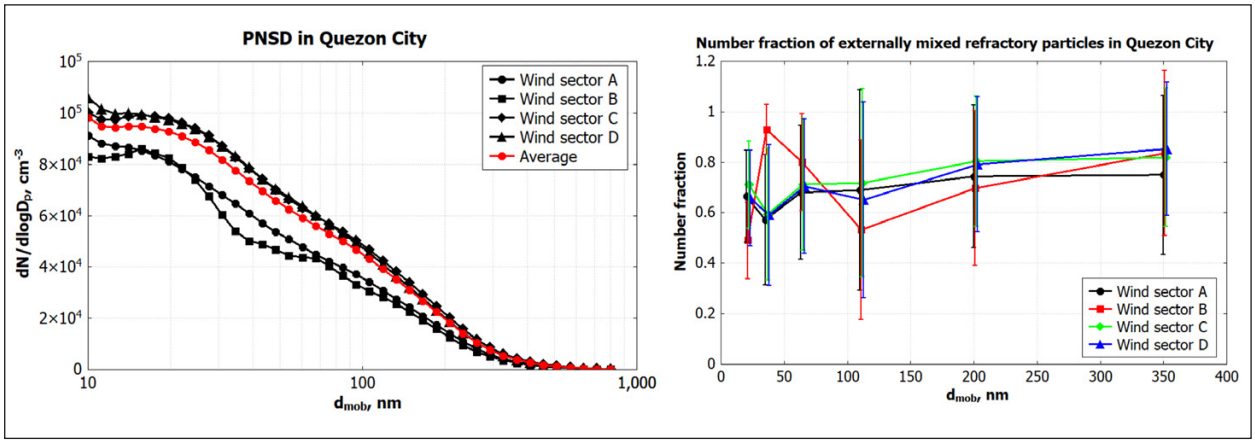

Fig. 8: Average particle number size distribution and number fraction of externally mixed refractory particles segregated by wind sector in East Avenue, Quezon City.

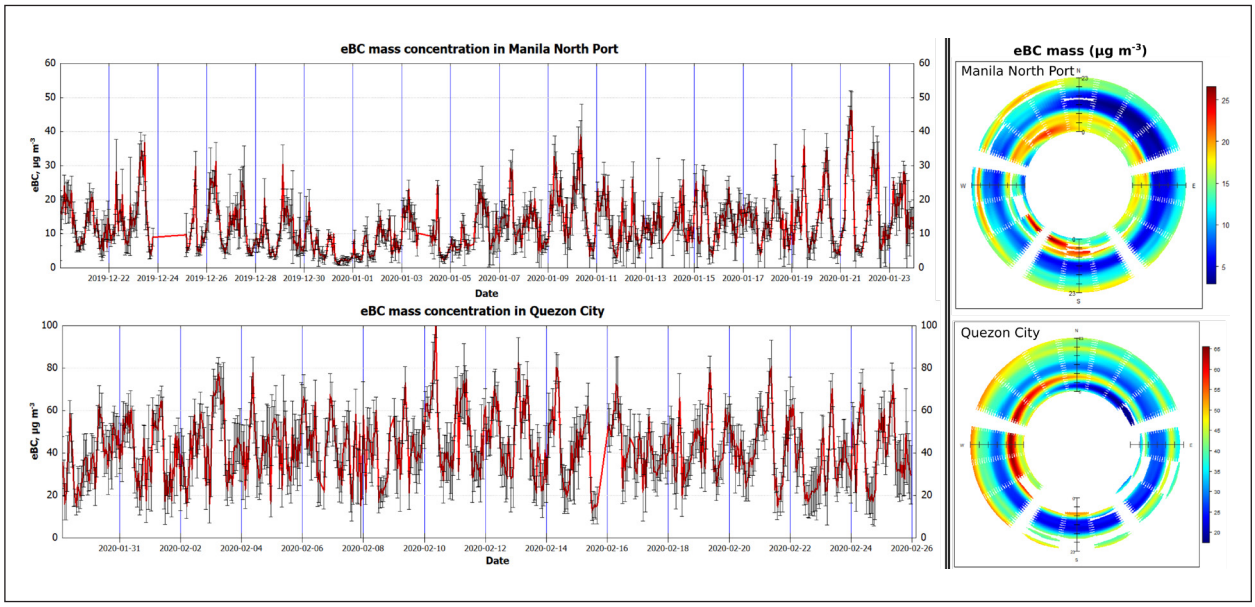

Fig. 9: Overall time series (left panel) and polar plot (right panel) of measured equivalent BC (eBC) mass concentration during the measurement period in Manila North Port (upper row) and Quezon City (bottom row).

showed slightly higher total PNC. In terms of NF of EMRP in Quezon City, unlike the results found in Manila North Port, the size segregated NF of EMPR resided in all measured size range (Fig. 8, Right panel), sectors A-C-D showed very similar particle volatility in different size ranges of EMRP contrary to sector B's results. The oddity of measurements from wind sector B is most likely a measurement artifact, which is a result of the parking building blocking the air mass from sector B (Fig.6); thus, data collected from this sector is restricted.

Equivalent Black Carbon Emissions in Metro Manila

The temporal variation and polar analysis of equivalent BC mass concentration in stationary measurement sites are presented in Fig. 9. The average equivalent BC mass concentration during the measurement period in Manila North Port and Quezon City was 12.7 ± 8.5 µg m^{-3} and 42.3 ± 17.6 µg m^{-3}, respectively. This shows that roadside equivalent BC emission in Quezon City is 3.3 times higher than the port activities in Manila North Port. Distressingly, the highest average equivalent BC mass concentration was above 60 µg m^{-3}, which was observed in Quezon City during rush hour; that is to say, this is the time when commuters have prolonged exposure to direct vehicular emissions. During midday, equivalent BC mass concentrations decreased on average to approx. 30 µg m^{-3}.

In comparison, the estimated average background equivalent BC mass concentration in Quezon City was 11.7 ± 0.8 µg m^{-3}, which is 2.8 times higher than in Manila North Port. The polar plot of equivalent BC mass concentration showed dependence on wind direction, which confirms that the highest equivalent BC mass concentrations are associated with winds prevailing from the direction of the streetside, East Avenue (Fig. 9). The similarity between equivalent BC variation during the day in both measurement sites suggests that primary emissions from road traffic predominantly contribute to poor air quality in Manila North Port and Quezon City.

Impact of Air Pollution on Personal Exposure and Respiratory Tract Deposition

The information about particle number size distribution, as well as externally mixed refractory particles collected from TROPOS measurement sites, were used to determine the respiratory tract deposition (RTD) of both ambient and refractory particles following the methodology used by *Kecorius et al.* [2019] (adopting generalized minute ventilation rate for males at 1.4 m^3 h^{-1}). Based on the observations in Manila North Port, we have estimated the total RTD dose rate of males from ambient particles to be 4.7 × 10^{10} particles per hour, where ultrafine particles contributed to 97% of the total deposited particle number. While an estimated RTD dose rate of 8.1 × 10^{10} particles per hour was observed on the roadside of Quezon City, where 95% of the total deposited particle number was in the ultrafine size range. This means that roadside dwellers in Quezon city have an RTD dose rate that is 1.7 times higher

than people around Manila North Port. Nevertheless, results suggest that inhabitants in Metro Manila may accumulate an order of magnitude higher particle dose than in Europe or the USA.

Moreover, we found that the RTD dose rate of externally mixed refractory particles in Manila North Port and Quezon city was 1.2×10^{10} particles per hour and 5.5×10^{10} particles per hour, where ultrafine EMRP was attributable to 90% and 95% of the total deposition dose, respectively. Concerningly, this means that the roadside dwellers in Quezon city have up to 4.8 times higher RTD of EMRP than people on the port side, and twice more elevated than the results we found in Taft Avenue from our previous study *Kecorius et al.* [2019].

In addition to the RTD derived from the data gathered at both stationary measurements sites, we were able to estimate the personal exposure and RTD of city dwellers during their commute by using the TROPOS-built mobile platform, MERDOC [*Madueño et al.,* 2019], to directly measure the personal exposure and eBC mass RTD. Shortly, the MERDOC measures the ambient aerosol inhaled exclusively through the nose during normal tidal breathing; it is then exhaled through a mouthpiece that flows to the mixing chamber and then dried (<20% RH) to be sampled in a micro-aethalometer and flowmeter. The RTD of equivalent BC is assessed based on the difference between inspired and expired mass concentration relative to the breathed air volume. The Lung Center of the Philippines – Institutional Ethics Review Board (LCP-IERB) granted ethical approval for this experiment. The initial results showed that commuters using PUJs inhale equivalent BC mass concentration twice higher than street pedestrians and up to three times higher respiratory deposition of equivalent BC due to their proximity to the source emission. Our initial results showed that the fraction of particles deposited in the respiratory tract is constant regardless of the amount of inhaled equivalent BC mass concentration. However, personal breathing parameters (e.g., minute ventilation, breathing rate) highly influence final RTD. This was the first study of this type in the highly polluted developing region.

Summary

The TAME-BC project presented a novel approach to integrate the environmental, social, and health sciences in Germany and the Philippines to provide a systematic integrative approach that aims at eBC reduction in Metro Manila. The project started by jointly defining the existing air pollution challenges (complex problem constellation) and investigating solution-orientated goals (plausible future constellations) that reflect the current state of the problem (sustainable constellation) by involving various stakeholders (transition strategies). TROPOS acted as the overall coordinator of the TAME-BC project and the leading institution to evaluate urban air quality and exposure concentrations. This report presents preliminary results from the intensive measurement campaign in Manila North Port and Quezon City that happened in November 2019 – March 2020. On average, lower background pollutant concentrations in Manila North Port suggest that its contribution to urban pollution budged is suppressed by local emissions. High emissions from heavy-duty diesel-powered vehicles and ships in Manila North Port were diluted with fresh air coming from the West. This lowers the observed concentrations of pollutants, which has a decreasing effect on environments further away from the sea.

Further inland, locally emitted high concentrations of pollutants are trapped by concrete canyon-like street topography. From the health perspective – extremely high concentrations of externally mixed refractory particles, observed in Manila North Port and Quezon city, determine an order of magnitude higher respiratory tract deposition doses of pollutants than more economically developed regions, such as Europe or the USA. The preliminary results presented here will be used as the basis of co-produced knowledge relayed to stakeholders for evidenced-supported pollution mitigation strategies. TAME-BC framework presents a practical transdisciplinary approach useful for research endeavors aiming to mitigate emissions in rapidly urbanizing regions beyond Metro Manila.

References

Alas, H. D., Müller, T., Birmili, W., Kecorius, S., Cambaliza, M. O., Simpas, J. B. B., … Wiedensohler, A. (2018). Spatial characterization of black carbon mass concentration in the atmosphere of a southeast Asian megacity: An air quality case study for Metro Manila, Philippines. *Aerosol Air Qual. Res.*, *18*(9), 2301–2317. https://doi.org/10.4209/aaqr.2017.08.0281

Costabile, F., Alas, H., Aufderheide, M., Avino, P., Amato, F., Argentini, S., … Gobbi, G. P. (2017). First results of the "Carbonaceous Aerosol in Rome and Environs (CARE)" Experiment: Beyond current standards for PM10. *Atmosphere*, *8*(12). https://doi.org/10.3390/atmos8120249

Kecorius, S., Müller, T., Birmili, W., Weinhold, K., Müller, K., Tamayo, E., Cayetano, M., Alas, H., Simpas, J., Vallar, E., Hermann, H., Wiedensohler, A., Spatial and temporal distribution of black carbon in the metropolitan area of Manila, Philippines. TROPOS Biennial Report 2014/2015, page 64-67.

Kecorius, S., Madueño, L., Löndahl, J., Vallar, E., Galvez, M. C., Idolor, L. F., … Wiedensohler, A. (2019). Respiratory tract deposition of inhaled roadside ultrafine refractory particles in a polluted megacity of South-East Asia. *Sci. Total Environ.*, *663*, 265–274. https://doi.org/10.1016/j.scitotenv.2019.01.338

Kecorius, S., Madueño, L., Vallar, E., Alas, H., Betito, G., Birmili, W., … Wiedensohler, A. (2017). Aerosol particle mixing state, refractory particle number size distributions and emission factors in a polluted urban environment: Case study of Metro Manila, Philippines. *Atmos. Environ.*, *170*, 169–183. https://doi.org/10.1016/j.atmosenv.2017.09.037

Kecorius, S., Tamayo, E. G., Galvez, M. C., Madueño, L., Betito, G., Gonzaga-Cayetano, M., … Wiedensohler, A. (2018). Activity pattern of school/university tenants and their family members in metro Manila – Philippines. *Aerosol Air Qual. Res.*, *18*(9), 2412–2419. https://doi.org/10.4209/aaqr.2018.02.0069

Madueño, L., Kecorius, S., Andrade, M., & Wiedensohler, A. (2020). Exposure and respiratory tract deposition dose of equivalent black carbon in high altitudes. *Atmosphere*, *11*(6), 1–14. https://doi.org/10.3390/atmos11060598

Madueño, L., Kecorius, S., Birmili, W., Müller, T., Simpas, J., Vallar, E., … Wiedensohler, A. (2019). Aerosol particle and black carbon emission factors of vehicular fleet in Manila, Philippines. *Atmosphere*, *10*(10), 1–15. https://doi.org/10.3390/atmos10100603

Madueño, L., Kecorius, S., Löndahl, J., Müller, T., Pfeifer, S., Haudek, A., … Wiedensohler, A. (2019). A new method to measure real-world respiratory tract deposition of inhaled ambient black carbon. *Environ. Pollut.*, *248*, 295–303. https://doi.org/10.1016/j.envpol.2019.02.021

Robert, A., Kennedy, C., Hoornweg, D., Slavcheva, R., Godfrey, N., Cities, L. S. E., … Gomes, A. (2014). Cities and the New Climate Economy : the transformative role of global urban growth Appendix : Methodology Note, (November), 1–70.

Tõnisson, L., Kunz, Y., Kecorius, S., Madueño, L., Tamayo, E. G., Casanova, D. M., … Macke, A. (2020). From transfer to knowledge co-production: A transdisciplinary research approach to reduce black carbon emissions in Metro Manila, Philippines. *Sustainability (Switzerland)*, *12*(23), 1–19. https://doi.org/10.3390/su122310043

Funding

This research was funded by the German Federal Ministry of Education and Research in the framework of TAME-BC (project number 01LE1903A).

Cooperation

TAME-BC Grant Recipients: Leibniz Institute for Tropospheric Research;
Leibniz Institute for Environmental Medicine; German Development Institute.

Modelling of biogenic VOC emissions and SOA formation

Ralf Wolke, Marie L. Luttkus, Kathrin Gatzsche, Erik H. Hoffmann, Andreas Tilgner, Laurent Poulain, Hartmut Herrmann

Einen wesentlichen Bestandteil des atmosphärischen Aerosols bildet die organische Partikelmasse, deren Großteil sekundär (sekundäres organisches Aerosol, SOA) entweder durch chemische Gasphasenprozesse und anschließender „Gas-to-Partikel"-Partitionierung oder durch chemische Prozesse in der wässrigen Phase entsteht. Durch die Vielzahl an organischen Vorläuferverbindungen und atmosphärischen Abbaupfade ist die SOA-Bildung sehr komplex. Prozess- und Sensitivitätsstudien mit dreidimensionalen atmosphärischen Modellen sind ein Schlüsselinstrument zur Vorhersage und Untersuchung dieser Effekte, bestehender Zusammenhänge und Wechselwirkungen. Deshalb wurden in den letzten Jahren unterschiedliche Modellansätze hierfür in das Modell COSMO-MUSCAT implementiert und für Untersuchungen zur Luftqualität eingesetzt. Mehrere Feld- und Modellstudien haben dabei die besondere Bedeutung von biogenen Emissionen und der genauen Beschreibung ihrer raumzeitlichen Variabilität gezeigt. In *Luttkus et al.* [2022] wurde hierbei der Einfluss des Detaillierungsgrads von Landnutzungsdaten auf Luftqualitätsvorhersagen untersucht. Dabei sind zwei verschiedene Landnutzungsdatensätze für Simulationen mit COSMO-MUSCAT für Deutschland verwendet worden. Einer der Datensätze enthält hierbei detaillierte Informationen für über 100 Baumarten, während der zweite Datensatz lediglich verallgemeinerte Landnutzungsklassen wie Misch- und Nadelwald beinhaltet. Die Modellstudien zeigten erhebliche Unterschiede in den BVOC-Emissionsmustern, wobei die Anwendung von detaillierten Baumarteninformationen zu komplexen Mustern mit einzelnen Emissionsspitzen führt. Im Unterschied dazu resultierten aus gröberen Waldinformationen im Mittel 50 % höhere BVOC-Emissionen.

Die Bildung von SOA wird in COSMO-MUSCAT mit dem 2-Produkt-Ansatz beschrieben, wobei das Ausgangmodul SORGAM [*Schell et al.*, 2001] aktualisiert und um wesentliche Komponenten (z.B. Isopren, Sesquiterpene, HOMs) erweitert wurde. Neben dem auf *Pankow* [1994] basierenden absorptivem Verteilungsansatz, bei dem von einem instantanen Gas-Partikel-Gleichgewicht der Reaktionsprodukte ausgegangen wird, wurde in COSMO-MUSCAT ein kinetischer Ansatz implementiert [*Gatzsche*, 2019]. Dieser Ansatz beschreibt die Aufnahme von gelösten Stoffen in Aerosolpartikeln unter Berücksichtigung von Gasphasendiffusion, Grenzflächenmassentransfer, Partikelphasendiffusion und Partikelphasenreaktionen. Die beiden Modellansätze wurden für Simulationen im Mai 2014 miteinander und mit Feldmessungen verglichen. Der kinetische Ansatz bietet zukünftig die Möglichkeit, die SOA-Partitionierung zeitabhängig und in Abhängigkeit von Partikelgröße und Zusammensetzung sowie in Konkurrenz zu Flüssighasenbildungsprozessen zu beschreiben.

Introduction

Organic aerosols (OA) are omnipresent major components of the atmospheric aerosol mixture and influence numerous atmospheric processes. The quantitative determination of climate and environmental impacts of OA is limited by a number of factors. These include in particular the incomplete understanding of their formation and processing, i.e., how emitted VOCs (volatile organic compounds) lead to the formation of highly oxidized VOCs and consequently to atmospheric OA. A large fraction of OA in the atmosphere is formed secondary (secondary organic aerosol, SOA) by chemical gas-phase processes and subsequent gas-particle-partitioning (gasSOA) or by chemical processes in the aqueous phase (aqSOA). SOA formation is very complex because of the variety of organic precursor

compounds and numerous atmospheric degradation pathways. Thus, the large number of mutually influencing interactions excludes a simple cause-effect analysis. Process and sensitivity studies with three-dimensional atmospheric models are therefore a key tool for predicting and investigating the above-mentioned effects. There are still considerable uncertainties regarding global SOA mass burden, formation mechanisms, and particle product distributions. Here, the impact of the SOA formation mechanisms is emphasized. Furthermore, also plant emissions of biogenic VOCs (BVOCs) are subject to great uncertainty which are important SOA precursors. Each plant species has its own unique VOC emission characteristics that define both emission strength and composition. The oxidation of these highly reactive compounds impacts the tropospheric chemical composition and oxidation budget, and thus is not only linked to SOA but also to ground-level ozone production.

SOA is formed via the oxidation of gas-phase organic precursor compounds by ozone (O_3), hydroxyl radical (OH), nitrate radical (NO_3), or photolysis. Thereby, the functionalization and binding ability of the product molecules result in a decreased volatility [*Hallquist et al.*, 2009]. If the vapor pressure of the oxidized organic compounds is low enough, they can condense on a pre-existing particle surface or form new particles through nucleation. The gas-to-particle partitioning of these highly oxidized VOCs is predominantly described by an absorptive partitioning approach based on gas-particle equilibrium for these compounds [*Pankow*, 1994]. However, recent measurements indicate that the viscosity of SOA particles increases with decreasing relative humidity and that a semi-solid phase state is very likely achieved (*Reid et al.* [2018] and the references therein). Consequently, absorptive partitioning approaches, which are based on a steady equilibrium between gas and particle phase, may indirectly overestimate particle-phase diffusion. Due to their complexity and the associated high computational effort, multiphase processes for SOA formation have so far often only been considered in a simplified form in higher-scale atmospheric models. Furthermore, the absorptive partitioning approach does not consider the influence of the gas-phase diffusion, the particle size and curvature for the gas-to-particle transport of organic compounds.

Significant progress in the development of non-equilibrium partitioning models has been made in recent years, where the particle phase is resolved in different ways. For the chemistry-transport model COSMO-MUSCAT, an approach based on bulk properties applicable not only in box model frameworks but also in CTMs was selected. The utilized kinetic model approach is based on previous studies of *Schwartz and Freiberg* [1981], *Schwartz* [1986], *Sander* [1999], and *Zaveri et al.* [2014], which describe the uptake of solutes in (aqueous) aerosol particles and related processes. Briefly, the model approach considers gas-phase diffusion, interfacial mass transfer, particle-phase diffusion, and particle-phase reactions.

The Chemistry Transport Model (CTM) system COSMO-MUSCAT [*Wolke et al.*, 2012] has been utilized to improve and analyse the SOA approach. Originally, SOA formation in COSMO-MUSCAT is described with SORGAM [*Schell et al.*, 2001] which is based on absorptive partitioning and has been updated and extended recently [*Gatzsche*, 2019; *Luttkus et al.*, 2022]. After successful implementation and testing of the kinetic partitioning approach, several simulations have been performed with COSMO-MUSCAT using both approaches. Simulations with the kinetic model have been performed without (SOA_{kin_A}) and with enabled particle-phase reactivity ($SOA_{kin\_B\text{-}D}$). The results of the different setups are compared with each other and a deactivated particle-phase reaction case (SOA_{kin_A}). Finally, an extended comparison with the TROPOS field site Melpitz was performed. From this detailed evaluation, possible shortcomings of the model framework for this process study have been derived. Up to now, the application of a kinetic partitioning approach with reversible SOA formation in a CTM is unique.

Biogenic emissions

Biogenic emissions from the terrestrial ecosystem are governed by plant species composition due to species-specific characteristics, such as biomass density (BD) and BVOC-specific standard emission potential (SEP). Additionally, climate and environmental impacts regulate BVOC emissions. Crucial for the simulation of BVOC emissions are (i) the applied land use dataset which describes the plant composition within a grid cell, (ii) the BVOC emission parameterization, and (iii) database containing the plant as well as plant and BVOC species specific parameters.

Land use (LU) datasets. Often LU datasets contain generalized LU categories such as plant functional types (PFT), but a more detailed representation on a species level is crucial when investigating the effect of different tree species on air quality. Here,

	coniferous forest	spruce	pine
	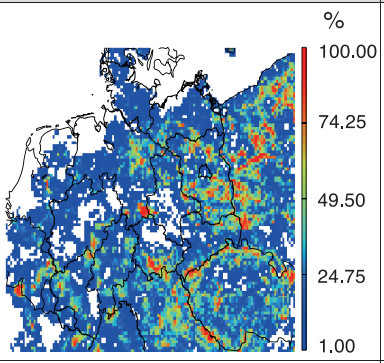	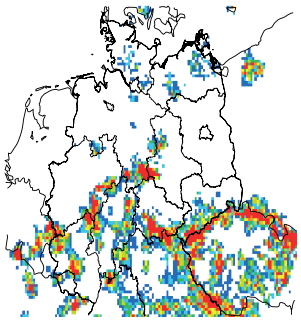	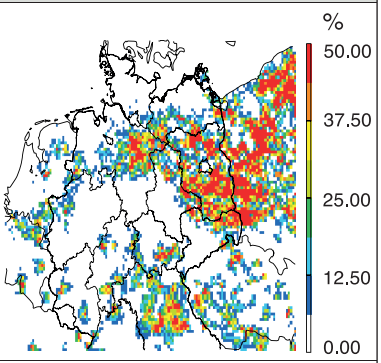
BD (ε)	1000 (5)	1600 (2.5)	700 (5)
α-pinene	71% of monoterpenes (3550)	83% of monoterpenes (3320)	98% of monoterpenes (3430)
limonene	23% of monoterpenes (1150)	10% of monoterpenes (400)	2% of monoterpenes (70)
p-cymene	4% of monoterpenes (200)	0% of monoterpenes (0)	0% of monoterpenes (0)
1.8-cineol	2% of monoterpenes (100)	7% of monoterpenes (280)	0% of monoterpenes (0)

Fig. 1: Main monoterpene emitting tree species with corresponding biomass density BD, emission factor ε, monoterpene emission split, and standard emission factor listed in the parenthesis.

a LU dataset comprising 10 generalized categories (urban areas, mixed land use, coniferous forest, mixed forest, meadow, heath, bushes, sand, mudflats, water bodies) (10_LU) is compared with a detailed dataset of 138 LU classes including 116 tree species, 11 agricultural LU types, and additional vegetated (green urban areas, wetlands, etc.) as well as non-vegetated classes (artificial structure, water bodies, etc.) (138_LU). The detailed LU dataset is based on *Köble and Seufert* [2001]. For both datasets, the percentage of every LU class is given for every grid cell. The spatial distribution and LU composition are crucial for the BVOC emission patterns which themselves govern the spatial distribution and temporal evolution of oxidizing agents, BVOCs and their reaction products. The predominant agricultural LU category for the 10_LU is mixed LU and for the 138_LU non-irrigated arable land, the largest portions of which are located in an area ranging from the Netherlands to Czech Republic with a maximum in central Germany. The LU class mixed forest of the 10_LU comprises all deciduous tree species with main contributions in the middle and south west of the model domain (see Fig. 1). The most common tree species of the 138_LU are beech (middle, south west of domain, spots in northern Poland and Germany), oaks (smaller spots around Berlin and in Poland, higher ratios in the west of domain), and birch (smaller spots throughout the domain, highest ratios in Poland). Needle-leaved tree species are grouped into conifer forest of the 10_LU with highest contribution in the east, especially Brandenburg, and the low mountain range in the south of the model domain. While the tree species distribution of the 138_LU reveals a clear separation between pine mainly in the north east, and spruce in the low mountain range (see Fig. 1).

Biogenic emission scheme. Due to individual LU characteristics, BVOC emission strengths and compositions varies between different tree species and LU categories [*Karl et al.*, 2009b; *Steinbrecher et al.*, 2009] causing various air quality impacts. The algorithm presented here is based on the approach presented by *Steinbrecher et al.* [2009]. The emission E_{SL} (1) for a given land use class L and a specific BVOC S is calculated as follows:

$$E_{SL} = A_L \times BD_L \times SEP_{SL} \times \gamma$$

Where A_L is the area covered by the land use class (in m^2), BD_L is the foliage biomass density (in g m^{-2}), SEP is the standard BVOC and land use specific emission potential (in µg g^{-1} h^{-1}) standardized for 30°C and 1000 µmol m^{-2} s^{-1} photosynthetically active photon flux density (PPFD). γ denotes a correction factor for seasonality, temperature, and light. BVOC emissions are highly dependent on temperature and light availability. The BVOC emission scheme considers isoprene, 17 monoterpenes, sesquiterpenes (β-caryophyllene), and oxygenated BVOCs (BOVOCs: methanol, acetone, ethanol, acetaldehyde, formaldehyde, formic acid, acetic acid).

Emission database. The parameters needed for the emission scheme, e.g., BD and SEP are taken from *Steinbrecher et al.* [2009] as well as from

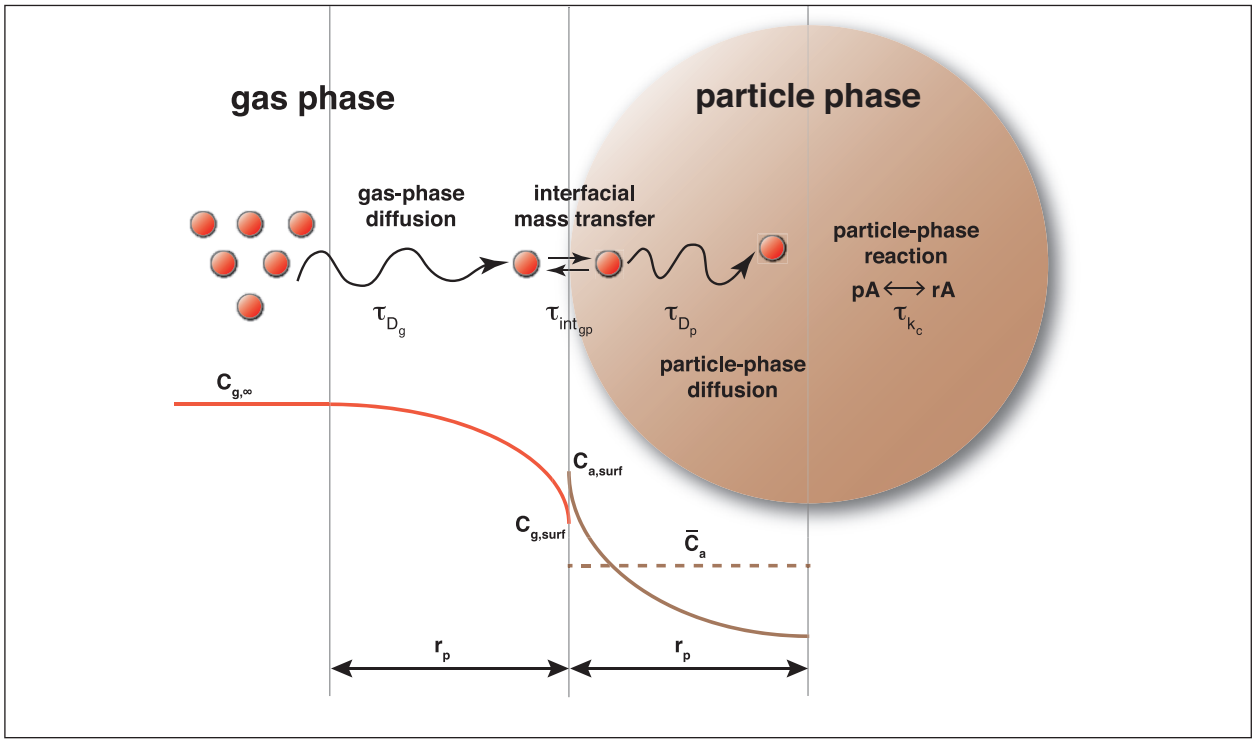

Fig. 2: Resistances of mass transfer included in COSMO-MUSCAT for partitioning of organic species. The quantities τ_{D_g}, τ_{int}, τ_{D_p}, and τ_{k_c} denote characteristic time scales for gas-phase diffusion, interfacial mass transfer, particle-phase diffusion, and chemical reactions that affect the partitioning in the kinetic approach (in contrast to the absorptive approach).

Oderbolz et al. [2013] but the use of other datasets (such as *Guenther et al.* [2006]; *Guenther et al.* [2012]; *Karl et al.* [2009b]) might modify the BVOC emission strengths as well as the compositions mainly due to varying emission splits and corresponding SEPs.

SOA formation

After the emission of biogenic as well anthropogenic VOCs (AVOCs), these highly reactive volatile compounds can quickly react with ozone, hydroxyl and nitrate radicals [*Atkinson and Arey*, 2003; *Luttkus et al.*, 2022; *Oderbolz et al.*, 2013] producing oxidized reaction products of lower volatility and thereby contributing to SOA formation via new particle formation or condensation onto pre-existing particles [*Jokinen et al.*, 2015; *Pankow*, 1994; *Riccobono et al.*, 2014]. So far, the intricate and highly complex SOA formation processes are highly simplified in chemistry mechanisms and SOA modules for the use in CTMs.

Chemistry mechanism. In COSMO-MUSCAT the chemistry mechanism RACM-MIM2-ext [*Karl et al.*, 2006; *Stockwell et al.*, 1997] is used but was equipped with additional reactions for sesquiterpenes [*Karl et al.*, 2009a]. Monoterpenes are grouped into α-pinene (API) and limonene (LIM), therefore the 17 monoterpenes considered in the BVOC emission algorithm from *Steinbrecher et al.* [2009] have been grouped as follows: (i) cyclic terpenes with one double bond are treated as API, (ii) monoterpene with more than one double bond as LIM, (iii) p-cymene as xylene, (iv) 1.8-cineol as RACM lumped species HC8. Individual VOCs have their preferred oxidising partner: (i) AVOCs mainly OH radicals, (ii) isoprene OH followed by NO_3 and ozone, (iii) API and LIM mainly OH during day and NO_3 during night but ozone also possible, (iv) p-cymene OH, (v) 1,8-cineol OH, (vi) sesquiterpene ozone followed by NO_3 and OH, and (vii) BOVOCs OH. Progressing chemical functionalisation leads to a further reduction of the volatility of reaction products and so produces SOA, whereby the SOA forming potential is VOC-oxidant reaction specific and additionally depends on the total absorbed organic matter available.

Updated SOA module for the absorptive partitioning approach. SOA formation for the absorptive partitioning approach is based on the 2-product approach SORGAM [*Schell et al.*, 2001]. As SORGAM only considers SOA pathways for AVOCs and monoterpene with OH and O_3 radicals, further pathways have been incorporated to ensure SOA formation from all BVOCs. Therefore, reactions of monoterpenes with NO_3 [*Griffin et al.*, 1999], isoprene

[*Kroll et al.*, 2006; *Ng et al.*, 2008], and sesquiterpenes [*Hoffmann et al.*, 1997; *Karl et al.*, 2009a] were added. Furthermore, also highly-oxidised multifunctional organic molecules (HOMs, monoterpene: [*Berndt et al.*, 2016b; *Jokinen et al.*, 2015]; sesquiterpenes: *Richters et al.* [2016]; isoprene: *Berndt et al.* [2016a]) are included (for more details see *Gatzsche et al.* [2018] and *Luttkus et al.* [2022]).

Kinetic partitioning approach. The kinetic partitioning approach even further improves the SOA description as it considers the reaction products as solutes in aerosol particles including their uptake and in-particle processes (gas- and particle-phase diffusion, interfacial mass transfer, particle-phase reactions; see Fig. 2). The second Fick's law is used to describe the diffusion flux of a solute in the particle phase considering a first order particle-phase reaction. The solution for taking into account of a first-order chemical reaction in the particle phase was already considered for droplets by *Schwartz and Freiberg* [1981]. This approach was already applied for various investigations in the aqueous phase (e.g., *Sander* [1999], *Shi and Seinfeld* [1991]) and in the particle phase [*Zaveri et al.*, 2014]. The approach utilized is based on a concentration profile in the particle (see Fig. 3), which is described by a steady state and a transient term. In the case of high viscosity or particle radii larger than 20 µm, this leads to concentration enrichment in the peripheral area of the particle. The basic derivation of the kinetic partitioning approach and the proof of convergence of the transient term as well as an approximation for this term are shown in *Gatzsche* [2019]. The transient term becomes more important for semi-solid and nonreactive particles.

This approach increases the degrees of freedom for phase transfer compared to the absorptive distribution approach and therefore measurements are required to characterize the particle phase properties.

For polydisperse aerosol populations, the following model equations are used for the gas-phase:

$$\frac{\mathrm{d}C_{g,i}}{\mathrm{d}t} = -\sum_{m=1}^{M} \frac{4}{3}\pi r_{p,m}^{3} N_m k_{trans,i,m} \left(C_{g,i} - \frac{\overline{C}_{a,i,m}}{Q_{i,m} K_{om,i,m} M_{o,m}} \right)$$

and the particle-phase:

$$\frac{\mathrm{d}\overline{C}_{a,i,m}^{tot}}{\mathrm{d}t} = \frac{4}{3}\pi r_{p,m}^{3} N_m k_{trans,i,m} \left(C_{g,i} - \frac{\overline{C}_{a,i,m}}{Q_{i,m} K_{om,i,m} M_{o,m}} \right) - k_{c,i} \overline{C}_{a,i,m}$$

For a certain size class m and compound i. Here, C_g denotes the gas-phase, $\overline{C}_a$ the average particle-phase and M_o the total organic mass concentration in the particle phase (µg m^{-3}). k_c describes the chemical reaction rate constant of the solute within the particle phase (s^{-1}), K_{om} the equilibrium gas/particle partitioning coefficient (m^3 µg^{-1}), and the combined mass transfer coefficient from the gas phase and the interface k_{trans} (s^{-1}). The steady state term of the concentration profile Q=Q(D_b,k_c,r_p) is a function of the particle-phase bulk diffusion coefficient D_b (m^2 s^{-1}), the rate constant k_c (s^{-1}), and the particle radius r_p (m). With the knowledge of the aerosol number N_m (m^{-3}) for each class m and the corresponding particle radius r_p, the associated average particle-phase concentration $\overline{C}_a^{tot}$ of the polydisperse aerosol population can be computed. Usually, the right-hand side of the equations contains additional reaction terms to describe the chemical

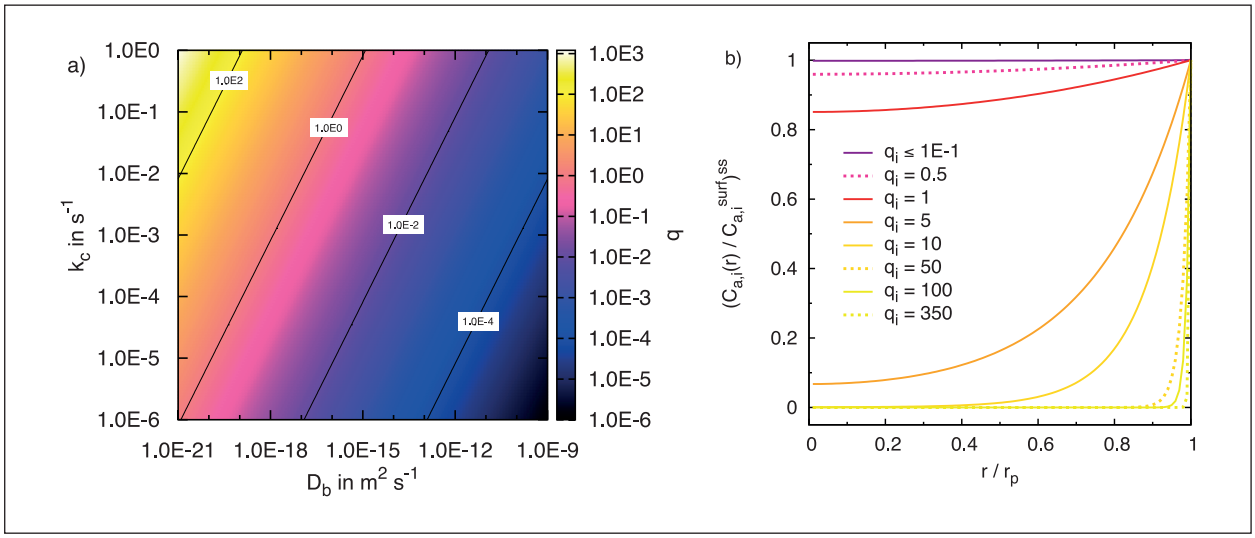

Fig. 3: a) Dimensionless diffusion-reaction parameter q_i ($q_i = r_p(k_{c,i}/D_{b,i})^{1/2}$), which is the square root of the second Damköhler number and b) the resulting particle-phase concentration profiles r / r_p at steady state.

transformations in the gas and particle phase, respectively. In this study, an additional backward reaction with the reaction constant k_b (s^{-1}) was implemented in the particle phase to further refine the approach of pseudo-first-order rate constants and, thus, investigate the influence of particle-phase chemical reactions in more detail [*Gatzsche et al.*, 2017]. Backward reactions describe the reaction of the aged organic particle-phase compounds to the original partitioned organic compounds that exchange directly with the gas phase.

The simulations here are obtained using the mass-based approach of COSMO-MUSCAT considering one size section for organic aerosol which comprises primary and secondary organic matter (POA, SOA). A fixed particle number of $N = 10^9$ m^{-3} and a particle radius of $r_p = 1$ µm were assumed. The initialized monodisperse particle population is representative for the accumulation mode, which accounts for most of the aerosol surface area. It is known, that particles in this mode have a relatively long lifetime and are formed from coagulation of particles in the nuclei mode or from condensation of vapours on pre-existing particles. Here, POA is obtained from the MACC emission database without any size classification.

Results of the case study May 2014

Setup. The simulations are performed without any data assimilation and nudging only by forcing via the boundaries. To keep the long-term evolution of meteorological fields as close as possible to observations, the integration period was divided into overlapping short term cycles. Each of these cycles consists of a one-day COSMO pre-run for spin-up of the meteorological fields initialized and forced with COSMO-DE re-analysis data provided by the German weather service (DWD, Offenbach) followed by a two-day run with the online-coupled model system COSMO-MUSCAT. MUSCAT restarts with the final chemical concentration fields of the previous cycle. COSMO-MUSCAT simulations are performed for May 2014 for the model domain centred over north Germany and with a grid resolution of 0.0625° x 0.0625° (7 km x 7 km). The chemical boundary values are generated by COSMO-MUSCAT runs on the European domain. A 10-day spin-up time is applied before simulating the time period of interest.

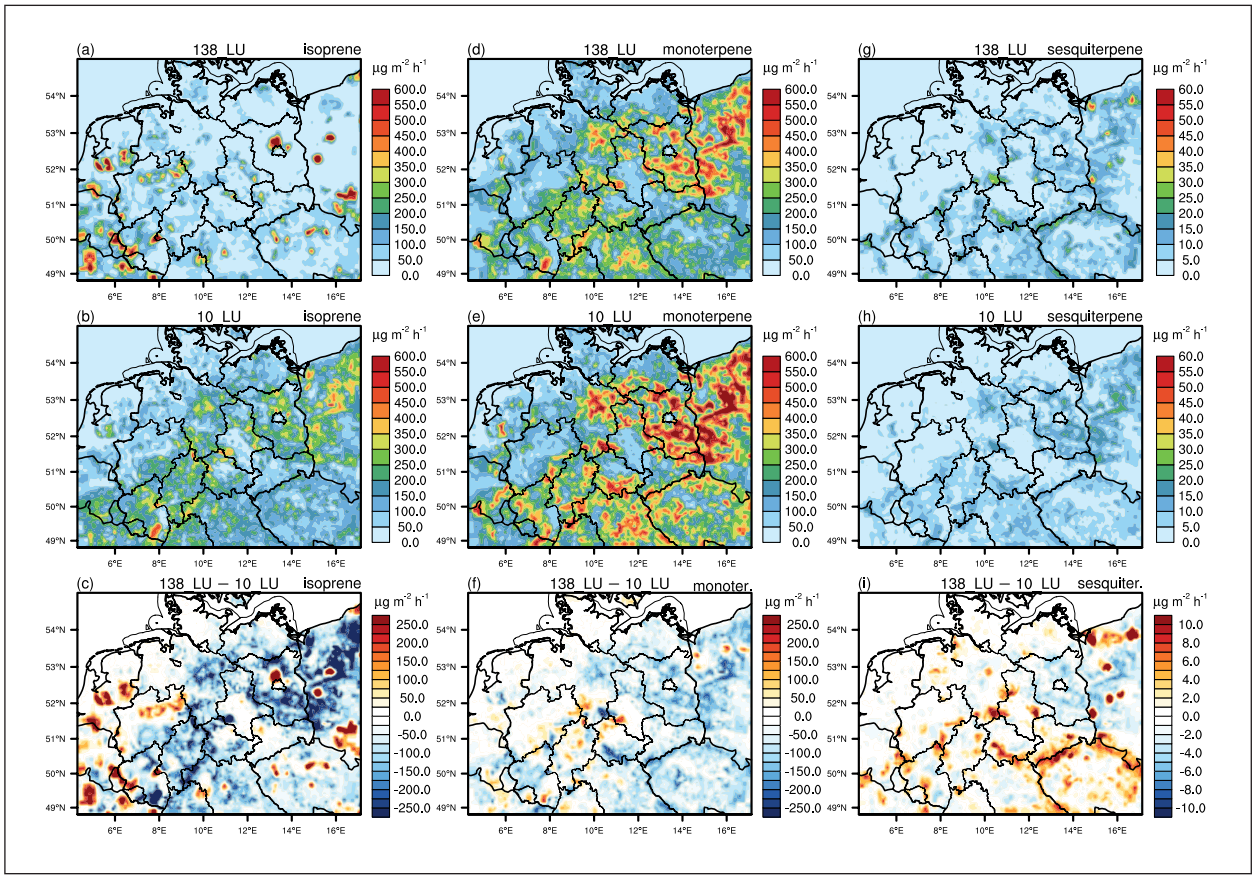

Fig. 4: Average isoprene emission for (a) the 138_LU and (b) 10_LU, monoterpene emission for (d) the 138_LU and (e) 10_LU, sesquiterpene emission for (g) the 138_LU and (h) 10_LU; as well as difference plots (c), (f) and (i) for the second half of May (15-31 May 2014).

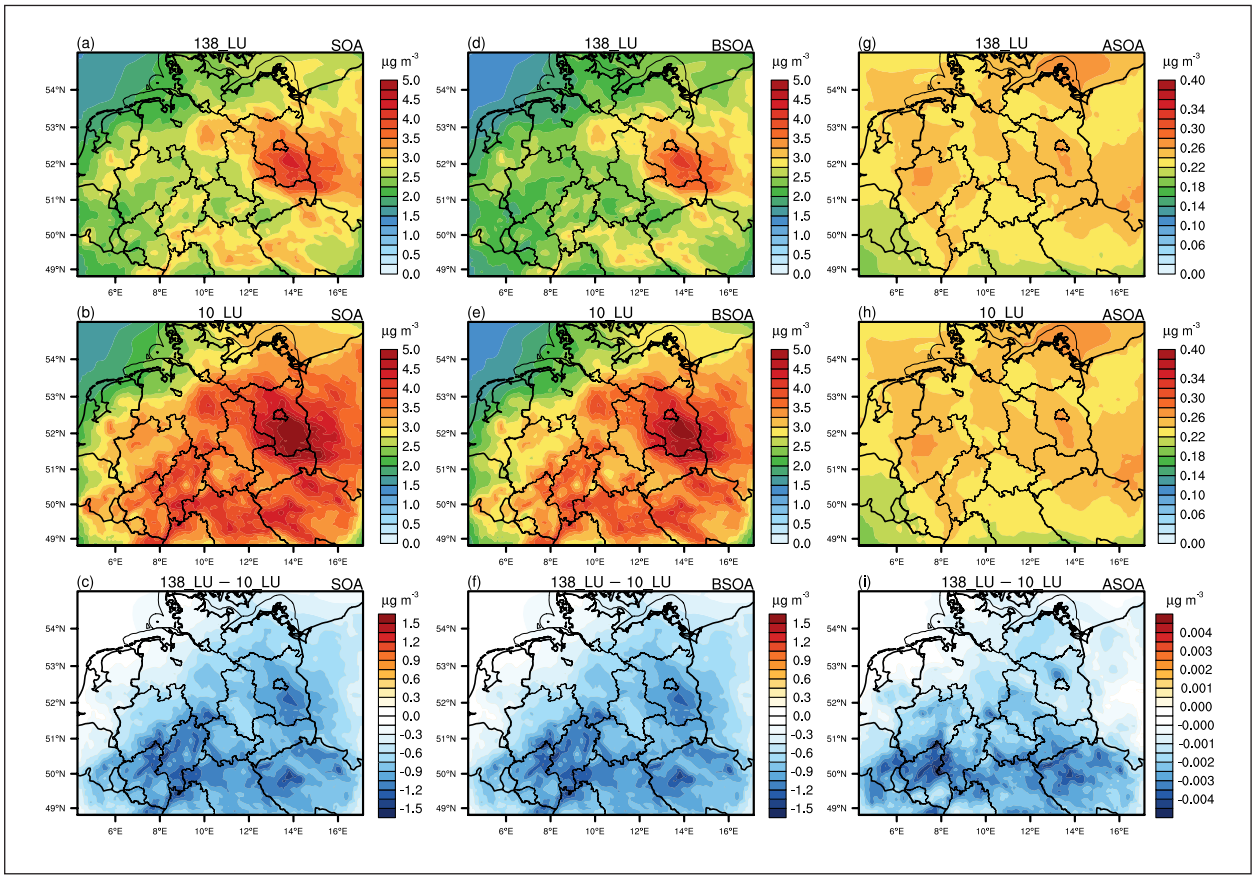

Fig. 5: Average total SOA for (a) the 138_LU and (b) 10_LU, biogenic SOA for (d) the 138_LU and (e) 10_LU SOA, anthropogenic SOA concentrations for (g) the 138_LU and (h) 10_LU; as well as difference plots (c), (f) and (i) for the second half of May (15-31 May 2014).

Tree species vs. forest level information. The influence of LU dataset detailedness on air quality is investigated using average map plots and the difference between the results using the two datasets: 138_LU – 10_LU. Figure 4 shows the isoprene, monoterpene, and sesquiterpene emission during the second half of May (15-31 May 2014). Compared to the generalized LU dataset, the detailed dataset leads to more distinct emission patterns. Isoprene emission is dominated by oaks resulting in high emission spots in the western model domain as well as few spots around Berlin and in Poland. Additional sources are poplar, maple, Douglas fir, robinia, willow, and elm which do not frequently occur in the model domain or show lower emission potentials than their generalized LU categories of the 10_LU. Therefore, the differences between the two datasets are negative except for the oak emission spots. LIM and p-cymene emissions are reduced for all tree species of the 138_LU. API emission is reduced for oak and spruce while for beech higher emissions are reached using 138_LU. Higher sesquiterpene emissions are linked to birch and spruce; BOVOC emissions to beech and spruce; 1.8-cineol to spruce. Overall, an overestimation of 50% of BVOC (without BOVOCs) emissions is invoked by the generalized LU during May 2014.

Different BVOCs have individual reaction rate constants resulting in species-specific dependencies between BVOCs and their oxidizing partners which affects the distribution and evolution of their concentrations. For isoprene, an inverse correlation with OH and for monoterpene with NO_3 radicals can be identified [*Luttkus et al.*, 2022]. Therefore, oaks decrease and pine trees (defined as non-isoprene emitters) increase the OH radical concentration, and, for NO_3 radical, beech are the dominating sink. For May 2014, the use of the generalized LU dataset leads to altered NO_x (±2.5%), ozone (+2.5%), OH (±50%), and NO_3 radical (-70%) concentrations. Monoterpene-NO_3 reaction products are the dominant SOA source in the model domain. The highest monoterpene emissions occur in coniferous forest for the 10_LU and beech and pine forests for the 138_LU. But the elevated BOVOC emissions in the southern model domain due to spruce and beech forests, suppresses SOA formation as OH is depleted and BOVOC oxidation itself does not yield to SOA. This reduces the overall organic matter available for the absorptive approach

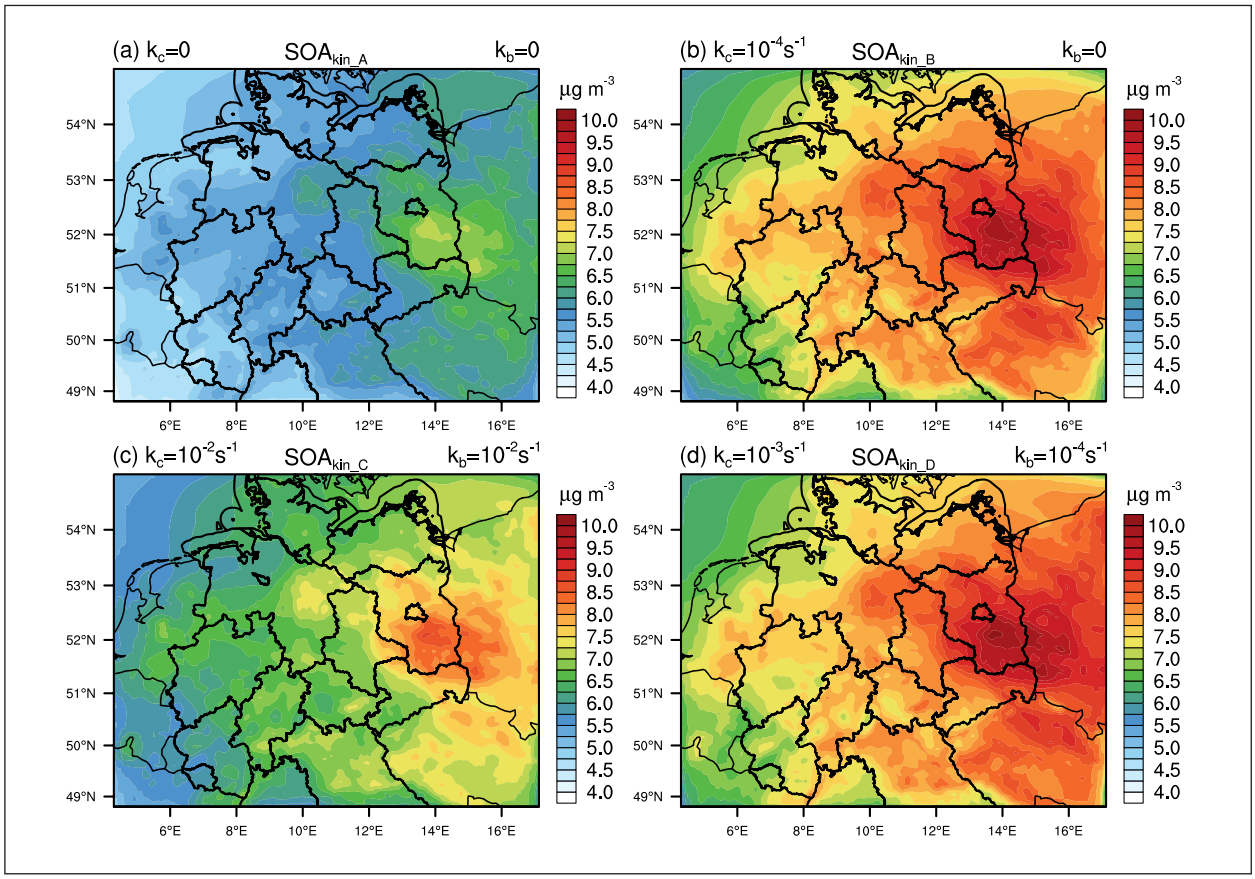

Fig. 6: Average SOA mass concentrations of the kinetic partitioning approach in the surface layer for different particle-phase reactivities (a) SOA_{kin_A}: k_c = 0 s^{-1}, (b) SOA_{kin_B}: k_c = 10^{-4} s^{-1}, (c) SOA_{kin_C}: k_c = k_b = 10^{-2} s^{-1} and (d) SOA_{kin_D}: k_c = 10^{-3} s^{-1} & k_b = 10^{-4} s^{-1} during 15-31 May 2014.

which additionally lowers the SOA contribution of the other SOA substances. This is evident by the reduced anthropogenic SOA contribution (ASOA) in Fig. 5 for which changes are solely invoked by BVOC emission changes and their entailed chemical degradation and SOA contribution (BSOA) as anthropogenic emissions are the same for both simulations. Therefore, pine trees are the main SOA source for the 138_LU (Fig. 5). Even though BOVOCs are not yielding SOA, their temporal evolution seems to be an excellent proxy for SOA [*Luttkus et al.*, 2022].

Intercomparison of the absorptive and kinetic partitioning approach. Model simulations using the absorptive partitioning approach with the SORGAM parametrization (SOA_{abs}) and the kinetic partitioning approach for liquid aerosol particles (D_b =10^{-9} m^2 s^{-1}) with a non-reactive particle-phase (SOA_{kin_A} (k_c = 0 s^{-1})) are compared in this section. In detail, we have analysed monthly average concentrations of May 2014. In Fig. 6, the average SOA surface layer mass concentration simulated for 15-31 May 2014 for four different scenarios using the kinetic approach is shown (a) SOA_{kin_A}: k_b=0 s^{-1}, k_c=0 s^{-1}; (b) SOA_{kin_B} with moderate irreversible particle-phase reactivity: k_c=10^{-4} s^{-1}, k_b=0 s^{-1}; (c) SOA_{kin_C} with reversible particle-phase reactions: k_c=10^{-2} s^{-1}, k_b=10^{-2} s^{-1}; (d) SOA_{kin_D} with reversible particle-phase reactions: k_c=10^{-3} s^{-1}, k_b=10^{-4} s^{-1}. Here, k_b denotes the backward reaction rate constant for a particle-phase reaction. The SOA mass distribution is very similar between simulations and only concentration differences can be observed. The maximum SOA mass occurs in the eastern part of the model domain and is highest for SOA_{kin_B} and SOA_{kin_D}. In this region and in the south of Germany (Bavaria), the kinetic partitioning approach forms more SOA. The region with the highest SOA mass concentrations is also the warmest and driest region in May 2014, this invokes higher emissions of SOA precursors (mainly monoterpenes) and ambient oxidant levels. Figure 7 shows the absolute differences between the average SOA concentrations between SOA_{kin_A} for 15-31 May 2014 for three different simulations with the kinetic and one with the absorptive approach (SOA_{abs}). The consideration of particle-phase reactions leads to an increased SOA formation. However, measuring the rates of these particle-phase reactions is difficult and therefore there are no solid measurements reported at this time. But, it is known from the literature [*Hallquist et al.*, 2009]

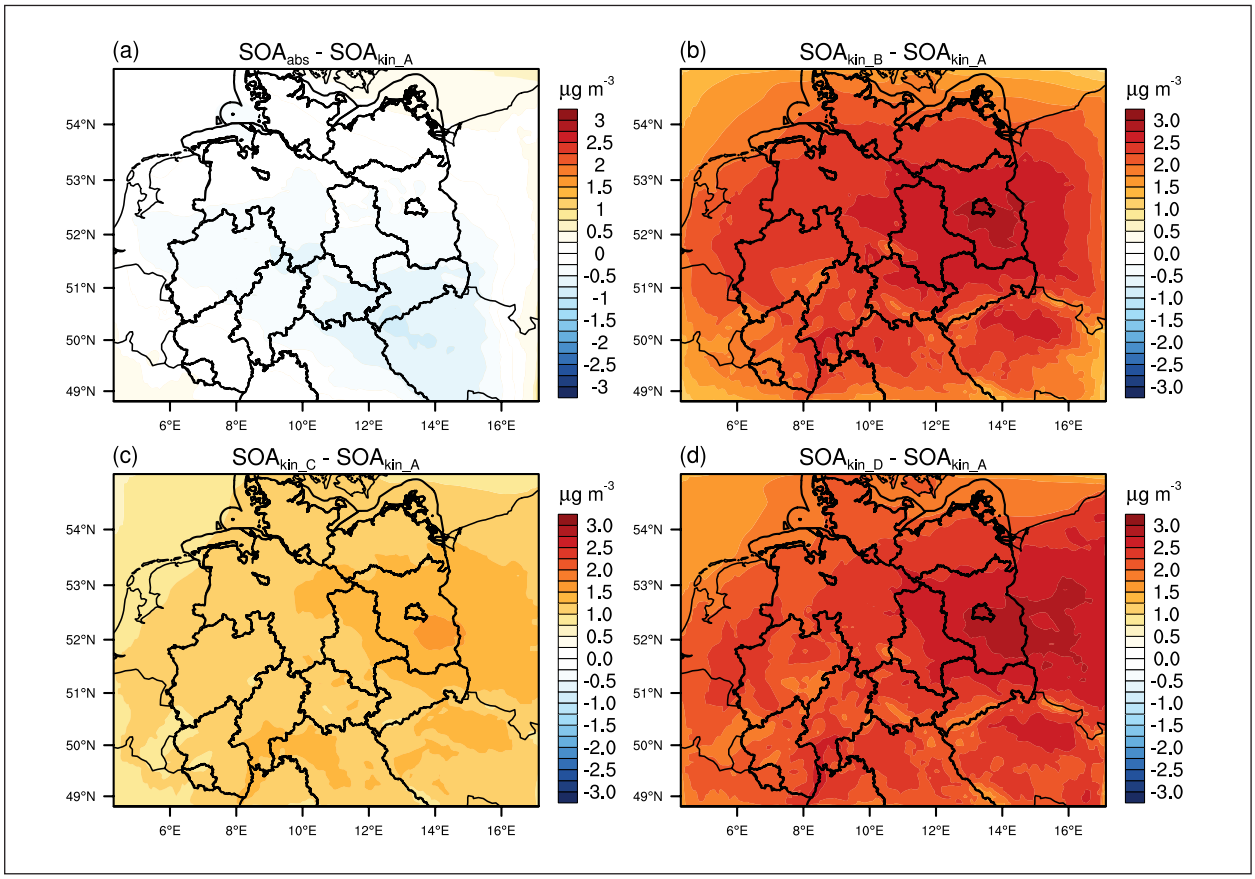

Fig. 7: Absolute differences of the average SOA mass concentrations (ΔSOA) in the surface layer for 15-31 May 2014 comparing the kinetic partitioning approach with different reactivities (a) ΔSOA = SOA$_{abs}$ - SOA$_{kin_A}$, (b) ΔSOA = SOA$_{kin_B}$ - SOA$_{kin_A}$, (c) ΔSOA = SOA$_{kin_C}$ - SOA$_{kin_A}$, and (d) ΔSOA = SOA$_{kin_D}$ - SOA$_{kin_A}$.

that these particle-phase reactions affect the properties of organic aerosols and may be the reason for the underestimated SOA formation in existing models in the past.

Comparison with measurements. The results of the different model scenarios were compared to the PM$_1$ organic mass (OM) concentration measured by an Aerodyne High-Resolution Time of Flight Aerosol Mass Spectrometer (HR-ToF-AMS, *DeCarlo et al.* [2006]). Figure 8 shows the measured and modelled time series for the OM concentration in Melpitz during the second half of May 2014. This figure indicates for the largest part an agreement between the measured

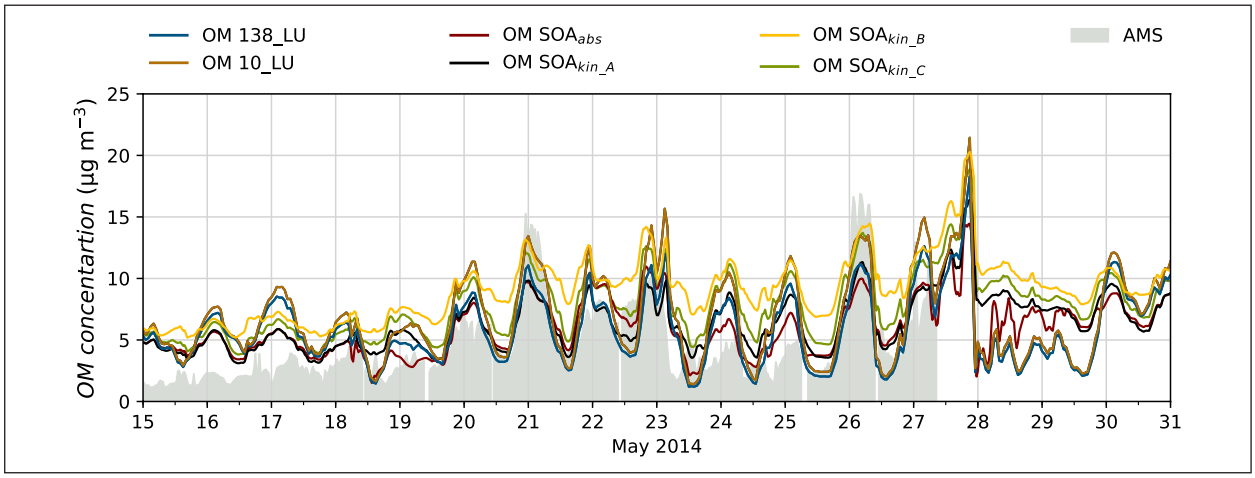

Fig. 8: Comparison of the modelled and measured organic mass concentrations for Melpitz (15-31 May 2014).

and simulated organic mass concentrations. The AMS measurements are representative of PM_1 and the simulated organic mass refers to PM_{10}. Since POA from the MACC emission database is considered and a mass-based approach is utilized for the SOA description, no differentiation of the organic mass according to the particle sizes is possible. The deviations between the simulations and the AMS measurements in this period could thus be partly ascribed to the distribution of the organic mass to different particle sizes.

The temporal development of the SOA mass concentration for both simulation methods (absorptive, kinetic) correlates very well. Due to the non-instantaneous partitioning of the kinetic approach, the organic mass evolves with a slight temporal delay with respect to the absorptive approach and shows higher day-time values.

Conclusions

To analyse the effect of LU dataset detailedness, a tree species specific BVOC emission split was integrated into the model system COSMO-MUSCAT. Furthermore, to include more BVOC SOA pathways, the SOA module SORGAM was further extended. The comparison between the two LU datasets reveals a significant impact on BVOC emission strengths, composition, and patterns which strongly influence the chemical composition of the troposphere including regional changes in SOA concentrations of up to 60%.

Moreover, the representation of SOA formation and related processes in atmospheric models has been improved by implementing a kinetic partitioning approach in order to gain an advanced understanding of atmospheric organic aerosol and its processing in the troposphere. Particularly, COSMO-MUSCAT was enhanced by a kinetic description of the gas-to-particle partitioning of organic compounds and was applied with a mass-based approach for process studies. An intercomparison of simulations and comparison with field measurements demonstrated the applicability of the kinetic partitioning approach. Simulations comparing both partitioning approaches for a non-reactive particle phase show similar results with slightly higher average SOA mass concentrations for the kinetic partitioning approach. Up to 0.54 µg m^{-3} or 11% more SOA was simulated with the kinetic approach in the modelled period. In the model region, the temporal variations of the organic mass concentration at Melpitz were captured by the model for both partitioning approaches. Moreover, the sensitivity of the SOA formation on the particle-phase reactivity was studied. The average SOA mass for May 2014 was increased between 13 – 50% depending on the particle-phase reaction rate coefficient and the reversibility of the reactions.

The described developments qualify the model system COSMO-MUSCAT to represent the important but very complex processes of SOA formation in a moderate way. However, the investigations also reveal significant potential for further model improvement, which will be addressed in the next years with different approaches (e.g., advanced chemical mechanisms, size-resolved and composition-dependent partitioning schemes, detailed emission models).

References

Atkinson, R., and J. Arey (2003), Atmospheric degradation of volatile organic compounds, *Chem. Rev.*, *103*(12), 4605-4638, https://doi.org/10.1021/cr0206420.

Berndt, T., H. Herrmann, M. Sipila, and M. Kulmala (2016a), Highly Oxidized Second-Generation Products from the Gas-Phase Reaction of OH Radicals with Isoprene, *J. Phys. Chem. A*, *120*(51), 10150-10159, https://doi.org/10.1021/acs.jpca.6b10987.

Berndt, T., S. Richters, T. Jokinen, N. Hyttinen, T. Kurten, R. V. Otkjaer, H. G. Kjaergaard, F. Stratmann, H. Herrmann, M. Sipila, M. Kulmala, and M. Ehn (2016b), Hydroxyl radical-induced formation of highly oxidized organic compounds, *Nat. Commun.*, *7*, 13677, https://doi.org/10.1038/ncomms13677.

DeCarlo, P. F., J. R. Kimmel, A. Trimborn, M. J. Northway, J. T. Jayne, A. C. Aiken, M. Gonin, K. Fuhrer, T. Horvath, K. S. Docherty, D. R. Worsnop, and J. L. Jimenez (2006), Field-deployable, high-resolution, time-of-flight aerosol mass spectrometer, *Anal. Chem.*, *78*(24), 8281-8289, https://doi.org/10.1021/ac061249n.

Gatzsche, K. (2019), Investigation of gasSOA formation by parcel and 3-D modeling, PhD thesis, 146 pp., University of Leipzig, Leipzig.

Gatzsche, K., Y. Iinuma, A. Tilgner, A. Mutzel, T. Berndt, and R. Wolke (2017), Kinetic modeling studies of SOA formation from α-pinene ozonolysis, *Atmos. Chem. Phys.*, *17*(21), 13187-13211, https://doi.org/10.5194/acp-17-13187-2017.

Gatzsche, K., Y. Iinuma, A. Mutzel, T. Berndt, L. Poulain, A. Tilgner, and R. Wolke (2018), Kinetic Modeling of SOA Formation for alpha- and beta-Pinene, paper presented at Air Pollution Modeling and its Application XXV, Springer International Publishing, Cham, 2018.

Griffin, R. J., D. R. Cocker, R. C. Flagan, and J. H. Seinfeld (1999), Organic aerosol formation from the oxidation of biogenic hydrocarbons, *J. Geophys. Res.*, *104*(D3), 3555-3567, https://doi.org/10.1029/1998jd100049.

Guenther, A. B., T. Karl, P. Harley, C. Wiedinmyer, P. I. Palmer, and C. Geron (2006), Estimates of global terrestrial isoprene emissions using MEGAN (Model of Emissions of Gases and Aerosols from Nature), *Atmos. Chem. Phys.*, *6*(11), 3181-3210, https://doi.org/10.5194/acp-6-3181-2006.

Guenther, A. B., X. Jiang, C. L. Heald, T. Sakulyanontvittaya, T. Duhl, L. K. Emmons, and X. Wang (2012), The Model of Emissions of Gases and Aerosols from Nature version 2.1 (MEGAN2.1): an extended and updated framework for modeling biogenic emissions, *Geosci. Model Dev., 5*(6), 1471-1492, https://doi.org/10.5194/gmd-5-1471-2012.

Hallquist, M., J. C. Wenger, U. Baltensperger, Y. Rudich, D. Simpson, M. Claeys, J. Dommen, N. M. Donahue, C. George, A. H. Goldstein, J. F. Hamilton, H. Herrmann, T. Hoffmann, Y. Iinuma, M. Jang, M. E. Jenkin, J. L. Jimenez, A. Kiendler-Scharr, W. Maenhaut, G. McFiggans, T. F. Mentel, A. Monod, A. S. H. Prévôt, J. H. Seinfeld, J. D. Surratt, R. Szmigielski, and J. Wildt (2009), The formation, properties and impact of secondary organic aerosol: current and emerging issues, *Atmos. Chem. Phys.*, *9*(14), 5155-5236, https://doi.org/10.5194/acp-9-5155-2009.

Hoffmann, T., J. R. Odum, F. Bowman, D. Collins, D. Klockow, R. C. Flagan, and J. H. Seinfeld (1997), Formation of Organic Aerosols from the Oxidation of Biogenic Hydrocarbons, *Atmos. Chem. Phys.*, *26*(2), 189-222, https://doi.org/10.1023/A:1005734301837.

Jokinen, T., T. Berndt, R. Makkonen, V. M. Kerminen, H. Junninen, P. Paasonen, F. Stratmann, H. Herrmann, A. B. Guenther, D. R. Worsnop, M. Kulmala, M. Ehn, and M. Sipila (2015), Production of extremely low volatile organic compounds from biogenic emissions: Measured yields and atmospheric implications, *Proc. Nat. Acad. Sci.*, *112*(23), 7123-7128, https://doi.org/10.1073/pnas.1423977112.

Karl, M., K. Tsigaridis, E. Vignati, and F. Dentener (2009a), Formation of secondary organic aerosol from isoprene oxidation over Europe, *Atmos. Chem. Phys.*, *9*(18), 7003-7030, https://doi.org/10.5194/acp-9-7003-2009.

Karl, M., A. Guenther, R. Köble, A. Leip, and G. Seufert (2009b), A new European plant-specific emission inventory of biogenic volatile organic compounds for use in atmospheric transport models, *Biogeosciences*, *6*(6), 1059-1087, https://doi.org/10.5194/bg-6-1059-2009.

Karl, M., H. P. Dorn, F. Holland, R. Koppmann, D. Poppe, L. Rupp, A. Schaub, and A. Wahner (2006), Product study of the reaction of OH radicals with isoprene in the atmosphere simulation chamber SAPHIR, *J. Atmos. Chem.*, *55*(2), 167-187, https://doi.org/10.1007/s10874-006-9034-x.

Köble, R., and G. Seufert (2001), Novel Maps for Forest Tree Species in Europe., Torino, Italy.

Kroll, J. H., N. L. Ng, S. M. Murphy, R. C. Flagan, and J. H. Seinfeld (2006), Secondary organic aerosol formation from isoprene photooxidation, *Environ. Sci. Technol.*, *40*(6), 1869-1877, https://doi.org/10.1021/es0524301.

Luttkus, M. L., E. H. Hoffmann, L. Poulain, A. Tilgner, and R. Wolke (2022), The effect of land use classification on the gas-phase and particle composition of the troposphere: tree species vs. forest type information., *J. Geophys. Res. - Atmos.*, *in review.*

Ng, N. L., A. J. Kwan, J. D. Surratt, A. W. H. Chan, P. S. Chhabra, A. Sorooshian, H. O. T. Pye, J. D. Crounse, P. O. Wennberg, R. C. Flagan, and J. H. Seinfeld (2008), Secondary organic aerosol (SOA) formation from reaction of isoprene with nitrate radicals (NO_3), *Atmos. Chem. Phys.*, *8*(14), 4117-4140, https://doi.org/10.5194/acp-8-4117-2008.

Oderbolz, D. C., S. Aksoyoglu, J. Keller, I. Barmpadimos, R. Steinbrecher, C. A. Skjøth, C. Plaß-Dülmer, and A. S. H. Prévôt (2013), A comprehensive emission inventory of biogenic volatile organic compounds in Europe: improved seasonality and land-cover, *Atmos. Chem. Phys.*, *13*(4), 1689-1712, https://doi.org/10.5194/acp-13-1689-2013.

Pankow, J. F. (1994), An absorption model of the gas/aerosol partitioning involved in the formation of secondary organic aerosol, *Atmos. Environ.*, *28*(2), 189-193, https://doi.org/10.1016/1352-2310(94)90094-9.

Reid, J. P., A. K. Bertram, D. O. Topping, A. Laskin, S. T. Martin, M. D. Petters, F. D. Pope, and G. Rovelli (2018), The viscosity of atmospherically relevant organic particles, *Nat. Commun.*, *9*(1), 956, https://doi.org/10.1038/s41467-018-03027-z.

Riccobono, F., S. Schobesberger, C. E. Scott, J. Dommen, I. K. Ortega, L. Rondo, J. Almeida, A. Amorim, F. Bianchi, M. Breitenlechner, A. David, A. Downard, E. M. Dunne, J. Duplissy, S. Ehrhart, R. C. Flagan, A. Franchin, A. Hansel, H. Junninen, M. Kajos, H. Keskinen, A. Kupc, A. Kurten, A. N. Kvashin, A. Laaksonen, K. Lehtipalo, V. Makhmutov, S. Mathot, T. Nieminen, A. Onnela, T. Petaja, A. P. Praplan, F. D. Santos, S. Schallhart, J. H. Seinfeld, M. Sipila, D. V. Spracklen, Y. Stozhkov, F. Stratmann, A. Tome, G. Tsagkogeorgas, P. Vaattovaara, Y. Viisanen, A. Vrtala, P. E. Wagner, E. Weingartner, H. Wex, D. Wimmer, K. S. Carslaw, J. Curtius, N. M. Donahue, J. Kirkby, M. Kulmala, D. R. Worsnop, and U. Baltensperger (2014), Oxidation products of biogenic emissions contribute to nucleation of atmospheric particles, *Science*, *344*(6185), 717-721, https://doi.org/10.1126/science.1243527.

Richters, S., H. Herrmann, and T. Berndt (2016), Highly Oxidized RO2 Radicals and Consecutive Products from the Ozonolysis of Three Sesquiterpenes, *Environ. Sci. Technol.*, *50*(5), 2354-2362, https://doi.org/10.1021/acs.est.5b05321.

Sander, R. (1999), Modeling Atmospheric Chemistry: Interactions between Gas-Phase Species and Liquid Cloud/Aerosol Particles, *Surveys Geophys., 20*(1), 1-31, https://doi.org/10.1023/a:1006501706704.

Schell, B., I. J. Ackermann, H. Hass, F. S. Binkowski, and A. Ebel (2001), Modeling the formation of secondary organic aerosol within a comprehensive air quality model system, *J. Geophys. Res. - Atmos.*, *106*(D22), 28275-28293, https://doi.org/10.1029/2001jd000384.

Schwartz, S. E. (1986), Mass-Transport Considerations Pertinent to Aqueous Phase Reactions of Gases in Liquid-Water Clouds, paper presented at Chemistry of Multiphase Atmospheric Systems, Springer Berlin Heidelberg, Berlin, Heidelberg, 1986.

Schwartz, S. E., and J. E. Freiberg (1981), Mass-transport limitation to the rate of reaction of gases in liquid droplets: Application to oxidation of SO2 in aqueous solutions, *Atmos. Environ.*, *15*(7), 1129-1144, https://doi.org/10.1016/0004-6981(81)90303-6.

Shi, B., and J. H. Seinfeld (1991), On mass transport limitation to the rate of reaction of gases in liquid droplets, *Atmos. Environ. Part A. General Topics*, *25*(10), 2371-2383, https://doi.org/10.1016/0960-1686(91)90111-j.

Steinbrecher, R., G. Smiatek, R. Köble, G. Seufert, J. Theloke, K. Hauff, P. Ciccioli, R. Vautard, and G. Curci (2009), Intra- and inter-annual variability of VOC emissions from natural and semi-natural vegetation in Europe and neighbouring countries, *Atmos. Environ.*, *43*(7), 1380-1391, https://doi.org/10.1016/j.atmosenv.2008.09.072.

Stockwell, W. R., F. Kirchner, M. Kuhn, and S. Seefeld (1997), A new mechanism for regional atmospheric chemistry modeling, *J. Geophys. Res. - Atmos.*, *102*(D22), 25847-25879, https://doi.org/10.1029/97jd00849.

Wolke, R., W. Schröder, R. Schrödner, and E. Renner (2012), Influence of grid resolution and meteorological forcing on simulated European air quality: A sensitivity study with the modeling system COSMO–MUSCAT, *Atmos. Environ.*, *53*, 110-130, https://doi.org/10.1016/j.atmosenv.2012.02.085.

Zaveri, R. A., R. C. Easter, J. E. Shilling, and J. H. Seinfeld (2014), Modeling kinetic partitioning of secondary organic aerosol and size distribution dynamics: representing effects of volatility, phase state, and particle-phase reaction, *Atmos. Chem. Phys.*, *14*(10), 5153-5181, https://doi.org/10.5194/acp-14-5153-2014.

Funding
Saxonian State Office for the Environment, Agriculture, and Geology (LfULG);
M.L.L is funded by the Ph.D. scholarship program (AZ 20016/452) of the German Federal Environment Foundation (Deutsche Bundesstiftung Umwelt, DBU).

Cooperation
Center for Information Services and High Performance Computing (ZIH), TU Dresden, Germany;
Deutscher Wetterdienst (DWD), Offenbach, Germany;
Helmholtz Center for Environmental Research, Leipzig, Germany.

Vertical profiling of aerosol, clouds, turbulence, and atmospheric structure close to the North Pole: An overview of first results from the MOSAiC expedition

Ronny Engelmann, Christian Pilz, Hannes Griesche, Martin Radenz, Julian Hofer, Dietrich Althausen, Kevin Ohneiser, Holger Siebert, Birgit Wehner, Albert Ansmann

Während der Arktischen Eisdrift MOSAiC mit dem Forschungseisbrecher Polarstern lieferte TROPOS einen Beitrag zur vertikalen Profilmessung des Atmosphärenzustands, insbesondere von Aerosol, Wolken, Wasserdampf und Turbulenz. Auf fünf Fahrtabschnitten von September 2019 bis Oktober 2020 haben insgesamt sechs Wissenschaftler die Messungen der OCEANET-Atmosphere Plattform betreut und zusätzlich im vierten Abschnitt Ballonaufstiege mit dem BELUGA-System durchgeführt.

Die so gewonnenen Daten liefern neue Erkenntnisse über das arktische Klimasystem. Die Entdeckung von sibirischem Waldbrandaerosol zwischen 7 und 18 km Höhe über den gesamten arktischen Winter hinweg war eins der unerwarteten Highlights. Der Rauch von immensen Waldbränden zwischen Juli und August 2019 konnte bis in die Stratosphäre gelangen und wurde im Polarwirbel eingeschlossen.

Die Konsequenzen dieses Ereignisses können weitreichend sein. Zum einen wurden viele heterogene Bildungsprozesse von Zirruswolken in den Waldbrandschichten beobachtet. Zum anderen waren arktischer Winter und Frühjahr 2019/20 durch einen überdurchschnittlich starken Rückgang von stratosphärischem Ozon gekennzeichnet, welcher neben dem starken Polarwirbel möglicherweise auch über Wechselwirkungen von polaren stratosphärischen Wolken mit dem Waldbrandaerosol zusammenhing.

Die Anwendung neu entwickelter Lidar- und Radarmethoden vom TROPOS auf den MOSAiC-Datensatz erlaubt es, Schließungsstudien zwischen Wolkenkondensationskeimen, Eiskeimen, Wolkentropfen- und Eiskristallanzahlen durchzuführen. Die Messungen mit dem BELUGA-Ballonsystem erlauben Studien zu Turbulenz, meteorologischen Parametern und mikrophysikalischen Aerosolparametern bis in eine Höhe von 1500 m über dem Meereis.

Introduction

Rapid sea ice loss, unusual Arctic warming, and our incomplete knowledge about the complex processes controlling the Arctic climate motivated the MOSAiC (Multidisciplinary drifting Observatory for the Study of Arctic Climate) expedition, the largest Arctic research initiative in history. On 20 September 2019, the German research icebreaker Polarstern left Tromsø in northern Norway heading towards the central part of the Arctic and started drifting through the Arctic Ocean trapped in the ice at the beginning of October 2019. The goal of the MOSAiC expedition was to take the closest look ever at the Arctic as the epicentre of global warming and to gain fundamental insights that are key to better understand global climate change. Hundreds of researchers of more than 70 research institutions from 20 countries were involved in this exceptional expedition. The MOSAiC campaign brought a modern research icebreaker close to the North Pole for a full year, especially, for the first time, in polar winter. The mission was spearheaded by the Alfred Wegener Institute, Helmholtz Center for Polar and Marine Research (AWI).

TROPOS took part in this endeavour and continuously operated the OCEANET-Atmosphere container aboard the research vessel Polarstern side by side with the ARM (Atmospheric Radiation

Measurement) mobile facility 1 (AMF-1) and collected tropospheric and stratospheric aerosol and cloud profile data throughout the expedition period from September 2019 to October 2020. During leg 4 of MOSAiC, the tethered balloon system BELUGA [Balloon-bornE moduLar Utility for profilinG the lower Atmosphere, *Egerer et al.* 2019] was deployed from a research camp at an ice floe drifting in the Fram Strait in Summer 2020.

Our role in the MOSAiC consortium was to provide a seasonally and height-resolved characterization of aerosols and clouds in the North Pole region from the surface up to 30 km height. Our specific focus was to explore the impact of aerosol particles on mixed-phase-cloud and cirrus evolution in the free troposphere up to tropopause level [*Engelmann*, 2021, *Ohneiser*, 2021]. Aerosol–cloud interaction, especially in the upper troposphere, is poorly understood. Advances in our understanding of the influence of pollution from local aerosol and that transported over long distances especially on ice formation processes is, however, of fundamental importance for an improved modelling of atmospheric and climate processes in the Arctic. Clouds in general sensitively influence the energy and water cycles; their accurate representation in models is thus critical for robust future climate projections.

Measurements and Datasets

OCEANET-Atmosphere and Cloudnet: The OCEANET-Atmosphere container of TROPOS, which is routinely operated aboard Polarstern since 2009 [e.g., *Baars et al.*, 2020], housed our multiwavelength Raman lidar Polly-XT [*Engelmann et al.*, 2016], two microwave radiometers for water vapour and cloud liquid-water measurements (one by the University of Cologne for low water-vapour paths), two photometers for aerosol optical thickness (AOT) observations (one by the University of Lille), a pyranometer and a pyrgeometer for solar and terrestrial radiation measurements, a total-sky imager, and basic surface meteorological sensors. For precipitation observations and for ice crystal morphological studies a one-dimensional and a two-dimensional disdrometer were operated as well. The TROPOS equipment was already involved in the Arctic field campaign PASCAL (Physical feedbacks of Arctic boundary layer, Sea ice, Cloud and AerosoL) [*Griesche et al.*, 2020, 2021] aboard Polarstern two years before. Figure 1 shows Polarstern as it was fixed to the ice camp and the setup of the different atmospheric measurement containers at the bow of the ship.

The MOSAiC expedition for the first time provided the unique opportunity to perform lidar observations north of 85° N over the entire winter half year 2019–2020. This part of the central Arctic is not covered by any other lidar measurement, neither by observations with the spaceborne CALIPSO lidar (only up to 81.8° N) nor by measurements of the ground-based Arctic lidar network [*Nott and Duck*, 2011]. Thus, we add a new data set to the global aerosol database [Pangaea: *Ohneiser*, 2021]. *Di Biagio et al.* [2018] were the first to run lidars (mounted on an ensemble of autonomous drifting buoys) in the central Arctic, even north of 82° N, to perform year-round aerosol profiling, including the winter half year of 2015–2016. These measurements

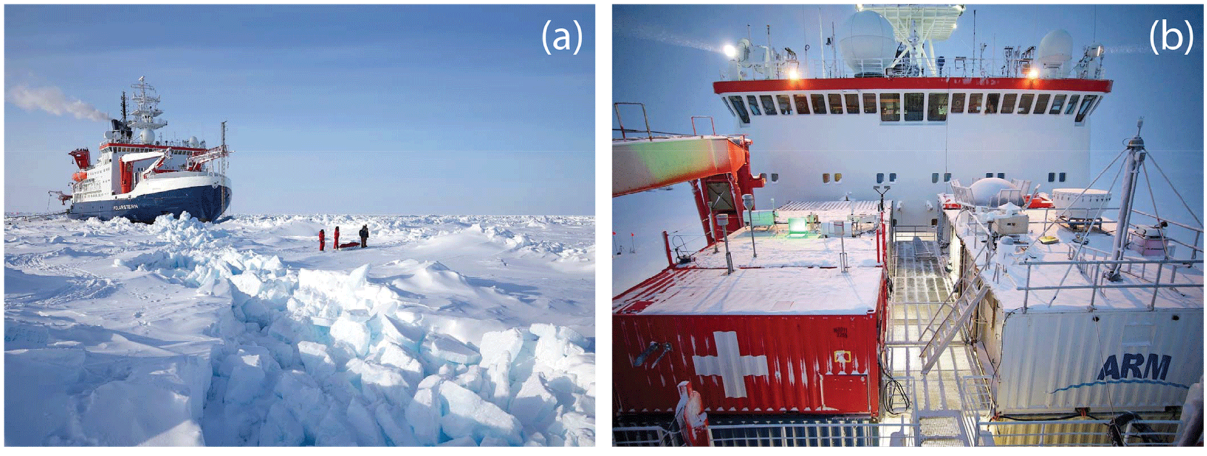

Fig. 1: The Polarstern (a) drifting in the Arctic ice on 10 April 2020 and (b) measurement containers for in situ aerosol monitoring (the first two containers on the left side and the first container on the right side) and for remote sensing of aerosols and clouds. The OCEANET-Atmosphere container of TROPOS is the third one on the left side (with the bright spot on the roof caused by green laser light). The ARM mobile facility (AMF-1) is shown on the right side. The photographs were taken by Michael Gutsche (CC-BY 4.0), AWI.

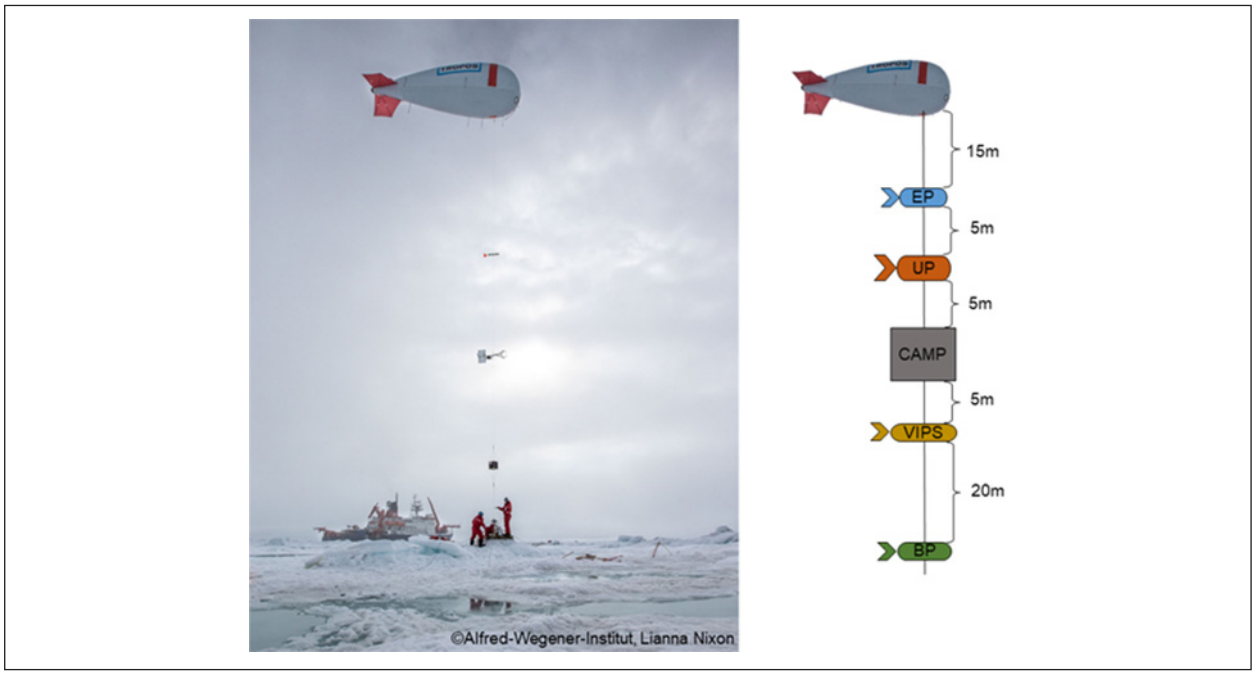

Fig. 2: The BELUGA system. Left: Instruments attached to the tether of the balloon, from top to bottom extended meteorology package (EP), ultrasonic anemometer package (UP), and cubic aerosol measurement platform (CAMP). Right: Sketch of the typical instrument arrangement with dimensions.

together with respective CALIPSO lidar observations are used in our contrasting analysis regarding the aerosol conditions during the MOSAiC year 2019–2020 and the year 2015–2016 characterized by unperturbed aerosol conditions [*Ohneiser et al.*, 2021].

Using the combined datasets from the ARM cloud radar [ARM data archive], the OCEANET-Atmosphere Polly-XT lidar, and microwave radiometer HATPRO (data retrievals of liquid-water path and integrated water vapour have been performed by the experts of the University Cologne, [Pangaea]) allowed us to generate a complete Cloudnet dataset for the entire MOSAiC campaign. The first dataset version was already processed in near-realtime on-board during the campaign. Finalized and improved data analysis of the individual datasets now led to a new post-processed Cloudnet dataset which is soon to be published in the Pangaea data archive.

Balloon-borne observations with BELUGA: As part of the "Arctic Amplification: Climate Relevant Atmospheric and Surface Processes, and Feedback Mechanisms (AC)[3]" project, the balloon-borne measurements focused on the characterization of the cloudy Arctic atmospheric boundary layer (ABL). The Arctic ABL shows various special features compared to mid-latitudes, such as generally stable stratification, capping temperature inversions, persistent low-level mixed-phase clouds, and cloud layers decoupled from the surface. Complex processes remain unclear and essential measurements in the remote Arctic environment, particularly above the sea ice, are still sparse. During leg 4 of MOSAiC, the BELUGA observations were carried out on 33 balloon flights in altitudes ranging from ground level to 1.5 km. With a modular setup of five custom-built instrument packages, comprehensive in situ measurements of atmospheric thermodynamic and dynamic state parameters (temperature, humidity, pressure, 3-D wind), broadband solar and terrestrial irradiance, aerosol particle microphysics, and cloud particle properties were made (Fig. 2). The observations enable detailed analysis of the Arctic ABL above the sea ice in summer, thus supporting model validation and improvements.

The data collected during the balloon measurements contain:

- 60 profiles of temperature, humidity, pressure, and wind with an extended meteorological package (EP),
- 20 profiles with high-resolution 3D-wind vectors and temperature with an ultrasonic anemometer package (UP),
- 36 profiles of particle number concentration, particle number size distribution, and particle light absorption with a cubic aerosol measurement platform,
- 36 profiles of up-and downward terrestrial and solar irradiances with a broadband radiation package,

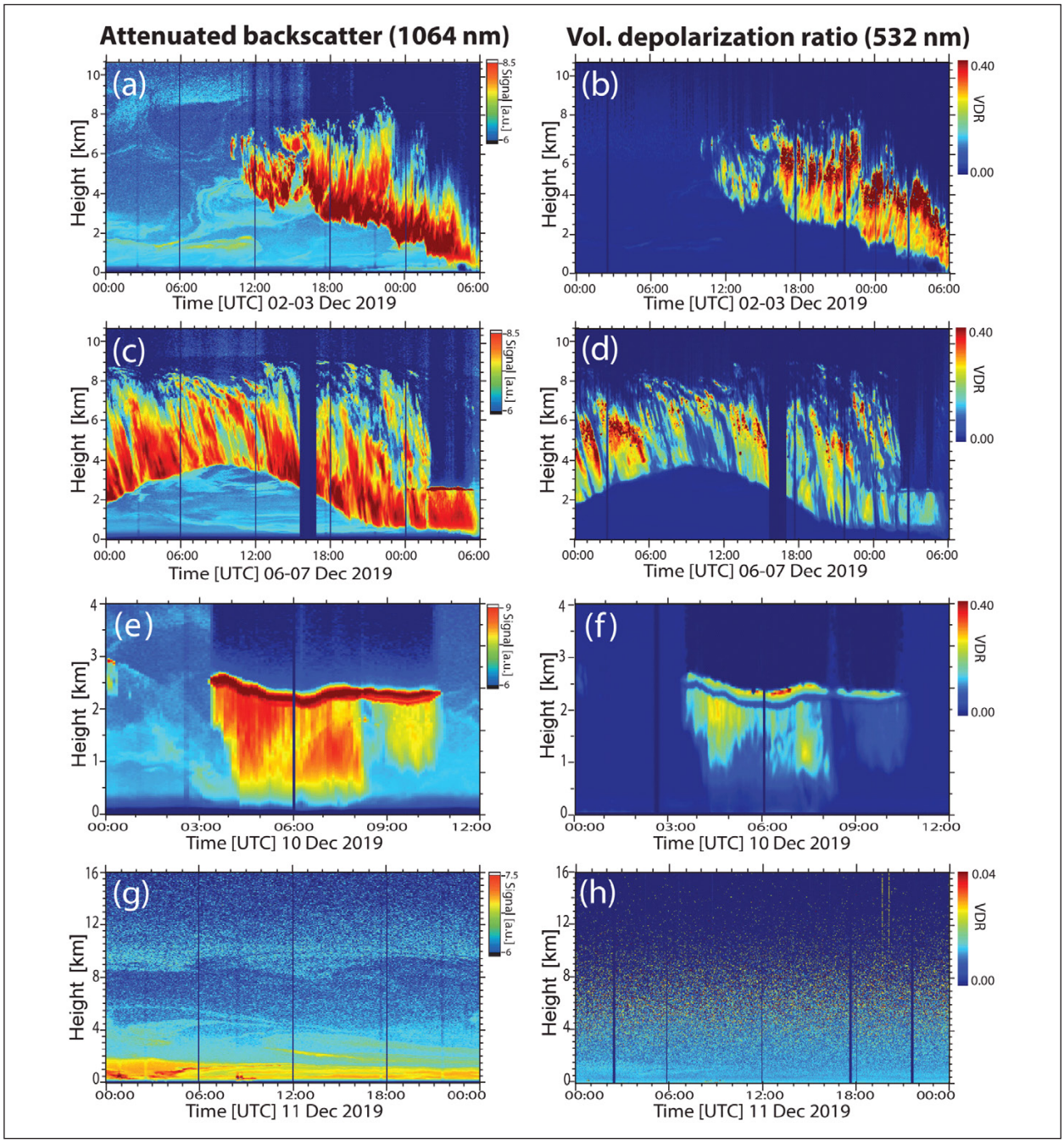

Fig. 3: Ice clouds, mixed-phase clouds, and aerosols monitored with Polly above the Polarstern from 2–11 December 2019. ***(a–d)*** *Evolution of cirrus layers with strong virga embedded in wildfire smoke and Arctic haze,* ***(e–f)*** *development of a long-lasting mixed-phase altocumulus with shallow liquid-water layer at the top and ice virga below, and* ***(g–h)*** *Arctic haze (below 5 km height) and wildfire smoke (above 8 km) during clear-sky conditions. The range-corrected 1064 nm signal (left panels, in arbitrary units (a.u.), logarithmic scale, the given exponents indicate the signal range) and the 532 nm volume linear depolarization ratio (VDR, right panels) are shown. Note that the colour scales vary from panel to panel.*

- 12 profiles of cloud particle images with a Video Ice Particle Sampler (VIPS).

Each data set will be published in the Pangaea data archive by March 2022. An associated data descriptor paper will be submitted to Nature Scientific Data in the near future.

Results

During the winter months of the expedition, Polarstern moved very slowly with the pack ice in December, January, and February and was mostly located between 86° and 88° N. The exceptionally strong polar vortex of 2019–2020 was well established during that time. Figure 3 shows a 10 day

measurement sequence (2–11 December 2019) from our lidar observations. Complex features of aerosol layering, cirrus evolution (Fig. 3a–d), and mixed-phase cloud life cycles (Fig. 3e–f) were found. Clear, i.e., fog and cloud-free, periods occurred frequently as well and provided excellent conditions for a detailed characterization of Arctic haze and wildfire smoke.

The measured volume linear depolarization ratio (VDR) in the right panels of Fig. 3 allows us to precisely distinguish cirrus from layered mixed-phase clouds. Ice crystals cause large depolarization ratios (green to red colours in Fig. 3b, d, f), and, in contrast, liquid-water layers produce rather low depolarization ratios of around zero in Fig. 3f (the increase in the depolarization values with increasing penetration of the laser beam into the water cloud layer is caused by multiple scattering). The depolarization ratio of aerosol particles was found to be generally small (Fig. 3h) in the free troposphere and stratosphere, which indicates spherical haze and smoke particles.

Wildfire smoke layer in the UTLS regime: Our most impressive and outstanding observation during the entire MOSAiC expedition was the detection of a persistent, 10 km deep aerosol layer of aged wildfire smoke [*Ohneiser et al.*, 2021]. We monitored this smoke layer in the upper troposphere and lower stratosphere (UTLS) from about 7–8 km up to 17–18 km height for more than 7 months from the beginning of the lidar observations in late September 2019 until May 2020. Extreme and long-lasting wildfires in central and eastern Siberia, in closest neighbourhood to the Arctic region, were most probably responsible for the UTLS smoke layer over the High Arctic in the winter half year of 2019–2020 [*Ohneiser et al.*, 2021].

In Fig. 4, we present an overview of our MOSAiC smoke-layer observations on board the drifting Polarstern in terms of geometrical and optical properties. One set of lidar products per day was considered. Gaps in the data time series are caused by fog and low cloud events, partly lasting over many days. We included Koldewey Aerosol Raman Lidar (KARL) observations at Spitsbergen in Fig. 4b and c to prolong the AOT and extinction time series preceding the MOSAiC expedition. According to the KARL observations, the stratospheric AOT reached values close to 0.15 at 532 nm at the beginning of August 2019 and decreased to values of 0.07–0.08 in September 2019.

Figure 4a shows the temporal evolution of the geometrical properties of the High-Arctic aerosol layer during the winter half-year. The layer base was frequently found below the tropopause. The vertical bars in Fig. 4a are coloured to distinguish different levels of the aerosol loading expressed in terms of the particle extinction coefficient. As can be seen in Fig. 4a, the maximum light extinction values were typically found just above the tropopause. They slowly decreased with time from values > 10 Mm^{-1} in October and November to < 5 Mm^{-1} in April 2020. Figure 4a also contains information about the occurrence of polar stratospheric clouds (PSC). Most of the PSCs over Polarstern were detected in January 2020. We observed a much lower number of PSCs over the North Pole region (86° to 88.6° N) during the winter and spring seasons of 2020 than the CALIPSO lidar within the latitudinal range from 60 to 81.8° N.

Figure 4b provides an overview of the development of the aerosol optical thickness (AOT) at 355 and 532 nm from August 2019 to May 2020. We computed the AOT from the particle backscatter height profiles in order to reduce the noise in the lidar AOT observations significantly and, thus, to better see trends in the evolution of the polar smoke layer (with mean lidar ratios of 55 sr at 355 nm and 85 sr at 532 nm). Subsequently, we integrated the extinction values between the aerosol layer base and top heights, as given in Fig. 4a, to obtain the AOT of the smoke layer.

The combined KARL and Polly observations show a coherent downward trend in the AOT time series until the beginning of December 2019. The 532 nm AOT observed over the Polarstern decreased from 0.05–0.12 in October and November to values of 0.03–0.06 from December to mid-March and then dropped to 0.01–0.02 in April 2020. Almost constant AOT conditions were observed from 10 December to 10 March. Based on the KARL and Polly observations, we can conclude that the UTLS perturbation decreased from about 0.15 (532 nm AOT) at the beginning of August 2019 to 0.02 at the end of April 2020 (within 9 months); thus, the e-folding decay time was about 5 months.

The layer-mean 532 nm smoke extinction coefficients in Fig. 4c (obtained from AOT divided by the respective layer geometrical depth in Fig. 4a) were of the order of 10 Mm^{-1} until mid-November 2019, around 4–5 Mm^{-1} during the main winter months until mid-March 2020, and mostly ≤ 3 Mm^{-1} at the end of the lifetime of the smoke layer. According to long-term observations at midlatitude lidar sites, the minimum 532 nm AOT value for a clean stratosphere is around 0.001–0.002 [*Baars et al.*, 2019], and the minimum extinction coefficients are of the order of 0.1–0.2 Mm^{-1}. From the measured layer mean extinction coefficients, mass concentrations of the smoke particles were derived and ranged from 0.4–2 $\mu g\,m^{-3}$ during the autumn and winter months. Minimum stratospheric mass concentrations (at midlatitudes) are close to 0.01–0.02 $\mu g\,m^{-3}$ [*Baars et al.*, 2019].

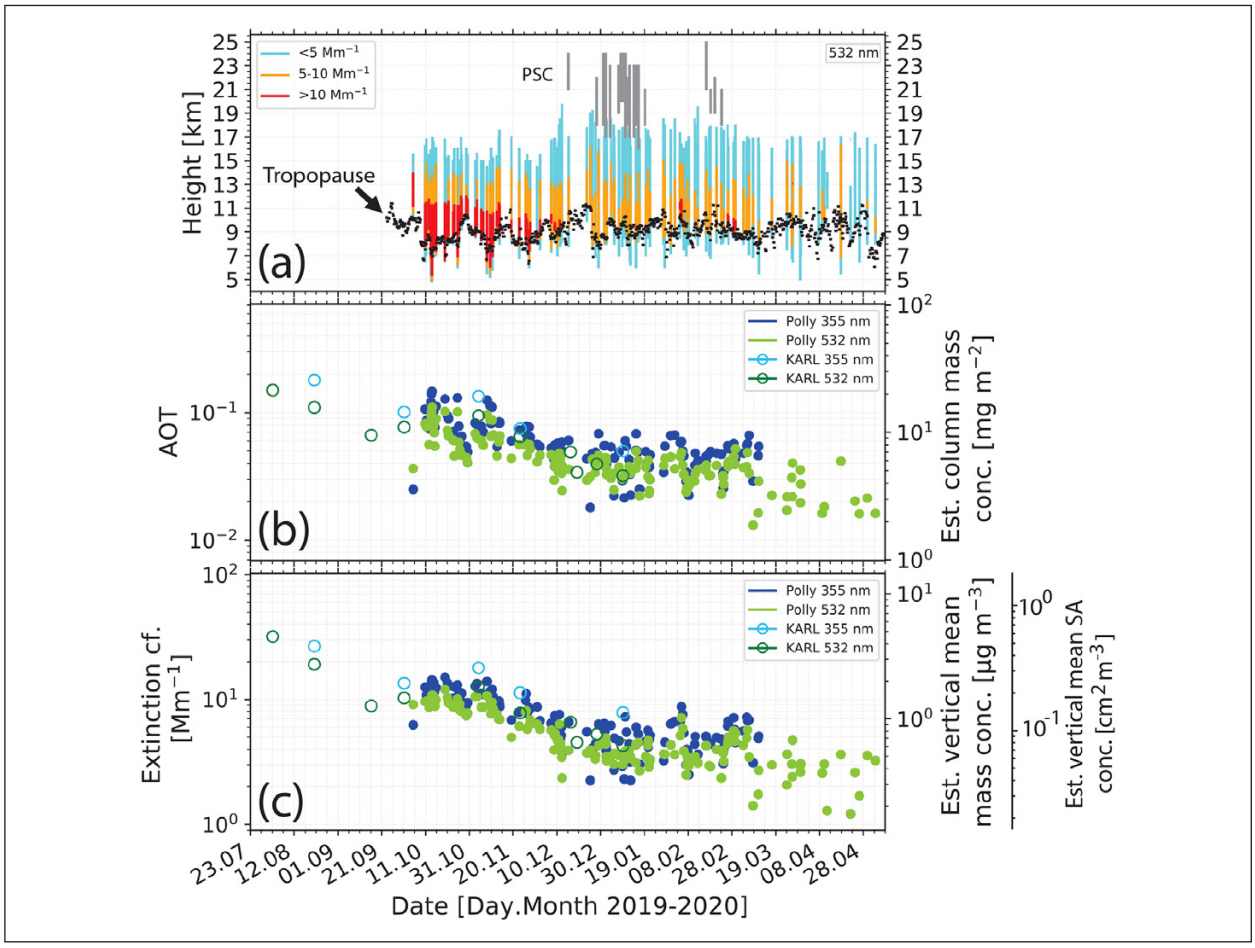

Fig. 4: (a) Overview of Polly observations of UTLS smoke layers (coloured bars from bottom to top; one bar per day) from 23 July 2019 to 8 May 2020. The colours in each bar indicate segments with different extinction coefficient levels. Furthermore, the tropopause and PSCs layers are shown as well. (b) Smoke layer AOT (KARL – open symbols; Polly – closed symbols) at 355 and 532 nm. Column mass concentrations are indicated as well. (c) Layer mean 355 and 532 nm particle extinction coefficient and respective estimated mass and surface area concentrations. For comparison, background AOT and extinction levels (532 nm) are of the order of 0.001–0.002 and 0.1–0.2 Mm^{-1}, respectively (Baars et al., 2019).

We finally estimated the smoke aerosol load over the Arctic by multiplying the area (considering latitudes > 66.7° N) by a mean smoke layer depth of 8 km, a mean smoke extinction coefficient of about 5 Mm^{-1}, a volume-to-extinction conversion factor of 0.124×10^{-12} Mm for wildfire smoke [*Ansmann et al.*, 2021], the smoke particle density of 1.15 g m^{-3}, and yield 0.2 Mt of smoke as a guess for the mean value of the smoke aerosol load over the Arctic during the winter half-year (2019–2020). The overall Siberian smoke particle mass injected into the UTLS height range of the Northern Hemisphere may have been a factor of 2 higher. For comparison, the particle mass injected into heights of 11–13 km during the record-breaking Canadian pyroCb smoke event in August 2017 was about 0.3 Mt [*Yu et al.*, 2019], and the rather strong Australian bushfires in December 2019 and January 2020 caused a stratospheric smoke particle mass of the order of 0.5–1 Mt [*Peterson et al.*, 2021].

Ohneiser et al. [2021] discuss a potential impact of the UTLS wildfire smoke on ozone depletion. First, a record-breaking ozone depletion was observed in the spring of 2020 [e.g. *Wohltmann et al.*, 2020], and second, at the same time, a strong perturbation of the stratospheric aerosol conditions occurred. A potential relationship between the high UTLS pollution levels and strong ozone reduction was not considered so far in any of the studies on ozone depletion. *Ohneiser et al.* [2021] compiled all information we have regarding PSC occurrence, smoke and sulphate conditions, and ozone depletion during the MOSAiC campaign. In general, two pathways to influence ozone depletion by aerosol pollution are possible. The particles could, on the one hand, influence the evolution of PSCs and specifically their microphysical properties (number concentration, size and surface distribution), and on the other hand, the particles could be directly involved in heterogeneous chemical processes by increasing the particle surface area available to

convert nonreactive chlorine components into reactive forms. Also, a third (indirect) impact of smoke, when well distributed over large parts of the Northern or Southern hemispheres, is via the influence on large-scale atmospheric dynamics. It will be the task of the future years to further investigate those hypotheses.

Arctic haze vertical structures: The original and primary goal of the shipborne MOSAiC lidar measurements was to provide, for the first time, a height-resolved characterization of tropospheric aerosols and clouds over the North Pole region during the winter half year. Because of its importance for the climate and environmental conditions, Arctic haze has been intensively studied for more than 50 years. However, knowledge about the vertical layering structures of these aged haze aerosols and about the composition and microphysical properties is still limited and mostly based on sporadic aircraft observations performed during field campaigns, preferably in spring. *Ritter et al.* [2016] presented a ground-based multiwavelength polarization Raman lidar study on Arctic haze in terms of backscatter, depolarization, and lidar ratios. The situation has improved since 2006 with the start of the CALIPSO mission.

In general understanding, long-range transport of cold, polluted air masses from northern Eurasian source regions (mainly north of the Arctic front)

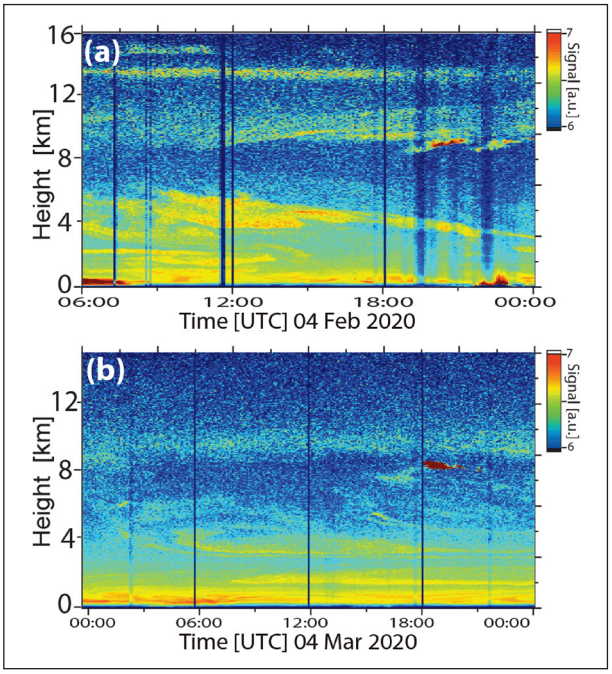

Fig. 5: Arctic haze (below 8 km height) and wildfire smoke (above 8 km height) over the North Pole region in late winter on ***(a)*** *4 February 2020 and* ***(b)*** *4 March 2020. PSC layers are present as well at 13.5 and 15 km height on 4 February (pronounced yellow layers). The range-corrected 1064 nm signal is shown in arbitrary units (a.u., logarithmic scale).*

prevails in winter and leads to the formation of Arctic haze with the highest mass concentrations in late winter and early spring. Such a low-level aerosol transport is missing in summer. *Stohl* [2006] pointed out that the winter transport of aerosols towards the High Arctic occurs at low heights. Long-transported aerosols may reach heights up to the middle troposphere (5–7 km height).

In Fig. 5, we present two typical MOSAiC cases of Arctic haze observed on 4 February and 4 March 2020. The Polarstern was drifting with the ice at latitudes of 87.5° N (4 February) and 88.1° N (4 March). The most striking feature in both figures is that aerosol layers occurred almost everywhere within the troposphere and in the lower stratosphere. Also, remnants of PSCs were visible around 13.5–14 km height on 4 February 2020 (Fig. 5a). Temperatures were around –76 °C at 13.5 km height and thus sufficiently low to allow the formation of type Ia PSC. Type Ia PSCs are thought to consist of nitric acid trihydrate (NAT) crystals and produce significant depolarization of backscattered laser light. Note that the Polarstern was fully below the strong polar vortex from the beginning of January to mid-April 2020 [*Ohneiser et al.*, 2021].

As for an example, values for the 532 nm extinction coefficients of 2–8 Mm^{-1} in the lower layer (up to 2.5 km height) and 1–7 Mm^{-1} in the lofted layer above 3 km height were observed on 4 February. These values are in good agreement with CALIPSO lidar observations [*Di Biagio et al.*, 2018). *Di Biagio et al.* [2018] showed 14 d mean and layer mean values of 2–8 Mm^{-1} (0–2 km layer), 2–10 Mm^{-1} (2–5 km), and 1–2 Mm^{-1} (5–10 km layer) measured in the area from 5–25° E (north of Svalbard) and 80–82° N in February and March 2015.

The atmospheric boundary layer observed with BELUGA on MOSAiC leg 4: First results of the BELUGA observations are presented in the recently submitted publication "Tethered balloon-borne profile measurements of atmospheric properties in cloudy conditions over Arctic sea-ice during MOSAiC: Overview and first results" by Lonardi et al. to the Elementa special feature for MOSAiC (Fig. 6).

The observed temperature profiles show different coupling states of cloud layers in the Arctic ABL. In the case of 13 and 24 July (Fig. 6), the warmer cloud layer is decoupled from the surface layer while on 23 July (Fig. 7) the constant temperature profile below the main inversion at 600 m indicates a coupling of the cloud layer with the sea ice.

Further preliminary results focused on the aerosol particle measurements were presented at the European Aerosol Conference 2021. During a warm

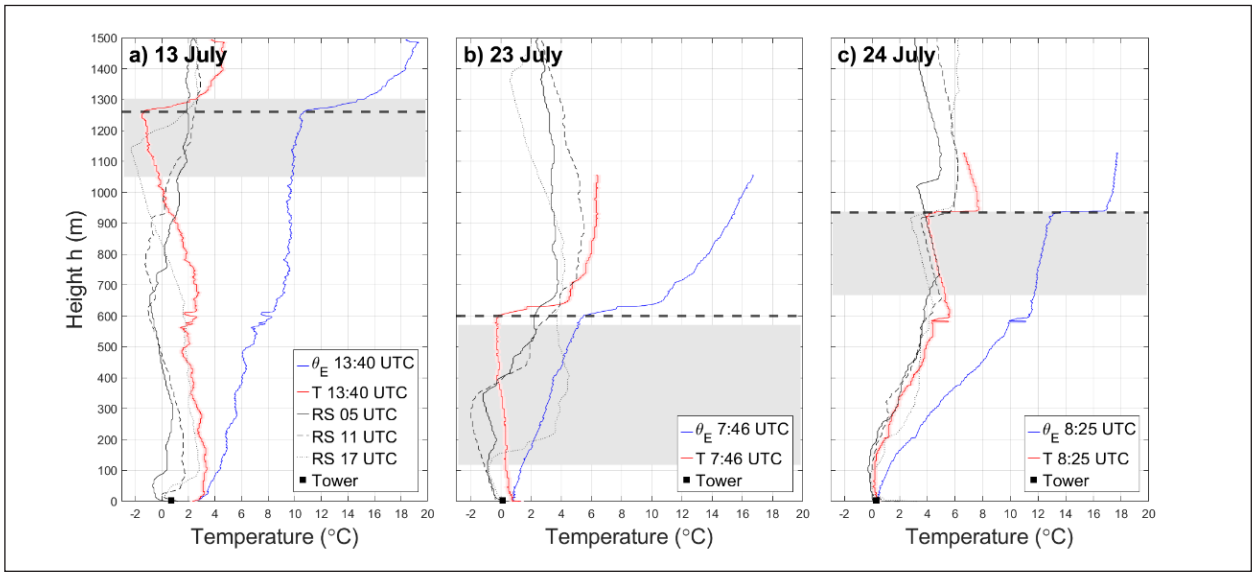

Fig. 6: Profiles of equivalent potential temperature (blue lines) and temperature (red lines) from EP measurements. Profiles from radio soundings at 5, 11, and 17 UTC are also shown (black lines).

air intrusion event end of July 2020, increased Black Carbon concentrations and one order of magnitude higher accumulation mode particle concentrations were observed below 1 km height. West-Siberian wildfires were identified as the source of long-range transported pollution by back-trajectory analysis and satellite-based wildfire detection (Fig. 7). The observations were made in the Fram Strait at about 79° N, 2° W.

Mixed-phase cloud evolution in Arctic haze: Stratiform mixed-phase clouds are predominant in the Arctic. Because of their sensitive influence on radiative transfer and the water cycle, they have been the focus of research for more than 15 years. However, because of the complexity of influencing meteorological and aerosol aspects, there are still many open questions concerning their long lifetime, especially of the longevity of liquid-water layers and

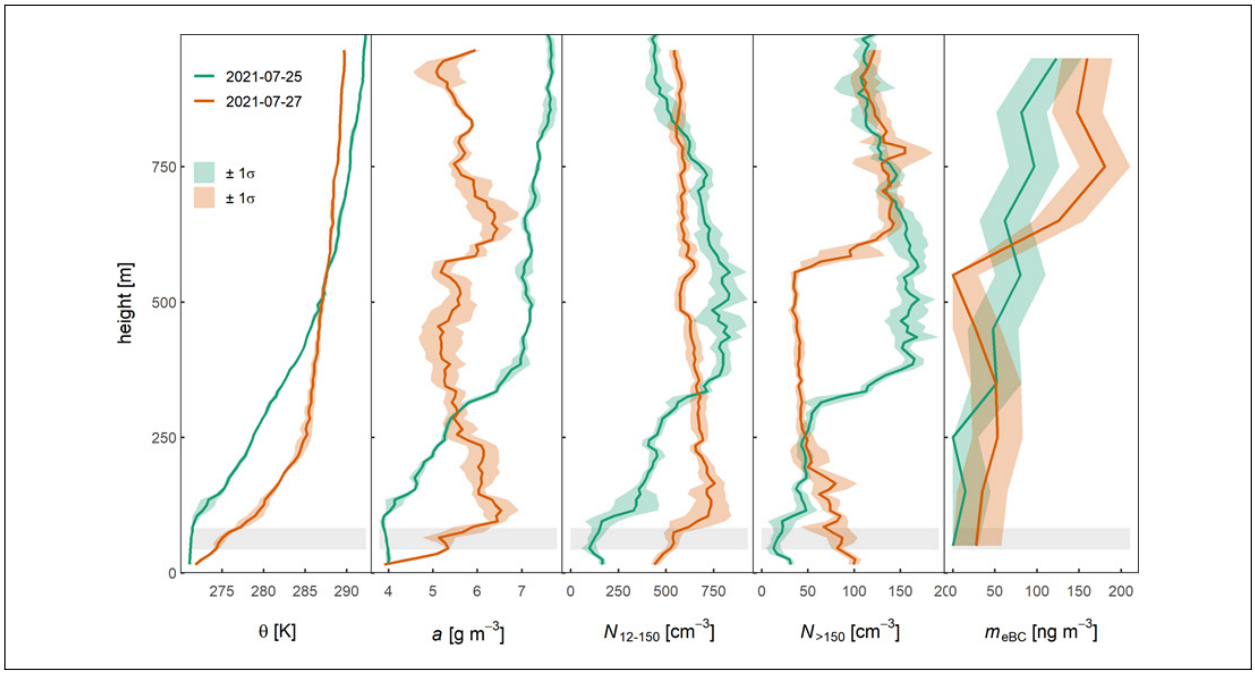

Fig. 7: Profiles of potential temperature (θ), absolute humidity (a), concentration of Aitken-mode particles between 12 and 150 nm size (N12-150), concentration of accumulation-mode particles above 150 nm size (N150), and equivalent Black Carbon mass concentration.

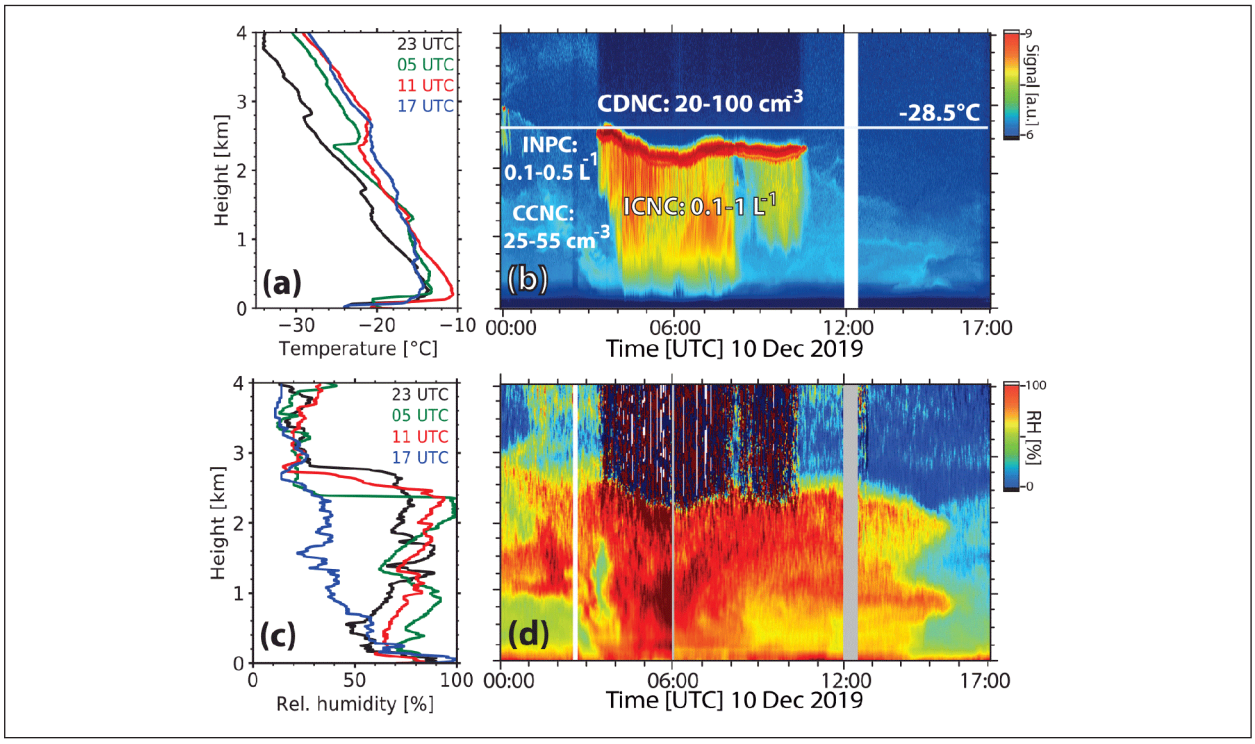

Fig. 8: Mixed-phase cloud closure study. (a, c) Profiles of temperature and relative humidity from MOSAiC radiosondes. (b) The 1064 nm range-corrected signal shows the mixed-phase cloud layer between 2 and 2.6 km height with ice virga below the main cloud layer, and (d) the height–time display of Raman lidar observations of relative humidity. In (b), CDNC as obtained from the dual-FOV lidar observations, CCNC and INPC estimated from the lidar observations at 2.5 - 2.6 km height before the cloud layer appeared, and ICNC (mean value) as estimated from combined lidar–radar observations are given as numbers.

thus of water droplets in the presence of ice crystals. MOSAiC contributes to this research field by means of combined lidar and radar observation.

One example is shown in Fig. 3e and f. The cloud layer was observed for more than 7 h over the Polarstern on 10 December 2019. The dark band in the depolarization ratio panel between 2–3 km height in Fig. 3f indicates the liquid-water-dominated cloud top layer. The increase in the depolarization ratio above the dark zone at the liquid cloud base is caused by multiple scattering by cloud droplets. Favourable conditions with cloud top temperatures around –28.5 °C at 2.6 km height (at 03:00 UTC) were given for heterogeneous ice formation via immersion freezing, i.e., ice nucleation on INPs immersed in the water droplets. After nucleation in the cloud top layer, ice crystals grow fast to sizes of 50–100 µm within minutes and immediately start to fall out. As visible in Fig. 3e and f, the crystals formed long virga below the shallow altocumulus layer. The ice crystals partly evaporated on the way down but partly reached the ground as precipitation. The liquid-water-dominated cloud top layer was not depleted at any time during the 7 h period.

About 40 long-lasting mixed-phase cloud events (ice-precipitating shallow altocumulus decks) with durations from 4–30 h were observed from October 2019 to March 2020. New lidar methods that have been developed at TROPOS allow to estimate cloud-condensation-nuclei concentration (CCNC) and ice-nucleating particle concentration (INPC) from lidar measurements [*Mamouri and Ansmann*, 2016] in the vicinity of the clouds. At the same time the cloud-droplet number concentration (CDNC) within the liquid cloud base can be obtained by the dual-field-of-view polarization method [*Jimenez et al.*, 2020] and the ice-crystal number concentration (ICNC) can be estimated from lidar-radar observations [*Bühl et al.*, 2019]. With these new methods closure studies between CCND and CDNC and between INPC and ICNC, respectively, can be performed.

Figure 8 summarizes our data analysis efforts and highlights the overall potential of our advanced aerosol/cloud lidar to contribute to cloud research. Since radiosondes were launched every 6 h (Fig. 8a and c) over the entire MOSAiC year, excellent conditions for a detailed lidar-based aerosol and cloud monitoring Fig. 8b), including a coherent monitoring of the relative-humidity field (Fig. 8b), were given during the MOSAiC winter half year [*Engelmann et al.*, 2021].

Conclusions and outlook

The highlight of our observations was the detection of the long-lasting UTLS wildfire smoke layer which was present over the North Pole region for more than 7 months [*Ohneiser et al.*, 2021]. Besides the smoke, we presented 2 days with typical Arctic haze layering features and properties, introduced the in-situ measurements from the balloon-borne platform BELUGA, and demonstrated the possibility for aerosol/cloud closure studies from remote sensing.

Our research focus is on aerosol–cloud interaction, especially on ice nucleation in mixed-phase clouds and cirrus in the middle and upper troposphere. We developed new techniques, data analysis concepts, and closure experiments and applied them for the first time to Arctic cloud studies. These successful closure experiments (demonstrated in two case studies so far) corroborate that aerosol particles are able to control cloud evolution and cloud microphysical properties in the Arctic as well. In the future, we will analyse all observed liquid-dominated cloud layers with our dual field of view polarization method in order to characterize the arctic cloud liquid phase from a statistical point.

The observed wildfire smoke layers during MOSAiC opened another chapter in TROPOS studies on heterogeneous ice formation. Figure 3a and c show great examples how cirrus clouds formed in the wildfire smoke. *Ansmann et al.* [2021] then developed methods to derive particle mass, volume, surface area, and number concentrations in the case of wildfire smoke layers as well as estimates of smoke-related cloud condensation nuclei and ice-nucleating particle concentrations from backscatter lidar measurements on the ground and in space.

Heterogeneous ice nucleation is a complex process, especially in the case of organic aerosol particles. A first successful closure study between the predicted ice crystal nucleation rate (from lidar-based the ice-crystal number parameterization) and the estimated ice crystal nucleation rate (from lidar–radar observations) was presented in *Engelmann et al.* [2021]. It was shown that the wildfire smoke was probably able to trigger cirrus formation before the ice supersaturation onset for homogeneous freezing was reached and to control the further evolution of the ice cloud system.

In the new project Smoke Cirrus Interaction in the Arctic in the framework of MOSAiC (SCiAMO) funded from BMBF, we will further analyze all smoke-cirrus interaction cases during MOSAiC to obtain a statistically trustworthy view on smoke and its role in cirrus ice nucleation. The respective extended data analysis will not only be part of our MOSAiC data analysis but it will be also put into context with our observed Australian bushfire smoke in Punta Arenas during the Dynamics, Aerosol, Cloud and Precipitation Observations in the Pristine Environment of the Southern Ocean (DACAPO-PESO). Furthermore, within the DFG-funded project Continuous Observations of Aerosol-cLoud interaction in Antarctica (COALA) we will perform similar combined lidar-radar measurements with OCEANET-Atmosphere at the Neumayer-III research station in Antarctica for a full year in 2023. These projects fully fit into the TROPOS strategy to contrast the northern and southern hemisphere up to the polar regions.

References

Ansmann, A., Ohneiser, K., Mamouri, R.-E., Knopf, D. A., Veselovskii, I., Baars, H., Engelmann, R., Foth, A., Jimenez, C., Seifert, P., and Barja, B.: Tropospheric and stratospheric wildfire smoke profiling with lidar: mass, surface area, CCN, and INP retrieval, Atmos. Chem. Phys., 21, 9779–9807, https://doi.org/10.5194/acp-21-9779-2021, 2021.

Bühl, J., Seifert, P., Radenz, M., Baars, H., and Ansmann, A.: Ice crystal number concentration from lidar, cloud radar and radar wind profiler measurements, Atmos. Meas. Tech., 12, 6601–6617, https://doi.org/10.5194/amt-12-6601-2019, 2019.

Baars, H., Herzog, A., Heese, B., Ohneiser, K., Hanbuch, K., Hofer, J., Yin, Z., Engelmann, R., and Wandinger, U.: Validation of Aeolus wind products above the Atlantic Ocean, Atmos. Meas. Tech., 13, 6007–6024, https://doi.org/10.5194/amt-13-6007-2020, 2020.

Baars, H., Ansmann, A., Ohneiser, K., Haarig, M., Engelmann, R., Althausen, D., Hanssen, I., Gausa, M., Pietruczuk, A., Szkop, A., Stachlewska, I. S., Wang, D., Reichardt, J., Skupin, A., Mattis, I., Trickl, T., Vogelmann, H., Navas-Guzmán, F., Haefele, A., Acheson, K., Ruth, A. A., Tatarov, B., Müller, D., Hu, Q., Podvin, T., Goloub, P., Veselovskii, I., Pietras, C., Haeffelin, M., Fréville, P., Sicard, M., Comerón, A., Fernández García, A. J., Molero Menéndez, F., Córdoba-Jabonero, C., Guerrero-Rascado, J. L., Alados-Arboledas, L., Bortoli, D., Costa, M. J., Dionisi, D., Liberti, G. L., Wang, X., Sannino, A., Papagiannopoulos, N., Boselli, A., Mona, L., D'Amico, G., Romano, S., Perrone, M. R., Belegante, L., Nicolae, D., Grigorov, I., Gialitaki, A., Amiridis, V., Soupiona, O., Papayannis, A., Mamouri, R.-E., Nisantzi, A., Heese, B., Hofer, J., Schechner, Y. Y., Wandinger, U., and Pappalardo, G.: The unprecedented 2017–2018 stratospheric smoke event: decay phase and aerosol properties observed with the EARLINET, Atmos. Chem. Phys., 19, 15183–15198, https://doi.org/10.5194/acp-19-15183-2019, 2019.

Di Biagio, C., Pelon, J., Ancellet, G., Bazureau, A., and Mariage, V.: Sources, load, vertical distribution, and fate of wintertime aerosols north of Svalbard from combined V4 CALIOP data, ground-based IAOOS lidar observations and trajectory analysis, J. Geophys. Res.-Atmos., 123, 1363–1383, https://doi.org/10.1002/2017JD027530, 2018.

Egerer, U., Gottschalk, M., Siebert, H., Ehrlich, A., and Wendisch, M.: The new BELUGA setup for collocated turbulence and radiation

measurements using a tethered balloon: first applications in the cloudy Arctic boundary layer, Atmos. Meas. Tech., 12, 4019–4038, https://doi.org/10.5194/amt-12-4019-2019, 2019.

Engelmann, R., Ansmann, A., Ohneiser, K., Griesche, H., Radenz, M., Hofer, J., Althausen, D., Dahlke, S., Maturilli, M., Veselovskii, I., Jimenez, C., Wiesen, R., Baars, H., Bühl, J., Gebauer, H., Haarig, M., Seifert, P., Wandinger, U., and Macke, A.: Wildfire smoke, Arctic haze, and aerosol effects on mixed-phase and cirrus clouds over the North Pole region during MOSAiC: an introduction, Atmos. Chem. Phys., 21, 13397–13423, https://doi.org/10.5194/acp-21-13397-2021, 2021.

Engelmann, R., Kanitz, T., Baars, H., Heese, B., Althausen, D., Skupin, A., Wandinger, U., Komppula, M., Stachlewska, I. S., Amiridis, V., Marinou, E., Mattis, I., Linné, H., and Ansmann, A.: The automated multiwavelength Raman polarization and water-vapor lidar PollyXT: the neXT generation, Atmos. Meas. Tech., 9, 1767–1784, https://doi.org/10.5194/amt-9-1767-2016, 2016.

Griesche, H. J., Ohneiser, K., Seifert, P., Radenz, M., Engelmann, R., and Ansmann, A.: Contrasting ice formation in Arctic clouds: surface-coupled vs. surface-decoupled clouds, Atmos. Chem. Phys., 21, 10357–10374, https://doi.org/10.5194/acp-21-10357-2021, 2021.

Griesche, H. J., Seifert, P., Ansmann, A., Baars, H., Barrientos Velasco, C., Bühl, J., Engelmann, R., Radenz, M., Zhenping, Y., and Macke, A.: Application of the shipborne remote sensing supersite OCEANET for profiling of Arctic aerosols and clouds during Polarstern cruise PS106, Atmos. Meas. Tech., 13, 5335–5358, https://doi.org/10.5194/amt-13-5335-2020, 2020.

Jimenez, C., Ansmann, A., Engelmann, R., Donovan, D., Malinka, A., Schmidt, J., Seifert, P., and Wandinger, U.: The dual-field-of-view polarization lidar technique: a new concept in monitoring aerosol effects in liquid-water clouds – theoretical framework, Atmos. Chem. Phys., 20, 15247–15263, https://doi.org/10.5194/acp-20-15247-2020, 2020.

Lonardi et al.: Tethered balloon-borne profile measurements of atmospheric properties in cloudy conditions over Arctic sea-ice during MOSAiC: Overview and first results, submitted for the MOSAiC special feature in Elementa.

Mamouri, R.-E. and Ansmann, A.: Potential of polarization lidar to provide profiles of CCN- and INP-relevant aerosol parameters, Atmos. Chem. Phys., 16, 5905–5931, https://doi.org/10.5194/acp-16-5905-2016, 2016.

Nott, G. J. and Duck, T. J.: Lidar studies of the polar troposphere. Met. Apps, 18, 383–405, https://doi.org/10.1002/met.289, 2011.

Ohneiser, K., Ansmann, A., Chudnovsky, A., Engelmann, R., Ritter, C., Veselovskii, I., Baars, H., Gebauer, H., Griesche, H., Radenz, M., Hofer, J., Althausen, D., Dahlke, S., and Maturilli, M.: The unexpected smoke layer in the High Arctic winter stratosphere during MOSAiC 2019–2020 , Atmos. Chem. Phys., 21, 15783–15808, https://doi.org/10.5194/acp-21-15783-2021, 2021.

Peterson, D. A., Fromm, M. D., McRae, R. H. D., Campbell, J. R., Hyer, E. J., Taha, G., Camacho, C. P., Kablick, G. P., Schmidt, C. C., and DeLand, M. T.: Australia's Black Summer pyrocumulonimbus super outbreak reveals potential for increasingly extreme stratospheric smoke events, NPJ Clim. Atmos. Sci., 4, 38, https://doi.org/10.1038/s41612-021-00192-9, 2021.

Pilz et al.: Data description for the Beluga measurements, in preparation for Nature Scientific Data. Est. submission: February 2022.

Ritter, C., Neuber, R., Schulz, A., Markowicz, K., Stachlewska, I., Lisok, J., Makuch, P., Pakszys, P., Markuszewski, P., Rozwadowska, A., Petelski, T., Zielinski, T., Becagli, S., Traversi, R., Udisti, R., and Gausa, M.: 2014 iAREA campaign on aerosol in Spitsbergen – Part 2: Optical properties from Raman-lidar and in-situ observations at Ny-Ålesund, Atmos. Environ., 141, 1–19, https://doi.org/10.1016/j.atmosenv.2016.05.053, 2016.

Stohl, A.: Characteristics of atmospheric transport into the Arctic troposphere, J. Geophys. Res., 111, D11306, https://doi.org/10.1029/2005JD006888, 2006.

Wohltmann, I., Gathen, P., Lehmann, R., Maturilli, M., Deckelmann, H., Manney, G. L., Davies, J., Tarasick, D., Jepsen, N., Kivi, R., Lyall, N., and Rex, M.: Near-Complete Local Reduction of Arctic Stratospheric Ozone by Severe Chemical Loss in Spring 2020, Geophys. Res. Lett., 47, e2020GL089547, https://doi.org/10.1029/2020GL089547, 2020.

Yu, P., Toon, O. B., Bardeen, C. G., Zhu, Y., Rosenlof, K. H., Portmann, R. W., Thornberry, T. D., Gao, R.-S., Davis, S. M., Wolf, E. T., de Gouw, J., Peterson, D. A., Fromm, M. D., and Robock, A.: Black carbon lofts wildfire smoke high into the stratosphere to form a persistent plume, Science, 365, 587–590, https://doi.org/10.1126/science.aax1748, 2019.

Data availability

ARM Data Archive:

Ka-Band ARM Zenith RADAR (KAZR); general mode, doi: 10.5439/1498936, https://www.arm.gov/data/.

PANGAEA:

Ohneiser, Kevin; Ansmann, Albert; Engelmann, Ronny; Griesche, Hannes; Radenz, Martin; Hofer, Julian; Althausen, Dietrich (2021): Optical aerosol profiles from the Raman Lidar Polly-XT during MOSAiC, PANGAEA, https://doi.org/10.1594/PANGAEA.935539.

Engelmann, Ronny; Griesche, Hannes; Radenz, Martin; Hofer, Julian; Althausen, Dietrich; Walbröl, Andreas; Ebell, Kerstin (2022): Brightness temperatures of the HATPRO microwave radiometer onboard the Polarstern during the MOSAiC expedition. PANGAEA, https://doi.pangaea.de/10.1594/PANGAEA.941356.

Walbröl, Andreas; Ebell, Kerstin; Engelmann, Ronny; Griesche, Hannes; Radenz, Martin; Hofer, Julian; Althausen, Dietrich; Crewell, Susanne (2022): Brightness temperatures of the MiRAC-P microwave radiometer onboard the Polarstern during the MOSAiC expedition. PANGAEA, https://doi.pangaea.de/10.1594/PANGAEA.941407.

Ebell, Kerstin; Walbröl, Andreas; Engelmann, Ronny; Griesche, Hannes; Radenz, Martin; Hofer, Julian; Althausen, Dietrich (2022): Temperature and humidity profiles, integrated water vapour and liquid water path derived from the HATPRO microwave radiometer onboard the Polarstern during the MOSAiC expedition. PANGAEA, https://doi.pangaea.de/10.1594/PANGAEA.941389.

Walbröl, Andreas; Orlandi, Emiliano; Crewell, Susanne; Ebell, Kerstin (2022): Integrated water vapour derived from the MiRAC-P microwave radiometer onboard the Polarstern during the MOSAiC expedition. PANGAEA, https://doi.pangaea.de/10.1594/PANGAEA.941470.

Long-term lidar measurements of Australian wildfire smoke layer in the stratosphere over southern South America in 2020-2021: Potential influence on ozone reduction?

Kevin Ohneiser, Albert Ansmann, Holger Baars, Patric Seifert, Cristofer Jimenez, Martin Radenz, Ronny Engelmann

Rekordwaldbrände in Verbindung mit starker Pyrokonvektion 2019/2020 in Südostaustralien führten zum Eintrag von enormen Mengen Waldbrandrauch in die Stratosphäre der Südhalbkugel. Der Rauch formte eine mehr als 10 Kilometer dicke Schicht, die auch im weit entfernten Punta Arenas (Chile) über 2 Jahre mit Lidarmessungen beobachtet werden konnte. Die Rauchpartikel beeinflussten das Strahlungsbudget, die Dynamik der Atmosphäre, Ozonabbau, sowie die heterogene Bildung von Zirruswolken.

Introduction

Record-breaking wildfires with an unprecedentedly strong pyroconvection series were raging in south east Australia in late December 2019 and early January 2020 [*Ohneiser et al*. 2020, *Khaykin et al*., 2020]. Never observed amounts of biomass-burning smoke were lifted into the stratosphere and formed 5-15 km thick aerosol layers from the tropopause up to around 20 km and partly even 30 km height. In 2020 and 2021, we monitored the stratospheric perturbation by smoke with lidar over Punta Arenas, in southern Chile, for two years. The smoke particles influenced the Earth's radiative balance, the dynamics of the atmosphere, ozone depletion in Antarctica, and the evolution of cirrus clouds in the upper troposphere via heterogeneous ice nucleation in which aged smoke particles served as ice-nucleating particles.

Method

Lidar observations in Punta Arenas (53.2°S, 70.9°W; 9m above sea level, a.s.l.), Chile, were conducted in the framework of the long-term DACAPO-PESO (Dynamics, Aerosol, Cloud And Precipitation Observations in the Pristine Environment of the Southern Ocean) campaign lasting from November 2018 to the end of 2021. The mobile Leipzig Cloudnet supersite LACROS (Leipzig Aerosol and Cloud Remote Observation System Lacros) [*Bühl et al*., 2013] was run continuously (with some short irregular measurement gaps) at the University of Magallanes (UMAG) in Punta Arenas. The Polly instrument (POrtabLle Lidar sYstem) [*Engelmann et al*., 2016] is the key instrument of LACROS for aerosol profiling, and it is installed inside a container. These polarization Raman lidar observations permit us to determine height profiles of the particle backscatter coefficient at the laser wavelengths of 355, 532, and 1064nm, particle extinction coefficients at 355 and 532nm, the particle linear depolarization ratio at 355 and 532nm.

Furthermore, lidar data from the Compact Rayleigh Autonomous Lidar (CORAL, [*Kaifler and Kaifler*, 2021]) is used. CORAL is located in Río Grande in southern Argentina. It is a powerful lidar that allows to detect aerosol optical properties at 532nm from 15km upwards through the whole stratosphere.

For auxiliary meteorological observations, we used GDAS1 (Global Data Assimilation System 1) temperature and pressure profiles with 1° horizontal resolution from the National Weather Service's National Centers for Environmental Prediction [*GDAS*, 2021].

Results and Discussion

The smoke that was injected into the stratosphere above Australia distributed quickly over the entire southern hemispheric stratosphere and was therefore measurable at remote places like Punta Arenas and Río Grande.

Figure 1 summarizes the smoke-related stratospheric lidar observations in Punta Arenas (Polly) and Río Grande (Coral) between January 2020 and November 2021. The geometrical properties in a) show that the first smoke layers in January 2020 were the most intense and well-defined in terms of extinction coefficient. Typically, the smoke boundaries were found to be located between 5km and 28km. Later, the smoke layers got blurrier and weaker and turned into an enhanced background aerosol. Still, 2 years after the injection of the smoke aerosols, the smoke aerosol optical thickness (AOT) is enhanced as can be seen in Fig. 1b). The corresponding AOT shows initial smoke AOT values of more than 0.4 in January, decreasing to 0.03-0.06 in March 2020, and 0.01-0.04 in November 2021, which is only slightly enhanced background aerosol. The CORAL data shows slightly lower AOT as Polly because CORAL only allows for retrieving profiles above 15km height and does therefore miss the lowest part of the smoke layers.

The fact that the Australian smoke was observed for 2 years in the stratosphere and that it coincided with record-breaking ozone hole events in 2020 and 2021 motivated us to discuss a potential impact of the smoke particles on the strong ozone depletion. The discussion is based on the observed overlapping height ranges of the smoke layers, polar stratospheric clouds, and the ozone hole regions that can be seen in Fig. 2. The surface area concentration shows an absolute maximum especially between 8-14km (see Fig. 2a). However, the particle surface area concentration deviation is strongly positive between around 7 and 24km, the polar stratospheric clouds are enhanced up to ~25km and the ozone hole is located between approximately 7 and 25km as can be seen in Fig. 2b. There are two pathways to influence ozone depletion by aerosol pollution. The particles can influence the evolution of PSCs and specifically their microphysical properties (number concentration and size distribution), and on the other hand, the particles can be directly involved in heterogeneous chemical

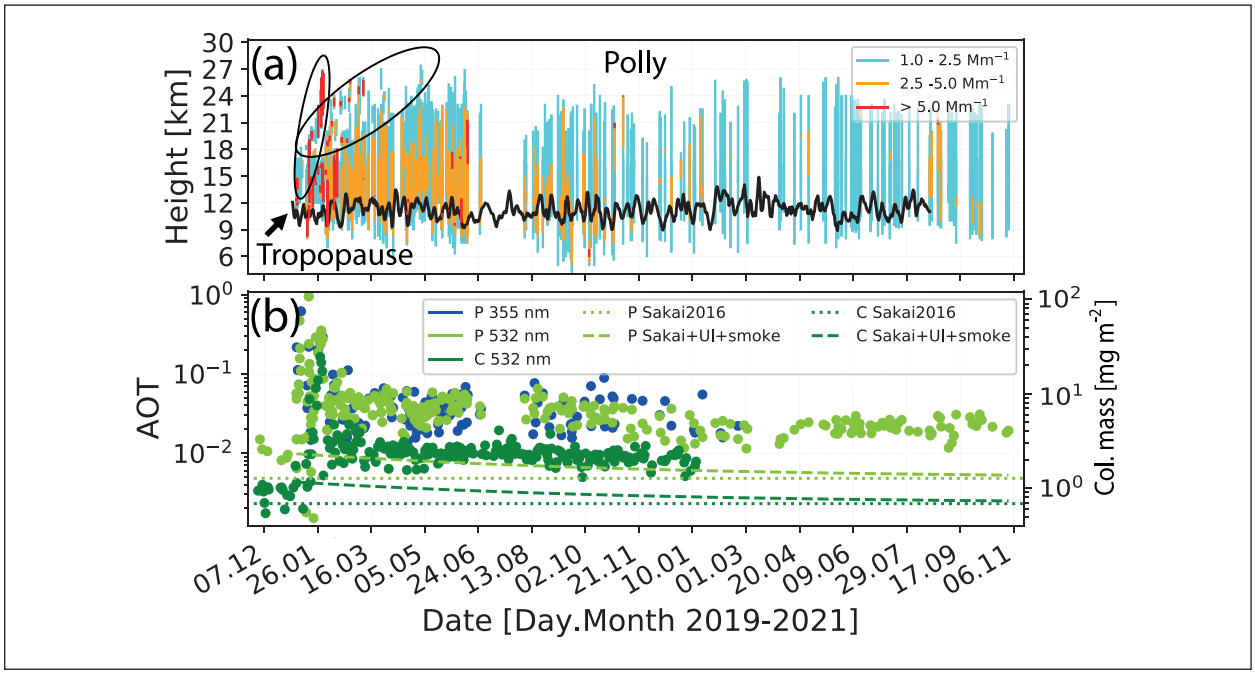

Fig. 1: (a) Overview of Polly observations of UTLS smoke layers (colored bars from bottom to top, one bar per day) from November 2019 to November 2021. Observational gaps between bars are caused by long periods of opaque clouds which do not allow for retrieving stratospheric aerosol profiles. The longer period with missing data in July 2020 is related to a longer Polly measurement gap. The colors in each bar indicate segments with different extinction coefficient levels (<5Mm−1, 5-10Mm−1, and >10Mm−1, see legend in the panel). Black edging highlights the ascending layers, separated from the non-highlighted main layers. (b) Smoke layer AOT and column mass (CORAL, "C", dark green; Polly, "P", bright green and blue) at 355nm and 532nm, calculated from the profiles of the extinction coefficients, multiplied by the layer depth in (a) (in case of CORAL multiplied by 13km being the layer between 15km and 28km height). Note that the Polly data shows the total smoke AOT and the CORAL data shows the AOT between 15 and 28km. CORAL AOT is therefore lower. The curves indicated by "Sakai 2016" represent the background found in Sakai et al., 2016 relevant for Polly "P" and CORAL "C". "Sakai+UI+smoke" curves include also the estimated enhanced background caused by Ulawun volcanic aerosol and smoke aerosol each injected before January 2020 into the lower stratosphere with an AOT relevant for Polly ("P") and Coral ("C").

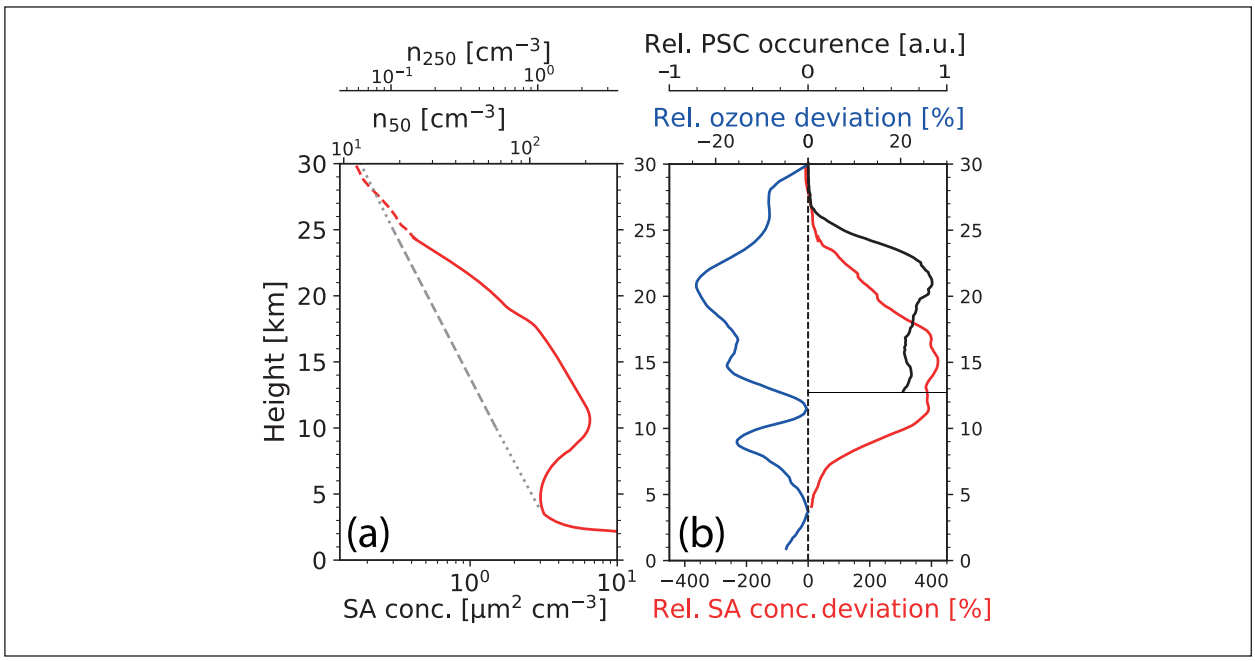

Fig. 2: (a) Estimated surface area concentration and number concentration of September to November 2020 Polly measurements at Punta Arenas (red) compared to the Sakai et al. (2016) background aerosol data (dotted line is extrapolated). (b) Relative estimated surface area concentration deviation, relative partial ozone pressure deviation (September to November 2020) of the mean values averaged at Lauder (New Zealand), Neumayer (Antarctica), and the South Pole (Antarctica) (data from NDACC, 2021). Relative ozone deviation is the 2020 partial ozone pressure profile with respect to the average of 2000-2020. Relative PSC occurence on the southern hemisphere north of 81.8°S in winter 2020 in arbitrary units using CALIPSO data (CALIPSO, 2021). Thin horizontal black line indicates the lower detection boundary of PSC; below this height cirrus clouds were frequently misclassified as PSC.

processes by increasing the particle surface area available to convert nonreactive chlorine components into reactive forms.

Extremely large fires and the injection of large amounts of smoke into the stratosphere is a new important aspect of climate change. It underlines the non-predictable complexity of climate change. Many processes that smoke can initiate in the stratosphere are not yet completely understood and this underlines the need to further investigate the effects of smoke in the stratosphere on chemical and physical processes.

References

Bühl, J., P. Seifert, U. Wandinger, H. Baars,T. Kanitz, J. Schmidt, A. Myagkov, R. Engelmann, A. Skupin, B. Heese, A. Klepel, D. Althausen, and A. Ansmann, (2013): LACROS: the Leipzig Aerosol and Cloud Remote Observations System, *Proc. SPIE 8890*, https://doi.org/10.1117/12.2030911

CALIPSO (Cloud-Aerosol Lidar and Infrared Pathfinder Satellite Observations) data (2021): available at: https://www-calipso.larc.nasa.gov/tools/data_avail/, last access: 26 November, 2021

Engelmann, R., T. Kanitz, H. Baars, B. Heese, D. Althausen, A. Skupin, U. Wandinger, M. Komppula, I. Stachlewska, V. Amiridis, E. Marinou, I. Mattis, H. Linné, and A. Ansmann (2016): The automated multiwavelength Raman polarization and water-vapor lidar PollyXT: the neXT generation, *Atmos. Meas. Tech., 9, 1767–1784,* https://doi.org/10.5194/amt-9-1767-2016

GDAS (Global Data Assimilation System, meteorological database) (2021): available at: https://www.ready.noaa.gov/gdas1.php, last access: 26 November, 2021

Kaifler, B. and N. Kaifler (2021): A Compact Rayleigh Autonomous Lidar (CORAL) for the middle atmosphere, *Atmos. Meas. Tech., 14, 1715–1732*, https://doi.org/10.5194/amt-14-1715-2021

Khaykin, S., B. Legras, S. Bucci, P. Sellitto, L. Isaksen, L. Tencé, S. Bekki, A. Bourassa, L. Rieger, D. Zawada, J. Jumelet, and S. Godin-Beekmann (2020): The 2019/20 Australian wildfires generated a persistent smoke-charged vortex rising up to 35km altitude, *Commun. Earth Environ., 1, 22,* https://doi.org/10.1038/s43247-020-00022-5

NDACC (Network for the Detection of Atmospheric Composition Change) (2021): available at: http://www.ndaccdemo.org/, last access: 26 November, 2021

Ohneiser, K., A. Ansmann, H. Baars, P. Seifert, B. Barja, C. Jimenez, M. Radenz, A. Teisseire, A. Floutsi, M. Haarig, A. Foth, A. Chudnovsky, R. Engelmann, F. Zamorano, J. Bühl, and U. Wandinger (2020): Smoke of extreme Australian bushfires observed in the stratosphere over Punta Arenas, Chile, in January 2020: optical thickness, lidar ratios, and depolarization ratios at 355 and 532nm, *Atmos. Chem. Phys., 20, 8003–8015*, https://doi.org/10.5194/acp-20-8003-2020

Sakai, T., O. Uchino, T. Nagai, B. Liley, I. Morino and T. Fujimoto (2016): Long-term variation of stratospheric aerosols observed with lidars over Tsukuba, Japan, from 1982 and Lauder, New Zealand, from 1992 to 2015, *J. Geophys. Res. Atmos., 121, 10,283–10,293*, https://doi.org/10.1002/2016JD025132

Dispersal and radiative forcing of stratospheric smoke injection from the extreme 2019-2020 Australian wildfires

Bernd Heinold, Holger Baars, Anne Kubin, Kevin Ohneiser, Kerstin Schepanski, Roland Schrödner, Fabian Senf, Ina Tegen

Die extremen Buschbrände in Südostaustralien 2019/2020 setzten gewaltige Mengen Rauchaerosol frei, die durch hochreichende Pyrokonvektion in die Stratosphäre der Südhemisphäre gelangten. Die mächtigen, langlebigen Rauchfahnen beeinflussten erheblich das Strahlungsbudget sowie die Dynamik der Atmosphäre der südlichen mittleren und hohen Breiten. Globale Aerosol-Klima-Modelle sind bisher nicht geeignet, intensive Pyrokonvektionsereignisse zu berücksichtigen. Die Auswirkungen starker Vegetationsbrände auf die Energiebilanz in Klimasimulationen werden dadurch potenziell unterschätzt.

Introduction

The exceptional wildfires in Southeast Australia between late December 2019 and early January 2020 produced enormous amounts of smoke aerosol of more than 1 Tg [*Khaykin et al.*, 2020, *Ohneiser et al.* 2020]. Triggered by the extreme fire heat, several deep pyroconvective events carried the smoke directly up to 14–16 km height into the stratosphere. The thick plumes were distributed eastwards across the mid and high-latitude Southern Hemisphere persistently reducing the atmospheric transparency. Global aerosol-climate models show significant uncertainties regarding the emission height of aerosols from intense wildfires. By combining aerosol-climate modelling and lidar observations, we demonstrate the importance of the representation of those high-altitude fire smoke layers for estimating the atmospheric energy budget.

Method

The 2019-2020 Australian wildfires were investigated with the global aerosol-climate model ECHAM6.3-HAM2.3 [*Tegen et al.*, 2019] as described in *Heinold et al.* [2021]. The simulations were performed at T63 horizontal resolution (~1.875°) in a mode nudged to ERA5 reanalysis and with prescribed sea surface temperature and sea ice extent as boundary condition. The modelled period covers November 2019 to March 2020.

The emissions of biomass burning aerosol were prescribed by daily satellite-based data from the Global Fire Assimilation System [GFAS; *Kaiser et al.*, 2012]. By default, 75% are emitted into the boundary layer (BL), 17% and 8% in the first and second layer above the BL, respectively (*'BASE'* case). As the coarse resolution does not allow to explicitly represent the strong pyroconvective events reported over Southeast Australia [*Kablick et al.*, 2020], we adapted the high-altitude smoke injection height in the model for the days 29–31 December 2019 and 4 January 2020. Without direct information available, the pyroconvective injection heights were varied in sensitivity experiments. A reasonably good representation is by a scenario with 100% smoke injection into the model layer above the tropopause (*'TP+1'* case) shown here as an example.

The pyroconvective injection heights in the model were verified with lidar observations at Punta Arenas (53.14°S, 70.89°W), Chile from the long-term DACAPO-PESO campaign (https://dacapo.tropos.de). Furthermore, measurements by the few mid and high-latitude sun photometer stations of the Aerosol Robotic Network (AERONET) in the Southern Hemisphere were used for evaluation. For more information on the Punta Arenas lidar measurements see *Ohneiser et al.* in this issue.

Results and Discussion

The 2019-2020 Australian wildfire plume considerably increased the aerosol optical thickness (AOT) of the usually pristine Southern Hemisphere [*Hirsch and Koren*, 2021]. Average AOT derived from satellite between 20–60°S was significantly increased to 0.16 for January 2020 implying an offset of approx. 50% from the long-term mean. One year later, observed AOTs were still increased up to 50% relative to 2019.

In Figure 1, the comparison of the ECHAM6.3-HAM2.3 results with the AERONET measurements for January to March 2020 show that the observed AOTs can only be reproduced by the model if the fire injection heights are prescribed accordingly for the observed deep pyroconvection. Whereas, the default results are biased low and less correlated with the observations (Fig. 1a, b).

The Australian wildfire smoke was also observed above Punta Arenas with a ground-based lidar. For three observations in January 2020, the exceptionally thick stratospheric smoke plume is reflected in the measured extinction coefficients in Fig. 1c–f. These remarkable features can only be captured by the model with stratospheric Australian fire injection heights, giving clear evidence that the deep pyroconvection in the Australian wildfire hotspots did emit smoke well above the usually assumed injection heights [*Val Martin et al.*, 2018]. The model results also indicate the role of absorptive aerosol heating for

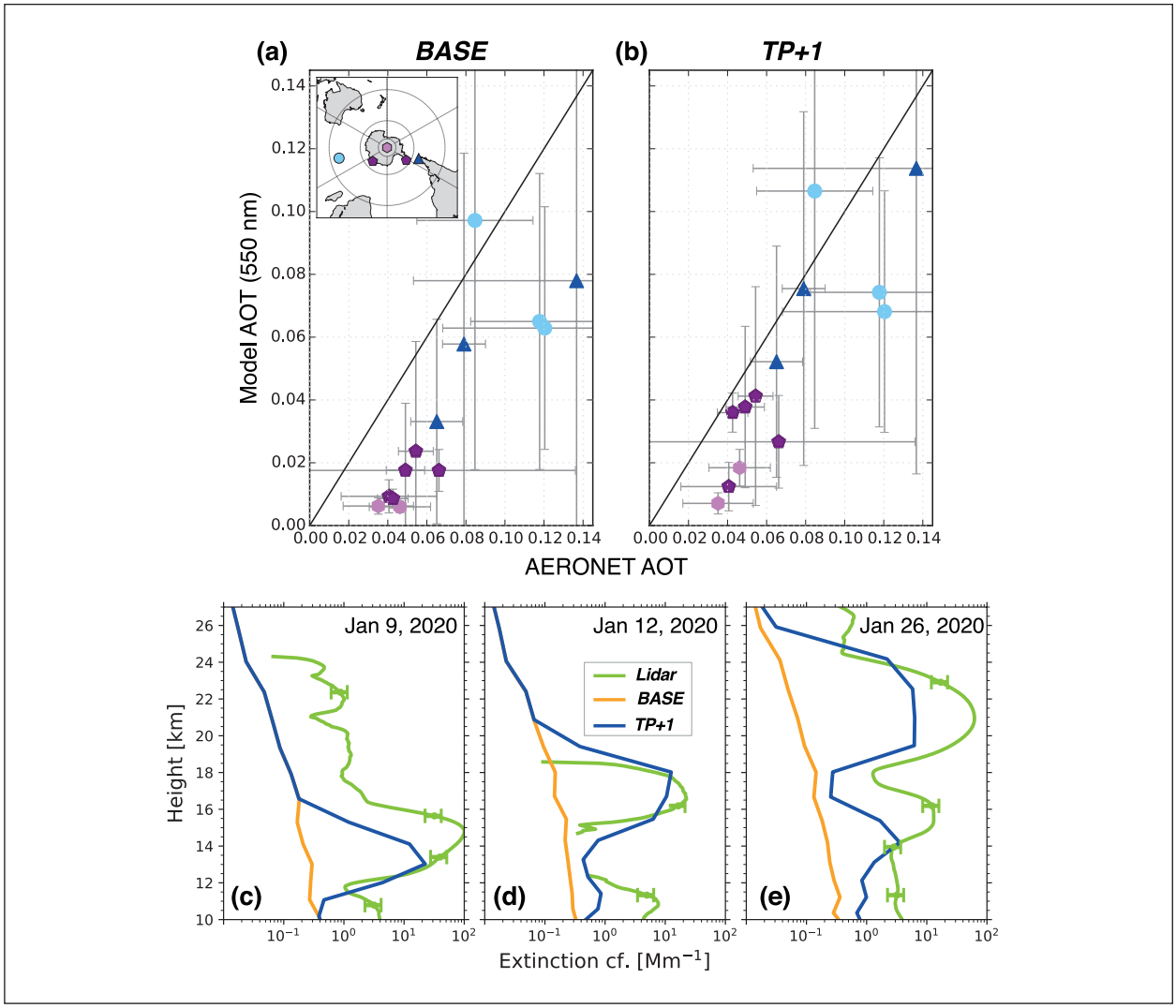

Fig. 1: (a, b) Scatter plots of observed versus simulated monthly mean 550-nm AOT at southern mid and high-latitude AERONET stations for January to March 2020. The error bars represent the standard deviation based on daily values. Compared are model results for the cases (a) BASE and (b) TP+1. The stations are colour-coded respectively: Punta Arenas, Chile (53.14°S, 70.89°W), blue triangle; Amsterdam Island (37.80°S, 77.57°E), light blue circles; Antarctic Stations Marambio (64.24°S, 56.63°W) and Vechernaya Hill (67.66°S, 46.16°E), purple pentagons; South Pole (90.00°S), light purple hexagons. (c-f) Comparison of modelled and observed profiles of aerosol extinction coefficients at the field site in Punta Arenas (53.14°S, 70.89°W) for 9, 12, and 26 January 2020. Error bars indicate the estimated lidar measurement uncertainties of 30%, values below the lidar detection limit are omitted from the graph.

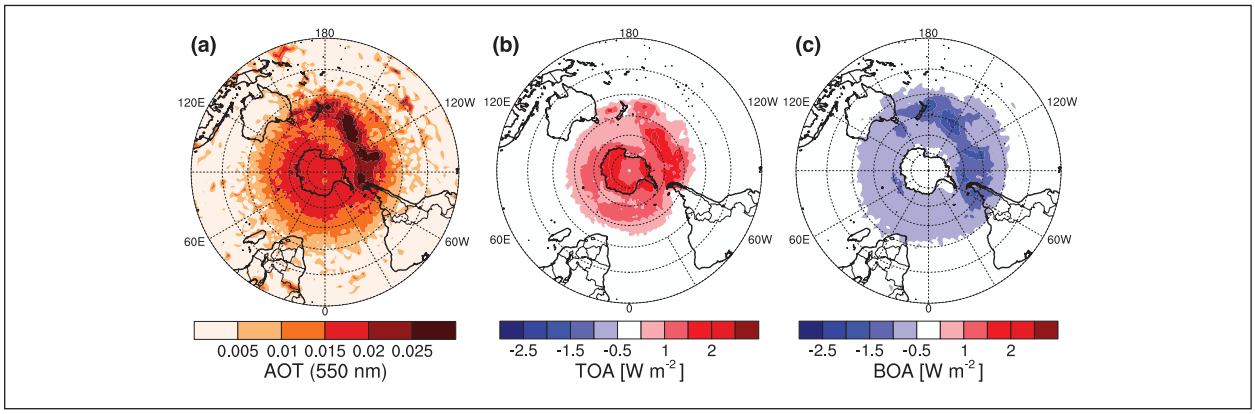

Fig. 2: AOT and solar radiative forcing of the 2019-2020 Australian wildfire smoke plume in the Southern Hemisphere. Model results of (a) AOT and (b, c) instantaneous shortwave radiative forcing of the elevated smoke aerosol layer, averaged over the months January to March 2020. All values are differences between ECHAM6.3-HAM2.3 results with Australian wildfire smoke injection into the model layer above tropopause for the pyroconvective days 29 – 31 December 2019 and 1 April 2020 (TP+1) as well as model results without the pyroconvective smoke emissions. The instantaneous radiative flux differences are shown for all-sky conditions at top (TOA; b) and surface/bottom of the atmosphere (BOA; c).

the vertical transport. There is a continuous rise of the smoke layer in the lidar profiles (Fig. 1c–f), which can only be reproduced if aerosol-radiation interactions are considered in the simulations that finally lead to a considerable absorptive heating.

This individual extreme Australian fire event caused a significant top-of-atmosphere (TOA) hemispheric instantaneous direct radiative forcing signal that reached a magnitude comparable to the radiative forcing by anthropogenic absorbing aerosol [*Thornhill et al.*, 2021]. Up to +0.50 W m^{-2} instantaneous direct radiative forcing was modelled at TOA, averaged for the Southern Hemisphere for January–March 2020 under all-sky conditions. At surface, an instantaneous solar radiative forcing of up to -0.81 W m^{-2} was found for clear-sky conditions, comparable to the short-term surface dimming by a large volcanic eruption [*Schmidt et al.*, 2018]. On the other hand, a significant absorptive heating with maximum heating rates in January 2020 of 1.7 K day^{-1} was modelled for the smoke-containing air layer. While the effective TOA radiative forcing is expected to be low due to stratospheric adjustment to the instantaneous forcing, these heating rate changes may trigger responses in the atmospheric dynamics [*Khaykin et al.*, 2020].

Since extreme wildfires are expected to occur more frequently in the rapidly changing climate, our findings suggest that deep wildfire plumes must be adequately considered in climate projections in order to obtain reasonable estimates of atmospheric energy budget changes.

References

Heinold, B., H. Baars, B. Barja, M. Christensen, A. Kubin, K. Ohneiser, K. Schepanski, N. Schutgens, F. Senf, R. Schrödner, D. Villanueva, and I. Tegen (2021): Important role of stratospheric injection height for the distribution and radiative forcing of smoke aerosol from the 2019/2020 Australian wildfires, *Atmos. Chem. Phys. Discuss.* [preprint], https://doi.org/10.5194/acp-2021-862, in review.

Hirsch, E. and I. Koren, I. (2021): Record-breaking aerosol levels explained by smoke injection into the stratosphere, *Science*, 371, 6535, 1269-1274, https://doi.org/10.1126/science.abe1415.

Kablick, G. P. III, D. R. Allen, M. D. Fromm, and G. E. Nedoluha (2020): Australian pyroCb smoke generates synoptic – scale stratospheric anticyclones, *Geophys. Res. Lett.*, 47, e2020GL088101, https://doi.org/10.1029/2020GL088101.

Kaiser, J. W., A. Heil, M. O. Andreae, A. Benedetti, N. Chubarova, L. Jones, J.-J. Morcrette, M. Razinger, M. G. Schultz, M. Suttie, and G. R. van der Werf (2012): Biomass burning emissions estimated with a global fire assimilation system based on observed fire radiative power, *Biogeosciences*, 9, 527–554, https://doi.org/10.5194/bg-9-527-2012.

Khaykin, S., B. Legras, S. Bucci, P. Sellitto, L. Isaksen, L. Tencé, S. Bekki, A. Bourassa, L. Rieger, D. Zawada, J. Jumelet, and S. Godin-Beekmann (2020): The 2019/20 Australian wildfires generated a persistent smoke-charged vortex rising up to 35km altitude, *Nature Communications Earth and Environment, 1, 22,* https://doi.org/10.1038/s43247-020-00022-5.

Ohneiser, K., A. Ansmann, H. Baars, P. Seifert, B. Barja, C. Jimenez, M. Radenz, A. Teisseire, A. Floutsi, M. Haarig, A. Foth, A. Chudnovsky, R. Engelmann, F. Zamorano, J. Bühl, and U. Wandinger (2020): Smoke of extreme Australian bushfires observed in the stratosphere over Punta Arenas, Chile, in January 2020: optical thickness, lidar ratios, and depolarization ratios at 355 and 532nm, *Atmos. Chem. Phys., 20, 8003–8015*, https://doi.org/10.5194/acp-20-8003-2020.

Schmidt, A., M. J. Mills, S. Ghan, J. M. Gregory, R. P. Allan, T. Andrews, C. G. Bardeen, A. Conley, P. M. Forster, A. Gettelman, R. W. Portmann, S. Solomon, and O. B. Toon (2018): Volcanic Radiative Forcing From 1979 to 2015, *J. Geophys. Res.-Atmos.*, 123, 12491–12508, https://doi.org/10.1029/2018JD028776.

Tegen, I., D. Neubauer, S. Ferrachat, C. Siegenthaler-Le Drian, I. Bey, N. Schutgens, P. Stier, D. Watson-Parris, T. Stanelle, H. Schmidt, S. Rast, H. Kokkola, M. Schultz, S. Schroeder, N. Daskalakis, S. Barthel, B. Heinold, and U. Lohmann (2019): The global aerosol–climate model ECHAM6.3–HAM2.3 – Part 1: Aerosol evaluation, *Geosci. Model Dev.*, 12, 1643–1677, https://doi.org/10.5194/gmd-12-1643-2019.

Thornhill, G. D., W. J. Collins, R. J. Kramer, D. Olivié, R. B. Skeie, F. M. O'Connor, N. L. Abraham, R. Checa-Garcia, S. E. Bauer, M. Deushi, L. K. Emmons, P. M. Forster, L. W. Horowitz, B. Johnson, J. Keeble, J.-F. Lamarque, M. Michou, M. J. Mills, J. P. Mulcahy, G. Myhre, P. Nabat, V. Naik, N. Oshima, M. Schulz, C. J. Smith, T. Takemura, S. Tilmes, T. Wu, G. Zeng, and J. Zhang (2021): Effective radiative forcing from emissions of reactive gases and aerosols – a multi-model comparison, *Atmos. Chem. Phys.*, 21, 853–874, https://doi.org/10.5194/acp-21-853-2021.

Val Martin M., R. A. Kahn, and M. G. Tosca (2018): A Global Analysis of Wildfire Smoke Injection Heights Derived from Space-Based Multi-Angle Imaging, *Remote Sens.*, 10, 1609, https://doi.org/10.3390/rs10101609.

Funding

Internal project, TROPOS.

Cooperation

Pacific Northwest National Laboratory (PNNL), Richland, WA, USA;
Deutscher Wetterdienst (DWD), Offenbach, Germany;
Freie Universität Berlin, Berlin, Germany;
Vrije Universiteit Amsterdam, Amsterdam, the Netherlands;
University of Magallanes, Punta Arenas, Chile.

VACCINE — Variation in Antarctic cloud condensation nuclei and Ice nucleating particle concentrations at Neumayer Station III

Silvia Henning[1], Rolf Weller[2], Linda Ort[2], Julia Loftfield[2], Marcus Schumacher[2], Heike Wex[1], Frank Stratmann[1]

[1] Leibniz Institute of Tropospheric Research, Leipzig, Germany

[2] Alfred Wegener Institute, Helmholtz Centre for Polar and Marine Research (AWI), Bremerhaven, Germany

Im Rahmen des vorgestellten Projekts VACCINE wurden die ersten kompletten Jahresgänge von Wolkenkondensations- (CCN) und Eisnukleationskeimkonzentrationen (INP) an der deutschen Antarktis-Station Neumayer III gemessen. Dies erlaubt zum ersten Mal CCN- und INP-Konzentrationen sowie deren Quellen in Abhängigkeit der Jahreszeiten in Dronning Maud Land zu untersuchen. Die CCN-Konzentration zeigt einen ausgeprägten Jahresgang mit um Faktor zehn höheren Werten im Sommer, der Jahresgang der Partikelhygroskopizität läuft dem entgegen und zeigt hygroskopischere Partikel in den Wintermonaten. Die INP-Konzentrationen liegen ganzjährig sehr niedrig und haben kaum einen Anteil an INP, die oberhalb von minus 15°C Gefrieren auslösen. Im weiteren Verlauf des Projekts werden mit Hilfe von Rückwärtstrajektorien CCN- und INP-Quellgebiete sowie Transportwege identifiziert werden. Die vorgestellten INP- und CCN-Daten repräsentieren einen extrem wertvollen Datensatz, der einen maßgeblichen Beitrag zur weiteren Optimierung von Klimamodellen beitragen wird.

Background

The earth's climate changes at rates unprecedented in thousands, if not hundreds of thousands of years, with the Polar Regions being the fastest warming areas on earth. Polar regions have also a strong global impact on climate conditions and therefore affect lives and livelihoods across the world. Despite the progress polar climate research made, poorly understood processes remain, one of those being the aerosol – cloud – climate interaction, which still cannot be modelled with satisfying accuracy. Clouds and their interactions with the climate system are one of the most difficult components to model, especially in the polar regions. This is, among others, due to difficulties in obtaining high-quality measurements. The availability of high-quality measurements is therefore of crucial importance for understanding processes and for driving and / or evaluating atmospheric models. Increasing the available data-base is one of the main objectives of VACCINE. Starting with December 2019, TROPOS continuously performs in-situ Cloud Condensation Nuclei (CCN) and Ice Nucleating Particles (INP) measurements at Neumayer Station III. In the future, the captured data such as number concentrations, particle hygroscopicity, INP freezing spectra etc. will be linked with meteorological information (e.g. back trajectories) and information on the chemical composition of the prevailing aerosol particles for identifying sources of INP and CCN (secondary vs. primary) and transport pathways (local vs. long-range transport) over the full annual cycle. A result of this project will be a deeper understanding about processes dominating the CCN and INP population in Antarctica.

Fig. 1: CCN instrument (left) and the low volume sample set-up (right) as installed in the AWI Air Chemistry Observatory at Neumayer Station III. Both units sample from the same whole air inlet as the other aerosol instrumentation, which is situated on top of the measurement container.

Fieldwork at Neumayer Station III

Starting with the austral summer season in December 2019, CCN-measurements were carried out at the AWI Air Chemistry Observatory with a commercially available CCN instrument [*Roberts and Nenes*, 2005]. With the instrument total CCN number concentrations can be determined as function of supersaturation in the range between 0.1 and about 1%. The instrument was installed at the observatory (Fig. 1, left) and has been measuring continuously since then. The remote access to the CCN proofed stable, allowing performance checks of the instrument from TROPOS. The daily / weekly on-site maintenance is being carried out by AWI-staff.

Besides CCN also INP sampling was established, using the low volume filter sampling setup available in the AWI Air Chemistry Observatory (Fig. 1, right). These activities aim at the number concentrations of INP in the air, active at temperatures above -25°C. Filter samples are collected on polycarbonate filters and immediately frozen for later analysis in the TROPOS laboratories [*Wex et al.*, 2019]. The weekly filter change and handling is done by the AWI-staff, as well. These samples are the first ever collected for INP analysis at Dronning Maud

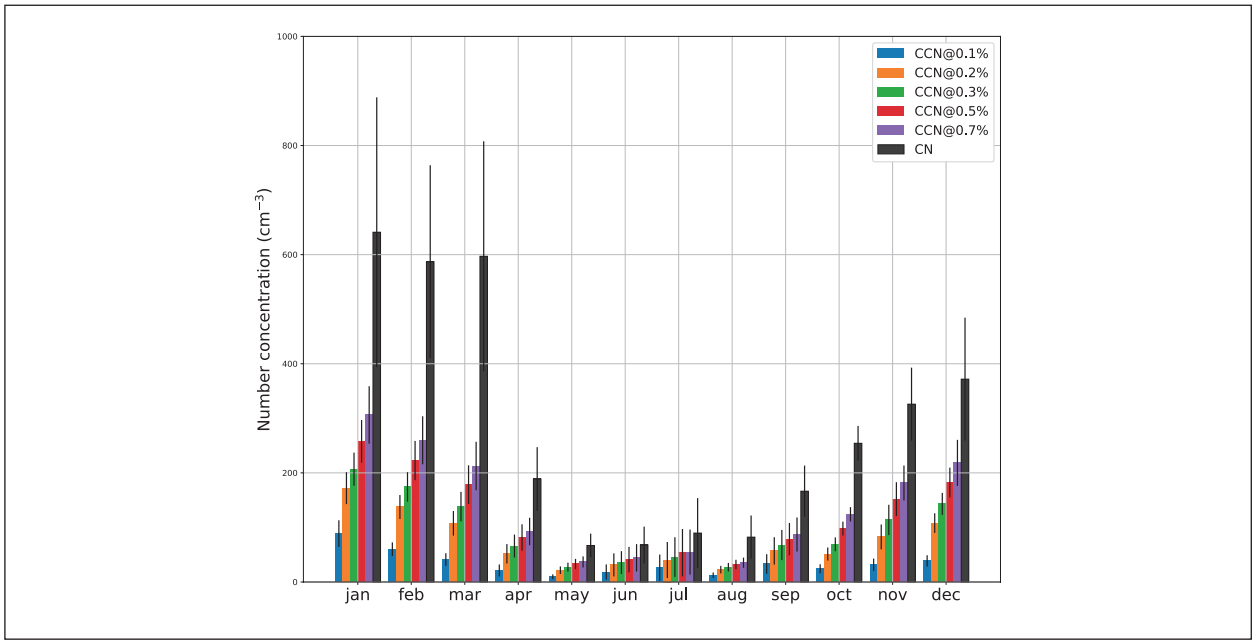

Fig. 2: Two-years annual cycle of the number concentration of cloud condensation nuclei between 0.1% and 0.7% supersaturation and the total particle concentration CN. The current data set ranges from December 2019 until November 2021.

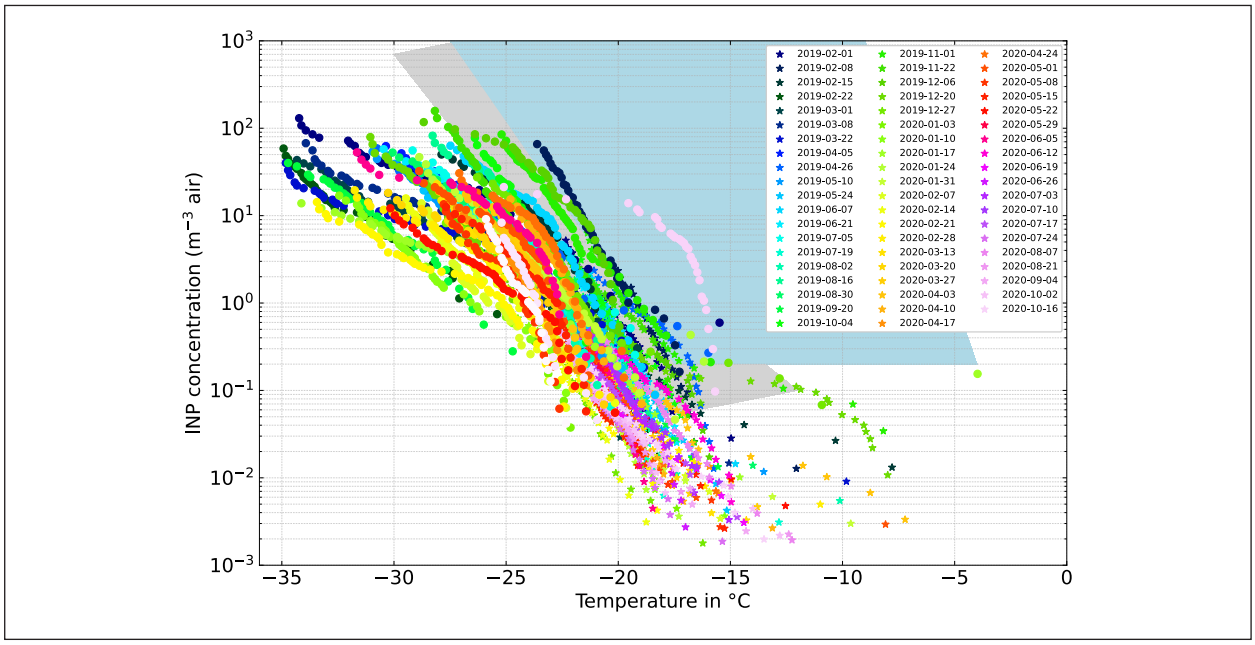

Fig. 3: INP freezing spectra (blue area: Tatzelt et al., 2021, grey area: McCluskey et al., 2018). Sample period ranges from Feb 2019 until Oct 2020 with weekly to biweekly resolution. The date gives the start day of the sampling period.

Land in Antarctica spanning the whole annual cycle. The here presented data cover the first 20 months of samples.

Preliminary results

CCN measurements. The CCN instrument measures CCN number concentrations at 5 different supersaturations. Combined with the particle number size distribution measurements, the particle hygroscopicity can be derived [*Petters and Kreidenweis*, 2006]. Running continuously since December 2019 two full years of CCN data for Neumayer station III have been gained (Figure 2). Number concentrations in general are low and a clear annual cycle is found for CCN as well as for the total particle number (CN). The latter is similar to results reported for the Belgian Princess Elisabeth Station, located 200 km inland in the escarpment zone of Dronning Maud Land at an altitude of 1400 m [*Herenz et al.*, 2019]. Lowest number concentrations are observed in austral winter months May to August with monthly averages below 20 cm^{-3} at, e.g., the supersaturation of 0.1% and an CN concentration below 100 cm^{-3} during this time. In January, CCN increased to 90 cm^{-3} at 0.1% and CN increased to 610 cm^{-3}.

New particle formation events were observed in the summer months. Some of them were followed by particle growth into the CCN diameter range. April is a transition month between summer and winter; while the ratio between winter and summer concentrations is about 10 for both CCN and CN, for April the ratio to the summer values is only 3 for CN, but 4.5 for CCN. In April new particle formation events do still occur, but might not be followed by particle growth to CCN sizes anymore. Also, the hygroscopicity parameter exhibits an annual cycle. In summer, low values were found, ranging from 0.3 at 0.7% to 0.6 at 0.1% supersaturation, suggesting a strong influence of organic matter for smaller particles. In winter the particle hygroscopicity was on average much higher - around 1 - at all supersaturations, which might be caused by an increasing influence of long-range transport to the station.

INP results. INP freezing spectra from the off-line analysis of all so far available filter samples is shown in Fig. 3. In general, the INP concentrations are very low even compared to other measurements in the southern hemisphere [blue area: *Tatzelt et al.*, 2021, grey area: *McCluskey et al.*, 2018]. As a preliminary result only very few samples are ice active at temperatures warmer than -15°C, which might point towards the absence of biological INP sources in the region. The INP freezing spectra will in the further course of the project be linked with meteorological information and information on the chemical composition of the prevailing aerosol particles for identifying sources of INP and CCN over the full annual cycle.

All results are preliminary and will be followed up by an in-depth analysis including a backward trajectory analysis. A further approach applied for source identification will be the potential source contribution

function (PSCF), which is a receptor modelling method that is based on air mass back trajectories. The PSCF [*Ashbaugh et al.*, 1985] has been successfully applied to high-latitude studies in the Antarctic [*Herenz et al. 2019*, *Dall´Osto et al.*, 2017]. This model is commonly used to identify regions that have the potential to contribute to high values of measured concentrations at a receptor site.

With the dataset resulting from the measurements introduced herein, we will be able to make significant progress in understanding the Antarctic aerosol in the future, helping to improve model predictions.

References

Ashbaugh LL, Malm WC, Sadeh WZ (1985), A residence time probability analysis of sulfur concentrations at Grand Canyon National Park. *Atmos. Environ.* (1967), 19(8), 1263-1270, https://doi.org/10.1016/0004-6981(85)90256-2.

Dall´Osto M, et al. (2017), Arctic sea ice melt leads to atmospheric new particle formation. Sci. Rep., 7(1), 3318, https://doi.org/10.1038/s41598-017-03328-1.

McCluskey, C. S., J. Ovadnevaite, M. Rinaldi, J. Atkinson, F. Belosi, D. Ceburnis, S. Marullo, T. C. J. Hill, U. Lohmann, Z. A. Kanji, C. O'Dowd, S. M. Kreidenweis, and P. J. DeMott (2018), Marine and Terrestrial Organic Ice-Nucleating Particles in Pristine Marine to Continentally Influenced Northeast Atlantic Air Masses, *J. Geophys. Res. - Atmos.*, *123*(11), 6196-6212, https://doi.org/10.1029/2017jd028033.

Herenz, P., H. Wex, A. Mangold, Q. Laffineur, I. V. Gorodetskaya, Z. L. Flemming, M. Panagi, and F. Stratmann (2019), CCN measurements at the Princess Elisabeth Antarctica Research Station during three austral summers, *Atmos. Chem. Phys*., 19, 275–294, https://doi.org/10.5194/acp-19-275-2019.

Petters MD, Kreidenweis SM (2007), A single parameter representation of hygroscopic growth and cloud condensation nucleus activity, *Atmos. Chem. Phys.*, 7(8), 1961-1971.

Roberts GC, Nenes A (2005), A continuous-flow streamwise thermal-gradient CCN chamber for atmospheric measurements. *Aerosol Sci. Technol.*, 39(3), 206-221.

Tatzelt, C., S. Henning, A. Welti, A. Baccarini, M. Hartmann, M. Gysel-Beer, M. van Pinxteren, R. L. Modini, J. Schmale, and F. Stratmann (2021), Circum-Antarctic abundance and properties of CCN and INP, *Atmos. Chem. Phys. Discuss. [preprint]*, https://doi.org/10.5194/acp-2021-700.

Weller R, Schmidt K, Teinila K, Hillamo R (2015), Natural new particle formation at the coastal Antarctic site Neumayer. *Atmos. Chem. Phys.*, 15(19), 11399-11410, https://doi.org/10.5194/acp-15-11399-2015.

Wex H, et al. (2019), Annual variability of ice-nucleating particle concentrations at different Arctic locations. *Atmos. Chem. Phys.*, 19(7), 5293-5311, https://doi.org/10.5194/acp-19-5293-2019.

Funding

DFG, German Research Foundation, HE 6770/3.

Cooperation

Alfred Wegener Institute, Helmholtz Centre for Polar and Marine Research (AWI), Bremerhaven, Germany.

Hemispheric contrasts in stratiform mixed-phase cloud properties observed with LACROS

Martin Radenz[1], Patric Seifert[1], Johannes Bühl[1], Holger Baars[1], Ronny Engelmann[1], Boris Barja González[2], Albert Ansmann[1]

[1] Leibniz Institute for Tropospheric Research (TROPOS), Leipzig, Germany

[2] Atmospheric Research Laboratory, University of Magallanes, Punta Arenas, Chile

Anhand dreier Langzeitdatensätze des Leipziger Aerosol- und Wolken- Fernerkundungssystem (Leipzig Aerosol and Cloud Remote Observations System; LACROS) wurden hemisphärische Unterschiede der Eisbildung in unterkühlten Schichtwolken untersucht. Für die Nordhemisphäre wurden zwischen 2014 und 2018 gesammelte LACROS-Datensätze aus Leipzig (Deutschland, 51,4°N, 12,4°E) und Limassol (Zypern, 34,7°N, 33,0°E) verwendet. Die Beobachtungen in mittleren Breiten der Südhemisphäre wurden zwischen November 2018 und Dezember 2021 in Punta Arenas (Chile, 53,1°S, 70,9°W) im Rahmen der Kampagne DACAPO-PESO (Dynamics Aerosol Clouds And Precipitation Observation in the Pristine Environment of the Southern Ocean; Beobachtung von Dynamik, Aerosol, Wolken und Niederschlag in der unverschmutzen Umgebung des Südozeans) erhoben. Dieser Datensatz stellt die ersten mehrjährigen bodengebundenen Fernerkundungsbeobachtungen in der westlichen Hälfte des Südozeans dar. Es konnte nachgewiesen werden, dass atmosphärische Schwerewellen die Bildung und Detektierbarkeit der Eisphase erschweren und dass eine Kopplung von Wolken mit der planetaren Grenzschicht die Häufigkeit der Eisbildung erhöht. Werden diese beiden Effekte berücksichtigt, tritt Eisbildung in Schichtwolken über Punta Arenas etwas weniger häufig auf als über Limassol und Leipzig. Dieser Unterschied kann auf eine geringere Verfügbarkeit von Eiskeimen in der freien Troposphäre über Punta Arenas zurückgeführt werden.

Introduction

Ice formation is a crucial process in supercooled clouds, affecting the radiative properties, lifetime, and precipitation formation. In the heterogeneous freezing regime, between 0 and -40°C aerosol particles with ice-nucleating properties are required to initiate the formation of ice. Globally, the availability of these ice-nucleating particles (INP) varies strongly, with a generally higher abundance in the northern hemisphere [*Gong*, 2020; *Welti*, 2020]. Poorer accuracy of weather predictions and climate simulations in the southern mid-latitudes compared to the northern hemisphere are frequently related to contrasts in the aerosol load [*Trenberth*, 2010; *Kuma*, 2020]. But, thermodynamics are the dominant driver of cloud microphysics and frequently mask the aerosol-related effects. Pinpointing the aerosol effect in such entangled systems requires comprehensive remote-sensing observations of aerosol load, cloud properties, and vertical motions. Thee long-term campaigns of the ground-based remote-sensing supersite LACROS (Leipzig Aerosol and Cloud Remote Observations System) in key regions of the climate system provide such observations. Focusing on shallow, stratiform, liquid-topped clouds in the multi-year dataset allows investigations of primary ice formation. This is done by analyzing the frequency of ice formation at a specific cloud-top temperature (CTT).

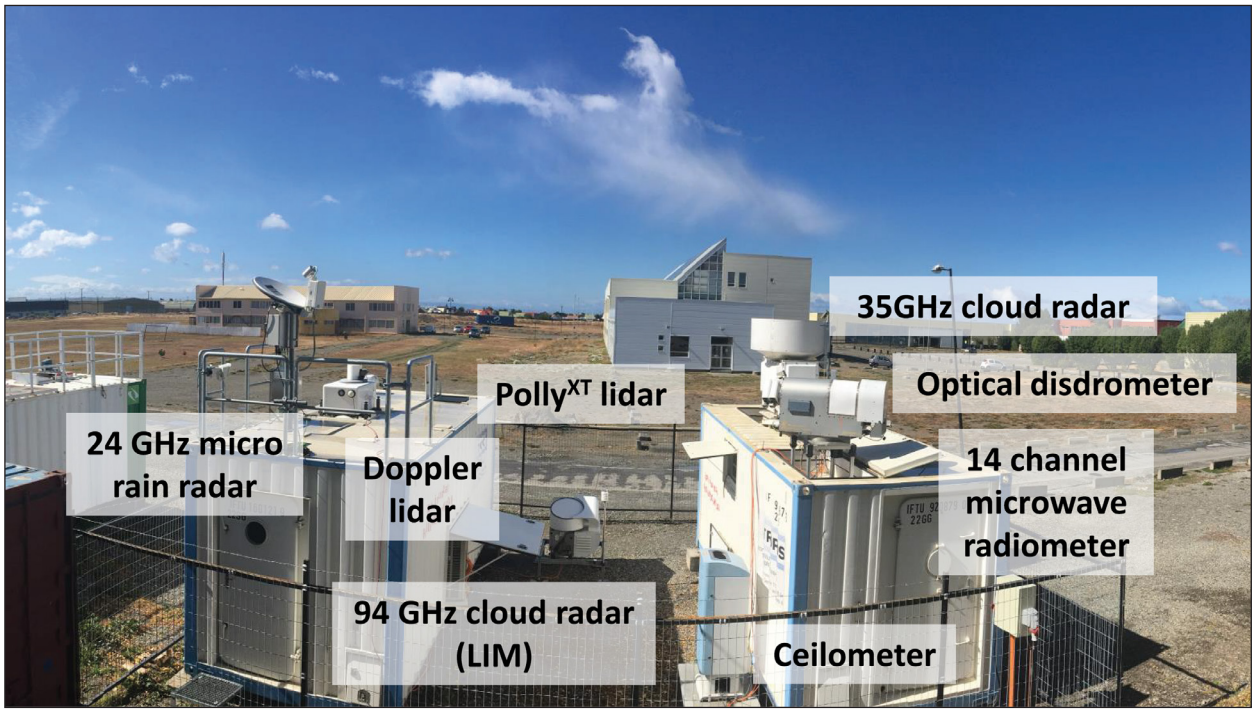

Fig. 1: The mobile facility LACROS deployed at the campus of the University of Magallanes at Punta Arenas, Chile.

LACROS observations at Leipzig, Limassol, and Punta Arenas

Between 2014 and 2018, LACROS conducted long-term observations at Leipzig (51.4°N, 12.4°E, Germany) and Limassol (34.7°N, 33.0°E, Cyprus) [*Bühl*, 2016; *Ansmann*, 2019]. From November 2018 to December 2021, LACROS was deployed to Punta Arenas (53.1°S, 70.9°W, Chile) for the campaign DACAPO-PESO (Dynamics Aerosol Clouds And Precipitation Observation in the Pristine Environment of the Southern Ocean) [*Radenz*, 2021]. These three datasets cover the aerosol conditions of a continental northern hemispheric background site, a hotspot of mineral dust in the eastern Mediterranean, and the marine-dominated pristine Southern Ocean, respectively. The datasets at Limassol and Punta Arenas resemble the first multi-year ground-based remote-sensing datasets in the Eastern Mediterranean and the western part of the Southern Ocean. A combination of state-of-the-art instrumentation, namely a MIRA-35 35 GHz scanning cloud radar, a Polly^{XT} multi-wavelength Raman polarization lidar, a Streamline XR 1.5 µm scanning Doppler lidar, a HATPRO 14-channel microwave radiometer, a 1064 nm ceilometer, an optical disdrometer, and radiation sensors covers the decisive properties of aerosols, dynamics, clouds, and precipitation for a more comprehensive picture of aerosol–cloud interaction. The analysis of the observations is based on well-established synergistic retrievals, such as Cloudnet [*Illingworth et al.*, 2007] and the lidar processing chain PollyNET [*Baars et al.*, 2016, 2017; *Yin and Baars*, 2021]. For the automatic extraction of the cloud cases from the extensive dataset an algorithm with objective criteria was developed [*Bühl*, 2016; *Radenz*, 2021]. Compared to prior lidar-only studies of the frequency of ice formation in supercooled layered clouds [*Kanitz*, 2011; *Seifert*, 2010], the synergistic dataset provides a better sensitivity for low ice-water contents and enables observations of in-cloud vertical motion.

Results

The low frequency of ice-forming clouds at Punta Arenas below -15°C can be related to orographic gravity waves. In the waves, stationary updrafts allow for persistent liquid saturation and the ice crystals are only observable downwind. These clouds could be identified by utilizing the autocorrelation function of the in-cloud vertical air velocity. Wave-driven clouds were identified in 30% of all clouds below -15°C over Punta Arenas. Additionally, a correlation between the surface-coupling of a cloud and the likelihood of ice formation was found for Punta Arenas and Leipzig. At T>-10°C, clouds coupled to the aerosol-rich boundary layer contained ice by a fraction of 0.3-0.4 more frequently. Taking both effects into account, free-tropospheric, fully turbulent clouds at Punta Arenas form ice less frequently than their northern-hemispheric counterparts (Fig 2a). This difference can be linked to a lower abundance of INPs in the free troposphere

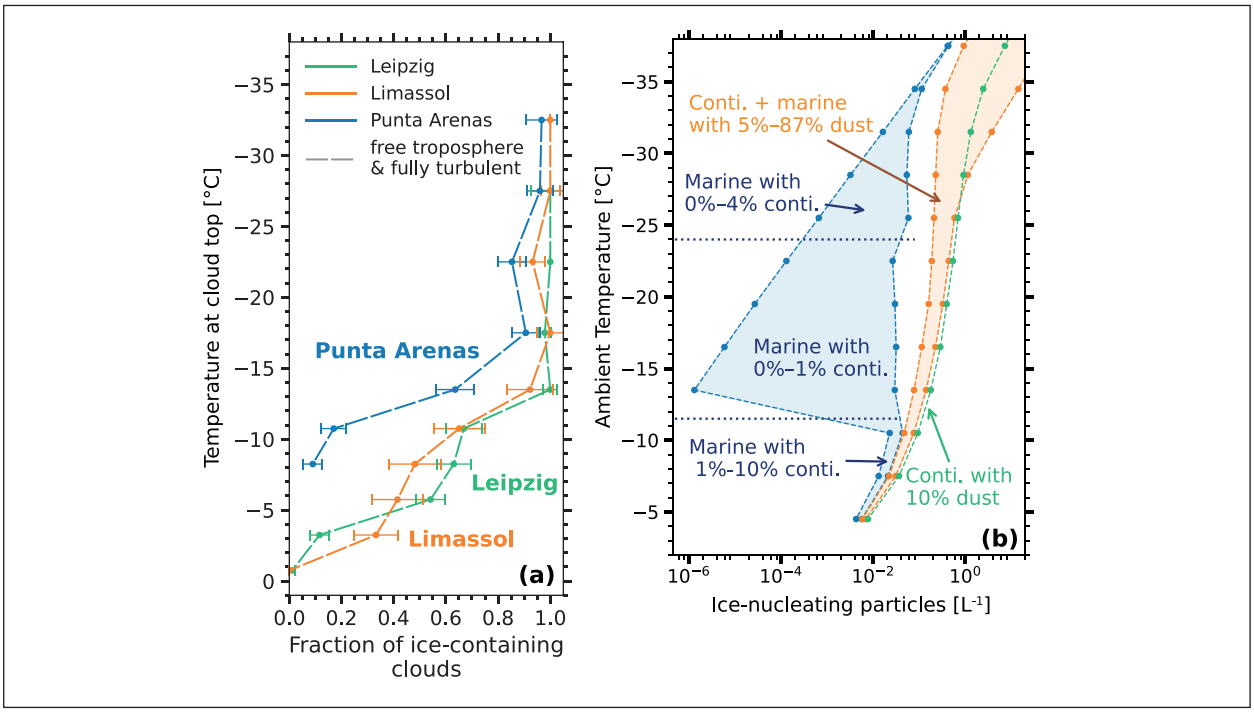

Fig. 2: (a) Fraction of clouds containing ice at a given cloud-top temperature for the locations of the LACROS deployments. Only free-tropospheric and turbulent clouds are shown after filtering for gravity waves and boundary layer coupling. (b) Estimated profiles of ice-nucleating-particle (INP) concentrations based on averaged lidar optical data, airmass source and well-established parametrizations. At Punta Arenas, a strong increase at -10°C is related to boundary-layer aerosol load.

at Punta Arenas. In Fig. 2b, profiles of lidar-estimated INP concentrations at ambient temperature are shown. The lower abundance of ice-containing clouds at Punta Arenas below -15°C can be linked to a factor of 10 times lower INP concentrations.

In a next step, the impact of the comparably high INP concentrations in the boundary layer on cloud microphysics will be more closely investigated. In terms of cloud microphysical properties, constraining the number and size of the ice particles will be an area of future research efforts.

References

Ansmann, A., R. E. Mamouri, J. Bühl, P. Seifert, R. Engelmann, J. Hofer, A. Nisantzi, J. D. Atkinson, Z. A. Kanji, B. Sierau, M. Vrekoussis, and J. Sciare (2019), Ice-nucleating particle versus ice crystal number concentrationin altocumulus and cirrus layers embedded in Saharan dust:a closure study, Atmos. Chem. Phys., 19(23), 15087-15115, https://doi.org/10.5194/acp-19-15087-2019.

Baars, H., P. Seifert, R. Engelmann, and U. Wandinger (2017), Target categorization of aerosol and clouds by continuous multiwavelength-polarization lidar measurements, Atmos. Meas. Tech., 10(9), 3175-3201, https://doi.org/10.5194/amt-10-3175-2017.

Baars, H., T. Kanitz, R. Engelmann, D. Althausen, B. Heese, M. Komppula, J. Preißler, M. Tesche, A. Ansmann, U. Wandinger, J. H. Lim, J. Y. Ahn, I. S. Stachlewska, V. Amiridis, E. Marinou, P. Seifert, J. Hofer, A. Skupin, F. Schneider, S. Bohlmann, A. Foth, S. Bley, A. Pfüller, E. Giannakaki, H. Lihavainen, Y. Viisanen, R. K. Hooda, S. N. Pereira, D. Bortoli, F. Wagner, I. Mattis, L. Janicka, K. M. Markowicz, P. Achtert, P. Artaxo, T. Pauliquevis, R. A. F. Souza, V. P. Sharma, P. G. van Zyl, J. P. Beukes, J. Sun, E. G. Rohwer, R. Deng, R. E. Mamouri, and F. Zamorano (2016), An overview of the first decade of PollyNET: an emerging network of automated Raman-polarization lidars for continuous aerosol profiling, Atmos. Chem. Phys., 16(8), 5111-5137, https://doi.org/10.5194/acp-16-5111-2016.

Bühl, J., P. Seifert, A. Myagkov, and A. Ansmann (2016), Measuring ice- and liquid-water properties in mixed-phase cloud layers at the Leipzig Cloudnet station, Atmos. Chem. Phys., 16(16), 10609-10620, https://doi.org/10.5194/acp-16-10609-2016.

Gong, X., H. Wex, M. van Pinxteren, N. Triesch, K. W. Fomba, J. Lubitz, C. Stolle, T. B. Robinson, T. Müller, H. Herrmann, and F. Stratmann (2020), Characterization of aerosol particles at Cabo Verde close to sea level and at the cloud level – Part 2: Ice-nucleating particles in air, cloud and seawater, Atmos. Chem. Phys., 20(3), 1451-1468, https://doi.org/10.5194/acp-20-1451-2020.

Illingworth, A. J., R. J. Hogan, E. J. O'Connor, D. Bouniol, M. E. Brooks, J. Delanoé, D. P. Donovan, J. D. Eastment, N. Gaussiat, J. W. F. Goddard, M. Haeffelin, H. K. Baltink, O. A. Krasnov, J. Pelon, J.-M. Piriou, A. Protat, H. W. J. Russchenberg, A. Seifert, A. M. Tompkins, G.-J. van Zadelhoff, F. Vinit, U. Willén, D. R. Wilson, and C. L. Wrench (2007), Cloudnet: Continuous Evaluation of Cloud Profiles in Seven Operational Models Using Ground-Based Observations, Bull. Amer. Meteor. Soc., 88(6), 883-898, https://doi.org/10.1175/bams-88-6-883.

Kanitz, T., P. Seifert, A. Ansmann, R. Engelmann, D. Althausen, C. Casiccia, and E. G. Rohwer (2011), Contrasting the impact of aerosols at northern and southern midlatitudes on heterogeneous ice formation, Geophys. Res. Lett., 38(17), https://doi.org/10.1029/2011GL048532.

Kuma, P., A. J. McDonald, O. Morgenstern, S. P. Alexander, J. J. Cassano, S. Garrett, J. Halla, S. Hartery, M. J. Harvey, S. Parsons, G. Plank, V. Varma, and J. Williams (2020), Evaluation of Southern Ocean cloud in the HadGEM3 general circulation model and MERRA-2 reanalysis using ship-based observations, Atmos. Chem. Phys., 20(11), 6607-6630, https://doi.org/10.5194/acp-20-6607-2020.

Radenz, M., J. Bühl, P. Seifert, H. Baars, R. Engelmann, B. Barja González, R. E. Mamouri, F. Zamorano, and A. Ansmann (2021), Hemispheric contrasts in ice formation in stratiform mixed-phase clouds: disentangling the role of aerosol and dynamics with ground-based remote sensing, Atmos. Chem. Phys., 21(23), 17969-17994, https://doi.org/10.5194/acp-21-17969-2021.

Seifert, P., A. Ansmann, I. Mattis, U. Wandinger, M. Tesche, R. Engelmann, D. Müller, C. Pérez, and K. Haustein (2010), Saharan dust and heterogeneous ice formation: Eleven years of cloud observations at a central European EARLINET site, Journal of Geophysical Research: Atmospheres, 115(D20), https://doi.org/10.1029/2009JD013222.

Trenberth, K. E., and J. T. Fasullo (2010), Simulation of Present-Day and Twenty-First-Century Energy Budgets of the Southern Oceans, J. Climate, 23(2), 440-454, https://doi.org/10.1175/2009jcli3152.1.

Welti, A., E. K. Bigg, P. J. DeMott, X. Gong, M. Hartmann, M. Harvey, S. Henning, P. Herenz, T. C. J. Hill, B. Hornblow, C. Leck, M. Löffler, C. S. McCluskey, A. M. Rauker, J. Schmale, C. Tatzelt, M. van Pinxteren, and F. Stratmann (2020), Ship-based measurements of ice nuclei concentrations over the Arctic, Atlantic, Pacific and Southern oceans, Atmos. Chem. Phys., 20(23), 15191-15206, https://doi.org/10.5194/acp-20-15191-2020.

Yin, Z., and H. Baars (2021), PollyNET - Pollynet Processing Chain: Version 3.0, edited, Zenodo.

Funding

This research has been supported by the European Commission, H2020 Research Infrastructures (grant nos. 654109 and 857510), the EU Seventh Framework Programme (grant no. 603445), the German Bundesministerium für Bildung und Forschung funded projects “High Definition Clouds and Precipitation for Climate Prediction HD(CP)2” (grant nos. 01LK1503F, 01LK1502I, 01LK1209C, and 01LK1212C), the DFG (grant nos. SE2464/1-1, KA4162/2-1, and 39828502), EU/Cyprus Research and Innovation Foundation EXCELLENCE/1216/0217, ANID/CONICYT/FONDECYT Iniciación (grant no. 11181335), and the German Bundesministerium für Wirtschaft und Energie (grant no. 50EE1721C).

Cooperation

Institute for Meteorology, University of Leipzig, Leipzig, Germany;
Atmospheric Research Laboratory, University of Magallanes, Punta Arenas, Chile;
ERATOSTHENES Centre of Excellence, Limassol, Cyprus.

Ice nucleating particle concentrations at cirrus level: First results from CIRRUS-HL

Sarah Grawe, Jonas Schaefer, Josephine Gundlach, Markus Hartmann, Frank Stratmann

Zirruswolken, deren Bildung und Strahlungseigenschaften von in die Höhe transportierten Eiskeimen beeinflusst werden, sind bislang nicht ausreichend genau in Wetter- und Klimamodellen repräsentiert. Während der Flugmission CIRRUS-HL im Sommer 2021 wurden Filter mit Aerosolpartikeln und Wolkenpartikelresiduen in 9-14 km Höhe besammelt, um erstmals umfassend Eiskeimkonzentrationen in der oberen Troposphäre und unteren Stratosphäre zu bestimmen. Vorläufige Ergebnisse zeigen potentielle Einflüsse von Flughöhe und Konvektion auf die Eiskeimkonzentration.

Introduction

Ice nucleating particles (INPs) have the potential to strongly influence cloud radiative properties due to the modulation of cloud particle number concentration and size. The most common pathway for primary ice formation in the atmosphere is immersion freezing, i.e., freezing of liquid droplets caused by an immersed INP. This process has rarely been investigated at cirrus level despite its relevance [*Kärcher and Lohmann*, 2003; *Krämer et al.*, 2016].

The abundance and sources of INPs at ground level have been a topic of numerous studies in recent years [e.g., *Kanji et al.*, 2017]. However, neither possible transport mechanisms of INPs from sources at the ground into the upper troposphere/lower stratosphere (UTLS), nor the actual abundance of INPs in the UTLS region are understood [*Kanji et al.*, 2017].

In June and July 2021, INPs were sampled on board of the High Altitude and Long Range Research Aircraft (HALO) in the framework of the CIRRUS-HL mission with the newly developed High-volume flow aerosol particle filter sampler (HERA). For the first time, elaborate sampling of aerosol particles and cloud particle residuals for INP analysis was performed in 9-14 km altitude in the course of 24 research flights.

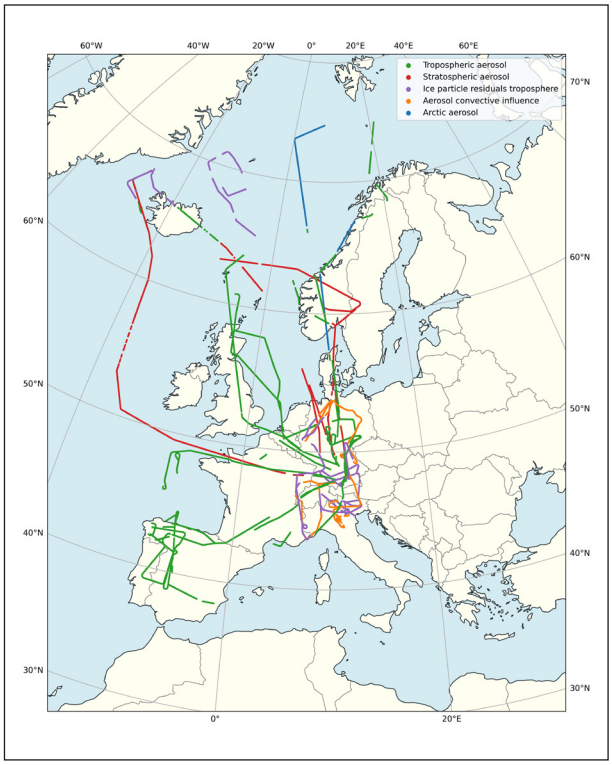

Fig. 1: Filter sampling tracks of evaluated samples above instrument background divided by categories. Filters were put into a certain category, if more than 80 % of the sampling time fit the classification condition. Sampling of IPRs behind the HALO-CVI is shown in purple.

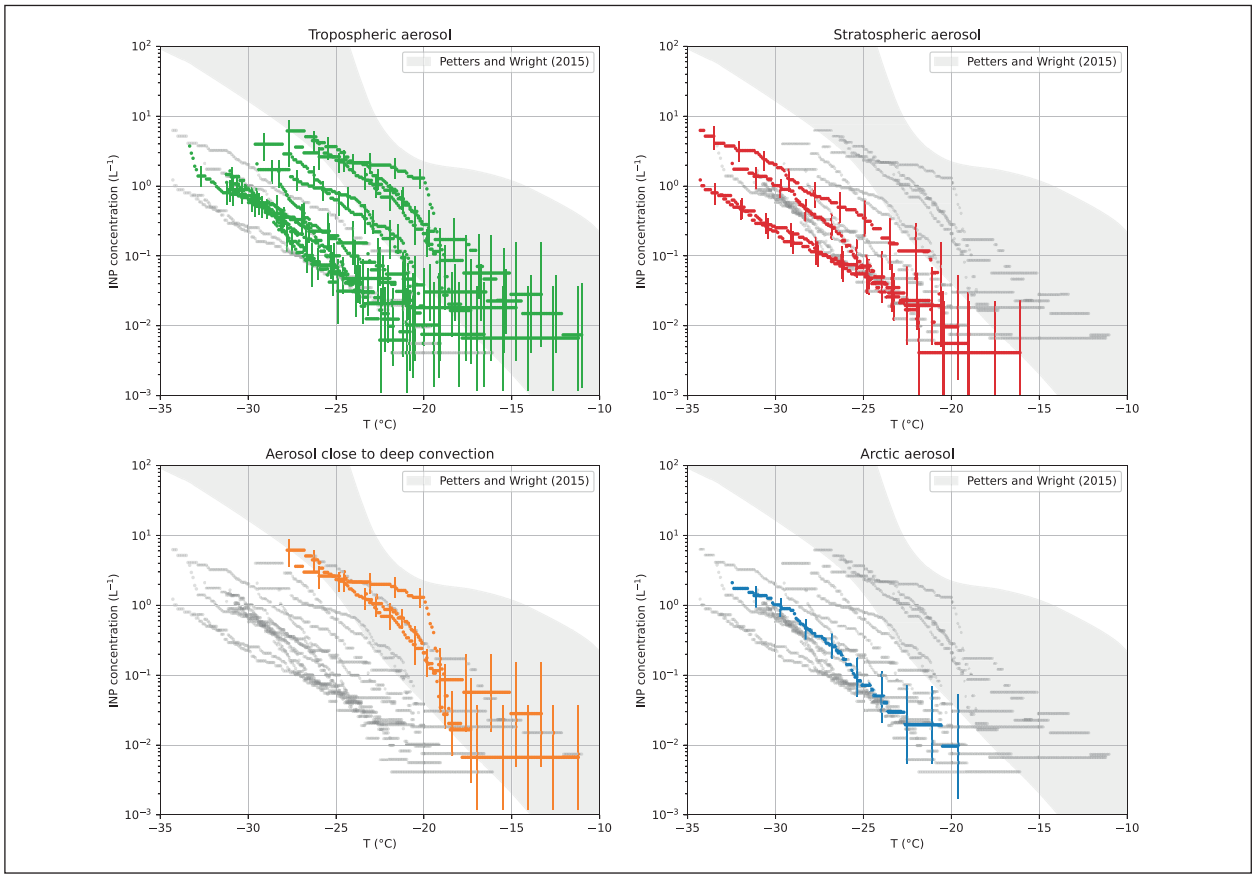

Fig. 2: INP concentrations by category with color code as shown in Fig. 1. Grey data points in the background denote all other filter samples. Typical INP concentrations measured in precipitation samples from mid-latitudes are indicated by the grey area. Note that INP concentrations behind the HALO-CVI could not yet be normalized and hence are not included.

Methods

Inlet configuration on HALO. During CIRRUS-HL, HALO was equipped with two aerosol inlets: Firstly, the HALO Submicrometer Aerosol Inlet (HASI), and secondly, the Counterflow Virtual Impactor Inlet [HALO-CVI, *Mertes et al.*, 2007]. HASI has been modified during the past years to allow for higher sampling flow rates and shifting the cut-off diameter towards larger particle sizes. Furthermore, a flow regulation system was developed in cooperation with enviscope GmbH, compensating changes in flow rate ensuring isokintetic sampling at all times. HASI was typically used for sampling aerosol particles outside of clouds. In contrast, the HALO-CVI was used for sampling ice particle residuals (IPRs) inside clouds.

Filter sampling with HERA. HERA was developed at TROPOS in cooperation with enviscope GmbH especially for aircraft sampling. It is a modular device consisting of an automated sampling unit and a powerful pump unit. The sampling unit is designed as a 7-way valve, enabling switching between 6 polycarbonate membrane filters and a bypass. The pump unit is made up of three vacuum scroll pumps and a flow meter for monitoring the volume of air sampled on each filter. During each CIRRUS-HL flight, at least one of the 6 filters in HERA was treated as a blank, i.e., no particles were sampled on it. The sampling strategy was specially planned for each flight, targeting differences in air mass origin, altitude, convective influence, and other parameters.

INP analysis. The filter samples were taken out of the aircraft and frozen at -20 °C directly after the flight. After transport to the TROPOS Icelab, filters were washed off with ultrapure water, separated into 1 µl droplets and placed onto a Silicon wafer. The wafer is cooled down by a Peltier element at a rate of 1 K min^{-1} and the freezing process of the droplets is monitored by a camera sitting above the cooled substrate. The number of frozen droplets at each temperature step is used to calculate the INP concentration, taking the volume of sampled air per filter, the droplet volume, and the volume of the washing water into account.

Preliminary results

First results suggest that the chosen sampling strategy was successful, i.e., the majority of the filter samples contain amounts of ice nucleation active material above the detection limit and variations in INP concentration can be observed. Figure 1 shows the sampling tracks of the so far analyzed filters, separated into different categories, i.e., tropospheric sampling of aerosol particles and IPRs, stratospheric sampling of aerosol particles, aerosol particles sampled under the influence of deep convection, and aerosol particles sampled in the Arctic. The categories and colors correspond to INP concentrations shown in Fig. 2, where each spectrum refers to one filter sample.

The overall variability in INP concentration is more than 2 orders of magnitude, with most of the spectra showing lower concentrations than the usually reported range for mid-latitudes derived from precipitation samples [*Petters and Wright*, 2015]. Clearly, highest concentrations were observed for filters sampled in proximity to deep convection, with values in the range of the precipitation samples, suggesting upward transport of lower tropospheric INPs. Outside deep convection, tropospheric, stratospheric, and Arctic concentrations seem somewhat similar. However, more detailed investigations, including the analysis of air mass origin, are needed and in progress.

References

Kanji, Z. A., L. A. Ladino, H. Wex, Y. Boose, M. Burkert-Kohn, D. J. Cziczo, and M. Krämer (2017), Overview of Ice Nucleating Particles, *Meteorol. Monogr.*, *58*, 1.1-1.33, https://doi.org/10.1175/amsmonographs-d-16-0006.1.

Kärcher, B., and U. Lohmann (2003), A parameterization of cirrus cloud formation: Heterogeneous freezing, *J. Geophys. Res. - Atmos.*, *108*(D14), https://doi.org/10.1029/2002JD003220.

Krämer, M., C. Rolf, A. Luebke, A. Afchine, N. Spelten, A. Costa, J. Meyer, M. Zöger, J. Smith, R. L. Herman, B. Buchholz, V. Ebert, D. Baumgardner, S. Borrmann, M. Klingebiel, and L. Avallone (2016), A microphysics guide to cirrus clouds – Part 1: Cirrus types, *Atmos. Chem. Phys.*, *16*(5), 3463-3483, https://doi.org/10.5194/acp-16-3463-2016.

Mertes, S., B. Verheggen, S. Walter, P. Connolly, M. Ebert, J. Schneider, K. N. Bower, J. Cozic, S. Weinbruch, U. Baltensperger, and E. Weingartner (2007), Counterflow Virtual Impactor Based Collection of Small Ice Particles in Mixed-Phase Clouds for the Physico-Chemical Characterization of Tropospheric Ice Nuclei: Sampler Description and First Case Study, *Aerosol Sci. Technol.*, *41*(9), 848-864, https://doi.org/10.1080/02786820701501881.

Petters, M. D., and T. P. Wright (2015), Revisiting ice nucleation from precipitation samples, *Geophys. Res. Lett.*, *42*(20), 8758-8766, https://doi.org/10.1002/2015GL065733.

Funding

This research is funded by the German Research Foundation (DFG priority program 1294, project number 442648163).

Hemispheric and seasonal contrast in cloud thermodynamic phase from A-Train spaceborne instruments

Diego Villanueva, Fabian Senf, Ina Tegen

Wolken und Aerosole beeinflussen den Energiehaushalt und den Wasserkreislauf der Erde. Es gibt zunehmend Hinweise darauf, dass Staubaerosol die Vereisung von Wolken, ihren Strahlungseffekt und ihre Reaktion auf die globale Erwärmung beeinflusst. Um den Klimawandel genauer zu projizieren, ist es daher wichtig, den Weg von staubinduzierten Gefrierprozessen zur Vereisung der Wolken besser zu verstehen. Basierend auf einem weltraumgestützten Lidar, einer Lidar-Radar Kombination und einer Radiometer-Polarimeter Kombination werden hemisphärische und saisonalen Kontraste in der Wolkenphase lokalisiert und quantifiziert. Die Ergebnisse zeigen, dass Beobachtungen des Kontrastes in der Wolkenphase dafür verwendet werden können, das staubgetriebene Gefrieren von Wolkentröpfchen in zu verstehen.

Introduction

Aerosol-cloud interactions are an important source of uncertainty in current climate projections. To understand and quantify the influence of ice-nucleating particles in cloud glaciation, it is crucial to have a reliable estimation of the hemispheric and seasonal contrast in cloud top phase, which is believed to result from the higher dust aerosol loading in boreal spring. For this reason, we locate and quantify these contrasts by combining three different A-Train cloud-phase products for the period 2007-2010. These products rely on a spaceborne lidar, a lidar-radar synergy, and a radiometer-polarimeter synergy. These results will help to improve our understanding of cloud glaciation processes, which can be valuable for future climate predictions and for understanding the impact of aerosols on radiation and precipitation.

Method

The Cloud-Aerosol LIdar with Orthogonal Polarization (CALIOP) onboard CALIPSO and the Cloud Profiling Radar (CPR) on board CloudSat are both active instruments. In the GCM-Oriented Cloud Calipso Product (CALIPSO-GOCCP v3.0) [*Cesana et al.*, 2013], the lidar depolarization measured by CALIOP is compared against an empirical threshold to retrieve the cloud-phase, where higher depolarization ratios are associated with ice crystals. In the liDAR-raDAR (DARDAR-MASK v2.0) product [*Delanoe et al.*, 2010], a decision tree is used to retrieve the cloud-phase, where a higher radar reflectivity is associated with larger particles such as ice crystals. The MODerate resolution Imaging Spectroradiometer (MODIS) onboard the Aqua satellite and the "Polarization and Directionality of the Earth Reflectance" (POLDER-3) instrument onboard the PARASOL satellite are both passive instruments. Different algorithms can be used with different radiometers to retrieve cloud top phase [*Riedi et al.*, 2010]. The PARASOL and Aqua/MODIS combination (PM-L2) product weights the MODIS-SWIR, MODIS-TIR and POLDER-3-POLAR products to make a final decision about the cloud-phase at cloud top. Similarly, we derived the GDP2 combination, in which the most frequent cloud top phase decision between the CALIPSO-GOCCP, DARDAR, and PM-L2 products is chosen to represent the cloud product ensemble.

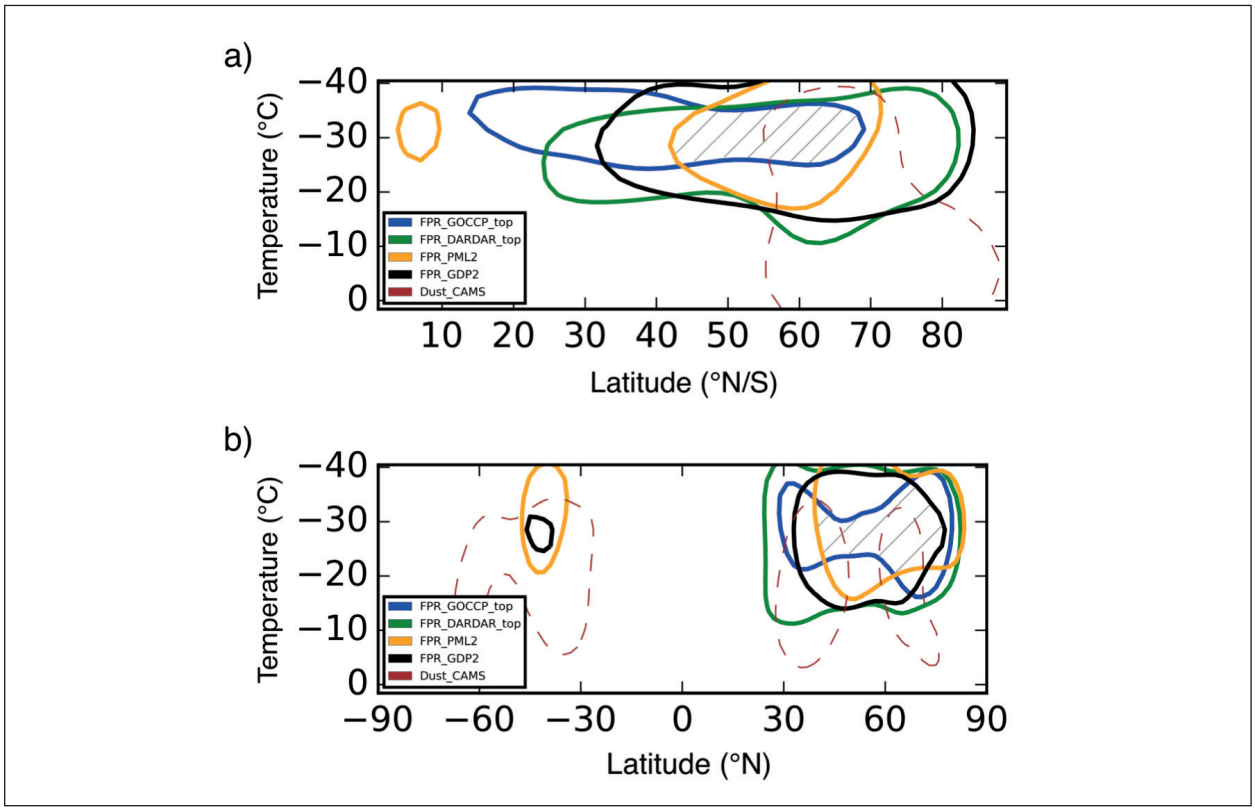

Fig. 1: Contour plot enclosing the regions in the temperature-latitude space where (a) the normalized north-south difference in FPR at cloud top is higher than +0.2 and (b) the normalized seasonal difference in FPR between MAM(SON) and SON(MAM) in the northern(southern) hemisphere is higher than +0.1.The hatched region corresponds to the zone where all products have a north-south(seasonal) contrast higher than +0.2(+0.1).The dashed contour encloses the regions where the dust loading is (a) 50 times higher in the northern hemisphere (b) 3 times higher during spring.A Gaussian filter was applied to smoothen the contours.

Results and Discussion

Fig. 1 shows the the hemispheric and seasonal contrast of cloud-phase for the different products and the GDP2 ensemble. For all products, the region is mostly located below -20°C (Fig. 1a). The magnitude of the north-south contrast is higher than previous estimates, where the contrast was reported to be about only +0.05 ice fraction or "Frequency Phase Ratio" (FPR) between -20°C and -30°C [*Tan et al.*, 2014].

The North-South contrast in FPR is attributed by several authors to the hemispheric difference in aerosol loading [*Kanitz et al.*, 2011; *Tan et al.*, 2014; *Villanueva et al.*, 2020]. More specifically, it is attributed to the higher concentration of INP-active mineral dust aerosol in the northern hemisphere, mostly originating from the Sahara and Gobi deserts. Moreover, the dust aerosol concentration in the northern hemisphere varies seasonally, with the highest concentrations during spring. For this reason, we also analyzed the average FPR differences between the months of March-April-May (MAM) and September-October-November (SON). We defined the seasonal contrast regions where the MAM-SON(SON-MAM) difference in FPR is higher than +0.1 in the northern(southern) hemisphere. Additionally, we locate the regions for which the dust loading is at least three times higher during spring compared to autumn. With this definition, similar to the hemispheric contrast, the seasonal cloud-phase contrast is mostly located below -20°C for all products (Fig. 1b), in agreement with previous reports [*Tan et al.*, 2014].

We can retrieve some interesting features from the location of the hemispheric and seasonal contrast of cloud top phase. First, the GDP2 ensemble agrees best with the DARDAR product on the location of the hemispheric contrast, and with the PM-L2 product on the location of the seasonal contrast. Second, the "overlap" zone, where all three products show a hemispheric or seasonal contrast, lays mostly between -35°C and -25°C and between 40--70°N. At this temperature, most types of mineral dust act as efficient INP [*Boose et al.*, 2016]. Therefore, this high-contrast region offers a good target for future campaigns looking to study the north-south contrast in cloud glaciation.

References

Boose, Y., Welti, A., Atkinson, J., Ramelli, F., Danielczok, A., Bingemer, H. G., . . . Lohmann, U. (2016). Heterogeneous ice nucleation on dust particles sourced from nine deserts worldwide - Part 1: Immersion freezing. Atmospheric Chemistry and Physics, 16(23), 15075–15095. https://doi.org/10.5194/acp-16-15075-2016

Cesana, G., & Chepfer, H. (2013). Evaluation of the cloud thermodynamic phase in a climate model using CALIPSO-GOCCP. Journal of Geophysical Research Atmospheres, 118(14), 7922–7937. https://doi.org/10.1002/jgrd.50376

Delanöe, J., & Hogan, R. J. (2010). Combined CloudSat-CALIPSO-MODIS retrievals of the properties of ice clouds. Journal of Geophysical Research Atmospheres, 115(4). https://doi.org/10.1029/2009JD012346

Kanitz, T., Seifert, P., Ansmann, A., Engelmann, R., Althausen, D., Casiccia, C., & Rohwer, E. G. (2011). Contrasting the impact of aerosols at northern and southern midlatitudes on heterogeneous ice formation. Geophysical Research Letters, 38(17). https://doi.org/10.1029/2011GL048532

Riedi, J., Marchant, B., Platnick, S., Baum, B. A., Thieuleux, F., Oudard, C., Dubuisson, P. (2010). Cloud thermodynamic phase inferred from merged POLDER and MODIS data. Atmospheric Chemistry and Physics. https://doi.org/10.5194/acp-10-11851-2010

Tan, I., Storelvmo, T., & Choi, Y. S. (2014). Spaceborne lidar observations of the ice-nucleating potential of dust, polluted dust, and smoke aerosols in mixed-phase clouds. Journal of Geophysical Research, 119(11), 6653–6665. https://doi.org/10.1002/2013JD021333

Villanueva, D., Heinold, B., Seifert, P., Deneke, H., Radenz, M., & Tegen, I. (2020). The day-to-day co-variability between mineral dust and cloud glaciation: a proxy for heterogeneous freezing. Atmospheric Chemistry and Physics, 20(4), 2177–2199. https://doi.org/10.5194/acp-20-2177-2020

Spectrally resolved cloud microphysical modeling in real case scenarios

Roland Schrödner, Fabian Senf, Jens Stoll, Oswald Knoth, Martin Simmel, Junghwa Lee, Johannes Bühl, Patric Seifert

Das spektral aufgelöste Wolkenmikrophysik-Modell COSMO-SPECS wurde erweitert und ist nun fähig reale Szenarien zu simulieren. Mit diesem Modell wurde die modellierte Struktur einer beobachteten Mischphasenwolke sowie der Einfluss der Annahmen des zu Grunde liegenden Aerosols auf die mikrophysikalischen Eigenschaften der Wolke untersucht. Es zeigt sich, dass eine Verringerung der Anzahl der eisbildenden Partikel als auch der verfügbaren Wolkenkondensationskeime die Niederschlagsbildung unterdrückt. Hierbei kommt das nicht-lineare Zusammenspiel zwischen primärer Eisbildung und sekundärem Eiskristallwachstum und der Anzahl und Größe der verfügbaren flüssigen Wolkentröpfchen zum Tragen.

Within mixed phase clouds several microphysical processes exchange water between the three compartments vapor, liquid phase (cloud and rain droplets) and ice phase (ice and snow crystals). In the recent years, TROPOS has investigated mixed-phase clouds at different places on Earth using remote sensing. The microphysical properties of these mixed phase clouds depend a lot on the availability of particles that serve as cloud condensation nuclei and ice nucleating particles. In order to investigate the complex interplay between the different microphysical processes in the observed clouds the spectrally resolved cloud microphysical model COSMO-SPECS is applied.

Methods

In order to be able to simulate the observed clouds under realistic conditions, COSMO-SPECS has been extended to consider dynamic lateral boundary conditions in a nested setup. With the new model system, a mixed-phase cloud case observed during the Cyprus Clouds, Aerosol, and Rain Experiment [CyCARE, *Radenz et al.*, 2021] on Cyprus has been simulated and investigated.

CyCare. The CyCare campaign took place at Limassol, Cyprus, between October 2016 and March 2018. Observations were done with the Leipzig Aerosol and Cloud Remote Observations System [LACROS, *Bühl et al.*, 2016]. In particular, the observations with cloud radar and lidar are used to setup and evaluate the model simulations.

COSMO-SPECS. The SPECtral bin cloud microphysicS model (SPECS) treats cloud hydrometeors and dry particles in fixed size bins, whereas two separate spectra are used for liquid droplets and ice crystals, respectively, including the contained aerosol mass. Various microphysical processes are considered that translate between water vapor, the liquid and the ice phase. SPECS has been continuously refined, with the latest process development introducing a separate field for ice nucleating particles (INP) and information on ice crystal shape and updates for several freezing processes [*Simmel et al.*, 2015; *Diehl and Grützun*, 2018]. SPECS is thus a comprehensive model of cloud microphysics, which in particular allows investigations of the importance of aerosol properties for the formation of cloud droplets, cloud ice and ultimately precipitation. Special attention is paid to the detailed description of aerosol-cloud interactions.

In addition to its original application as a box-model, SPECS was coupled to the meteorological forecast model of the German Weather Service COSMO [COnsortium for Small-Scale MOdelling, formerly LM, now ICON, *Grützun et al.*, 2008]. With

COSMO-SPECS, the feedback of the more complex description of the cloud microphysics by SPECS compared to COSMO's original 1- or 2-moment cloud microphysics on the dynamics can be investigated. Very recently, the usage of lateral boundary conditions of the hydrometeor quantities (e.g., liquid water and ice mass mixing ratio) in nested simulations was enabled. In this setup, realistic meteorological driving data for a three-dimensional COSMO-SPECS domain are provided by external simulations on a larger domain. Technically, this can be any meteorological model, however, for the present study, a multi-nested high-resolved COSMO simulation is used to provide the boundary data. The enhanced model system allows the simulation of real scenarios, which can be used to accompany field campaigns.

Simulation setup. During CyCare an interesting mixed-phase cloud case was observed on 24th January 2017 from 15 UTC (see Fig. 1e), in which an altocumulus cloud field arrived at the site with a vertical extent of about 3 km. The clouds frequently produced virgae, but the precipitation almost never reached the surface due to very dry air masses in the upper boundary layer. For this particular day, a nested COSMO simulation was created. Thereby, the domain horizontal resolution is stepwise increased from European reanalysis data on ~14 km resolution to the final domain around Limassol, Cyprus, with a mesh-size of only 400 m, a typical resolution of cloud-resolving models. On this innermost domain, SPECS was used instead of the standard bulk microphysics parameterization of COSMO. Since SPECS is computationally very expensive, only the period from 15 UTC to 21 UTC was simulated. In order to investigate the effect the assumed aerosol properties have on the properties and evolution of the simulated cloud, in a set of sensitivity studies the number of CCN-sized particles and INP was varied (base scenario: 1000 particles cm^{-3} in the CCN-size range, ~1 INP L^{-1} at -20 °C).

Results

Exemplary, here the base scenario is compared to a simulation with 10 times less CCN-sized particles and a simulation with 100 times less INP. Figure 1 presents the liquid water mass of the simulated clouds at Limassol. For comparison, the Cloudnet classification of the observed cloud is shown.

Overall, it can be seen that the simulations with COSMO-SPECS differ more from the COSMO standalone simulation, which share the same driving data, than from each other. Whereas COSMO frequently and early in the simulation produces a lot of precipitation in the particular scenario, this is not the case

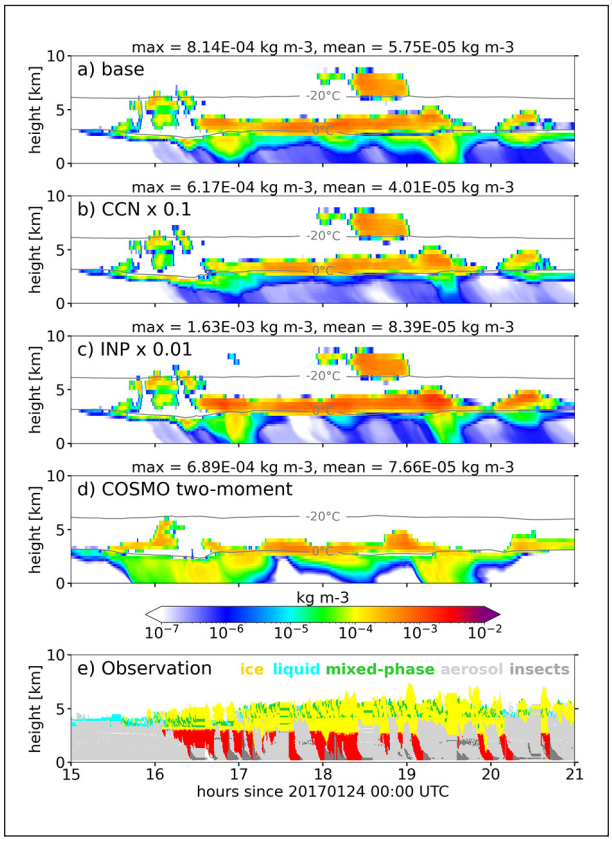

Fig. 1: Time-height cross-section of liquid water content simulated with COSMO-SPECS (a-c) and COSMO (d). Observed cloud targets as classified by Cloudnet.

when the spectrally resolved microphysics of SPECS are used. The reason for this is a much stronger ice phase simulated by COSMO. Moreover, in agreement with the observations, precipitation in SPECS sets on later and does only rarely and in little amounts reach the ground. However, despite the high horizontal resolution, the small-scale cell structure of the cloud field cannot be reproduced by the simulations. In contrast to the observed cloud field, the ice fraction is underestimated by COSMO-SPECS and the vertical extent of the simulated clouds is often much larger. Despite the decreased precipitation compared to COSMO, the formed precipitation humidifies the already too moist boundary layer more than observed.

The reduction of CCN as well as of INP leads to a decrease of the precipitation rates throughout the simulation. This is caused by a reduction of the number of liquid droplets, which decreases the efficiency of ice crystals colliding with liquid droplets ("riming"). Hence, less sufficiently large snow crystals are formed that would fall out as precipitation. Although for the wrong reasons (CCN and INP concentrations as in the base scenario have been observed), a more inhibited precipitation formation fits well to the observations.

Further investigations will target the effect of different ice particle shapes (currently spheres are assumed) and secondary ice multiplication (currently not implemented). Both processes can play an important role for riming. In addition, any ice particle shape other than spheres will lower their sedimentation velocity but might enhance their depositional and collisional growth. Apart from that, the influence of potential misrepresentations of liquid and frozen condensate masses of the driving model in the outer domains need to be investigated since these very much determine the overall simulated cloud dynamics.

References

Bühl, J., P. Seifert, A. Myagkov, and A. Ansmann (2016), Measuring ice- and liquid-water properties in mixed-phase cloud layers at the Leipzig Cloudnet station, *Atmos. Chem. Phys.*, *16*(16), 10609-10620, https://doi.org/10.5194/acp-16-10609-2016.

Diehl, K., and V. Grützun (2018), Model simulations with COSMO-SPECS: impact of heterogeneous freezing modes and ice nucleating particle types on ice formation and precipitation in a deep convective cloud, *Atmos. Chem. Phys.*, *18*(5), 3619-3639, https://doi.org/10.5194/acp-18-3619-2018.

Grützun, V., O. Knoth, and M. Simmel (2008), Simulation of the influence of aerosol particle characteristics on clouds and precipitation with LM-SPECS: Model description and first results, *Atmos. Res.*, *90*(2-4), 233-242, https://doi.org/10.1016/j.atmosres.2008.03.002.

Radenz, M., J. Bühl, P. Seifert, H. Baars, R. Engelmann, B. B. Gonzalez, R. E. Mamouri, F. Zamorano, and A. Ansmann (2021), Hemispheric contrasts in ice formation in stratiform mixed-phase clouds: disentangling the role of aerosol and dynamics with ground-based remote sensing, *Atmos. Chem. Phys.*, *21*(23), 17969-17994, https://doi.org/10.5194/acp-21-17969-2021.

Simmel, M., J. Bühl, A. Ansmann, and I. Tegen (2015), Ice phase in altocumulus clouds over Leipzig: remote sensing observations and detailed modeling, *Atmos. Chem. Phys.*, *15*(18), 10453-10470, https://doi.org/10.5194/acp-15-10453-2015.

Funding

The work was funded by DFG under grant number 398285025 and from European Commission's Horizon 2020 program grant number 857510 (EXCELSIOR).

How Aerosol Absorption Affects Cloud Cover over Germany

Fabian Senf[1], Ina Tegen[1], Johannes Quaas[2]

[1] Leibniz Institute for Tropospheric Research, Leipzig.

[2] Leipzig Institute for Meteorology, University Leipzig, Leipzig.

Absorbierendes Aerosol spielt eine wichtige Rolle im Klimasystem der Erde und trägt zu den Auswirkungen des Menschen auf das Klima bei. Absorbierendes Aerosol wie z.B. schwarzer Kohlenstoff in Ruß absorbiert die einfallende Sonnenstrahlung und verändert den Energiegehalt der Atmosphäre. Dies führt zu Veränderungen der atmosphärischen Stabilität, die sich auf die Wolkenbildung und Wolkenentwicklung auswirken, und verursacht komplexe Rückwirkungseffekte, die in aktuellen Klimaprojektionen äußerst unsicher sind. Daher wurde sich in der vorliegenden Studie der Thematik der Aerosol-Strahlungs-Wechselwirkungen und daraus folgender schneller Anpassungen aus der Perspektive einer großräumigen, hochauflösenden Modellierung genähert.

Introduction

Absorbing aerosol plays an important role in Earth's climate system and contributes to the human impact on climate [*Bond et al.*, 2013]. Absorbing aerosol such as black carbon in soot absorbs incoming solar radiation [*Ramanathan et al.*, 2001], changing the energy content of the atmosphere. It leads to perturbations in the thermal structure of the atmosphere also influencing clouds [*Koch and Del Genio*, 2010]. Aerosol also reduces the downwelling solar radiation at the surface referred to as surface dimming [*Wild*, 2009]. Over the land surface, this dimming by absorbing aerosols can lead to a substantial reduction in surface latent and sensible heat fluxes.

In previous climate assessments, a negative value is assigned to the net global effective radiative forcing of aerosol–radiation interactions (ARI) – but it has also been made clear that the current scientific understanding is low in terms of agreement and confidence level [*Flato et al.*, 2014]. It has been further stated that "while there is robust evidence for the existence of rapid adjustment of clouds in response to aerosol absorption, these effects are multiple and not well represented in climate models, leading to large uncertainty" [*Boucher et al.*, 2013, p.573]. Reasons for the disagreements between global models and regional high-resolution simulations are not always understood, making it difficult to infer a consistent picture [*Bond et al.*, 2013].

Methods

In modelling studies, the net effect of aerosol on radiation is usually inferred from two sets of simulations – one with and one without conditions perturbed by pollution aerosol [*Bond et al.*, 2013]. Here, this strategy has been applied to cloud-resolving ICOsahedral Non-hydrostatic Large-Eddy Model (ICON-LEM) simulations to investigate the impact of aerosol absorption over Germany. In the applied ICON-LEM version, aerosol perturbations can be formulated such that only direct and semi-direct effects of aerosol forcing are considered, whereas indirect effects via cloud microphysical adjustments are excluded.

Two distinct model experiments were conducted: In the first experiment (*absorbing experiment*), unmodified aerosol optical properties after *Tegen et al.* [1997] are included in radiative transfer calculations. Aerosol optical properties are taken from the Global Aerosol Climatology Project (GASP) providing representative, monthly-mean data. Simplified aerosol profiles are specified such that the largest amount

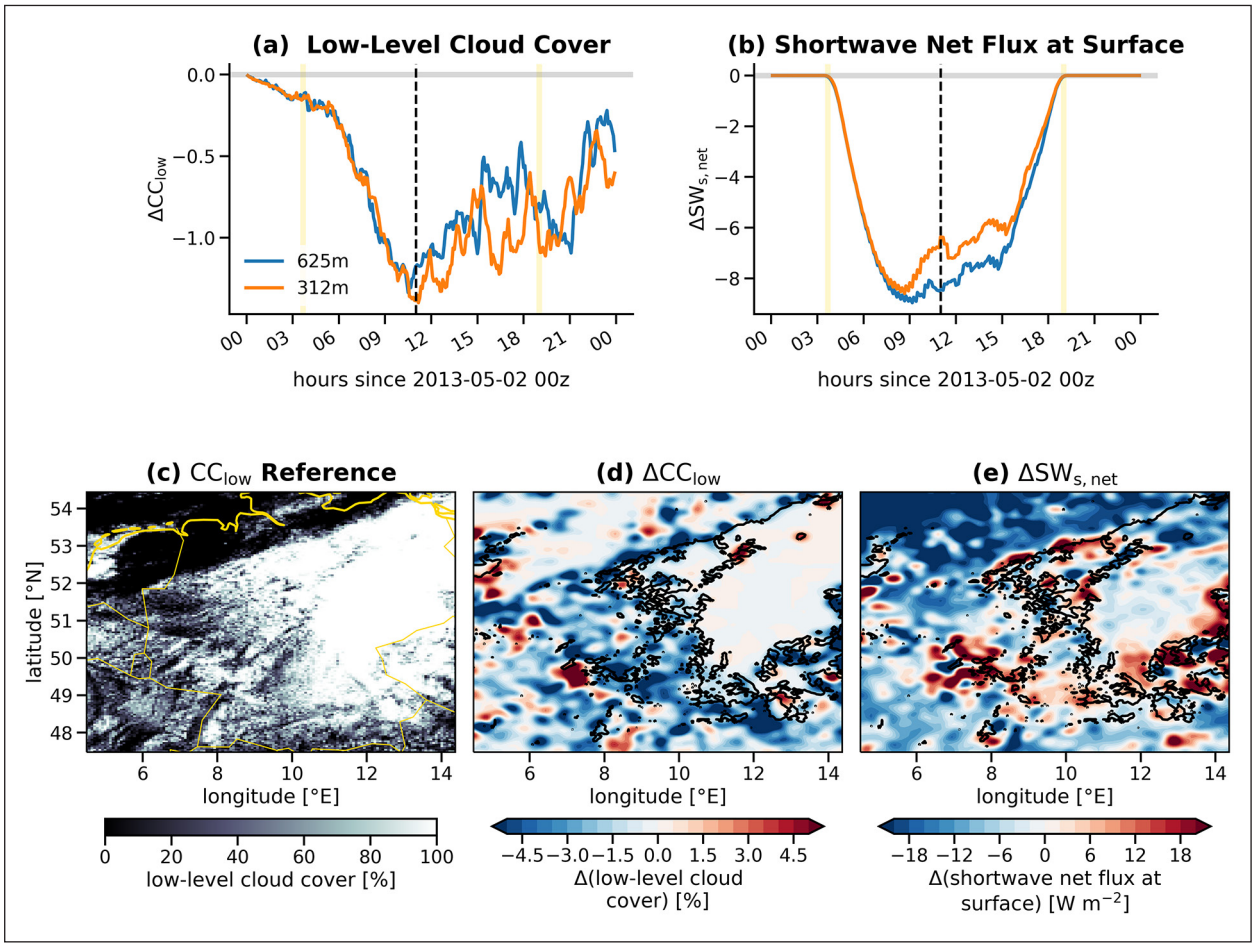

Fig. 1: The time series of (a) low-level cloud cover anomaly and (b) net short-wave radiation flux anomalies at the surface (sum of up- and downwelling components) are presented for ICON at 312 m (orange) and 625 m (blue) grid spacing. (c–e) provide an overview of the cloud scenery and resulting anomalies for 312 m and 1100 UTC. (c) The low-level cloud cover from the scattering experiment is compared to anomalies of (d) low-level cloud cover and (e) net short-wave radiation at the surface [see Senf et al., 2021 for more detail].

of aerosol is found in the planetary boundary layer. In the second experiment (*scattering experiment*), absorption coefficients for all aerosol species are set to zero, but keeping scattering properties at the predefined values. In this experiment, the broadband AODs decrease from 0.163 to 0.146. The *scattering experiment* with no aerosol absorption is taken as a reference. In that way, we can answer the question of how much the atmosphere is changed by increasing aerosol absorption to current levels.

Results and Conclusions

Due to the high computational cost, we only consider 24-hr forecasts for one single day during midlatitude spring, that is, 02 May 2013. This day falls into a period of intensive observations during the High-Definition Clouds and Precipitation for Climate Prediction (HD(CP)2) Observational Prototype Experiment [HOPE; *Macke et al.*, 2017]. The cloud scenery is characterised by a complex mixture of stratiform and convective cloud types during high-pressure weather. As time proceeds, a negative cloud cover anomaly develops at night (Fig. 1a). After sunrise, cloud cover is depleted even more efficiently. Direct short-wave heating due to absorbing aerosol induces a positive temperature anomaly and a negative humidity anomaly which both negatively influence liquid cloud amount. In addition, reduced surface fluxes due to surface dimming cause an increase in atmospheric stability of the boundary layer which partially hinders convective cloud development. The net short-wave radiation at surface is reduced up to – 8 W m^{-2} between 0800 and 0900 UTC. At this time and earlier, the reduction in net short-wave radiation is mainly caused by the dimming effect of absorbing aerosol. Later, the short-wave radiation anomaly becomes smaller again due to the response of low-level clouds. One could think of the boundary layer–cloud coupling as a buffered system which tries to minimise the loss of incoming energy by reducing the amount of low-level cloud which would otherwise

shade the surface in addition to the aerosol-induced surface dimming.

Based on the complete analysis of our perturbation experiments, the further main conclusions could be formulated [see *Senf et al.*, 2021]: Net TOA radiation fluxes increase by around 5 W m^{-2}, indicating a positive radiative forcing in which the atmosphere gains energy. Radiative forcing from direct and semi-direct aerosol effects are both positive and have similar magnitudes. Domain-average values of liquid water path (LWP) and precipitation reduce by similar amounts (–5 to –7%) until afternoon due to the decreased availability of moisture from the surface. Changes in LWP are dominated by a shrinking of large, stratiform cloud decks. Moreover, the number of small, convective clouds is also diminished by aerosol absorption. Future work will be dedicated to further disentangle the relative roles of surface dimming and local atmospheric heating effects.

References

Bond, et al. (2013) Bounding the role of black carbon in the climate system: a scientific assessment. *J. Geophys. Res. Atmos., 118,* 5380–5552, https://doi.org/10.1002/jgrd.50171

Boucher, et al. (2013) Clouds and aerosols. In: Climate change 2013: The Physical Science Basis. Contribution of Working Group I to the Fifth Assessment Report of the Intergovernmental Panel on Climate Change, pp. 571–657. Cambridge, UK: Cambridge University Press.

Flato, et al. (2014) Evaluation of climate models. In: Climate change 2013: The Physical Science Basis. Contribution of Working Group I to the Fifth Assessment Report of the Intergovernmental Panel on Climate Change, pp. 741–866. Cambridge, UK: Cambridge University Press.

Koch, D. and Del Genio, A.D. (2010) Black carbon semi-direct effects on cloud cover: review and synthesis. *Atmos. Chem. Phys., 10,* 7685–7696, https://doi.org/10.5194/acp-10-7685-2010

Macke, et al. (2017) The HD(CP)2 Observational Prototype Experiment (HOPE) – an overview. *Atmos. Chem. Phys., 17*, 4887–4914, https://doi.org/10.5194/acp-17-4887-2017

Ramanathan, V., Crutzen, P.J., Kiehl, J.T. and Rosenfeld, D. (2001) Aerosols, climate, and the hydrological cycle. *Science, 294*, 2119–2124, https://doi.org/10.1126/science.1064034

Senf, F., Quaas, J. & Tegen, I.(2021) Absorbing aerosol decreases cloud cover in cloud-resolving simulations over Germany. *Q J R Meteorol Soc, 147(741),* 4083– 4100, https://doi.org/10.1002/qj.4169

Tegen, I., Hollrig, P., Chin, M., Fung, I., Jacob, D. and Penner, J. (1997) Contribution of different aerosol species to the global aerosol extinction optical thickness: estimates from model results. *J. Geophys. Res. Atmos., 102,* 23895–23915, https://doi.org/10.1029/97JD01864

Wild, M. (2009) Global dimming and brightening: a review. *J. Geophys. Res. Atmos., 114 (D10),* https://doi.org/10.1029/2008JD011470

Funding

The study was supported by the HD(CP)2 project funded by the German Ministry for Education and Research (BMBF) under grant 01LK1507C and 01LK1503F and by the Research EU Horizon 2020 project CONSTRAIN under grant GA 820829. Computational resources were provided by DKRZ through the projects bm0834 and bb1174.

Results from the MetPVNet project

Jonas Witthuhn[1], Hartwig Deneke[1], Anja Hünerbein[1], Carola Barrientos-Velasco[1], Sebastian Bley[1], Stephan Lenk[1], Fabian Senf[1], Andreas Macke[1], Frank Werner[2], Ping Wang[3], Jan Fokke Meirink[3],Marion Schroedter-Homscheidt[4], Florian Filipitsch[5], Stefan Wacker[5], Stefanie Meilinger[6]

[1] Leibniz Institute for Tropospheric Research, Leipzig, DE.
[2] Jet Propulsion Laboratory, Pasadena, USA.
[3] Royal Netherlands Meteorological Institute, De Bilt, NL.
[4] German Aerospace Centre, Oldenburg, DE.
[5] German Weather Service, Lindenberg, DE.
[6] International Centre for Sustainable Development (IZNE), Bonn-Rhein-Sieg University of Applied Sciences, Sankt Augustin, Germany

MetPVNet (http://metpvnet.de/) war ein vom Wirtschaftsministerium gefördertes Verbundprojekt, dass im Februar 2021 abgeschlossen wurde, und die Entwicklung innovativer Energie-meteorologischer Methoden zu satellitenbasierten Vorhersagen von Einstrahlung und PV-Leistung auf Anlagenebene zum Ziel hatte. Die Abteilung der Fernerkundung war an den Arbeitspaketen zur Ableitung von hoch-aufgelöster Globalstrahlung aus Satelliten- und Beobachtungsdaten sowie an der Durchführung von Bodenmessungen im Rahmen zweier Messkampagnen maßgeblich beteiligt. Im Rahmen des Projekts wurde eine Methode zur Erhöhung der räumlichen Auflösung von Satellitendaten entwickelt sowie die optischen Eigenschaften und der direkter Strahlungseffekt von Aerosol über Deutschland mit verschiedenen Ansätze quantifiziert und verglichen.

MetPVNET

MetPVNet was a collaborative research project funded by the German Ministry of Commerce which ended in February 2021. Its central goal was to develop innovative energy-meteorological methods for the satellite-based prediction of solar irradiance and photovoltaic (PV) power production at the solar plant level [*Meilinger et al.*, 2021]. The project benefited from the synergies of the inter- and transdisciplinary cooperation of experts from the fields of meteorology, physics, renewable energies and electricity grids. The remote sensing department mainly contributed to work packages for deriving high-resolution global radiation from satellite observations as well as ground-based measurements as part of two field campaigns. A method was developed to improve the spatial resolution of satellite-based cloud and radiation products, and the optical properties and radiative effects of aerosol were analyzed and compared based on complementary approaches.

Increasing the spatial resolution of cloud property retrievals from Meteosat SEVIRI

An existing cloud property retrieval scheme for the Spinning Enhanced Visible and Infrared Imager (SEVIRI) instrument on board the geostationary Meteosat satellites has been modified to utilize its high-resolution visible (HRV) channel for increasing the spatial resolution of its physical outputs. This results in products with a nadir spatial resolution of 1x1 km^2 compared to the standard 3x3 km^2 resolution offered by the narrowband channels. Details about this work have been described in *Werner and Deneke* [2020] and *Deneke et al.* [2021].

Several scientific applications are expected to benefit from the improved spatial resolution, as illustrated in *Deneke et al.* [2021] for three examples: the retrieval of cloud properties for shallow convective cloud fields with respect to their small-scale variability; the detection and analysis of the initiation and growth of severe convective storms; and the retrieval of solar surface irradiance, which showed a reduction of the root-mean-square error by about 10 % in comparison to observations from a dense pyranometer network at least for some cases.

The comparison and the synergistic combination of satellite and ground-based observations crucially depends on the atmospheric volume sampled by the observations. In this respect, the improved spatial resolution of satellite products is expected to be advantageous as ground-based observations are able to resolve much finer cloud structures.

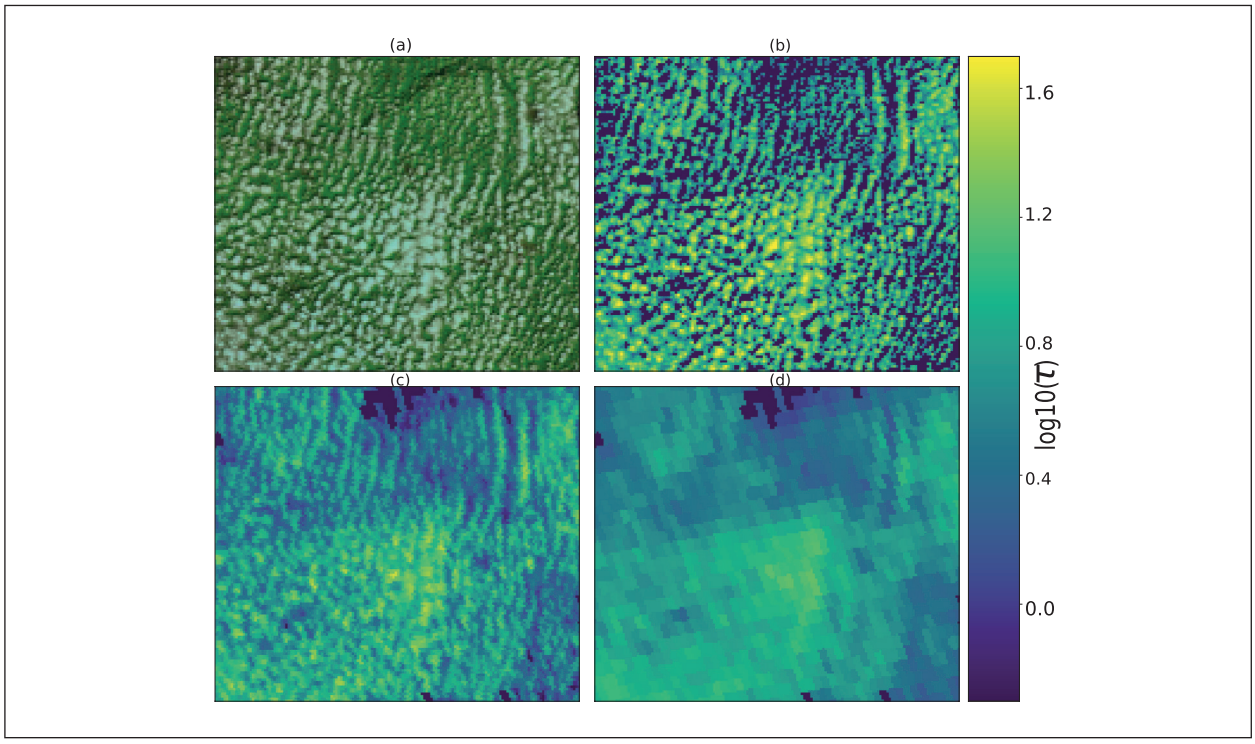

Fig. 1: Shallow convective cloud field observed over northeastern France at 3°25′E and 48°7′N on 2 June 2013 at 10:50 Z. MODIS reflectances are displayed as a day-natural color RGB composite in ***(a)****, and retrieved values of cloud optical depth (τ) are shown for the operational Terra MODIS C6.1 retrieval* ***(b)****, the improved Meteosat SEVIRI retrieval* ***(c)****, and the standard-resolution Meteosat SEVIRI retrieval* ***(d)*** *using a logarithmic color scale. Obtained from Deneke et al. [2021].*

Aerosol properties and aerosol–radiation interactions in clear-sky conditions over Germany

Within MetPVNet, aerosol optical properties and radiative effect (REari) have also been investigated for the region of Germany and for the year 2015 [*Witthuhn et al.*, 2021]. A particular focus was placed on seasonal and regional variations. Two complementary sources of information were considered: First, high-quality broadband global and diffuse irradiance measurements from the radiation observations within the station network of the German weather service (DWD) in combination with various semi-physical clear sky irradiance models. Secondly, explicit radiative transfer calculations conducted with the T-CARS (TROPOS - Clouds and Aerosol Radiative effect Simulator) framework utilizing the ECMWF radiation scheme (ecRad) and atmospheric and aerosol properties from the Copernicus Atmosphere Monitoring Service reanalysis (CAMS RA) as input database. Given the fundamental differences of both approaches, the consistency of the underlying aerosol properties and radiative effect have been discussed.

A detailed comparison of the CAMS RA aerosol information to AERONET direct solar and inversion products showed a high level of agreement of the aerosol optical depth (AOD) and asymmetry parameter (ASY) product. A larger inconsistency was found for the single scattering albedo (SSA), and reflected in a significant bias of –0.03 or about 30 %, introducing an overestimation of atmospheric heating caused by aerosol absorption.

The sensitivity of the REari to changes in aerosol optical properties was also determined. The results show that the REari is most sensitive to changes in SSA, followed by ASY and AOD. The SSA as a measure of absorption of aerosol has the strongest influence on the REari. This finding highlights the importance of a realistic representation of the aerosol mixture for a correct representation of REari. Empirical models are highly dependent on the assumptions of the optical properties of the aerosol particles and atmospheric gases. As they are mainly based on a fixed aerosol mixture, the annual variability of REari cannot be realistically reproduced by empirical models.

Based on the sensitivity study and CAMS RA evaluation, a best estimate of REari over Germany was obtained, showing a mean cooling of -10.6 Wm^{-2} at the surface and -6.5 Wm^{-2} at the top of the atmosphere. This results in a warming REari of 4.1 Wm^{-2} of the entire atmosphere.

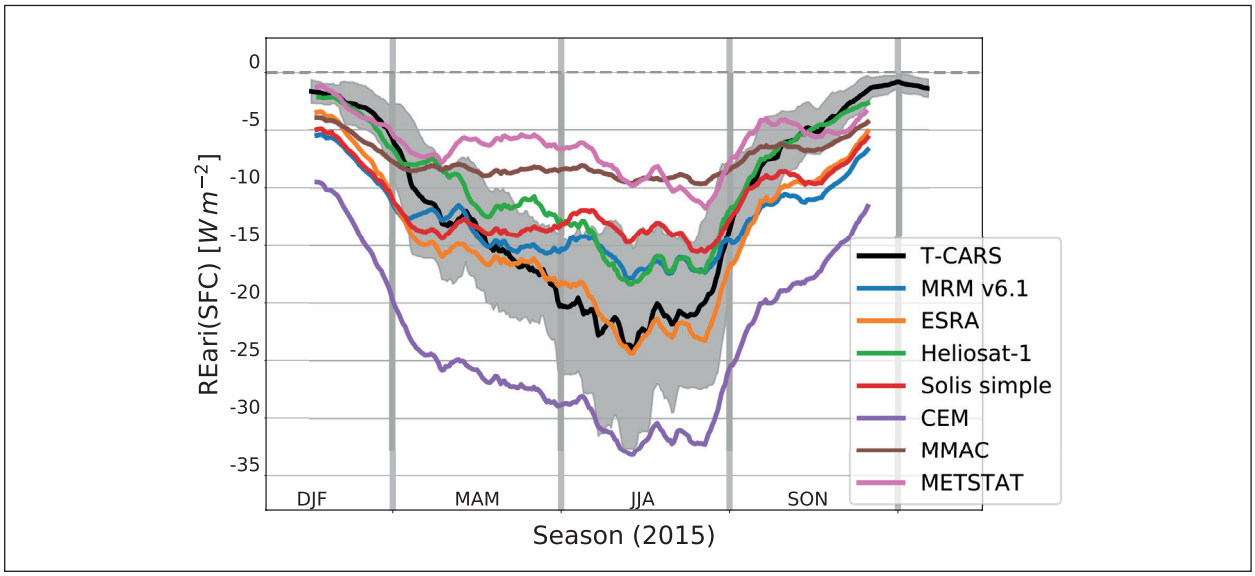

Fig. 2: The 30 days rolling mean of REari at the surface over all DWD stations in the year 2015 utilizing clear sky irradiance models (coloured lines), and explicit radiative transfer calculation (black line & grey shaded standard deviation). The figure is obtained from Witthuhn et al. [2021].

References

Deneke, H., Barrientos-Velasco, C., Bley, S., Hünerbein, A., Lenk, S., Macke, A., Meirink, J. F., Schroedter-Homscheidt, M., Senf, F., Wang, P., Werner, F., and Witthuhn, J. (2021), Increasing the spatial resolution of cloud property retrievals from Meteosat SEVIRI by use of its high-resolution visible channel: implementation and examples, Atmos. Meas. Tech., 14, 5107–5126, https://doi.org/10.5194/amt-14-5107-2021 .

Meilinger, S., Herman-Czezuch, A., Kimiaie, N., Schirrmeister, C., Yousif, R., Geiss, S., Scheck, L., Weissmann, M., Gödde, F., Mayer, B., Zinner, T., Barry, J., Pfeilsticker, K., Kraiczy, M., Winter, K., Altayara, A., Reise, C., Rivera, M., Deneke, H., Witthuhn, J., Betcke, J., Schroedter-Homscheidt, M., Hofbauer, P., and Rindt, B. (2021), Entwicklung innovativer satellitengestützter Methoden zur verbesserten PV-Ertragsvorhersage auf verschiedenen Zeitskalen für Anwendungen auf Verteilnetzebene: Schlussbericht, Hochschule Bonn-Rhein-Sieg, https://doi.org/10.18418/OPUS-5955 .

Werner, F. and Deneke, H. (2020), Increasing the spatial resolution of cloud property retrievals from Meteosat SEVIRI by use of its high-resolution visible channel: evaluation of candidate approaches with MODIS observations, Atmos. Meas. Tech., 13, 1089–1111, https://doi.org/10.5194/amt-13-1089-2020 .

Witthuhn, J., Hünerbein, A., Filipitsch, F., Wacker, S., Meilinger, S., and Deneke, H. (2021), Aerosol properties and aerosol–radiation interactions in clear-sky conditions over Germany, Atmos. Chem. Phys., 21, 14591–14630, https://doi.org/10.5194/acp-21-14591-2021 .

Funding

This research has been supported by the German Ministry of Commerce (grant no. 0350009E).

Oceanic transfer and atmospheric processing of marine carbohydrates: results from the PI-ICE study

Sebastian Zeppenfeld[1], Manuela van Pinxteren[1], Dominik van Pinxteren[1], Heike Wex[1], Elisa Berdalet[2], Dolors Vaqué[2], Manuel Dall'Osto, Hartmut Herrmann[1]

[1] Leibniz-Institute for Tropospheric Research, Leipzig, Germany
[2] Institut de Ciències del Mar-Consejo Superior de Investigaciones Científicas (ICM-CSIC), Barcelona, Catalonia, Spain

Der Südliche Ozean umgibt den Kontinent Antarktika und gehört noch zu den unberührtesten Orten der Erde. Seine Atmosphäre wird daher vordergründig von marinen Aerosolpartikeln dominiert, welche die Wolkenbildung in Form von Kondensations (CCN) - und Eiskeimen (INP) unterstützen können. Diese Fähigkeit der marinen Aerosolpartikeln ist unter anderem sehr stark von deren chemischen Zusammensetzung abhängig.
Marine Kohlenhydrate, eine bedeutende organische Stoffgruppe, werden im ozeanischen Oberflächenwasser durch mikrobielle Aktivitäten freigesetzt. Diese können durch windgesteuerte Prozesse, welche zum Eintrag und Platzen von Luftblasen führen, als Teil des sogenannten Sea Spray Aerosols (SSA) in die Luft getragen werden. Der Übergang von marinen Kohlenhydraten in die Atmosphäre, deren atmosphärische Alterung und deren Beitrag bei der Kondensation und Eiskeimbildung ist hierbei noch nicht ausreichend verstanden.
Während der PI-ICE Kampagne, welche von Januar bis März 2019 westlich der antarktischen Halbinsel stattfand, wurde der primäre Transfer von Kohlenhydraten vom Ozean über den Meeresoberflächenfilm (SML) in die Atmosphäre und deren sekundäre atmosphärische Veränderungen erforscht. Dazu erfolgte eine konzertierte Wasser- und größenaufgelöste Aerosolprobenahmen koordiniert von Bord des spanischen Forschungsschiffes RV Hespérides und der antarktischen Landstation Juan Carlos I auf der Livingston-Insel.

Introduction

The Southern Ocean surrounds the continent Antarctica and belongs to the most pristine places on Earth. Its atmosphere is strongly dominated by marine aerosol particles that can support the formation of clouds by acting as cloud condensation nuclei (CCN) or ice nucleating particles (INP). This capability of marine aerosol particles is, among other parameters, strongly dependent on their chemical composition.

Marine carbohydrates, an important class of organic substances, are released by microbial activities in the oceanic surface water. They can enter the atmosphere as part of sea spray aerosol (SSA) through wind-driven processes leading to bubble bursting. The emission processes of marine carbohydrates to the atmosphere, their atmospheric aging and their contribution for the condensation and ice nucleation is not yet well understood.

The primary transfer of carbohydrates from the ocean via the sea surface microlayer (SML) to the atmosphere and their secondary atmospheric modifications were studied during the PI-ICE campaign, which took place from January until March 2019 west of the Antarctic Peninsula. To this end, a concerted sampling of water and size-resolved aerosol particles was conducted on board the Spanish research vessel RV Hespérides and the Antarctic land station Juan Carlos I on Livingston Island.

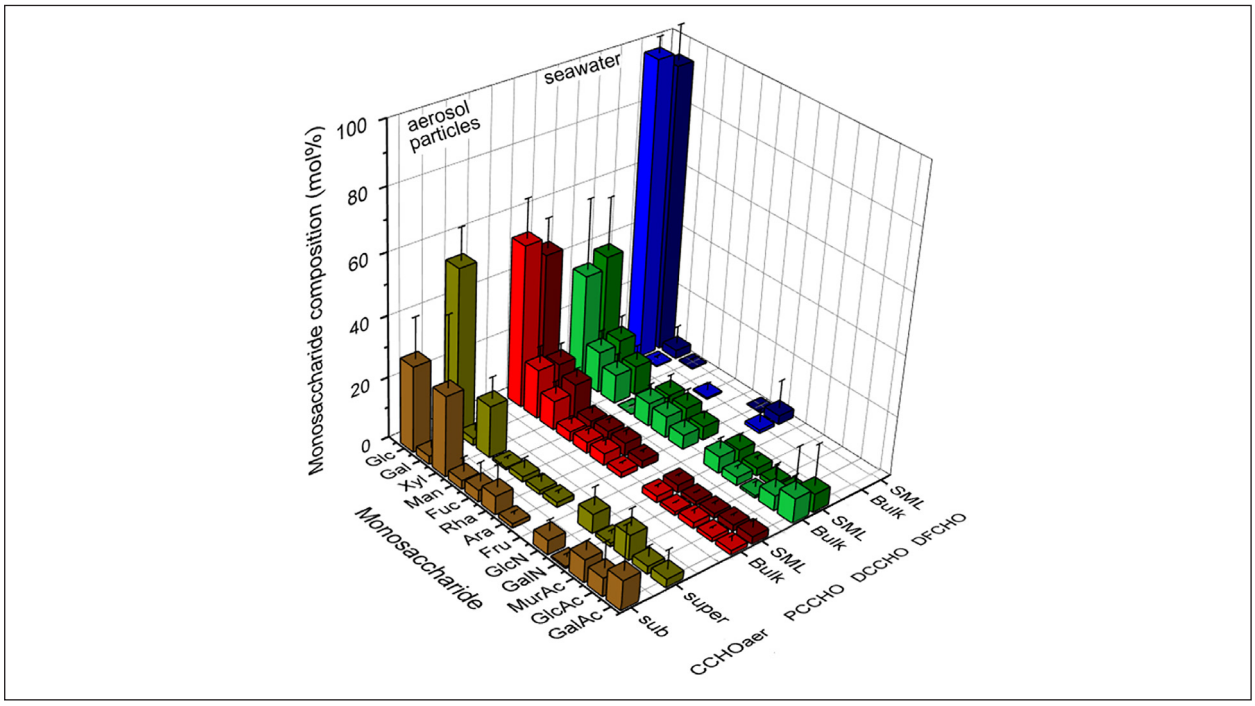

Fig. 1: Three-dimensional (3D) bar graph showing the average and standard deviation of the relative monosaccharide composition of combined carbohydrates in sub-/supermicron aerosol particles ($CCHO_{aer}$), particulate combined carbohydrates (PCCHO), dissolved combined carbohydrates (DCCHO) and dissolved free carbohydrates (DFCHO) in seawater and SML samples.

Methods

Size-resolved aerosol particles were collected on aluminium foils using a five-stage low-pressure Berner impactor (Hauke, Austria) equipped with a 3 m long heated tube to avoid the condensation of atmospheric water on the substrate and a wind sensor to minimize contaminations by local anthropogenic exhausts. SML samples were acquired using the glass plate technique [*van Pinxteren et al.*, 2017] and bulk water was scooped at a depth of approximately 25 cm. Dissolved and particulate carbohydrates were quantified in the bulk seawater, SML and size-resolved aerosol samples following the protocols described by [*Zeppenfeld et al.*, 2020, 2021] using high-performance anion-exchange chromatography coupled with amperometric detection (HPAEC-PAD) with and without the application of an acid hydrolysis. Furthermore, major inorganic ions, organic carbon (OC) and chlorophyll-a measurements were measured using state-of the art analytical methods *[Zeppenfeld et al.*, 2021]. The interpretation of the data was supported by air back-trajectories computed by the NOAA HYSPLIT model [*Stein et al.*, 2015].

Results and Discussion

Marine carbohydrates were found in bulk seawater, SML and size-resolved aerosol particles and contributed approximately 2-4% to organic carbon (OC). Air back-trajectories and strong correlations between the aerosolized carbohydrates, sodium and the wind speed strongly suggest local and regional wave breaking and bubble bursting processes as the driving emission source for the carbohydrates contained in the aerosol particles. High concentrations of carbohydrates were preferably found in two size modes. Increased concentrations of carbohydrates were found in a supermicron (1.2-10 µm) and a submicron mode (0.05-0.42 µm) and might be attributed to the release of jet and film droplets, respectively, during the bubble bursting process.

Sodium is considered as a conservative tracer for marine emissions and was used to calculate carbohydrate to sodium ratios. The direct comparison of these ratios in the different media water and air revealed a chemo-selective transfer of carbohydrates over sodium during the transfer from the ocean to the atmosphere. In contrast to very small enrichment factors within the SML (EF, median=1.4), very high enrichment factors for carbohydrates relative to the bulk seawater were estimated for supermicron (20-4000) and submicron (40-167 000) particles.

The monosaccharide composition of the carbohydrates detected in the aerosol and water samples showed quite different patterns (Fig. 1). Most noticeable was the low presence of galactose in aerosol particles in comparison to its more dominant

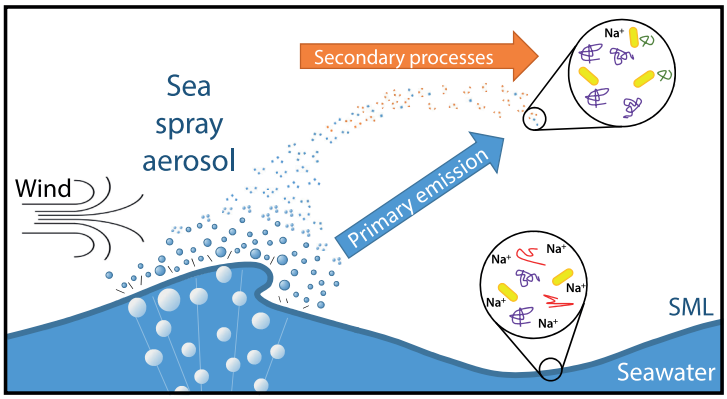

Fig. 2: Illustration of the primary emission and secondary transformation of carbohydrates in the marine atmosphere.

occurrence in seawater. Other monosaccharides, such as xylose, arabinose and glucose, strongly correlated with sodium suggesting a higher stability within the atmosphere. Furthermore, bacterial monosaccharides such as muramic acid and glucosamine were represented within the aerosol particles. Overall, the results of detailed analyses gave strong evidence for a bacterial degradation and modification of the aerosolized carbohydrates in the atmosphere after their oceanic emission. These bacteria might be released together with SSA from the ocean to the atmosphere and survive there by metabolizing organic substances, such as selected carbohydrates, within these particles. Abiotic reactions and processes as an alternative explanation to the bacterial metabolism were considered possible, but eventually rated as less likely.

In summary, we could show strong indications for the transport of carbohydrates from the ocean to the atmosphere by wind-driven processes (Fig. 2). However, strong changes in the monosaccharide composition indicate additional secondary processes in the atmosphere influencing the overall molecular composition, likely due to metabolic activities by heterotrophic bacteria.

References

van Pinxteren, M., Barthel, S., Fomba, K. W., Müller, K., Von Tümpling, W., and Herrmann, H.: The influence of environmental drivers on the enrichment of organic carbon in the sea surface microlayer and in submicron aerosol particles – measurements from the Atlantic Ocean, 5, https://doi.org/10.1525/elementa.225, 2017.

Stein, A. F., Draxler, R. R., Rolph, G. D., Stunder, B. J. B., Cohen, M. D., and Ngan, F.: NOAA's HYSPLIT Atmospheric Transport and Dispersion Modeling System, Bull. Amer. Meteor. Soc., 96, 2059–2077, https://doi.org/10.1175/BAMS-D-14-00110.1, 2015.

Zeppenfeld, S., van Pinxteren, M., Engel, A., and Herrmann, H.: A protocol for quantifying mono- and polysaccharides in seawater and related saline matrices by electro-dialysis (ED) – combined with HPAEC-PAD, 16, 817–830, https://doi.org/10.5194/os-16-817-2020, 2020.

Zeppenfeld, S., van Pinxteren, M., van Pinxteren, D., Wex, H., Berdalet, E., Vaqué, D., Dall'Osto, M., and Herrmann, H.: Aerosol Marine Primary Carbohydrates and Atmospheric Transformation in the Western Antarctic Peninsula, ACS Earth Space Chem., 5, 1032–1047, https://doi.org/10.1021/acsearthspacechem.0c00351, 2021.

Funding

We gratefully acknowledge the funding by the Deutsche Forschungsgemeinschaft (DFG, German Research Foundation, Projektnummer 268020496–TRR 172) within the Transregional Collaborative Research Center "ArctiC Amplification: Climate Relevant Atmospheric and SurfaCe Processes, and Feedback Mechanisms (AC)³" in subprojects B04. Additional support through the Leibniz Association SAW funding of the project "Marine biological production, organic aerosol particles and marine clouds: a Process Chain (MarParCloud)" (SAW-2016-TROPOS-2) is also gratefully acknowledged.

Cooperation

National and international project partners.

Photosensitizers and their kinetics in the aqueous phase

Thomas Schaefer, Tamara Felber, Kifle. Z. Aregahegn, Hartmut Herrmann

Die Bildung von sekundärem organischem Aerosol in der atmosphärischen Flüssig-/Partikelphase (aqSOA) ist ein schlecht verstandener Reaktionsweg. Es gibt Hinweise, dass lichtabsorbierende Verbindungen photochemische Prozesse in Aerosolpartikeln und/oder an der Gas-Partikel-Grenzfläche auslösen, die zur Aerosolalterung und SOA-Bildung führen, die Photosensibilisierung. Das Ziel der Studie ist es, Photosensibilisatoren, deren Kinetik sowie Reaktionsprodukte der Reaktion mit ungesättigten Carbonylverbindungen wie Methylvinylketon, Methacrolein und Methacrylsäure in wässriger Phase zu charakterisieren. Dazu wurde die Laserblitzanregung-Laser-Langwegabsorption und die Ultra-Performance-Flüssigkeitschromatographie verwendet. Es wurden Quantenausbeuten der Bildung der angeregten Zustände, sowie die Reaktionskonstanten und Reaktionsprodukte von Imidazol-2-carboxaldehyd und von 3,4-Dimethoxybenzaldehyd mit ungesättigten Carbonylverbindungen bestimmt.

Introduction

The formation of secondary organic aerosol in the atmospheric liquid/particle phase (aqSOA) is a poorly understood reaction pathway. There is evidence that light-absorbing compounds can initiate photochemical processes in aerosol particles or at the gas-particle interface that lead to aerosol aging and SOA formation, namely photosensitization. The aim of the present study is to investigate photosensitizers and kinetics, and to identify the products of aqueous phase reactions with unsaturated carbonyl compounds [*Felber et al., 2020, 2021*].

Methods

Kinetic studies. To study the reactivity of the excited triplet-state photosensitizers toward organic compounds, a thermostatted laser flash excitation - laser long-path absorption setup was used [*Felber et al., 2020, 2021*]. The excited triplet state of the photosensitizer was produced by exciting the photosensitizer with an excimer laser flash.

Product studies. The photolysis experiments were performed in a 300 mL thermostated aqueous-phase photoreactor. The photolysis was initiated by irradiation with a xenon short arc lamp equipped with a series of optical filters to filter UV light below 290 nm and infrared radiation [*Aregahegn et al., 2022*]. Product analysis was performed using ultra-performance liquid chromatography coupled with high-resolution electrospray ionization ion mobility spectrometry and quadrupole time-of-flight mass spectrometry (UPLC/(+)ESI-IMS-QTOFMS, waters Synapt HDMS).

Results and Discussion

The quantum yields of excited photosensitizers in the triplet state were investigated by the SCN^- trapping method [*Felber et al., 2020, 2021*]. The following compounds were used: Imidazole-2-carbox-aldehyde (2-IC), 2-furaldehyde (2 FA), 2-acetylfuran (2-AF), 3-methoxyacetophenone (3-MAP), 2-hydroxy-5-methylacetophenone (HMAP), benzophenone (BPh), 4-benzoylbenzoic acid (4-BBA), xanthone (Xan), 1-nitronaphthalene (1-NN), 2-acetonaphthone (2-AN), 3,4-dimethoxybenzaldehyde (DMB), vanillin (Van), 2-methoxybenzaldehyde (2 MBA), 3-methoxybenzaldehyde (3-MBA) and 4-methoxybenzaldehyde (4-MBA).

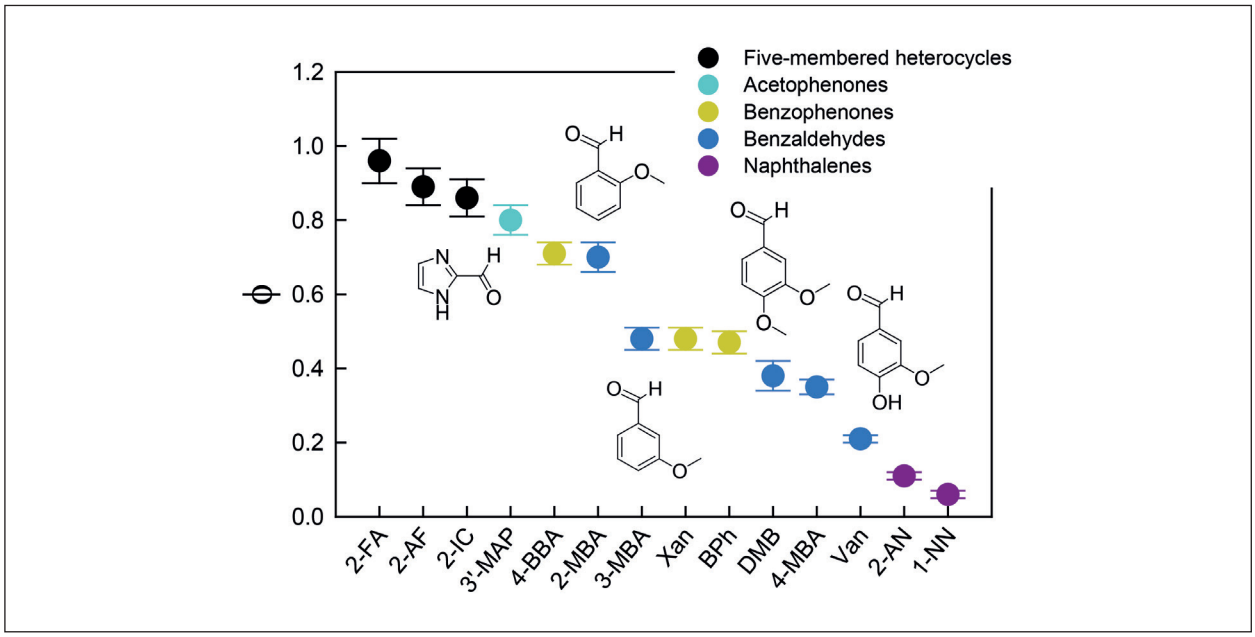

Fig. 1: Characterization of quantum yields (ϕ) of a variety of excited photosensitizers in the triplet state.

Figure 1 shows the quantum yields (ϕ) in order from the highest to the lowest value. The highest quantum yield was obtained with five-membered heterocycles, followed by acetophenones, benzophenones, benzaldehydes and naphthalenes. In the group of methoxybenzaldehydes, the quantum yield is affected by the position of the methoxy group in the following way: ortho > meta > para position. In addition, the nature of the para substituent in benzaldehydes affects ϕ in the following way: -H > -OMe > -OH, i.e. the ϕ decreases with higher electron donor capability. Based on the characterization of ϕ, two photosensitizers (2-IC and DMB) were selected for further investigation in terms of kinetic and productive studies. Table 1 summarizes the second order rate constants determined from photosensitized reactions with alkenes at different pH values [*Aregahegn et al., 2022*].

Using the results of reactivity studies, the photosensitized reaction of methyl vinyl ketone (MVK) and methacrolein (MACR) with 2-IC and DMB as photosensitizers was investigated. As shown by the HPLC chromatograms, new peaks are formed at different retention times, which increase with the irradiation time. These findings suggests that different products are formed in the photosensitized reaction between 2-IC and MVK. There are two possible reaction mechanisms for the photosensitized reaction of ^{3}2-IC* with MVK: either nucleophilic addition between the amine of 2-IC and the α,β-unsaturated C atom of MVK, followed by ring closure, or a Paterno-Büchi cycloaddition, where the excited carbonyl group reacts with substituted alkenes in a [2+2] cycloaddition to form an oxetane. A similar reaction mechanism is observed for the reaction of MACR with the excited ^{3}2-IC. A similar addition reaction of excited ^{3}DMB with MVK involves subsequent radical reactions with a C-C-bond formation between the excited DMB and the MVK or a Paterno-Büchi cycloaddition [*Aregahegn et al., 2022*].

Table 1: Second order rate constants (k_{2nd} /L mol^{-1} s^{-1})) of the reaction of excited 2-IC or excited DMB with different organic compound classes at T = 298 K under acidic and alkaline conditions.

PS	2-IC		DMB	
pH	**4-5**	**9**	**2**	**9**
Methyl vinyl ketone	(1.0 ± 0.1) × 10^9	(1.0 ± 0.1) × 10^9	n/d	(1.5 ± 0.2) × 10^8
Methacrolein	(1.4 ± 0.4) × 10^9	(1.5 ± 0.1) × 10^9	(1.1 ± 0.1) × 10^8	(2.8 ± 0.5) × 10^8
Methacrylic acid	(1.4 ± 0.4) × 10^9	(1.1 ± 0.4) × 10^8	n/d	(5.2 ± 1.2) × 10^6

References

Felber, T., Schaefer, T., and Herrmann, H. *Five Membered Heterocycles as Potential Photosensitizers in the Tropospheric Aqueous Phase: Photophysical Properties of Imidazole 2-carboxaldehyde, 2-Furaldehyde, and 2-Acetylfuran*. J. Phys. Chem. A, 2020, 124, (48), 10029 10039, https://doi.org/10.1021/acs.jpca.0c07028.

Felber, T., Schaefer, T., He, L., and Herrmann, H. *Aromatic Carbonyl and Nitro Compounds as Photosensitizers and Their Photophysical Properties in the Tropospheric Aqueous Phase.* J. Phys. Chem. A, 2021, 125, 23, 5078-5059, https://doi.org/10.1021/acs.jpca.1c03503.

Aregahegn, K. Z., Felber, T., Schaefer, T., and Herrmann, H. *Kinetics and Mechanisms of Aqueous-Phase Photosensitized Reactions of Imidazole-2-carboxaldehyde and 3,4-Dimethoxybenzaldehyde with α,β-Unsaturated Carbonyl Compounds.* 2022, in preparation.

Funding

Joint ANR/DFG research project PHOTOSOA - Photosensitization: A novel pathway to SOA generation and property change in tropospheric particles (grand number HE 3086/32-1) funded by the DFG (German Research Foundation).

Hydrotrioxide (ROOOH) formation in the atmosphere

Torsten Berndt,[1] Jing Chen,[2] Eva R. Kjærgaard,[2] Kristian H. Møller,[2] Andreas Tilgner,[1] Erik H. Hoffmann,[1]
Hartmut Herrmann,[1] John D. Crounse,[3] Paul O. Wennberg,[3,4] Henrik G. Kjaergaard[2]

[1] Atmospheric Chemistry Department (ACD), Leibniz Institute for Tropospheric Research (TROPOS), 04318 Leipzig, Germany.
[2] Department of Chemistry, University of Copenhagen, DK-2100 Ø, Denmark.
[3] Division of Geological and Planetary Sciences, California Institute of Technology, Pasadena, California 91125, United States.
[4] Division of Engineering and Applied Science, California Institute of Technology, Pasadena, California 91125, United States.

Hydrotrioxide, ROOOH, sind starke Oxidationsmittel in der organischen Synthese, welche bei tiefen Temperaturen durch Ozonolyse von Kohlenwasserstoffen in Lösungsmitteln erhalten werden. Deren mögliches Auftreten in der Atmosphäre, ausgehend von der Gasphasenreaktion von RO_2 Radikalen mit OH, wurde kürzlich postuliert. Es wird über den direkten Nachweis der ROOOH Bildung für verschiedene atmosphärenrelevante RO_2 Radikale berichtet. Kinetische Untersuchungen bestätigen schnelle RO_2 + OH Reaktionen, die zu Hydrotrioxiden führen. Ergebnisse einer Globalmodellierung weisen auf eine jährliche Produktion von 5 - 10 Millionen Tonnen an ROOOH ausgehend von der OH-initiierten Oxidation des Isoprens hin. Die atmosphärische Lebenszeit der ROOOHs wird auf Minuten bis zu Stunden abgeschätzt basierend auf deren thermischen Zerfall und der Reaktion mit OH Radikalen. Hydrotrioxide stellen eine neue Substanzklasse mit stark oxidierenden Eigenschaften in der Atmosphäre dar.

Introduction

Hydrotrioxides (ROOOH) are known, thermally unstable products formed in the low-temperature ozonolysis of saturated organic compounds in organic solvents. They are a chemical source of the powerful oxidant singlet molecular oxygen ($^1O_2$) released during their decomposition [*Stary et al*., 1976].

In atmospheric gas-phase chemistry, theoretical calculations have proposed the formation of hydrotrioxides as intermediates in the reaction of RO_2 radicals with OH, pathway (1) [*Müller et al.*, 2016]. The rapid radical recombination reaction is exothermic with about 130 kJ mol^{-1}, nearly independent of the RO_2 radical, forming initially the energy-rich ROOOH*. This chemically excited species can decompose leading to the corresponding alkoxy radical RO and HO_2, pathway (2), or to a lesser extent to an alcohol and O_2, pathway (3). In competition with decomposition, collisions with bath gas molecules, M, result in thermalized ROOOH, pathway (4).

RO_2 + OH	→	ROOOH*	(1)
ROOOH*	→	RO + HO_2	(2)
ROOOH*	→	ROH + O_2	(3)
ROOOH* + M	→	ROOOH + M	(4)

Theoretical calculations in the literature suggest that at 298 K and 1 bar N_2 channel (4) represent the dominant fate of ROOOH* in the case of $C_2H_5O_2$ and larger RO_2 radicals, while for CH_3O_2 radicals decomposition into CH_3O and HO_2 via channel (2) still dominates [*Assaf et al.*, 2018]. Thus, with exception of CH_3O_2 radicals, efficient formation of the thermalized ROOOH from RO_2 + OH reactions in the atmosphere is expected. This means that there is likely a strong gas-phase oxidant “hydrotrioxide” present which has not generally considered yet.

Here, we conclusively demonstrate via their direct detection that hydrotrioxides (ROOOH) are formed by RO_2 + OH reactions under atmospheric conditions.

Methods

The investigations were carried out in a free-jet flow system at 295 ± 2 K, a pressure of 1 bar air and a reaction time of 7.5 s using product monitoring by chemical ionization mass spectrometry. Additional experiments were conducted in a 1 m^3 Teflon chamber at the California Institute of Technology, Caltech, as well as quantum chemical calculations were performed to support the findings of the flow experiments.

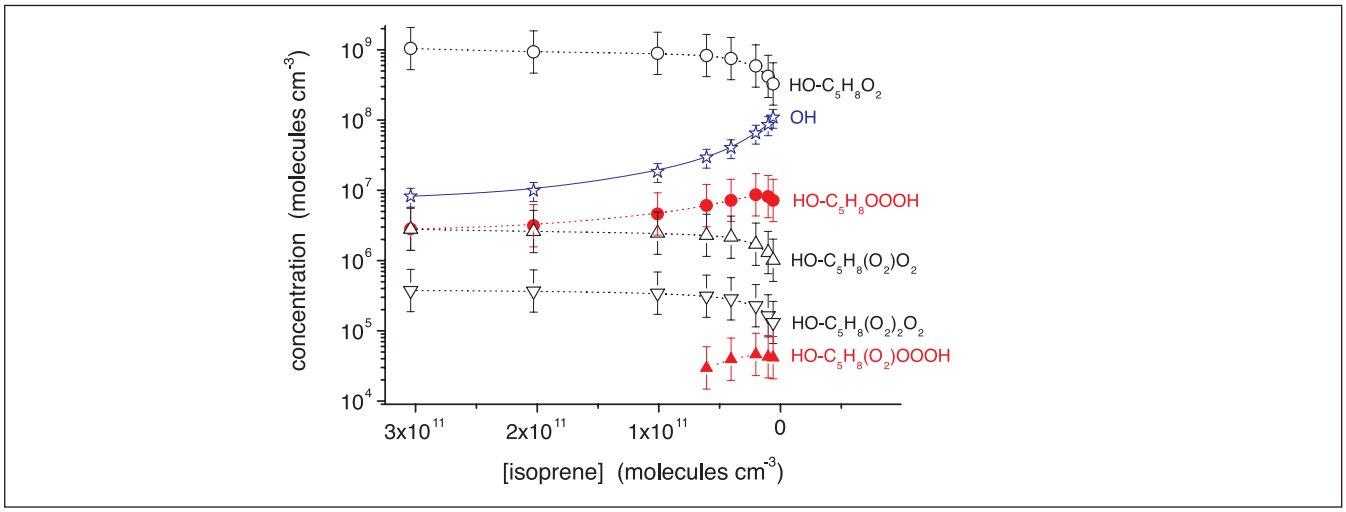

Fig. 1.: Formation of RO_2 radicals and hydrotrioxides from the OH + isoprene reaction. Increasing OH concentrations (blue stars) arise from constant OH production in the IPN photolysis ([IPN] = 2.15 × 10^{11} and [NO] = 1.0 × 10^{10} molecules cm^{-3}) while lowering of the OH loss rate by reducing the isoprene concentration. Iodide served as the reagent ion for product ionization.

Results and Discussion

For instance, ROOOH formation was probed in the reaction of OH radicals with isoprene (C_5H_8), one of the most important non-methane hydrocarbons in the atmosphere. Here, different isomeric RO_2 radicals are formed due to isoprene´s structure and the different positions of OH and O_2 addition as well as the RO_2 interconversion in this system. Moreover, RO_2 autoxidation leads to a suite of different oxidized RO_2 radicals HO-$C_5H_8(O_2)_xO_2$, x = 0, 1, 2. In Figure 1, results from an experiment with rising OH level due to lowering of isoprene in the reaction gas for constant isopropyl nitrite (IPN) photolysis for OH generation is shown. Signals consistent with the hydrotrioxides HO-$C_5H_8(O_2)_x$OOOH, x = 0 and 1, emerged beside those from the corresponding RO_2 radicals. Both substance classes showed the expected behavior, i.e., the RO_2 radical concentrations decreased with lowering of the isoprene feed while the ROOOH compounds increased proportional to the product [RO_2] × [OH].

The ROOOH´s formation kinetics was assessed based on the measured ROOOH, RO_2 and OH radical concentrations. From the linear dependence of [ROOOH] vs. [RO_2] × [OH] in the case of HO-C_5H_8OOOH, a rate coefficient k(HO-$C_5H_8O_2$+OH) = 5.1 × 10^{-11} cm^3 $molecule^{-1}$ s^{-1} follows. For the higher oxidized HO-$C_5H_8(O_2)$OOOH, the analysis yields k(HO-$C_5H_8(O_2)O_2$+OH) = 1.1 × 10^{-10} cm^3 $molecule^{-1}$ s^{-1}. These rate coefficients have an uncertainty of a factor of 3 - 4. Previously, high rate coefficients of RO_2 + OH reactions were reported for C_1 - C_4 RO_2 radicals via detection of the OH decay, e.g., k($C_4H_9O_2$+OH) = (1.5 ± 0.3) × 10^{-10} cm^3 $molecule^{-1}$ s^{-1} at 298 K [*Assaf et al.*, 2018], supporting our findings.

Global simulations permitted an assessment of ROOOH production from the OH radical-initiated oxidation of isoprene lumping all isoprene-derived RO_2 radicals ($RO_{2,isoprene}$) for simplicity. Using our experimentally observed rate coefficients k($RO_{2,isoprene}$+OH) = 5.1 × 10^{-11} (or 1.1 × 10^{-10}) cm^3 $molecule^{-1}$ s^{-1}, an overall ROOOH production of 5.0 (or 10.8) million metric tons per year was calculated.

The general validity of hydrotrioxide formation from RO_2 + OH reactions was demonstrated in the OH radical-initiated oxidation of dimethyl sulfide (DMS), α-pinene, toluene, 1-butene and 2-methylpropene.

References

Stary, F. E., D. E. Emge, and R. W. Murray (1976), Ozonization of organic substrates. Hydrotrioxide formation and decomposition to give singlet oxygen, *J.Amer. Chem. Soc.*, *98*(7), 1880-1884, https://doi.org/10.1021/ja00423a039.

Muller, J. F., Z. Liu, V. S. Nguyen, T. Stavrakou, J. N. Harvey, and J. Peeters (2016), The reaction of methyl peroxy and hydroxyl radicals as a major source of atmospheric methanol, *Nat. Commun.*, *7*(13213), 1-11, https://doi.org/10.1038/ncomms13213.

Assaf, E., C. Schoemaecker, L. Vereecken, and C. Fittschen (2018), Experimental and theoretical investigation of the reaction of RO_2 radicals with OH radicals: Dependence of the HO_2 yield on the size of the alkyl group, *Int. J. Chem. Kinet.*, *50*(9), 670-680, https://doi.org/10.1002/kin.21191.

No evidence for a productive rime-splintering mechanism at IDEFIX so far

Susan Hartmann[1], Alice Keinert[2], Alexei Kiselev[2], Johanna Seidel[1], Frank Stratmann[1]

[1] Leibniz Institute of Tropospheric Research, Leipzig, Germany

[2] Karlsruhe Institute of Technology (KIT), Institute of Meteorology and Climate Research, Karlsruhe, Germany

Atmosphärische Beobachtung von Mischphasenwolken zeigen gelegentlich eine starke Diskrepanz zwischen Eispartikel- und Eiskeimanzahlkonzentration von mehreren Größenordnungen. Als Erklärung für die Diskrepanz wurden Sekundäreisbildungsprozesse, die zur Vervielfältigung vorhandener Eispartikel führen können, vorgeschlagen. In dieser Studie untersuchen wir den bekanntesten Sekundäreisbildungsprozess, benannt nach Hallett und Mossop, bei dem unterkühlte Tropfen mit einem Eispartikel/Graupel kollidieren und Sekundäreispartikel produzieren. Bisher fehlt es an einem quantitativen und detaillierten mechanistischen Verständnis des Hallett-Mossop Prozesses. Erste vorläufige Ergebnisse des am TROPOS neu-entwickelten experimentellen Aufbaus IDEFIX (engl.: Ice Droplets splintEring on FreezIng eXperiment) geben keine Hinweise auf einen produktiven Hallett-Mossop Prozess. Vielmehr wurden einzelne Ereignisse mit geringer Anzahl von Sekundäreispartikeln im Zusammenhang mit dem mechanischen Abbrechen und der Sublimation von Reiftürmen beobachtet. Dies spricht zunächst gegen einen in der Literatur vorgeschlagenen Mechanismus, der die Bildung einer Eisschale um einen angelagerten gefrierenden Tropfen mit anschließender Fragmentierung beschreibt.

Introduction

Atmospheric observations of mixed-phase clouds occasionally demonstrate a strong discrepancy between the ice particle and ice nucleating particle number concentrations of one to four orders of magnitude at modest supercooling [*Crosier et al.*, 2011; *Hogan et al.*, 2002; *Mossop*, 1985; *Taylor et al.*, 2016]. Different secondary ice production (SIP) mechanisms have been hypothesized to increase the total ice particle number concentration by multiplication of pre-existing ice particles and hence explain the observed discrepancies [*Field et al.*, 2016; *Sotiropoulou et al.*, 2020]. The most well-known SIP process is the Hallett-Mossop [*Hallett and Mossop*, 1974] or rime-splintering process, in course of which small supercooled droplets freeze on impact on a larger ice particle (so-called rimer) and thereby produce secondary ice particles. Concerning rime splintering, several mechanisms have been proposed. These mechanisms are based on the release of stresses due to mechanical action, pressure or thermal gradients during riming, as well as on the sublimation of frail ice crystal elements [*Choularton et al.*, 1980; *Dong and Hallett*, 1989; *Mossop*, 1976]. An illustrative example of these mechanisms is the fragmentation of the ice shell forming around a freezing accreted droplet. However, the exact mechanism is not clear yet. Further, existing experimental data concerning the Hallett-Mossop process is inconsistent [*Korolev and Leisner*, 2020]. To overcome the missing quantitative and detailed mechanistic understanding, a new experimental set-up IDEFIX has been developed at TROPOS, in close cooperation with KIT.

Method - IDEFIX

IDEFIX is designed to investigate rime-splintering under realistic atmospheric conditions, i.e., temperature ranging from 0°C to -15°C, humidity at near ice saturation, impact velocities of around 1 m/s, which corresponds to the fall velocity of graupel having a diameter of 1 mm, and droplet-ice particle collision rates resulting in dry riming growth, i.e., the actual rimer surface temperature always is below 0°C. IDEFIX (Fig. 1) is an axial-symmetric laminar flow chamber with cooled walls in which two air flows pre-conditioned with respect to temperature,

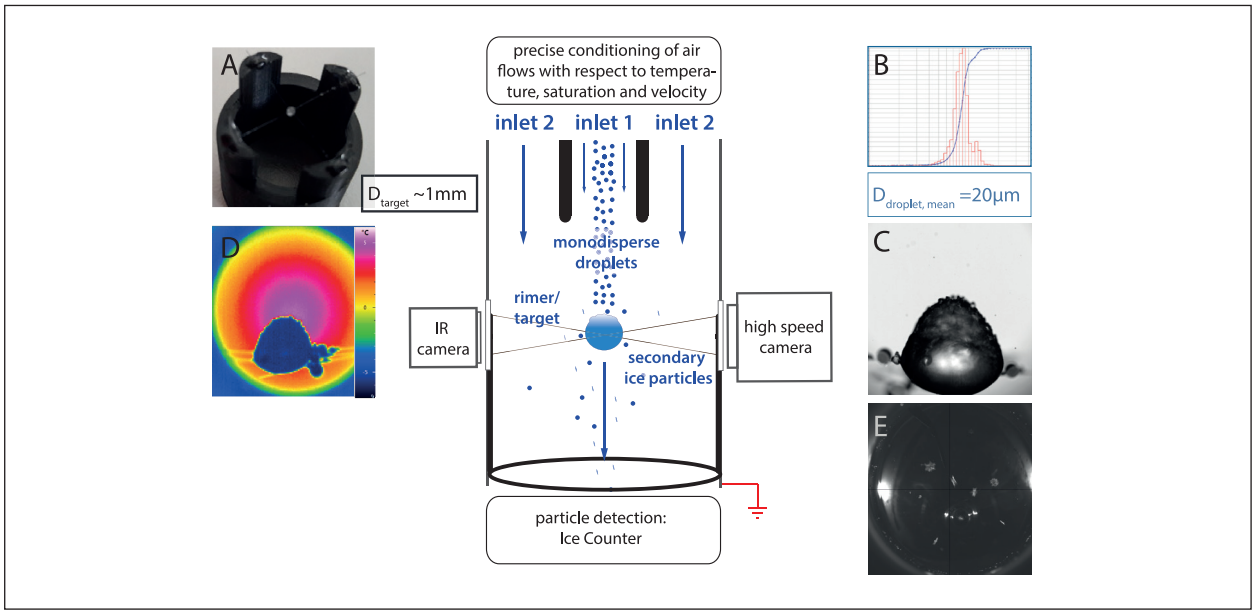

Fig. 1: Sketch of the IDEFIX collision chamber including (A) image of previously frozen ice target with a diameter of approx. 1 mm placed on electrically conductive carbon fibers, (B) number size distribution of supercooled droplets with mean diameter of 20 µm produced by a monodisperse droplet generator and measured with optical particle counter WELAS, images from (C) high speed video microscopy, and (D) infrared camera of rimed ice target and (E) image of secondarily produced ice crystals growing while immersed in the sugar solution inside the ice particle counter (developed by KIT) installed underneath IDEFIX. The chamber is grounded to avoid accumulation of charges on the rimer.

humidity and velocity are combined. In the center of the chamber, supercooled monodisperse droplets (mean diameter of 20 µm) collide with the rimer (diameter of 1 mm) which is fixed at the intersection of two crossing carbon fibers. The riming process is observed with high-speed video microscopy and an infrared camera to visualize the rimer surface structure and temperature, respectively. For detection, the SIP particles are impacted into a supercooled sugar solution and optically counted while being immersed and slowly growing in the sugar solution.

Results and Discussion

To quantitatively investigate SIP in the parameter range for which rime-splintering has been suggested to be effective, the air temperature and impact velocity were varied in the ranges from -3 °C to -15 °C and 0.5 m/s to 3 m/s, respectively. It was found that during droplet accreting with a collision rate of 10 droplets per second and mm² area cross section, the rimer surface temperature was increased by approximately 1.5 K, compared to conditions without droplet collisions, and always stayed below 0 °C. I.e., the rimer growth took place in the so-called dry growth regime.

At -5°C, only during one out of five experiments performed close to the ideal conditions for rime-splintering according to *Hallett and Mossop* [1974] SIP was observed (Fig. 2). The observed SIP cases were examined regarding their underlying physical mechanisms. We found evidence for mechanical fracturing and/or detachments of rime spires during sublimation in two out of four observed SIP cases after droplet collisions were stopped. Analyzing the rimer surface structure, it turned out that with increasing temperature and/or impact velocity the droplets tend to wet the ice surface on impact instead of freezing spherically. These findings argue against the proposed mechanism of fragmentation of the ice shell forming around a freezing accreted droplet [*Choularton et al.*, 1980; *Griggs and Choularton*, 1983; *Mossop*, 1976], but is in line with studies of *Dong and Hallett* [1989] and *Emersic and Connolly* [2017].

In summary, the preliminary results from first measurements conducted at IDEFIX suggest that we (a) observed single SIP events but (b) did not find evidence for a productive rime-splintering mechanism so far (Fig. 2).

Outlook

In the near future, we plan to continue the rime-splintering experiments in order to obtain better statistics and to expand the parameter space (e.g., polydisperse droplet size distributions, supersaturated conditions with respect to ice). With a more extensive database, we plan to develop a new parameterization for describing the rime-splintering process inside atmospheric models.

30 riming targets in total 21 SIP experiments		A	B		C	D
	v/ m/s	0.6	1	1	2	1
	T /°C	-5		-7		-15
number of valid experiments	9	1	5	1	1	1
valid with observed SIP	4	1	1	0	1	1
number of SIP particles		19	39	0	1	2

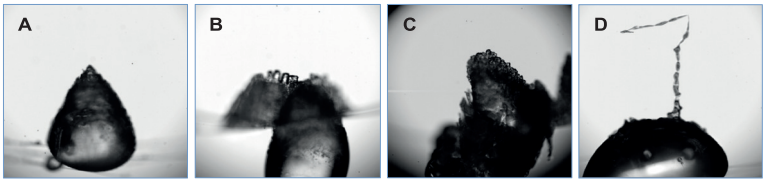

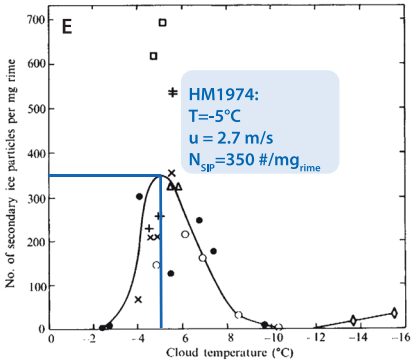

Fig. 2: Preliminary results of the first IDEFIX measurement campaign conducted at TROPOS. The table presents quantitative results of SIP in dependence of air temperature T and impact velocity v. Respective images from the highspeed microscopy are assigned to the individual observed SIP cases (A-D). For SIP cases A and B no direct evidence of any proposed rime-splintering mechanism could be found. In SIP case C & D after riming and/or subsequent sublimation, respectively, rime spire break-off was detected at the ice particle counter. In panel E the graph adopted from Hallett and Mossop [1974] (HM1974) is presented for comparison. HM1974 found in average 350 SIP particles per accreted mg rime at the maximum. In contrast, in this study only in one out of five experiments close to the ideal conditions for rime-splintering according to HM1974 SIP was observed, although two up to three mg rime was accreted during an individual, three up to five minutes long experiment at IDEFIX.

References

Choularton, T. W., D. J. Griggs, B. Y. Humood, and J. Latham (1980), Laboratory studies of riming, and its relation to ice splinter production, Q. J. R. Meteorol. Soc., 106(448), 367-374, https://doi.org/10.1002/qj.49710644809.

Crosier, J., K. N. Bower, T. W. Choularton, C. D. Westbrook, P. J. Connolly, Z. Q. Cui, I. P. Crawford, G. L. Capes, H. Coe, J. R. Dorsey, P. I. Williams, A. J. Illingworth, M. W. Gallagher, and A. M. Blyth (2011), Observations of ice multiplication in a weakly convective cell embedded in supercooled mid-level stratus, Atmos. Chem. Phys., 11(1), 257-273, https://doi.org/10.5194/acp-11-257-2011.

Dong, Y. Y., and J. Hallett (1989), Droplet accretion during rime growth and the formation of secondary ice crystals, Q. J. R. Meteorol. Soc., 115(485), 127-142, https://doi.org/10.1002/qj.49711548507.

Emersic, C., and P. Connolly (2017), Microscopic observations of riming on an ice surface using high speed video, Atmospheric Research, 185, 65-72.

Field, P. R., R. P. Lawson, P. R. A. Brown, G. Lloyd, C. Westbrook, D. Moisseev, A. Miltenberger, A. Nenes, A. Blyth, T. Choularton, P. Connolly, J. Buehl, J. Crosier, Z. Cui, C. Dearden, P. DeMott, A. Flossmann, A. Heymsfield, Y. Huang, H. Kalesse, Z. A. Kanji, A. Korolev, A. Kirchgaessner, S. Lasher-Trapp, T. Leisner, G. McFarquhar, V. Phillips, J. Stith, and S. Sullivan (2016), Chapter 7. Secondary Ice Production - current state of the science and recommendations for the future, Meteorol. Monogr., 0(0), null, https://doi.org/10.1175/amsmonographs-d-16-0014.1.

Griggs, D. J., and T. W. Choularton (1983), Freezing modes of riming droplets with application to ice splinter production, Q. J. R. Meteorol. Soc., 109(459), 243-253, https://doi.org/10.1002/qj.49710945912.

Hallett, J., and S. C. Mossop (1974), Production of secondary ice particles during riming process, Nature, 249(5452), 26-28, https://doi.org/10.1038/249026a0.

Hogan, R. J., P. R. Field, A. J. Illingworth, R. J. Cotton, and T. W. Choularton (2002), Properties of embedded convection in warm-frontal mixed-phase cloud from aircraft and polarimetric radar, Q. J. R. Meteorol. Soc., 128(580), 451-476, https://doi.org/10.1256/003590002321042054.

Korolev, A., and T. Leisner (2020), Review of experimental studies of secondary ice production, Atmos. Chem. Phys., 20(20), 11767-11797, https://doi.org/10.5194/acp-20-11767-2020.

Mossop, S. C. (1976), Production of secondary ice particles during growth of graupel by riming, Q. J. R. Meteorol. Soc., 102(431), 45-57, https://doi.org/10.1002/qj.49710243104.

Mossop, S. C. (1985), The origin and concentration of ice crystals in clouds, Bull. Am. Meteorol. Soc., 66(3), 264-273, https://doi.org/10.1175/1520-0477(1985)066<0264:toacoi>2.0.co;2.

Sotiropoulou, G., S. Sullivan, J. Savre, G. Lloyd, T. Lachlan-Cope, A. M. L. Ekman, and A. Nenes (2020), The impact of secondary ice production on Arctic stratocumulus, Atmos. Chem. Phys., 20(3), 1301-1316, https://doi.org/10.5194/acp-20-1301-2020.

Taylor, J. W., T. W. Choularton, A. M. Blyth, Z. Liu, K. N. Bower, J. Crosier, M. W. Gallagher, P. I. Williams, J. R. Dorsey, M. J. Flynn, L. J. Bennett, Y. Huang, J. French, A. Korolev, and P. R. A. Brown (2016), Observations of cloud microphysics and ice formation during COPE, Atmos. Chem. Phys., 16(2), 799-826, https://doi.org/10.5194/acp-16-799-2016.

Cooperation

Karlsruhe Institute of Technology (KIT), Institute of Meteorology and Climate Research, Karlsruhe, Germany.

Funding

This project is funded by the German Research Foundation DFG (grant HA 8322/1-1).

Verification of the Aeolus Wind Product in the Upper Troposphere and Lower Stratosphere using Super Pressure Balloon Observations

Sebastian Bley[1,2], Michael Rennie[3], Montserrat Pinol Sole[5], James Antifaev[4], Salvatore Candido[4], Rob Carver[4], Frithjof Ehlers[5], Thorsten Fehr[5], Jonas von Bismarck[5], Nedjeljka Zagar[6], Anne Grete Straume[5], Anja Hünerbein[1], Hartwig Deneke[1]

[1] Leibniz Institute for Tropospheric Research, Leipzig, Germany [2] ESA-ESRIN, Centre for Earth Observation, Frascati, Italy
[3] ECMWF, European Centre for Medium-Range Weather Forecasts, Reading, UK
[4] Loon, Mountain View, CA, United States
[5] ESA-ESTEC, European Space Research and Technology Centre, Noordwijk, Netherlands
[6] University of Hamburg, Hamburg, Germany

Dynamische Prozesse in der oberen Troposphäre und unteren Stratosphäre (UTLS) umfassen planetare Wellen sowie kurzskalige Schwerewellen. Deren typische Charakteristiken wie Windscherung oder Temperaturperturbation sind allerdings schwer zu modellieren oder zu messen. Beobachtungen des neuartigen Windsatelliten Aeolus füllen eine Lücke im globalen Beobachtungssystem, insbesondere in der UTLS, einer Region, in der Winddaten nur spärlich zur Verfügung stehen. Um diesen einzigartigen Datensatz zu validieren, wurden Aeolus-Windbeobachtungen mit Messungen von Stratosphärenballons des Google-Loon-Netzwerks verglichen. Diese Ballons können für mehrere Monate in Höhen zwischen 16-20 km verweilen und liefern dabei wertvolle Daten über die Dynamik in der UTLS. Vergleiche mit modellierten Windfeldern des ECMWF-Modells deuten auf eine systematische Überschätzung der modellierten Windgeschwindigkeit hin.

Introduction

Model winds are known to have significant uncertainties in the tropics, particularly in the Upper Troposphere and Lower Stratosphere (UTLS) [*Podglajen et al.,* 2014, *Zagar et al.,* 2021]. Quantifying these uncertainties and estimating errors on a global scale is generally difficult due to the lack of reference wind observations in the UTLS. Accurate observations of wind profiles from radiosondes, aircraft data or wind profilers are mostly concentrated over the northern hemisphere. Traditional satellite-based wind observations are limited to the cloud top layer for AMVs, or to the surface for scatterometers.

Wind observations from the novel Aeolus satellite that carries the world's first Doppler Wind Lidar in space, fill a significant gap in the global observing system, particularly in the UTLS. In order to validate this unique dataset, winds measured by Aeolus are compared against observations from the super pressure balloon network Loon. Beyond that, this synergistic dataset can be used to quantify uncertainties in wind speed forecasts.

Methods

We used the full dataset of 229 individual super pressure balloon flights between June 2019 and December 2020 and calculated collocated Aeolus wind profiles applying a horizontal and temporal collocation criterion of 100km/200 km and 2 hours. Figure 1 shows the global distribution of collocated wind observations between Loon and Aeolus. Using a maximum collocation distances of 100 km yields in 3227 collocated wind observations. This number increases to 5847, when applying a threshold of 200 km. To gain a high number of data points, we have considered all collocated measurements within the 200 km radius. In a second step, we have rejected data, if the standard deviation of measured winds is larger than 2 m/s.

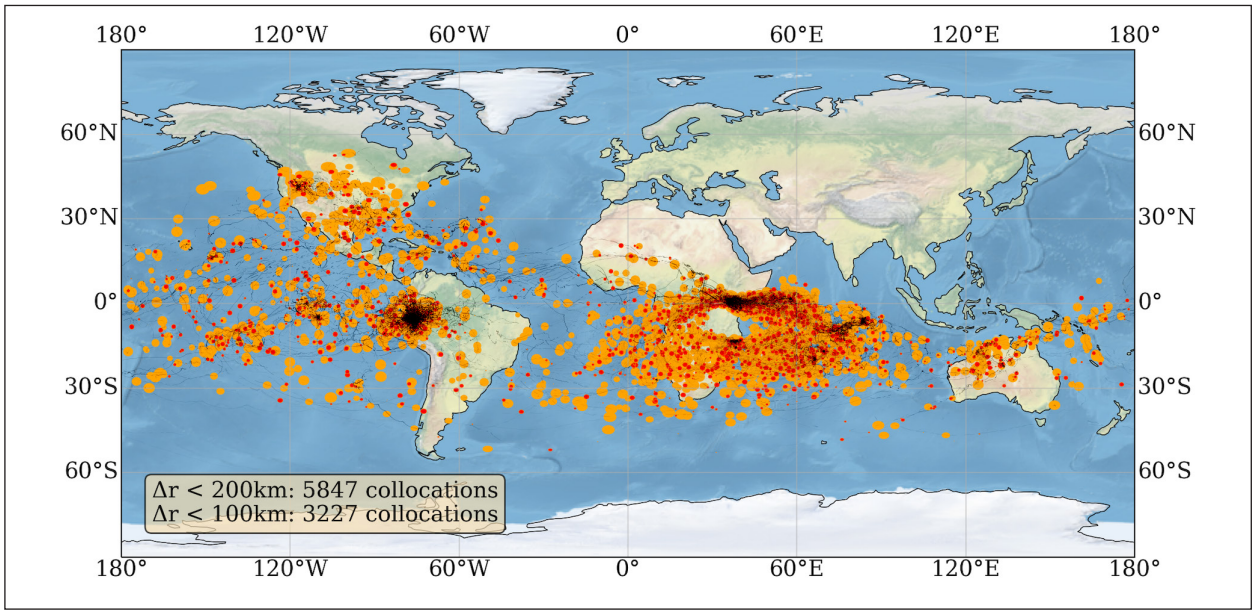

Fig. 1: Global collocated wind observations acquired from Aeolus and Loon in the time period from August 2019 until November 2020. The loon trajectories are shown by the thin lines in the background, while orange and red circles indicate collocated observations from Aeolus and Loon, for maximum collocation radii of 200 km and 100 km, respectively.

The balloons are assumed to be carried with the horizontal air flow and thus, the horizontal wind speed can be directly derived from changes in the balloon location. The observations of GPS position have uncertainties of approximately 10 m, which converts to approximately 0.23 m/s uncertainty [*Friedrich et al.,* 2017]. Further uncertainties in the Loon wind observations arise from the inertia of the large balloons, which may cause some underestimation of changes of the wind speed on short time scales [*Coy et al.,* 2019].

As model reference, we have used the forecasted wind fields from the ECMWF model, averaged and converted to the Aeolus horizontal line-of-sight (HLOS) wind vector. Also the Loon dataset provides the full zonal and meridional wind vector information, which we have converted to the HLOS wind speed by applying HLOS = –u sin(ϕ) –v cos(ϕ), where u and v are the zonal and meridional wind vectors and ϕ being the satellite's azimuth angle.

Results and Discussion

Using Loon balloon observations as reference, systematic and random errors of Aeolus HLOS winds are found to be -0.23 m/s and 6.13 m/s on average in the tropical UTLS between 16-20 km. ESAs pre-launch missing requirements recommend a precision of 3 m/s in that altitude range [*Ingmann and Straume,* 2016]. Furthermore, the target for the Aeolus HLOS wind systematic bias was to be below a value of 0.7 m/s over all vertical range bin levels. While the systematic bias, elaborated in this study, is in the range of the mission requirements, the HLOS random error is significantly larger for Rayleigh clear winds. The main reason for not reaching the targeted HLOS random error is the higher than expected signal loss in optical emit and receive path on the instrument. A comprehensive view on the causes for this are given in *Rennie et al* [2021].

The Aeolus HLOS estimated random error seems to be not representative as measure of the wind uncertainty in the tropical UTLS region. Looking into Aeolus HLOS profiles, we found mean wind shear values of 10 m/s/km, while the maximum values might be much higher in situations with strong wind shear. Figure 2 shows two example Rayleigh-clear HLOS wind profiles including the collocated Loon and ECMWF winds. Only a small change in the altitude of the balloons can cause a significant difference in wind speed, particularly in situations with strong wind shear. Therefore, we have linearly interpolated the Aeolus HLOS wind result between the Aeolus range bin below and above the Loon observation in order to better approximate the Aeolus measurement at the altitude of the balloon. Applying this method reduces the wind difference between Aeolus and Loon in the majority of cases. This finding highlights the need for a more realistic HLOS wind observation operator for assimilating Aeolus winds, instead of considering them as point winds, as it is currently done in the ECMWF foreward model.

Observation minus background statistics using the ECMWF model indicate a positive systematic

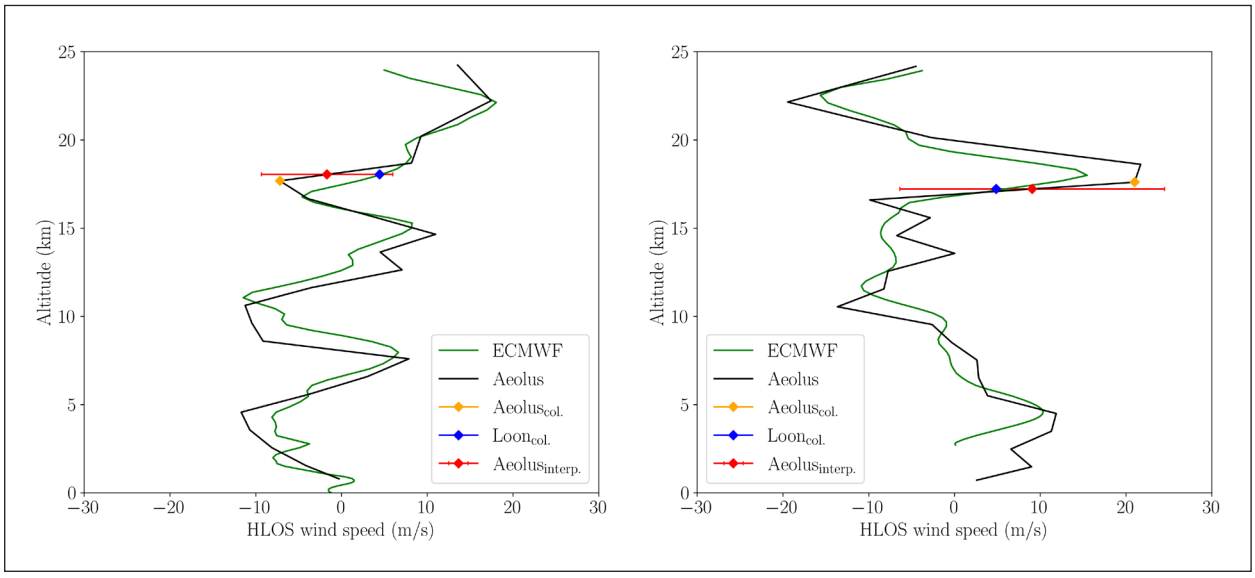

Fig. 2: Two example Aeolus Rayleigh-clear HLOS wind profiles (black solid line) including the collocated Loon wind observation (blue) and the ECMWF model winds (green lines). The yellow marker indicates the Aeolus wind speed of the vertical range bin, closest to the Loon altitude, while the red marker shows the HLOS wind observations interpolated between the range bin below and above the Loon altitude. The horizontal errorbars represent the standard deviation.

HLOS wind bias of 1 m/s, when comparing Aeolus against the model winds in the tropical UTLS. The wind difference between Aeolus and Loon however, show mean biases around 0 m/s. This finding indicates that the positive bias, seen in the O-B statistics, is attributable to model uncertainties of the predicted wind speed in the UTLS.

This study confirms the importance of validating the Aeolus HLOS winds against independent reference measurements for a better understanding of dynamical processes in the tropics in the UTLS, where model winds are known to have significant uncertainties. Super pressure balloon networks, such as Loon, provide a unique long-term reference dataset for validation of Doppler Wind Lidar missions such as Aeolus and model simulations.

References

Coy, L., Schoeberl, M. R., Pawson, S., Candido, S., and Carver, R. W.: Global Assimilation of Loon Stratospheric Balloon Observations, J. Geophys. Res. - Atmos., 124, 3005–3019, DOI: 10.1029/2018JD029673, URL: https://doi.org/https://doi.org/10.1029/2018JD029673, 2019.

Friedrich, L. S., McDonald, A. J., Bodeker, G. E., Cooper, K. E., Lewis, J., and Paterson, A. J.: A comparison of Loon balloon observations and stratospheric reanalysis products, Atmos. Chem. Phys., 17, 855–866, DOI: 10.5194/acp-17-855-2017, URL: https://acp.copernicus.org/articles/17/855/2017/, 2017.

Ingmann, P. and Straume, A.: ADM-AEOLUS mission requirements document, Centre ESRaT, URL: https://earth.esa.int/eogateway/documents/20142/1564626/Aeolus-Mission-Requirements.pdf, 2016.

Podglajen, A., Hertzog, A., Plougonven, R., and Žagar, N.: Assessment of the accuracy of (re) analyses in the equatorial lower stratosphere, J. Geophys. Res. - Atmos., 119, 11–166, DOI: 10.1002/2014JD021849, URL: https://doi.org/10.1002/2014JD021849, 2014.

Rennie, M. P., Isaksen, L., Weiler, F., de Kloe, J., Kanitz, T., and Reitebuch, O.: The impact of Aeolus wind retrievals on ECMWF global weather forecasts, Q. J. Roy. Meteor. Soc., DOI: 10.1002/qj.4142, URL: https://doi.org/10.1002/qj.4142, 2021.

Žagar, N., Rennie, M., and Isaksen, L.: Uncertainties in Kelvin waves in ECMWF analyses and forecasts: insights from Aeolus observing system experiments, Geophys. Res. Lett., p. e2021GL094716, DOI: 10.1029/2021GL094716, URL: https://doi.org/10.1029/2021GL094716, 2021.

Cooperation

European Space Agency - Centre for Earth Observation (ESA-ESRIN), European Centre for Medium-Range Weather Forecasts (ECMWF), University of Hamburg, Loon, The German Aerospace Center (DLR).

The Joint Aeolus – Tropical Atlantic Campaign (JATAC)

Holger Baars[1], Ronny Engelmann[1], Dietrich Althausen[1], Martin Radenz[1], Sofia Gómez Maqueo Anaya[1], Annett Skupin[1], Ulla Wandinger[1], Cordula Zenk[2,3], Eleni Marinou[4], Oliver Lux[5], Benjamin Witschas[5], Oliver Reitebuch[5], Torsten Fehr[6]

[1] Leibniz Institute for Tropospheric Research (TROPOS), Leipzig, Germany
[2] GEOMAR Helmholtz Centre for Ocean Research Kiel, Kiel, Germany
[3] Ocean Science Centre Mindelo (OSCM), Mindelo, Cape Verde
[4] National Observatory of Athens (NOA), Athens, Greece
[5] DLR, Institute of Atmospheric Physics, Oberpfaffenhofen, Germany
[6] European Space Agency (ESA), Noordwijk, The Netherlands

Im Sommer/Herbst 2021 hat TROPOS zusammen mit Kooperationspartnern eine temporäre ACTRIS-Supersite in Cabo Verde aufgebaut, um im Rahmen der „Joint Aeolus – Tropical Atlantic Campaign" die Messungen des ESA-Satelliten „Aeolus" zu validieren. Während der 3-wöchigen Intensivphase im September 2021, bei der auch mehrere Forschungsflugzeuge zum Einsatz kamen, konnten neben komplexen Saharastaubfahnen auch Aerosole vulkanischen Ursprungs (Las Palmas Eruption) beobachtet werden. Die atmosphärischen Messungen mit den bodengebundenen Instrumenten werden benutzt, um sowohl die Wind- als auch die Aerosolprodukte von Aeolus zu validieren.

Aeolus

On 22 August 2018, ESA successfully launched the Earth Explorer Mission Aeolus [*Stoffelen et al.*, 2005]. The scope of this mission is to measure profiles of one horizontal wind component (mainly the west-east direction) in the troposphere and stratosphere [*Baars et al.*, 2020] and to improve the weather forecast while assimilating the Aeolus wind profile data in near real-time [*Rennie & Isaksen* 2020]. Onboard of this satellite is the Atmospheric Laser Doppler Instrument (ALADIN), which is a high-spectral-resolution (HSR, *Wandinger* [1998]) Doppler lidar. While the main focus of the mission is to obtain atmospheric horizontal winds, the lidar is also capable to retrieve aerosol and cloud optical properties as spin-off products [*Ansmann et al.*, 2007; *Flament et al.*, 2021, *Baars et al.*, 2021] via the HSR lidar (HSRL) technique, which is a spaceborne novelty.

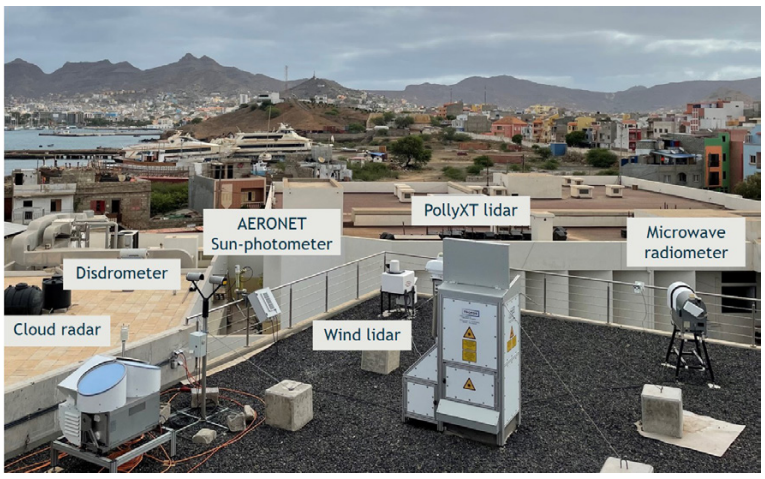

Fig. 1: Patchwork ACTRIS station on the roof of OSCM as photographed in September 2021.

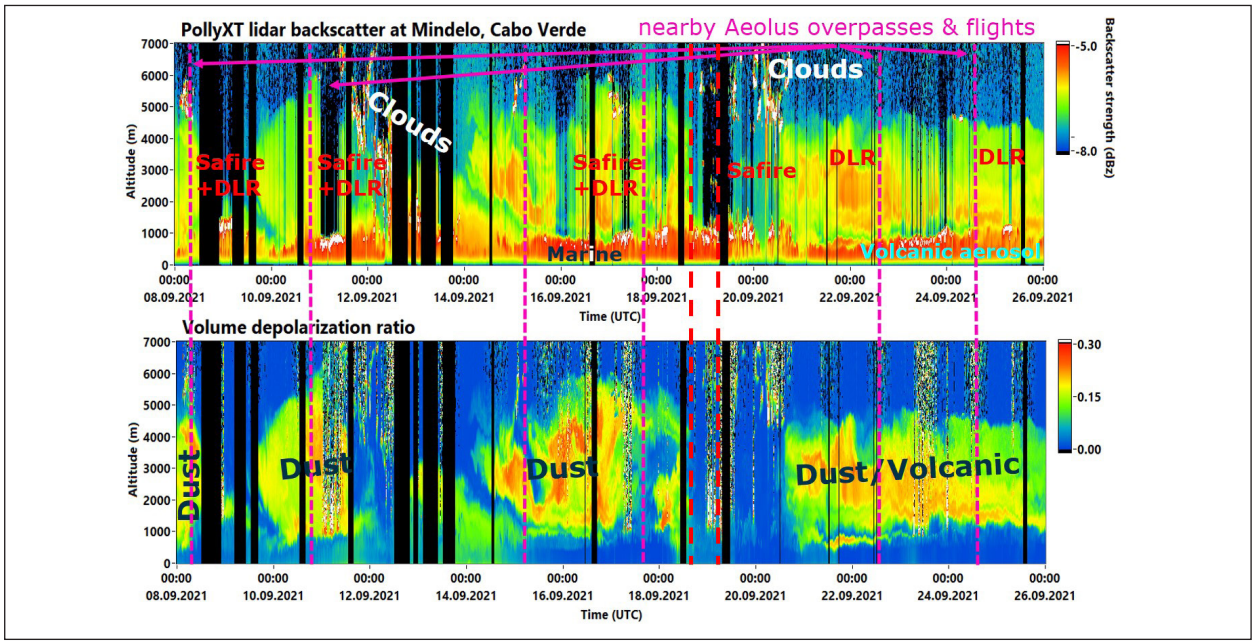

Fig. 2: Overview of atmospheric conditions over Mindelo during the 3-weeks intensive JATAC period. Top panel: Attenuated backscatter coefficient from PollyXT at 1064 nm. Bottom panel: Volume depolarization ratio at 532 nm. The overpasses of Aeolus and/or the DLR and LATMOS (Safire) airplanes are indicated as dashed vertical lines.

Thus, one of the goals of this Earth Explorer Mission is to prove the concept of this new technology in space and, therefore, intensive validation efforts are required.

JATAC

The Joint Aeolus – Tropical Atlantic Campaign (JATAC) has been performed in summer/autumn 2021 in Cabo Verde with the main objective to validate the observations of Aeolus – the first lidar mission of the European Space Agency (ESA). Next to an impressive airborne fleet based on the island of Sal, intense ground-based remote-sensing and airborne in-situ measurements took place on and above Mindelo (island of São Vicente).

For that reason, a dedicated orbit drift was performed in June 2021, so that the measurements of ESA's Aeolus satellite were directly performed over Mindelo on each Friday evening. Furthermore, the campaign has been dedicated to science studies for, e.g., the upcoming EarthCARE and WIVERN missions.

Patchwork ACTRIS station in Mindelo

At the Ocean Science Center Mindelo (OSCM), a full temporary ACTRIS remote sensing supersite was set up from June 2021. The instrumentation included a multiwavelength-Raman-polarization lidar PollyXT, an AERONET Sun photometer, a scanning Doppler wind lidar, a microwave radiometer - all provided by TROPOS - and a cloud radar belonging to ESA's fiducial reference network (FRM4Radar). The setup on the roof of the OSCM is shown in Fig. 1.

Results and Discussion

During the intensive observational period in September 2021, very different aerosol conditions were observed above and around Mindelo as shown in Fig. 2. Usually, the marine boundary layer up to an altitude of about 1 km was topped with a layer of Saharan dust reaching up to 6 km altitude. The amount and height of the Saharan dust aerosol varied during the 3-weeks campaign, providing a wide variety of aerosol conditions. Finally, volcanic aerosol from the "La Palma volcano" was observed in the local boundary layer and partly above.

Wind observations from the ground-based scanning Doppler lidar have been used to validate the Aeolus wind products above the island. First comparisons with airborne observations show that the ground-based Doppler lidar can observe winds up to the top of the Saharan air layer and agree with the Aeolus observation within the uncertainty range – see Fig. 3.

Aeolus aerosol products have been intensively validated for the direct overpasses with the PollyXT lidar. One example comparison covering the period of volcanic aerosol transport from La Palma to Cabo Verde is shown in Fig. 4. It was found that the backscatter coefficient can be well retrieved with Aeolus in the lofted aerosol layer with all algorithms (SCA

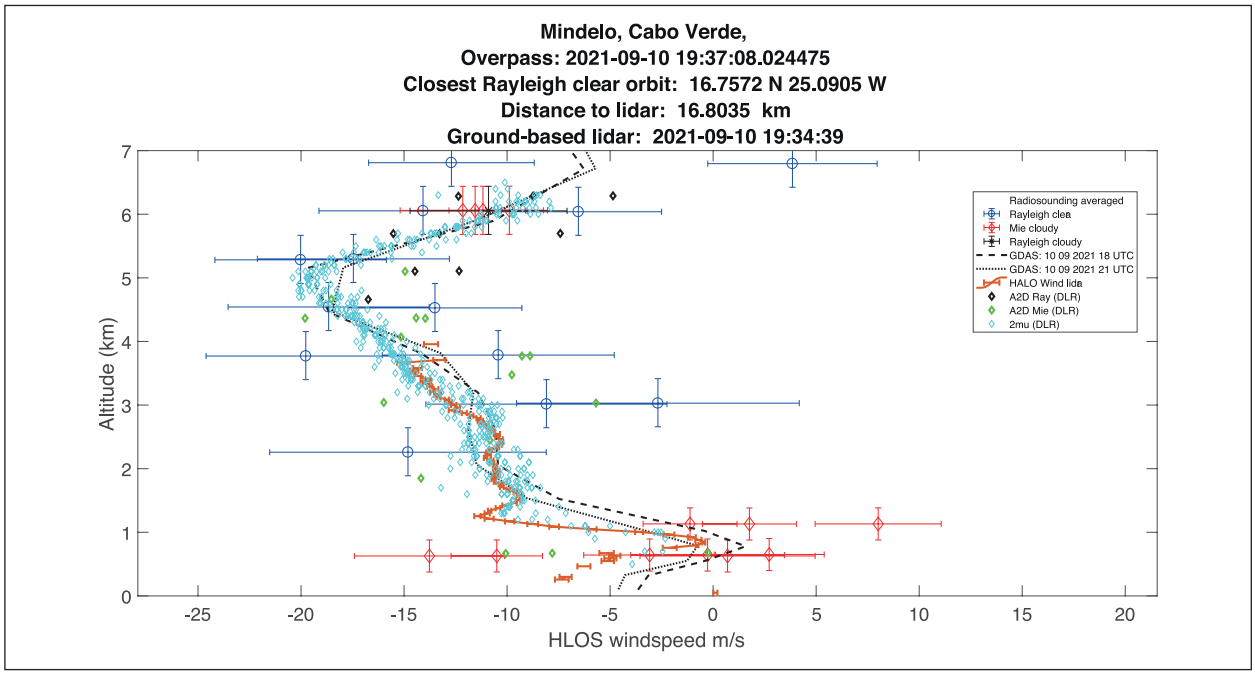

Fig. 3: Comparison of vertical profiles of horizontal line-of-sight wind (mainly west-east component) for Aeolus Rayleigh and Mie products, GDAS model data, ground-based HALO Doppler lidar, and airborne DLR wind lidars (A2D and 2mu). Aeolus data is shown within a radius of 100 km around Mindelo.

and SCA-mid for HSR and MCA for elastic lidar technique) - having in mind the coarse resolution of 87 km horizontally and 0.5 to 2 km vertically. Below 3 km, the HSR algorithms are not able to resolve the high backscatter values due to the low Aeolus signal return that is observed at this time of the mission

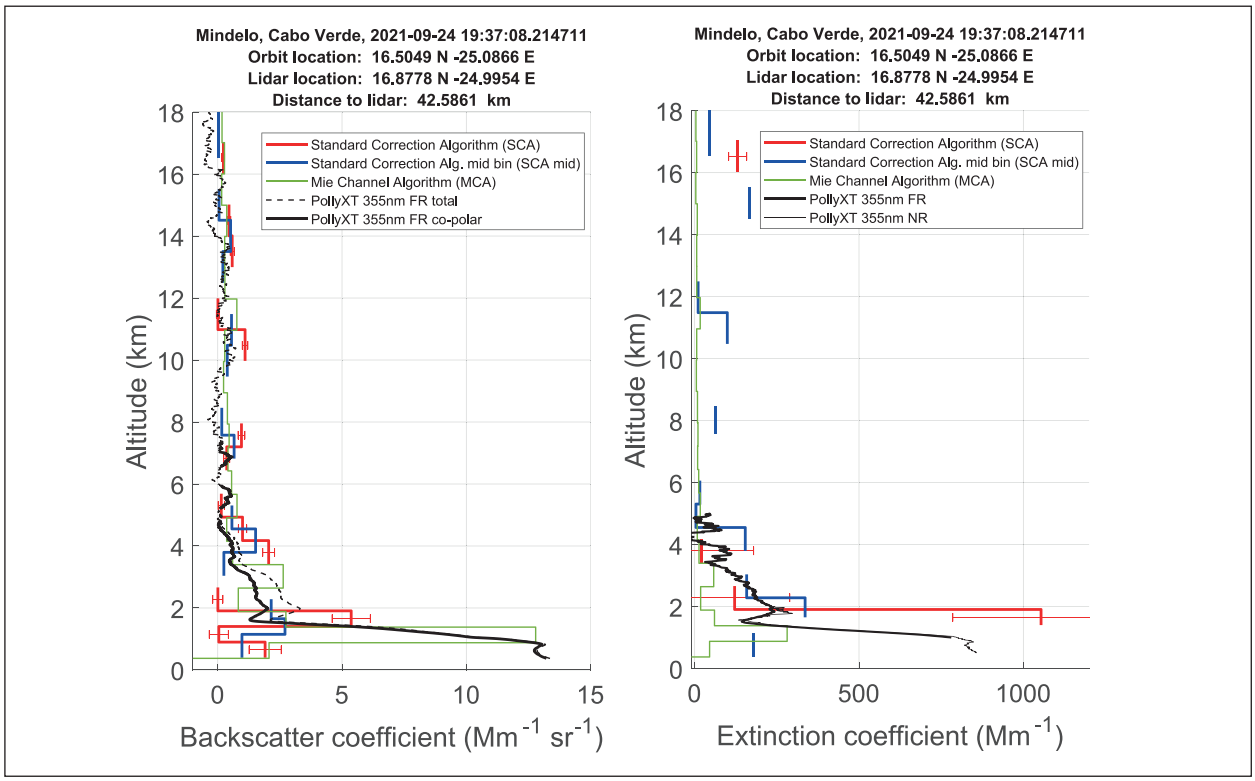

Fig. 4: Comparison of backscatter (left) and extinction (right) coefficients from PollyXT (black) and Aeolus (3 different algorithms: SCA, SCA-mid, and MCA).

(near end of lifetime). For the same reason, the HSR extinction retrievals suffer in general from noise, but could partly resolve the high extinction values up to around 1000 Mm^{-1} close to ground. The Mie channel algorithm (MCA) provides more robust results, but the fixed lidar ratio of 20 sr prevents to resolve the high extinction values while the backscatter coefficient agrees well.

Outlook

Another intensive campaign is planned for spring/summer 2022 on the Sao Vicente island, comprising a bigger instrument suite and covering the prime Saharan dust outbreak season. TROPOS will thus continue the operation of its instruments until this time.

Furthermore, TROPOS plans to setup a permanent ACTRIS aerosol and cloud remote sensing supersite at Mindelo in the framework of ACTRIS-D together with enhanced aerosol in-situ observations at the Cabo Verde Atmospheric Observatory on the same island. All these facilities are foreseen to operate continuously for more than 25 years and thus provide an excellent observational lighthouse in a region of the world where measurements are sparse.

References

Ansmann, A., U. Wandinger, O. Le Rille, D. Lajas, and A. G. Straume (2007), Particle backscatter and extinction profiling with the spaceborne high-spectral-resolution Doppler lidar ALADIN: methodology and simulations, Appl. Optics, 46(26), 6606-6622, https://doi.org/10.1364/AO.46.006606.

Baars, H., A. Herzog, B. Heese, K. Ohneiser, K. Hanbuch, J. Hofer, Z. Yin, R. Engelmann, and U. Wandinger (2020), Validation of Aeolus wind products above the Atlantic Ocean, Atmos. Meas. Tech., 13(11), 6007-6024, https://doi.org/10.5194/amt-13-6007-2020.

Baars, H., M. Radenz, A. A. Floutsi, R. Engelmann, D. Althausen, B. Heese, A. Ansmann, T. Flament, A. Dabas, D. Trapon, O. Reitebuch, S. Bley, and U. Wandinger (2021), Californian Wildfire Smoke Over Europe: A First Example of the Aerosol Observing Capabilities of Aeolus Compared to Ground-Based Lidar, Geophys. Res. Lett., 48(8), e2020GL092194, https://doi.org/10.1029/2020GL092194.

Flament, T., D. Trapon, A. Lacour, A. Dabas, F. Ehlers, and D. Huber (2021), Aeolus L2A aerosol optical properties product: standard correct algorithm and Mie correct algorithm, Atmos. Meas. Tech., 14(12), 7851-7871, https://doi.org/10.5194/amt-14-7851-2021.

Rennie, M., and L. Isaksen (2020), The NWP impact of Aeolus Level-2B winds at ECMWF, ECMWF Technical Memoranda, https://doi.org/10.21957/alift7mhr.

Stoffelen, A., J. Pailleux, E. Källén, J. M. Vaughan, L. Isaksen, P. Flamant, W. Wergen, E. Andersson, H. Schyberg, A. Culoma, R. Meynart, M. Endemann, and P. Ingmann (2005), THE ATMOSPHERIC DYNAMICS MISSION FOR GLOBAL WIND FIELD MEASUREMENT, Bull. Amer. Meteor. Soc., 86(1), 73-88, https://doi.org/10.1175/bams-86-1-73.

Wandinger, U. (1998), Multiple-scattering influence on extinction- and backscatter-coefficient measurements with Raman and high-spectral-resolution lidars, Appl. Optics, 37(3), 417-427, https://doi.org/10.1364/AO.37.000417.

Funding

Financial support by the German Federal Ministry for Economic Affairs and Energy (BMWi) under grant no. 50EE1721C, by European Union's Horizon 2020 research and innovation program through ACTRIS-2 under grant agreement no. 654109, and by the German Federal Ministry of Education and Research (BMBF) through PoLiCyTa under grant no. 01LK1603A.

Cooperation

European Space Agency (ESA), The German Aerospace Center (DLR), US National Aeronautics and Space Administration (NASA), Météo-France, Laboratoire atmosphères, milieux, observations spatiales (LATMOS), National Observatory of Athens (NOA), University of Nova Gorica (UNG), National Institute for Research and Development for Optoelectronics – (INOE), Ocean Science Centre Mindelo (OSCM), GEOMAR, and many more.

Transport and transformation of atmospheric aerosol across Central Europe with emphasis on anthropogenic sources (TRACE)

Laurent Poulain[1], Shubhi Arora[1], Hanna Wiedenhaus[1], Birgit Hesse[1], Petra Pokorna[2], Radek Lhotka[2], Jacub Ondracek[2], Petr Vodicka[2], Ralf Wolke[1], Vladimír Ždímal[2], Hartmut Herrmann[1]

[1] Leibniz Institute for Tropospheric Research, Leipzig, Germany
[2] Institute of Chemical Process Fundamentals of the CAS, Prague, Czech Republic

Da die erlaubten luftgetragenen Partikel-Massenkonzentrationen (PM) durch EU-Grenzwerte zum Schutz der menschlichen Gesundheit geregelt werden, ist es notwendig, die wichtigsten PM-Quellen genau zu identifizieren, um die lokale Luftqualität zu kontrollieren. Das Hauptziel des ProjektsTRACE ist es daher, die Transportwege und Umwandlungsprozesse des atmosphärischen Aerosols aus anthropogenen Quellen (insbesondere der Kohle- und Holzverbrennung) mit Hilfe komplementärer Messmethoden (offline und online) und modernster Modellierungswerkzeuge (Chemie-Transport-Modelle und Rezeptor-orientierte Modelle) für Mitteleuropa zu analysieren und zu bewerten. Die Messungen werden während zweier intensiver Kampagnen (Sommer und Winter) an den beiden ACTRIS-Stationen Melpitz (MEL, DE) sowie dem Nationalen Atmosphärenobservatorium Košetice (NOAK, CZ) durchgeführt und durch Messungen an einem dritten Standort (Frýdlant, FRÝ, CZ) an der tschechisch-polnisch-deutschen Grenze ergänzt. Um eine größere Skala abzudecken, werden Simulationen mit dem Chemie-Transportmodell COSMO-MUSCAT durchgeführt und die Ergebnisse durch die Messungen an den drei Probenahmestellen validiert.

Introduction

The emissions of primary particles and precursors of secondary particles in Europe have declined significantly over the past 20 years [*EEA*, 2018]. Until the year 2000, these emission reductions have reflected themselves in clear corresponding trends of particulate matter, PM_{10}. However, since 2000, the trend in PM_{10} concentrations in Europe has stagnated, only showing limited inter-annual fluctuations [*EEA*, 2018]. This pattern is in notable contrast to the continued reductions in PM emissions. The stagnating concentrations of ambient PM_{10} are therefore not fully understood and merit detailed examination. Similar trends in PM concentrations are also observed in Central Europe [*EEA*, 2018] like for example in Germany as well as in the Czech Republic based on long-term measurements at the rural background research sites Melpitz [*Poulain et al.*, 2011; *Spindler et al.*, 2013] and Košetice [*Holubová Šmejkalová*, 2018; *Pokorná et al.*, 2018]. The atmospheric aerosol particles are an extremely complex mixture of directly emitted particles (primary sources) from anthropogenic sources (e.g. traffic, residential heating, and energy production), biogenic sources (e.g. resuspension of dust, wildfires, volcano eruptions…), and secondary formed particles resulting of aging processes associated to atmospheric reactivity and the gas-to-particle partitioning which are either locally emitted or transported over long distances, e.g. [*van Pinxteren et al.*, 2019; *Waked et al.*, 2018]. Organic aerosol (OA) accounts for 20 – 90 % of the

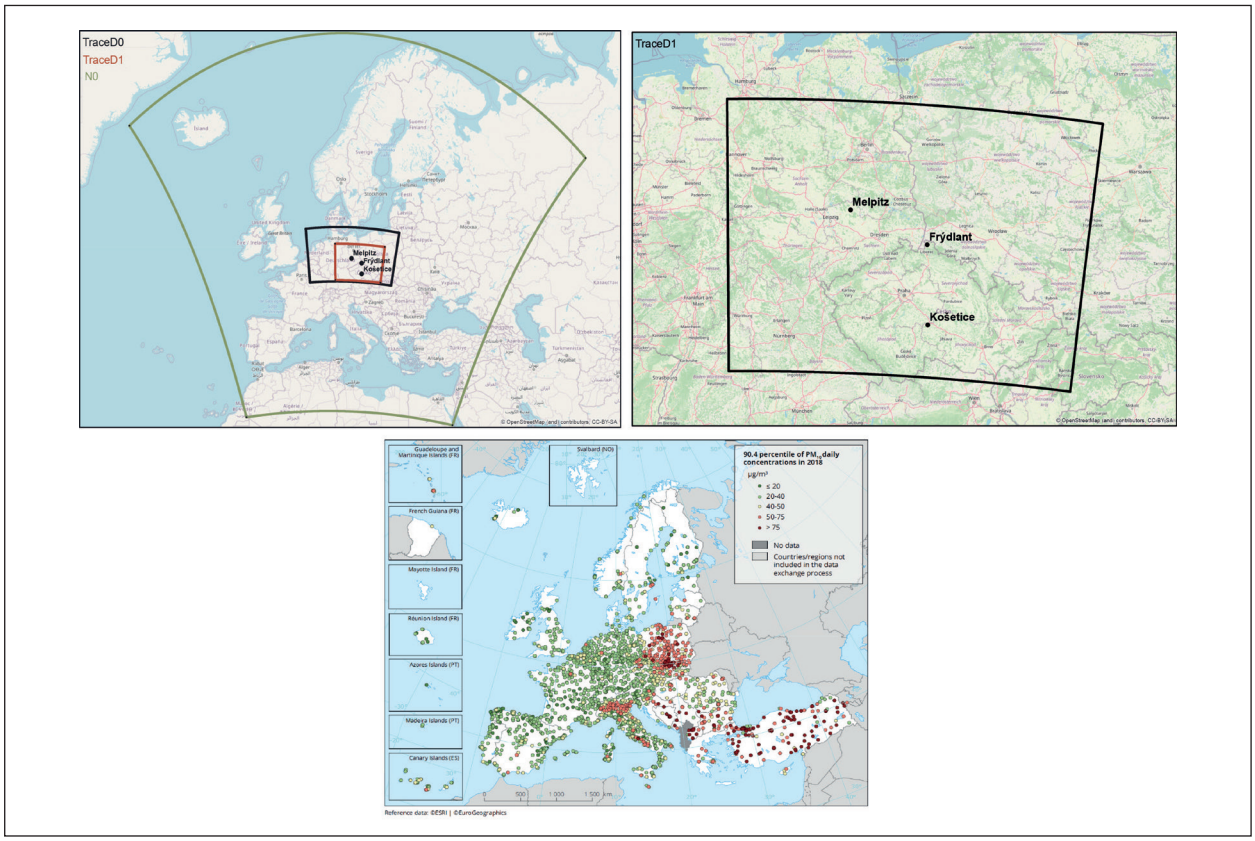

Fig. 1: Nesting of COSMO-MUSCAT runs, localization of the three rural background sampling sites used during TRACE (top) and the observed 90.4 percentile of the PM10 daily mean concentration in 2018 (source20) (bottom).

fine particles mass concentration [*Jimenez et al.*, 2009] made of thousands of compounds. To identify the aerosol sources, different source apportionment approaches have been used in Europe: chemical transport models (CTMs) and receptor-oriented models (RMs). However, due to the multiple origins of atmospheric aerosol the source apportionment and consequently the development of efficient mitigation strategies are difficult. Therefore, the application of advanced RMs on complementary data sets and adjustment or interconnection of their outputs in combination with CTMs enables precise and detailed identification of PM sources. However, this approach is lacking in Central European source apportionment studies.

Concept of the project

The TRACE project aims to combine the expertise of ICPF-CAS (Czech Republic) and TROPOS where all four departments of TROPOS are involved (ACD, EXAWOMP, Remote sensing, and Modeling) to combine state-of-the-art techniques including online aerosol mass spectrometers, offline comprehensive chemical characterization with receptor and chemical transport models to properly identify the contribution of primary and secondary aerosol sources and their geographical origin over one of the most polluted areas in Europe. A special focus on coal and biomass burning emissions will be made in order to better predict the impact of the future regulation regarding these two sources on air quality across Central Europe.

Results

Aerosol characterization

Measurements were performed during two intensive campaigns (February-March 2021 and July-August 2021 for the winter and summer campaigns, respectively) at the three sites: the two ACTRIS stations of Melpitz (MEL, DE) and the National Atmospheric Observatory Košetice (NOAK, CZ), completed by a third one (Frýdlant, FRÝ, CZ) located at the Czech-German-Polish border (Fig. 1).

All three stations were equipped with the same set of instruments provided by both partners combining online and offline measurements to provide a comprehensive chemical characterization of the atmospheric aerosols. The two campaigns ran successfully as can be seen on the preliminary results

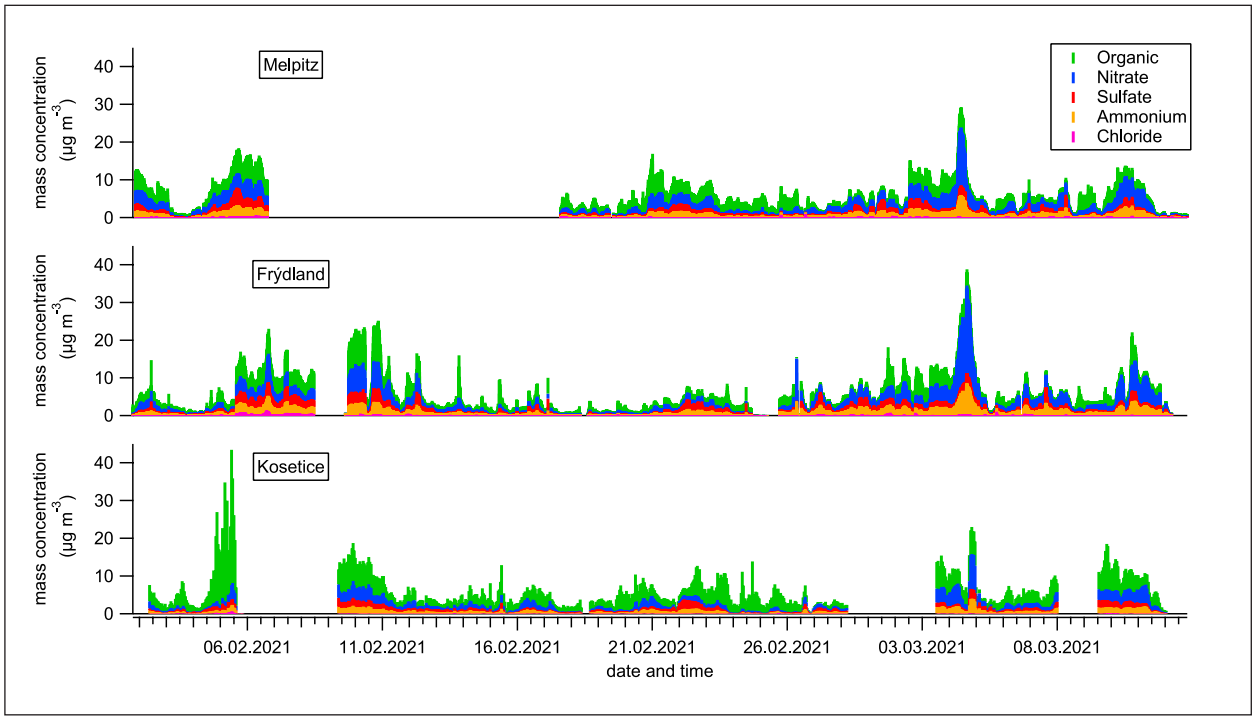

Fig. 2: Preliminary results of the aerosol chemical composition measured by the Aerosol Mass Spectrometers at the three sites during the winter campaign.

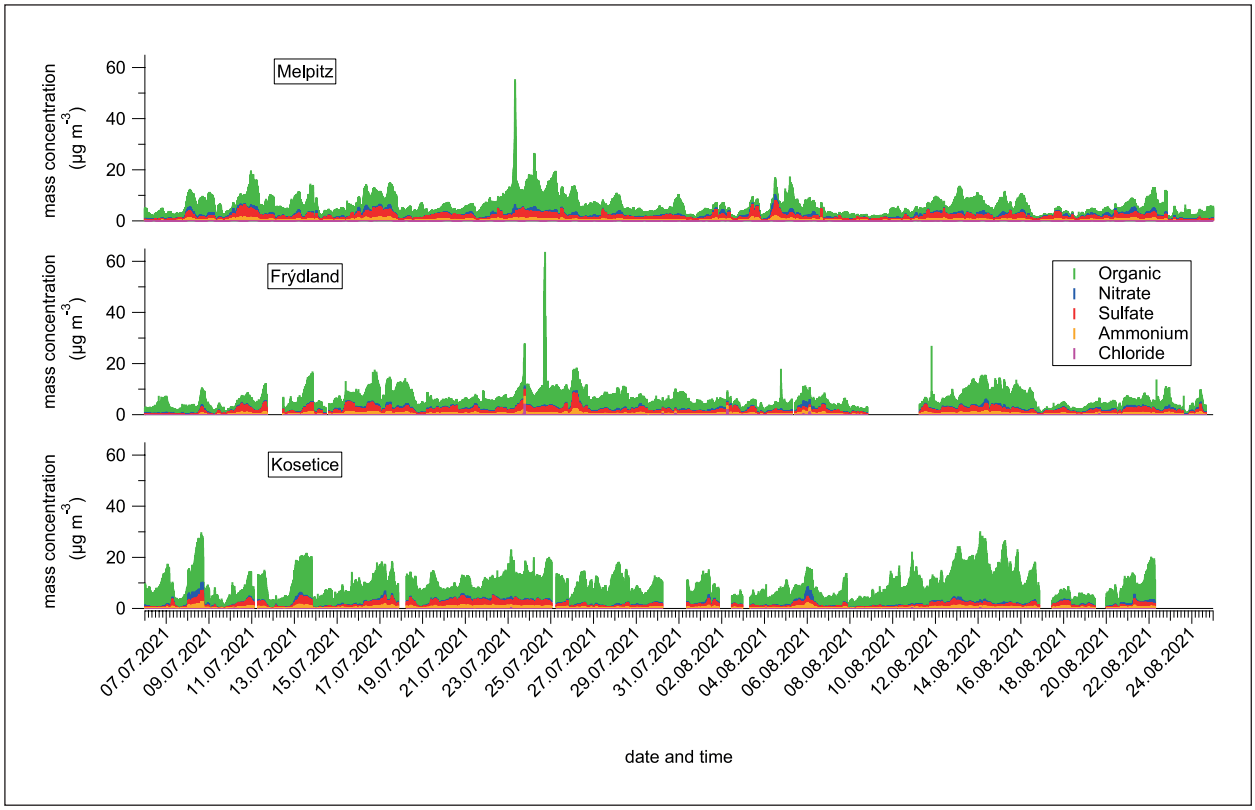

Fig. 3: Preliminary results of the aerosol chemical composition measured by the Aerosol Mass Spectrometers at the three sites during the winter campaign.

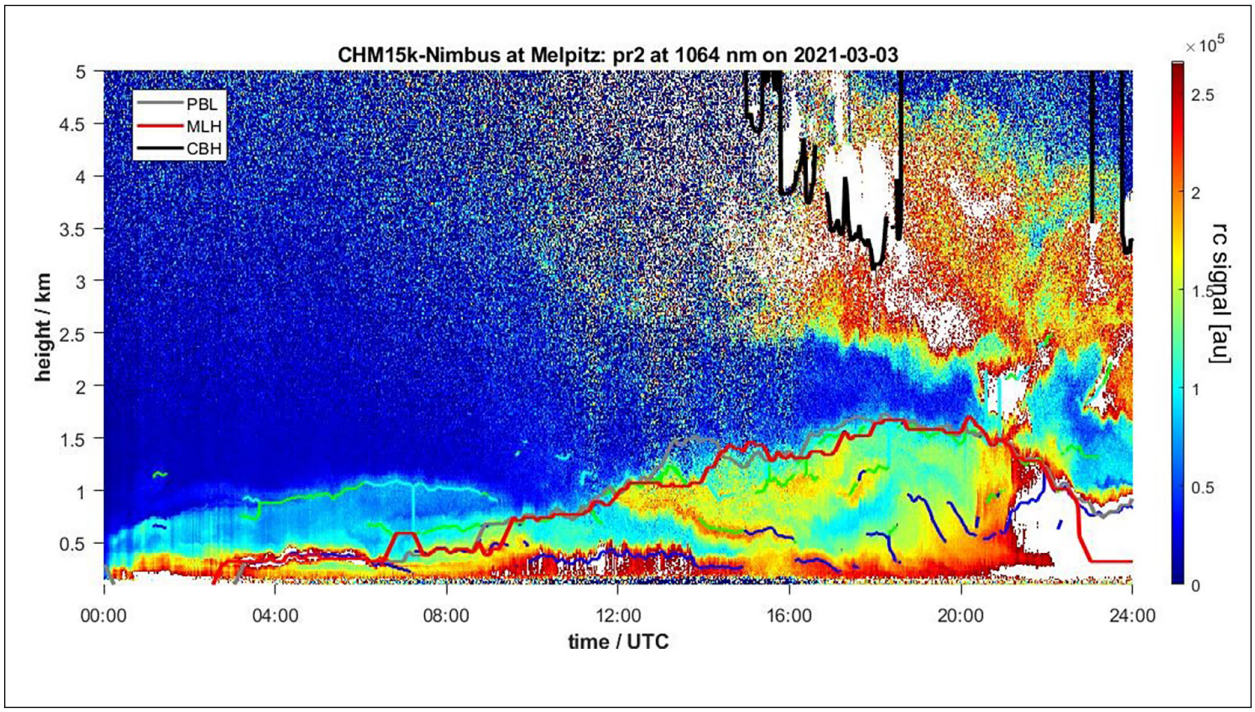

Fig. 4: Color plot of the vertical distribution of the range corrected backscatter signal at Melpitz on March 3, 2021. Layers of aerosol are visible as different intensities of this signal. The thin, green, blue, and cyan lines are the three aerosol layer heights, that are detected by the ceilometer itself and are given in the raw data of the instrument. These heights are not continuous and their number can change so that the color of the line may jump between the layers. See for example the nighttime residual layer that is marked by green and cyan lines between 4 and 8 UTC at about 1 km height. The continuous, thicker lines are determined using the STRATfinder algorithm: the planetary boundary layer height (PBLH) is marked in grey, the mixing layer height (MLH) in red, and the cloud base height (CBH) in black.

of the three Aerosol Mass Spectrometers measurements presented in Fig. 2 and 3. At each station, high volume $PM_{2.5}$ filter sampling was performed at a 12h time resolution on quartz filters. From them, total particle mass, OC/EC, water-soluble ions, anhydrous sugars, alkanes, PAHs, and secondary organic tracers will be analyzed.

Determination of the Planetary boundary layer height (PBLH) / mixing layer height (MLH)

All three stations were equipped with a ceilometer to detect aerosol layers in the atmosphere [*Heese et al.*, 2010] and thus to determine the heights of the PBL and the MLH, and data were submitted to the European E-Profile network (https://e-profile.eu). Calculation of the PBLH for the two field campaigns was performed using the routine STRATfinder [*Kotthaus et al.*, 2020]. STARTfinder follows the detected gradients and completes them to gain continuous layer heights. An example for a single day of the winter campaign is shown in Fig 4.

Chemical transport modeling

The chemical transport model COSMO-MUSCAT was prepared for the simulations of the measurement campaign periods. For this purpose, new model domains were adapted to the locations of the three measuring stations (Fig. 1) and the setup of the model was optimized by test runs. The period of the winter measurement campaign has already been simulated and must be further validated by the measurement data.

References

EEA (2018), European Environmental Agency, Report No 12/2018, https://doi.org/10.2800/777411.

Heese, B., H. Flentje, D. Althausen, A. Ansmann, and S. Frey (2010), Ceilometer lidar comparison: backscatter coefficient retrieval and signal-to-noise ratio determination, *Atmos. Meas. Tech.*, *3*(6), 1763-1770, https://doi.org/10.5194/amt-3-1763-2010.

Holubová Šmejkalová, A. (2018), 21 years of measurement of PM10 particles concentrations at the Košetice Observatory, *Meteorological Bulletin*, *3*, 80-85.

Jimenez, J. L., M. R. Canagaratna, N. M. Donahue, A. S. H. Prevot, Q. Zhang, J. H. Kroll, P. F. DeCarlo, J. D. Allan, H. Coe, N. L. Ng, A. C. Aiken, K. S. Docherty, I. M. Ulbrich, A. P. Grieshop, A. L. Robinson,

J. Duplissy, J. D. Smith, K. R. Wilson, V. A. Lanz, C. Hueglin, Y. L. Sun, J. Tian, A. Laaksonen, T. Raatikainen, J. Rautiainen, P. Vaattovaara, M. Ehn, M. Kulmala, J. M. Tomlinson, D. R. Collins, M. J. Cubison, E, J. Dunlea, J. A. Huffman, T. B. Onasch, M. R. Alfarra, P. I. Williams, K. Bower, Y. Kondo, J. Schneider, F. Drewnick, S. Borrmann, S. Weimer, K. Demerjian, D. Salcedo, L. Cottrell, R. Griffin, A. Takami, T. Miyoshi, S. Hatakeyama, A. Shimono, J. Y. Sun, Y. M. Zhang, K. Dzepina, J. R. Kimmel, D. Sueper, J. T. Jayne, S. C. Herndon, A. M. Trimborn, L. R. Williams, E. C. Wood, A. M. Middlebrook, C. E. Kolb, U. Baltensperger, and D. R. Worsnop (2009), Evolution of organic aerosols in the atmosphere, *Science*, *326*(5959), 1525-1529, https://doi.org/10.1126/science.1180353.

Kotthaus, S., M. Haeffelin, M. A. Drouin, J. C. Dupont, S. Grimmond, A. Haefele, M. Hervo, Y. Poltera, and M. Wiegner (2020), Tailored Algorithms for the Detection of the Atmospheric Boundary Layer Height from Common Automatic Lidars and Ceilometers (ALC), *Remote Sensing*, *12*(19), https://doi.org/10.3390/rs12193259.

Pokorná, P., J. Schwarz, R. Krejci, E. Swietlicki, V. Havranek, and V. Ždímal (2018), Comparison of PM2.5 chemical composition and sources at a rural background site in Central Europe between 1993/1994/1995 and 2009/2010: Effect of legislative regulations and economic transformation on the air quality, *Environ. Pollut.*, *241*, 841-851, https://doi.org/10.1016/j.envpol.2018.06.015.

Poulain, L., Y. Iinuma, K. Müller, W. Birmili, K. Weinhold, E. Bruggemann, T. Gnauk, A. Hausmann, G. Löschau, A. Wiedensohler, and H. Herrmann (2011), Diurnal variations of ambient particulate wood burning emissions and their contribution to the concentration of Polycyclic Aromatic Hydrocarbons (PAHs) in Seiffen, Germany, *Atmos. Chem. Phys.*, *11*(24), 12697-12713, https://doi.org/10.5194/acp-11-12697-2011.

Spindler, G., A. Grüner, K. Müller, S. Schlimper, and H. Herrmann (2013), Long-term size-segregated particle (PM_{10}, $PM_{2.5}$, PM_1) characterization study at Melpitz - influence of air mass inflow, weather conditions and season, *J. Atmos. Chem.*, *70*(2), 165-195, https://doi.org/10.1007/s10874-013-9263-8.

van Pinxteren, D., F. Mothes, G. Spindler, K. W. Fomba, and H. Herrmann (2019), Trans-boundary PM10: Quantifying impact and sources during winter 2016/17 in eastern Germany, *Atmos. Environ.*, *200*, 119-130, https://doi.org/10.1016/j.atmosenv.2018.11.061.

Waked, A., A. Bourin, V. Michoud, E. Perdrix, L. Y. Alleman, S. Sauvage, T. Delaunay, S. Vermeesch, J. E. Petit, and V. Riffault (2018), Investigation of the geographical origins of PM10 based on long, medium and short-range air mass back-trajectories impacting Northern France during the period 2009-2013, *Atmos. Environ.*, *193*, 143-152, https://doi.org/10.1016/j.atmosenv.2018.08.015.

Funding

TRACE is founding within the GAČR-DFG German-Czech Cooperation Research Program under the grand numbers 431895563 for the DFG and 20-08304J for the GAČR.

Cooperation

Institute of Chemical Process Fundamentals of the CAS (ICPF-CAS), Prague, Czech Republic.

Dust emission in agriculture A model study

Matthias Faust, Ralf Wolke, Kerstin Schepanski

In der Landwirtschaft ist die Bodenbearbeitung mit schweren Geräten gängige Praxis. Durch die mechanische Einwirkung auf den Boden wie z. B. beim Pflügen werden Partikel vom Boden aufgewirbelt, es entsteht eine Staubfahne. Aber auch andere typische Prozesse in der Landwirtschaft wie das Ausbringen von Trockendünger oder die Getreideernte gehen immer mit der Emission von Staub einher. Da derartige Staubquellen nicht windinduziert sind, lassen sie sich auch nicht mit klassischen Staubemissionsmodellen abbilden. Vielmehr müssen einzelne Emissionsereignisse gesondert betrachtet werden um den Transportpfad der Staubfahne durch die Atmosphäre zu simulieren. Aufgrund des turbulenten Charakters der atmosphärischen Grenzschicht ist eine einzelne Trajektorie dafür jedoch nur bedingt geeignet. Daher haben wir ein Model entwickelt, das unter Berücksichtigung der Turbulenz ein Trajektorien Set berechnet, welches die Dispersion einer Staubwolke in der Atmosphäre beschreibt.

Introduction

The simulation of agricultural emissions is challenging since they occur on a local scale, but the emitted dust particles are transported in a mesoscale range. Therefore, it is necessary to describe both the emission and transport of the particles accurately. We described the source using measurements of typical fieldwork. The experiments were performed by colleagues from ZALF (Leibniz Centre for Agricultural Landscape Research) and took place in the east of Berlin in April 2019 [*Münch et al*., 2020]. In the morning, a tractor spread dry fertiliser to the field and ploughed the field in the early afternoon, as shown in Fig.1. During the experiment, the Aerosol concentration was measured by two environmental dust monitors in two different heights upwind of the field. From this data, we recreated a digital model of the emitted dust plumes and traced them on their way through the atmosphere.

Method

A common approach for trajectory-based dispersion studies within the atmospheric boundary layer (ABL) is the application of Lagrangian particle dispersion models (LPDMs) [e.g. *Pisso et al*., 2019; *Stein et al*., 2015]. The main idea of the LPDM is to handle the deviations due to turbulence as a stochastic deviation from the mean transport path. So, a single trajectory becomes one possible solution of the transport in the chaotic system, and an extensive set of trajectories statistically describes the range of possible pathways, which can also be seen as particle dispersion. We used the trajectory model of *Miltenberger et al*. [2013] as a basis to develop the

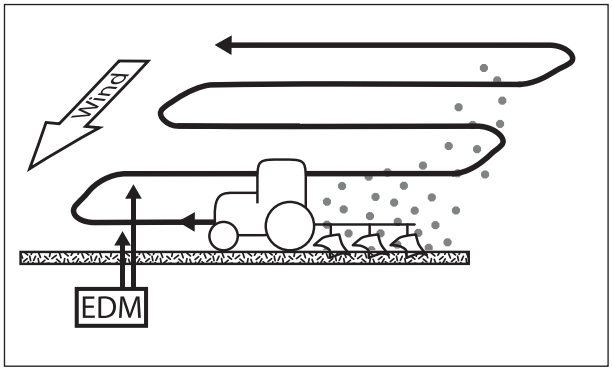

Fig. 1: Sketch of the experimental set-up: the tractor drives in parallel orientated tracks over the field. Downwind the emitted particle plume is measured by two vertically stacked Environmental Dust Monitors.

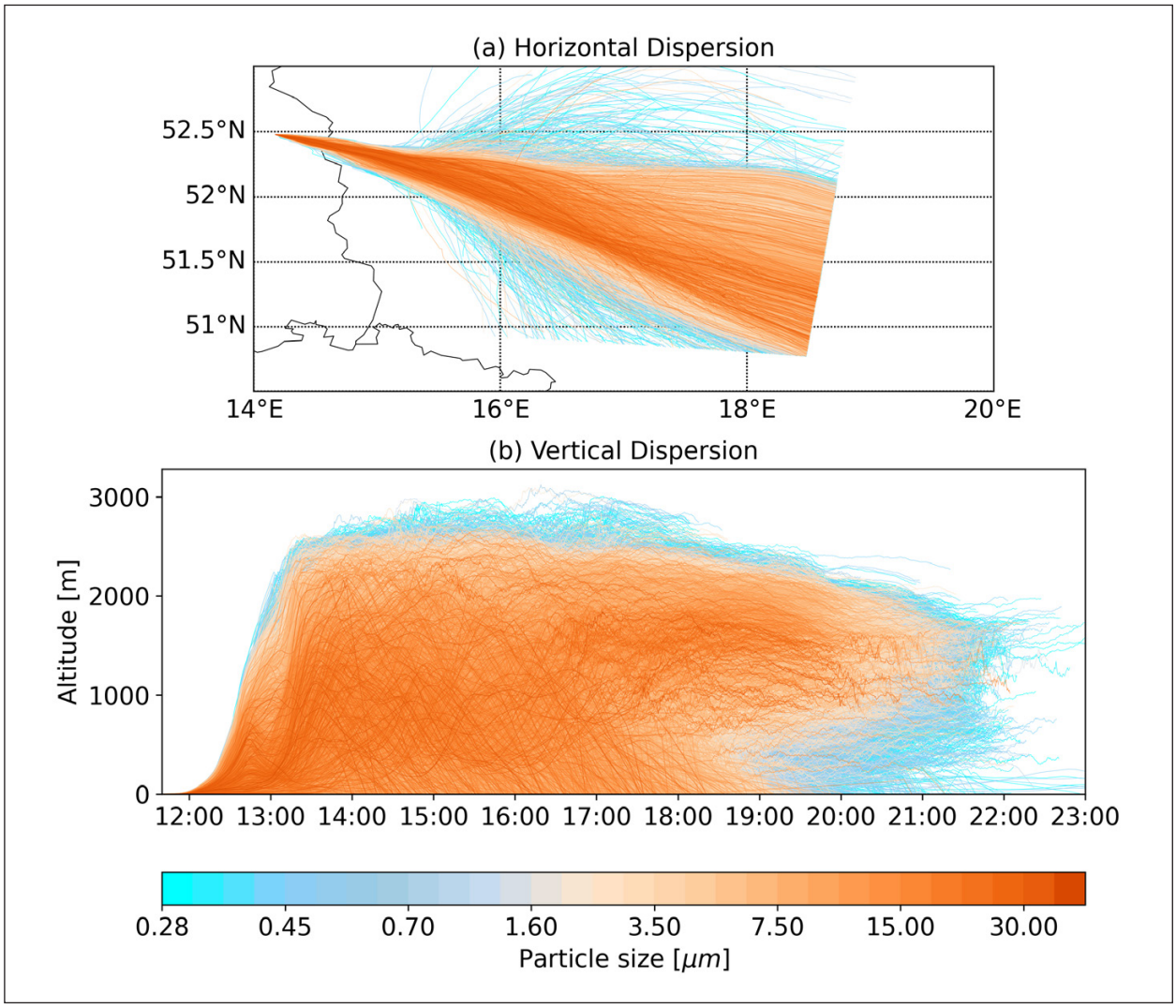

Fig. 2: Particle motion, early afternoon: (a) horizontal trajectories, (b) vertical trajectories.

particle dispersion model ltpas (In time particle simulation) and coupled it directly to the numerical weather forecast model COSMO of the German weather service. In this way, we can benefit from high resolved wind data and prognostic turbulent kinetic energy model data from the COSMO model. This novel approach allows us to simulate dispersion processes in the ABL with high accuracy [*Faust et al*., 2021].

Results and Discussion

We simulated the particle dispersion for both parts of the field experiment (fertilisation and ploughing), where each simulation consisted of more than one hundred thousand individual trajectories. Our results reflect the boundary layer development conceptual model throughout the day. Entrained into a rather stable and stratified ABL (morning hours), the particles reside only for a few minutes within the atmosphere. The bunch of trajectories launched at the source travels as a bundle with only little spreading. Finally, particles do not experience much uplift and settle down relatively close to the source, within a radius of about 10 km. Compared to the morning experiment, Fig. 2 shows that particles entrained during the early afternoon into the convective daytime boundary layer experienced significant vertical updraft and eventually were mixed over the entire depth of the boundary layer. Travelling longer distances by remaining aloft due to turbulent updraft, the particle trajectory plume further highlights another feature of the conceptual model of the boundary layer development: the formation of the nocturnal boundary layer and the residual layer as the upper part of the former daytime boundary layer above. Dust particles situated within the nocturnal boundary layer deposit due to the lack of turbulent buoyancy, whereas particles suspended within the residual layer remain aloft. Trajectories representing the first group of particles will terminate during nighttime, whereas trajectories

representing the latter group may continue travelling within the airflow.

In essence, particles entrained into a well-developed convective ABL will more likely be mixed deeper into the boundary layer, travel longer distances and reside longer within the atmosphere. This furthermore emphasises the need to develop prognostic TKE-based LPDMs, particularly for studies on, for example, aerosol transport whose source is located within the atmospheric boundary layer. The further development and application of this approach clearly would benefit from a thorough data validation such as in an extensive measurement framework. Our approach opens up the possibility of an improved simulation of dust emissions from agricultural activities such as tillage or harvest. These emissions occur mainly in weather conditions characterised by low wind speeds and affect an area several times larger than that by wind erosion. The identification of source areas and transport paths of agricultural dust thus remains an important task, to which the presented modelling approach can make an important contribution.

References

Faust, M., R. Wolke, S. Münch, R. Funk, and K. Schepanski (2021), A new Lagrangian in-time particle simulation module (ltpas v1) for atmospheric particle dispersion, *Geosci. Model Dev.*, *14*(4), 2205-2220, https://doi.org/10.5194/gmd-14-2205-2021.

Miltenberger, A. K., S. Pfahl, and H. Wernli (2013), An online trajectory module (version 1.0) for the nonhydrostatic numerical weather prediction model COSMO, *Geosci. Model Dev.*, *6*(6), 1989-2004, https://doi.org/10.5194/gmd-6-1989-2013.

Münch, S., N. Papke, N. Thiel, U. Nübel, P. Siller, U. Roesler, O. Biniasch, R. Funk, and T. Amon (2020), Effects of farmyard manure application on dust emissions from arable soils, *Atmos. Pollut. Res.*, *11*(9), 1610-1624, https://doi.org/10.1016/j.apr.2020.06.007.

Pisso, I., E. Sollum, H. Grythe, N. I. Kristiansen, M. Cassiani, S. Eckhardt, D. Arnold, D. Morton, R. L. Thompson, C. D. Groot Zwaaftink, N. Evangeliou, H. Sodemann, L. Haimberger, S. Henne, D. Brunner, J. F. Burkhart, A. Fouilloux, J. Brioude, A. Philipp, P. Seibert, and A. Stohl (2019), The Lagrangian particle dispersion model FLEXPART version 10.4, *Geosci. Model Dev.*, *12*(12), 4955-4997, https://doi.org/10.5194/gmd-12-4955-2019.

Stein, A. F., R. R. Draxler, G. D. Rolph, B. J. B. Stunder, M. D. Cohen, and F. Ngan (2015), NOAA's HYSPLIT Atmospheric Transport and Dispersion Modeling System, *Bull. Amer. Meteor. Soc.*, *96*(12), 2059-2077, https://doi.org/10.1175/BAMS-D-14-00110.1.

Funding

This research has been supported by the Leibniz Association (grant no. SAW-2017-DSMZ-2).

Cooperation

Leibniz Centre for Agricultural Landscape Research (ZALF), Müncheberg, Germany.

Ozon in Sachsen

Dominik van Pinxteren, Yaru Wang, Vanessa Engelhardt, Bernd Heinold, Jacob Schacht, Ralf Wolke, Hartmut Herrmann

Im Projekt „Ozon in Sachsen“ (SAXOZONE) werden Trends, Verursacher und Auswirkungen der bodennahen Ozonbelastung für das sächsische Landesamt für Umwelt, Landwirtschaft und Geologie (LfULG) untersucht. Trendanalysen zeigen steigende mittlere Ozonkonzentrationen an vielen städtischen und ländlichen Messstationen, wohingegen die Spitzenwerte früherer Jahrzehnte nur noch selten erreicht werden. Um die beobachteten Trends besser zu verstehen, werden mittels statistischer, sowie Chemie-Transport-Modellierung wichtige Einflussgrößen des Ozons quantitativ beschrieben. Im Ergebnis sollen Empfehlungen für das sächsische Messnetz, sowie Möglichkeiten zur Weiterentwicklung von Luftqualitätsmaßnahmen insbesondere im Hinblick auf eine wärmere Klimazukunft abgeleitet werden.

Introduction

Ozone is a trace gas that acts both as an air pollutant and a greenhouse gas, and has a three-fold significant impact on human health, vegetation including forests and agricultural crops, and the Earth's climate. Understanding the fundamental relationships of its formation has led to a decline in peak ozone levels, particularly in the 1990s, through emission reductions of the precursor compounds nitrogen oxides (NO_x) and volatile organic compounds (VOCs). However, mean ozone concentrations in Germany and Saxony have not shown clear changes during the past 2 decades. Legal target values for the protection of health and vegetation are not met at some stations and chronic ozone pollution is still too high. The current project intends to contribute to a better understanding of ozone specifically with regard to concentrations in Saxony.

Methods

Hourly ozone concentrations from the Saxon air quality measurement network statistically analysed and modelled. The focus is on long-term trends over several decades, the impacts of NO_x, VOC and particles (PM), as well as meteorological conditions as important factors influencing ozone.

These investigations are carried out by statistical analysis of the measured data, with machine learning methods, in particular so-called regression trees [*Carslaw und Taylor*, 2009] and partial dependence plots [*Friedman*, 2001], as well as by chemical transport modelling (CTM) with the mesoscale COSMO-MUSCAT model [*Wolke et al.*, 2012].

Results

In the following, examples of some initial results in the project are given.

Trends. Trend investigations are performed with the robust Theil-Sen estimator and usually show increasing or stagnating ozone concentrations at the measuring stations. Figure 1 shows the frequency distributions of hourly ozone concentrations in different concentration intervals for the past 24 years at the traffic station Dresden-Nord.

There is a clear decrease in the frequency of the lowest concentrations over the study period, while concentrations in the higher intervals increase significantly. These shifts in the frequency distributions can be explained by changes in NO_x emissions at the station. The higher these emissions are, the less they need to be enriched by meteorological conditions such as low wind speeds or low mixing layer heights to cause very high NO concentrations and thus very high depletion of ozone. In turn, this increases the frequency of medium and high concentrations as local ozone depletion from traffic emissions becomes progressively lower.

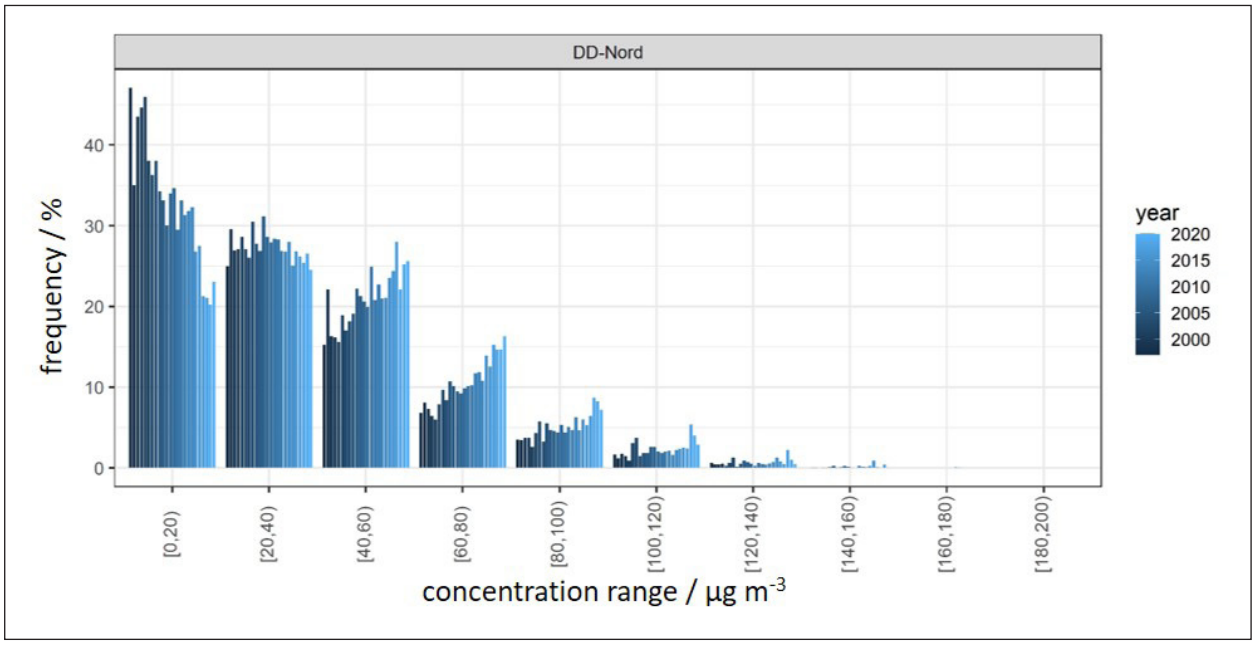

Fig. 1: Frequency distributions of hourly ozone concentrations in Dresden-Nord.

Influencing factors. The ozone concentration is determined by various factors which often overlap each other. In order to better identify these influencing variables, powerful models from the field of machine learning are trained ("gradient boosting machines"), with which so-called partial dependence plots can be derived, showing the marginal effects of individual factors, i.e. the isolated influences of one factor when all other factors are kept constant. Figure 2 shows the partial dependence plots for selected factors at the traffic station Dresden-Nord.

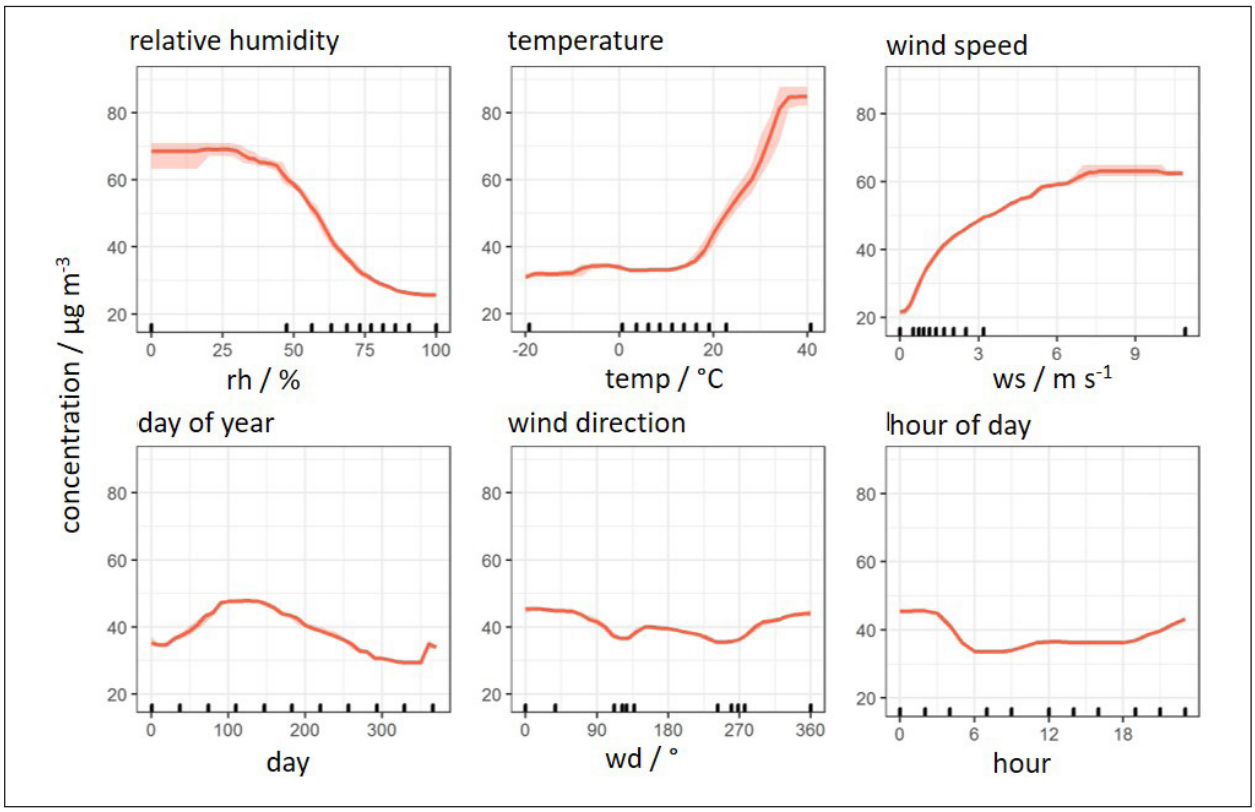

Fig. 2: Partial dependence plots for ozone in DD-Nord.

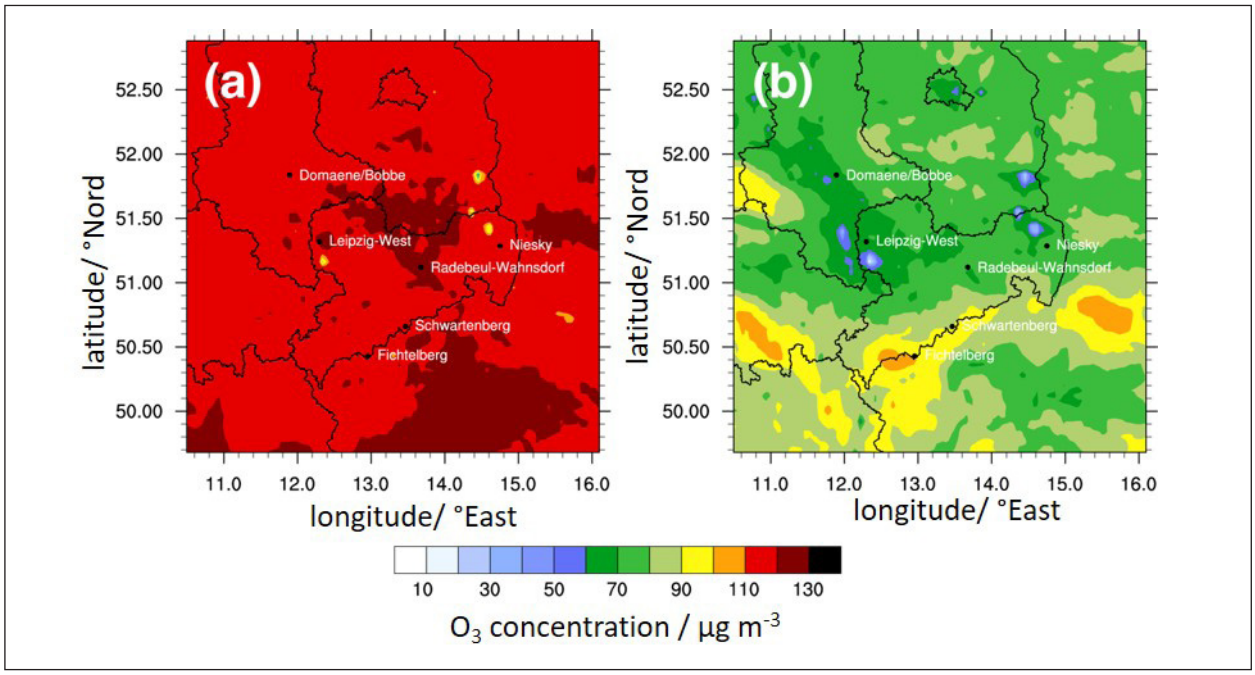

Fig. 3: (a) Midday (10:00 - 18:00) and (b) night-time (22:00 - 06:00) ozone concentrations for June - August 2018 simulated with COSMO-MUSCAT on the 4 km grid (D0).

Among the explanatory variables provided to the model, relative humidity (RH) has the largest influence on ozone concentration. Starting at about 25 % RH, the ozone concentration drops very sharply, which can be explained by the influence of dry deposition as an important ozone sink. Plants close their stomata under dry conditions to reduce evaporation of water over leaf surfaces, which also reduces ozone deposition. For temperature, there is a strong nearly linear increase from about 15°C on. Possible reasons are on the one emissions of biogenic ozone precursors, which are strongly coupled to temperature, and on the other hand the photochemical formation of ozone via a correlation of radiation intensity with temperature. For wind speed, ozone concentrations increase from low values at calm to high values at > 6 m s^{-1}. This is probably related to reduced ozone depletion by NO, since local NO_x emissions are rapidly removed and diluted at high wind speeds. Further impacts results from the annual cycle with maximum biogenic precursor emissions especially at the beginning of the vegetation period, from wind directions, when the road-side traffic emissions are particularly well transported to the station, and from the diurnal profile with lower ozone concentrations especially during the morning rush-hour due to elevated titration with NO.

Case study summer 2018. Even though the summer of 2018 was among the hottest and driest ever, the legal information threshold of 180 µg m^{-3} ozone was exceeded on only 4 days in Saxony. This follows an observed trend that despite an increase in hot days, the number of hours with extremely high ozone concentrations on average decreased over the past decades. The extreme weather and the complex relationships of meteorological parameters and precursor substances make the summer 2018 an interesting period of study for chemistry transport modelling. Figure 3 shows modelled mean ground-level ozone concentrations in June and July 2018 for daytime (10:00 -18:00) and night-time (22:00 - 06:00) hours in Saxony and surrounding areas.

In both periods, the locations of the Jänschwalde and Schwarze Pumpe coal-fired power plants in Brandenburg, and the Boxberg and Lippendorf coal-fired power plants in Saxony are clearly visible. The NO_x emitted by the power plants leads to a significant ozone depletion and thus lower ozone concentrations than in the surrounding area. During the day, the mean ozone concentrations in the vicinity of the cities of Leipzig, Dresden, Chemnitz and Zwickau are slightly above the mean value with values above 120 µg m^{-3}, while they are slightly below it at the Erzgebirge ridge. This modelled spatial distribution of daytime ozone deviates from station observations, which tend to show higher concentrations in the mountains than in the lowlands. A possible explanation is an overestimation of maximum concentrations in the model. This overestimation is higher in the lowlands than in the mountains, which compensates

for the observed contrast. At night, the ozone concentrations at the ridge of the Ore Mountains decrease significantly less and are still above 100 µg m^{-3} in some places, which is only about 10 µg m^{-3} below the mean daytime concentrations. In the lower-lying regions, the average night-time concentrations are less than 80 µg m^{-3}.

In the course of the project, more detailed analyses of the results from both statistical and chemical transport modelling will lead to a deeper understanding of ozone pollution in Saxony, from which recommendations for action will be derived for monitoring of the most important precursor compounds, as well as for further air pollution mitigation measures in the context of a warmer climate future.

References

Carslaw, D. C., and P. J. Taylor (2009), Analysis of air pollution data at a mixed source location using boosted regression trees, *Atmos. Environ.*, *43*(22-23), 3563-3570, https://doi.org/10.1016/j.atmosenv.2009.04.001.

Friedman, J. H. (2001), Greedy function approximation: A gradient boosting machine, *Annals of Statistics*, *29*(5), 1189-1232, https://doi.org/10.1214/aos/1013203451.

Wolke, R., W. Schröder, R. Schrödner, and E. Renner (2012), Influence of grid resolution and meteorological forcing on simulated European air quality: A sensitivity study with the modeling system COSMO-MUSCAT, *Atmos. Environ.*, *53*(SI), 110-130, https://doi.org/10.1016/j.atmosenv.2012.02.085.

Funding

Saxonian State Office for the Environment, Agriculture, and Geology (LfULG).

Measuring of the distribution of air pollution (MesSBAR)

Sebastian Düsing, Birgit Wehner, Ralf Käthner, Jens Voigtländer

Im Rahmen des Projektes „MesSBAR“ wurde mit mehreren Kooperationspartnern eine Drohne zum Messen atmosphärischer Parameter wie der Temperatur und Feuchte aber auch der Anzahlkonzentration von Aerosolpartikeln sowie deren Massenkonzentration und atmosphärischer Gase entwickelt. Eine einwöchige Feldkampagne nahe der Autobahn A555 bei Wesseling erlaubte die Beobachtung der morgendlichen Entwicklung der planetaren Grenzschicht mittels dieser Parameter und zeigte, dass die Drohne in der Lage ist, hochaufgelöst Schadstoffverteilungen im urbanen Raum zu messen und dass im 2. Schritt mit weiteren Drohnen durch parallele Messungen im Luv und Lee direkter Emissionen untersucht werden können.

Introduction

Despite being part of radiative forcing, aerosol particles consist of different compounds, e.g., black carbon (BC) from combustion processes, and can adversely affect health. Hence, monitoring and forecasting aerosol in terms of health risk is required. Public authorities in Germany, like the *Bundesanstalt für Straßenwesen* (BASt) or Umweltbundesamt (UBA), already monitor the aerosol load in different environments. Especially in urban areas, with aerosol produced during fuel combustion in vehicles, observation is required by European regulations. However, these measurements represent only a point, and information on the horizontal and vertical distribution of pollution is scarcely measured and available through air pollution dispersion models like the “EURopean Air pollution Dispersion-Inverse Modell” (EURAD-IM). In the course of the *Automatisierte luftgestützte Messung der Schadstoffbelastung in der erdnahen Atmosphäre in urbanen Räumen* (MesSBAR) project, fully autonomous drones are under development for observing important metrics of air quality to enrich air-pollution-dispersion models. Mass concentrations of particulate matter (PM), equivalent black carbon *m*(eBC)), nitrogen oxides (NO_x), and ozone (O_3) are observed. Multiple project partners, specialists in its field contribute to this project. TROPOS, in particular, contributes by developing an aerosol particle measurement kit (PM, *m*(eBC)). The drone prototype is shown in Fig. 1.

Methods

m(eBC) is derived with a miniaturized Aethalometer© (mod. MA200, AethLabs) based on the measurements of the aerosol particle light absorption at multiple wavelengths. Lab measurements have shown that *m*(eBC) is up to 23% larger than derived with a Multi-Angle Absorption Photometer (MAAP).

The setup also allows to derive the absorption Ångström exponent (AAE) providing insights into the observed black carbon material source but is not shown here.

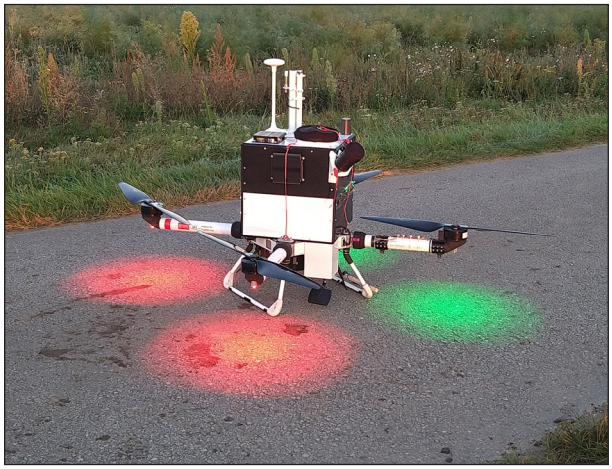

Fig. 1: MesSBAR quadrocopter during a field campaign at Wesseling during September 2021 before taking off.

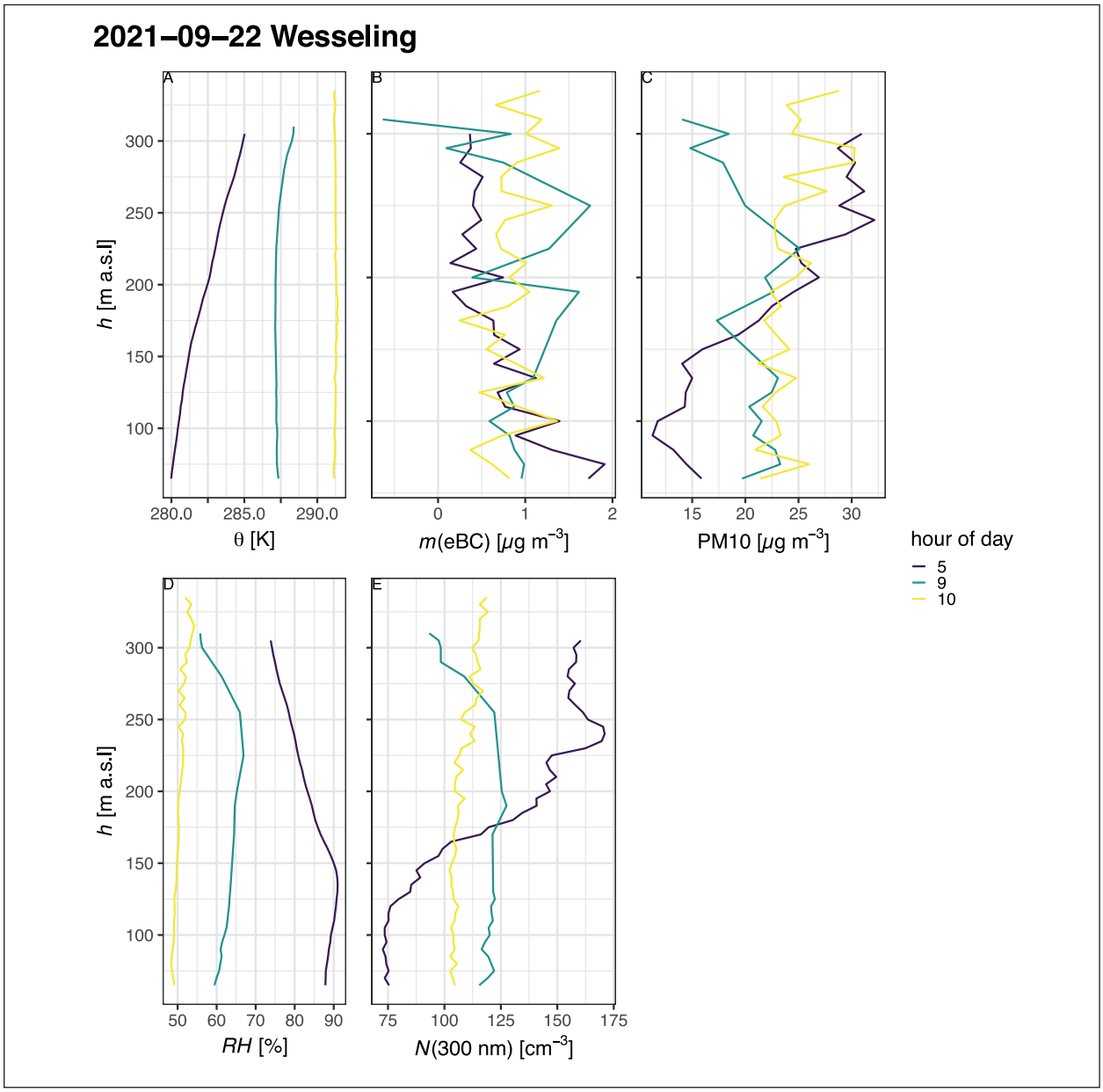

Fig. 2: Profiles of potential temperature θ and RH (A, D), m(eBC) (B), PM10 (C), and N(300 nm) (E) observed on 22 September 2021 nearby highway near Wesseling. Colors represent the hour of the day.

An optical particle size spectrometer (OPSS; mod. GT526-S, MetOne) is used to detect aerosol particles larger than 300 nm in diameter and provides their total number concentration *N* (300 nm) and particle number size distribution (PNSD) directly. PM up to 1 µm (PM1), 2.5 µm (PM2.5), and 10 µm (PM10) is estimated indirectly based on the PNSD. Laboratory calibrations have shown that this device, despite its six size channels, has a sufficient accuracy in sizing at least in smaller size ranges, since for large particles, there is no calibration standard available yet. A Personal Ozone Monitor (POM) operated by Forschungszentrum Jülich GmbH observed the mass concentration of ozone but is not shown here.

During the first campaigns in the vicinity of Wesseling at (50.79°N, 7°E, 55 m a.s.l.) close to highway A555 and a monitoring station of BASt, the drone was tested, and learnings were used to adapt the drone to the project's needs.

First results

Exemplarily, the vertical distribution of atmospheric and aerosol parameters up to an altitude of 330 m a.s.l. is shown in Fig. 2 for 22 September 2021. At 05:10 UTC, two distinct layers are observed, separated with an interface layer (IL) at around 150 m (slightly steeper gradient of *θ* and decreasing *RH*

above). Both layers were characterized by $d\theta/dz>0$ (stable layering), which prevented their mixing. At 9:28 UTC, the IL was lifted to around 250 m a.s.l. due to radiative heating and could not be observed during the profile conducted around 10:50 UTC.

The increased concentration of PM10 and N(300 nm) above the IL with values more than double as large as below IL is remarkable since we would have suspected to observe larger PM concentrations near the ground in the vicinity of a pollution source (highway). The vertical distribution of m(eBC) does not follow the vertical distribution of PM10 in the profile at 5:10 UTC showing a decrease up to the IL followed by a relatively constant m(eBC) of around 0.4 µg m^{-3} above. Until 10:50 UTC, m(eBC) increased and had a mean of around 0.8 µg m^{-3}. Likewise, the vertical gradient in PM10 changes during the observed time frame.

These observations demonstrate that the newly developed copter can observe the changes in the atmospheric and aerosol parameters with relatively high spatio-temporal.

Outlook

The project is ongoing, and copter II and III construction must be finished. Unfortunately, the copter cannot reach 1000 m yet because of safety regulations and battery capacity if the spatio-temporal resolution is not decreased. At least on safety regulations allowing to increase flight height is worked ongoing.

Future measurement campaigns will measure emissions directly from pollution sources utilizing parallel measurements in the Luv and Lee of the observed location with two copters available. Air pollution models will then be enriched with the data updating the emission representation in those.

Funding:
This work has been funded by the Modernity Fund (mFUND) of the Federal Ministry of Transport and Digital Infrastructure(BMVI) under grant agreement 19F2097A.

Cooperation:
Institute of Flight Guidance, TU Braunschweig; Leichtwerk Research GmbH; Federal Highway Research Institute (BASt); National Metrology Institute of Germany (PTB); Institute of Energy and Climate Research - Troposphere (IEK-8), Forschungszentrum Jülich GmbH; Federal Environment Agency (UBA).

Assessment methods to determine real-world respiratory tract deposition of inhaled ambient black carbon

Leizel Madueño, Thomas Müller, Simonas Kecorius, Alfred Wiedensohler, Mira Pöhlker

In diesem Artikel stellen wir die Entwicklung und Anwendung eines mobilen Messsystems vor, mit dem die Gesamtdeposition von eingeatmetem Ruß (BC) in den Atemwegen unter realen Bedingungen gemessen werden kann. Diese Informationen können das vorhandene Wissen über die Auswirkungen der Luftverschmutzung auf die Gesundheit ergänzen, insbesondere in Regionen, in denen die Verwendung von Standardmethoden und komplizierter Instrumentierung begrenzt ist.

Introduction

Exposure to air pollution is a significant contributor to the global burden of disease. Ambient particulate matter (PM) is classified as a group 1 carcinogen to humans, causing millions of premature deaths worldwide per year [*World Health Organization*, 2021]. Although many cohort studies have widely accepted the associations of PM with an aerodynamic diameter less than 2.5 m ($PM_{2.5}$) to induce all-cause cardiovascular and cardiopulmonary mortality, individual components of PM2.5 may have unequal health effects. Several studies propose that especially particles from incomplete combustion, such as black carbon (BC), are considered potentially more harmful to health than generalized PM.

To better understand the health effects of inhaled aerosol, it is crucial to quantify particles deposited in the respiratory tract during exposure, commonly defined as deposition dose (DD). There are several numerical (*in silico*) and semi-empirical models, e.g., International Commission of Radiological Protection (ICRP) and Multiple-Path Particle Dosimetry (MPPD) models, human subject (*in situ*) measurements, single breath measurements, and other prior approaches (*ab initio*) to assess the DD of a pollutant. Most of the important parameters to determine deposition of particles in the respiratory tract, such as personal breathing pattern, deposition fraction, particle deposition mechanisms, and uptake kinetics, are still scarce, fragmented, and non-coherent as a consequence of nonexistent methodological standards.

This article presents a novel, TROPOS-designed, respiratory tract deposition measurement platform called MERDOC (MEasuring Real-world deposition DOse of black Carbon), which was tested in two intensive field studies in La Paz/El Alto, Bolivia, and Metro Manila, Philippines. The first study was conducted in a high-altitude city in Bolivia, to demonstrate the potential of the proposed method to determine the DD of BC, followed by a clinical trial study performed in Metro Manila by a number of study volunteers (20 males, 20 females). Details of the experiment and results are published in *Madueño et al.*, [2019].

MEasuring Real-world deposition DOse of black Carbon (MERDOC)

The experimental setup to measure the respiratory tract deposition (RTD) of equivalent black carbon is shown in Fig.1. Briefly, the ambient aerosol is inhaled exclusively through the nose during normal tidal breathing, which is then exhaled through the mouthpiece into a mixing chamber (filled with silica

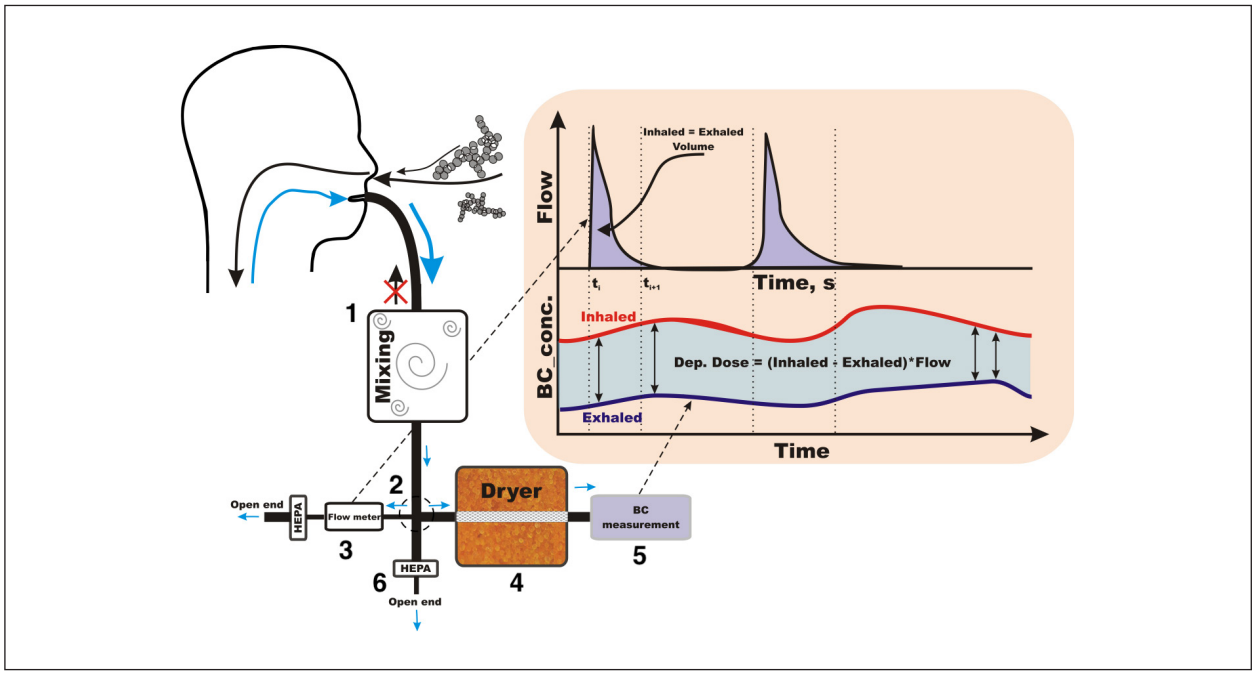

Fig.1: MERDOC experimental setup to measure respiratory tract deposition of black carbon. 1—mixing chamber where walls are filled with silica gel for drying; 2—four-way flow splitter; 3—mass flowmeter; 4—extra drying chamber; 5—MA200 micro-aethalometer. An identical micro-aethalometer, not shown in this figure, was used to record ambient BC mass concentration.

gel for drying). The aerosol is collected from the stream of air at ambient pressure onto the filter of a micro-aethalometer (at a flow rate of 100 ml/min). In parallel to exhaled air measurements, a separate mobile system monitoring the ambient BC mass concentration was taken alongside. The MERDOC measurement platform was placed in a backpack and was carried by the study volunteers during their public commute, which allowed the investigation of real-world measurements of breathing parameters, micro-environment exposure, and RTD of BC.

The difference between the inhaled and exhaled BC mass concentration represents the mass concentration (microgram m^{-3}) of BC that was deposited in the respiratory tract during one normal tidal breathing. The flow rate of exhaled air, integrated from the start

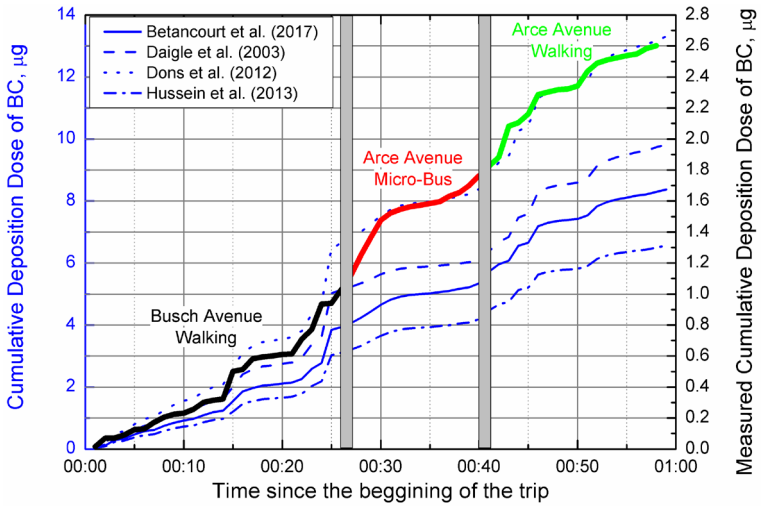

Fig.2: Cumulative deposition dose (DD) of black carbon (BC) during 1-h commuting trip in La Paz, Bolivia. Different means of commuting (walking, riding public transport called Micro-Bus) and location of commute (Busch and Arce Avenue) are indicated in the figure. Additionally, cumulative DD of BC, calculated using minute ventilation and assessment method (ab initio) from references are shown in blue lines.

and end time of exhalation, was used to calculate the minute ventilation (m^3 min^{-1}). The product of the mass concentration deposited in the respiratory tract and the minute ventilation was treated as the real deposited dose rate.

Results

The feasibility study done in Bolivia showed the potential of the proposed method to determine the DD of BC. The results showed a cumulative total respiratory tract deposition dose over a 1-h commuting trip resulted in an approximately 2.6 micrograms of BC. The amount of air breathed per one cycle (tidal volume) ranged from 0.8 L (while sitting in a public transport called micro-bus) to 1.1 L (while walking). The average breathing rate was 11 ± 1 breaths/min for different commuting activities. In comparison to other widely used RTD assessment methods, e.g., ab initio, where all inhaled aerosol is assumed to be deposited in the respiratory tract and uses physical parameters taken from previously reported values, the RTD of BC was up to 5 times (Fig. 2). Measured total respiratory tract deposited BC fraction varied from 39% to 48% during walking and commuting inside a public transport, respectively.

The clinical trial study done in Metro Manila [*Madueno et al.*, in prep.] where a number of study volunteers used the MERDOC during their daily commute showed that the mode of transportation (driving inside public transport versus walking) had no significant influence on the breathing frequency, tidal volume, and minute ventilation. While the exposure and RTD of BC were significantly higher during use of public transport than walking. The segregation of data based on gender showed a statistically significant difference between males and females. Males had higher tidal volume, but lower breathing rate than females. Interestingly, the difference between male and female breathing parameters did not show a significant effect on the total RTD of BC. The deposition fraction did not show dependence on gender nor the magnitude of inhaled BC concentration.

Outlook

The experiments presented here showed the potential of MERDOC to measure real-world respiratory tract deposition of inhaled ambient black carbon. The results found during the experiment will be used in subsequent studies to establish an association between heart rate variability and real BC deposited dose. In the future, it is planned to expand the capabilities of MERDOC to measure other aerosol particle information such as particle sizing of inhaled and exhaled breath, potential investigation of bioaerosols and microplastics present on breath, and possible evolution tracking of virus-like particles from inspired to expired air.

References

Madueño, L., Kecorius, S., Löndahl, J., Müller, T., Pfeifer, S., Haudek, A., Mardoñez, V., and Wiedensohler, A.: A new method to measure real-world respiratory tract deposition of inhaled ambient black carbon, Environ. Pollut., 248, 295–303, https://doi.org/10.1016/j.envpol.2019.02.021, 2019.

Madueño, L., Kecorius, S., Löndahl, J., Schnell-Kreis, J., Wiedensohler, A., Pöhlker, M., Respiratory tract deposition of ambient black carbon particles: Application of a novel experimental method in real-world conditions, 2022, in preparation.

World Health Organization: WHO Global Air Quality Guidelines. Particulate matter (PM2.5 and PM10), ozone, nitrogen dioxide, sulfur dioxide and carbon monoxide, 1–300 pp., 2021.

Funding

This research was funded by the German Federal Ministry of Education and Research in the framework of TAME-BC (project number 01LE1903A).

Appendices

Publications

Publication statistics

	2020	2021
Total number of publications	**360**	**248**
Books (author, editor) *	-	-
Book sections *	2	2
Contributions to collected editions *	1	3
Articles in peer reviewed journals *	116	105
Articles (others)	80	28
Presentations (invited)	4	4
Presentations (others)	123	95
Reports/Datasets/Software *	34	12

Publications *

2020

ACTRIS-Data-Centre-ARES-Aerosol-Remote-Sensing 2020. ACTRIS Aerosol Remote Sensing Data during the COVID-19 pandemic - GARRLiC products (Version 2.11) [Data set]. *Data from: AERIS*, https://doi.org/10.25326/69.

ACTRIS-Data-Centre-ARES-Aerosol-Remote-Sensing 2020. ACTRIS Aerosol Remote Sensing Data during the COVID-19 campaign held in May 2020 - GARRLiC products (Version 2.11) [Data set]. *Data from: AERIS*, https://doi.org/10.25326/70.

Ahlawat, A., Mishra, S. K., Birks, J. W., Costabile, F. and **Wiedensohler, A.** 2020. Preventing airborne transmission of SARS-CoV-2 in hospitals and nursing homes. Int. J. Environ. Res. Public Health, **17**, 8553. https://doi.org/10.3390/ijerph17228553.

Ahlawat, A., **Wiedensohler, A.** and Mishra, S. K. 2020. An overview on the role of relative humidity in airborne transmission of SARS-CoV-2 in indoor environments. Aerosol Air Qual. Res., **20**, 1856–1861. https://doi.org/10.4209/aaqr.2020.06.0302.

Alas, H. D. C., **Müller, T.**, **Weinhold, K.**, **Pfeifer, S.**, Glojek, K., Gregorič, A., Močnik, G., Drinovec, L., Costabile, F., Ristorini, M. and **Wiedensohler, A.** 2020. Performance of microAethalometers: Real-world field intercomparisons from multiple mobile measurement campaigns in different atmospheric environments. Aerosol Air Qual. Res., **20**, 2640-2653. https://doi.org/10.4209/aaqr.2020.03.0113.

Allen, R. J., Turnock, S., Nabat, P., Neubauer, D., Lohmann, U., Olivié, D., Oshima, N., Michou, M., Wu, T., Zhang, J., Takemura, T., Schulz, M., Tsigaridis, K., Bauer, S. E., Emmons, L., Horowitz, L., Naik, V., van Noije, T., Bergman, T., Lamarque, J.-F., Zanis, P., **Tegen, I.**, Westervelt, D. M., Le Sager, P., Good, P., Shim, S., O'Connor, F., Akritidis, D., Georgoulias, A. K., Deushi, M., Sentman, L. T., John, J. G., Fujimori, S. and Collins, W. J. 2020. Climate and air quality impacts due to mitigation of non-methane near-term climate forcers. Atmos. Chem. Phys., **20**, 9641-9663. https://doi.org/10.5194/acp-20-9641-2020.

Ashworth, K., Bucci, S., Gallimore, P. J., **Lee, J.**, Nelson, B. S., Sanchez-Marroquin, A., Schimpf, M. B., Smith, P. D., Drysdale, W. S., Hopkins, J. R., Lee, J. D., Pitt, J. R., Di Carlo, P., Krejci, R. and McQuaid, J. B. 2020. Megacity and local contributions to regional air pollution: An aircraft case study over London. Atmos. Chem. Phys., **20**, 7193-7216. https://doi.org/10.5194/acp-20-7193-2020.

Appendices: Publications

Baars, H., **Herzog, A.**, **Heese, B.**, **Ohneiser, K.**, **Hanbuch, K.**, **Hofer, J.**, **Yin, Z.**, **Engelmann, R.** and **Wandinger, U.** 2020. Validation of Aeolus wind products above the Atlantic Ocean. Atmos. Meas. Tech., **13**, 6007-6024. https://doi.org/10.5194/amt-13-6007-2020.

Baars, H. and **Yin, Z.** 2020. PollyNET/Pollynet_Processing_Chain: Version 2.0. Zenodo, http://doi.org/10.5281/zenodo.3774689.

Barlakas, V., **Deneke, H.** and **Macke, A.** 2020. The sub-adiabatic model as a concept for evaluating the representation and radiative effects of low-level clouds in a high-resolution atmospheric model. Atmos. Chem. Phys., **20**, 303-322. https://doi.org/10.5194/acp-20-303-2020.

Barrientos Velasco, C., **Deneke, H.**, **Griesche, H.**, **Seifert, P.**, **Engelmann, R.** and **Macke, A.** 2020. Spatiotemporal variability of solar radiation introduced by clouds over Arctic Sea ice. Atmos. Meas. Tech., **13**, 1757-1775. https://doi.org/10.5194/amt-13-1757-2020.

Barry, J., Böttcher, D., Pfeilsticker, K., Herman-Czezuch, A., Kimiaie, N., Meilinger, S., Schirrmeister, C., **Deneke, H.**, **Witthuhn, J.** and Gödde, F. 2020. Dynamic model of photovoltaic module temperature as a function of atmospheric conditions. Adv. Sci. Res., **17**, 165-173. https://doi.org/10.5194/asr-17-165-2020.

Barry, J., Böttcher, D., Pfeilsticker, K., Herman-Czezuch, A., Kimiaie, N., Meilinger, S., Schirrmeister, C., **Deneke, H.**, **Witthuhn, J.** and Gödde, F. 2020. Supplement to "Dynamic model of photovoltaic module temperature as a function of atmospheric conditions" (Version 1) [Data set]. *Data from: Zenodo*, http://doi.org/10.5281/zenodo.3958820.

Bauch, M., Labbé, T., Engel, A. and **Seifert, P.** 2020. A prequel to the Dantean Anomaly: The precipitation seesaw and droughts of 1302 to 1307 in Europe. Clim. Past, **16**, 2343-2358. https://doi.org/10.5194/cp-16-2343-2020.

Beer, C. G., Hendricks, J., Righi, M., **Heinold, B.**, **Tegen, I.**, Groß, S., Sauer, D., Walser, A. and Weinzierl, B. 2020. Modelling mineral dust emissions and atmospheric dispersion with MADE3 in EMAC v2.54. Geosci. Model Dev., **13**, 4287-4303. https://doi.org/10.5194/gmd-13-4287-2020.

Berndt, T., Chen, J., Møller, K. H., Hyttinen, N., Prisle, N. L., **Tilgner, A.**, **Hoffmann, E. H.**, **Herrmann, H.** and Kjaergaard, H. G. 2020. SO_2 formation and peroxy radical isomerization in the atmospheric reaction of OH radicals with dimethyl disulfide. Chem. Commun., **56**, 13634-13637 https://doi.org/10.1039/D0CC05783E.

Birmili, W., Pietsch, A., Niemeyer, T., Kura, J., Hoffmann, S., Daniels, A., **Zhao, J.**, **Sun, J.**, **Wehner, B.** and **Wiedensohler, A.** 2020. Abundance and sources of ultrafine particles in indoor and ambient air - current state of knowledge (Vorkommen und Quellen ultrafeiner Partikel im Innenraum und in der Außenluft – Aktueller Kenntnisstand). Gefahrst. Reinhalt. L., **80**, 33-43. https://doi.org/10.37544/0949-8036-2020-01-02-35.

Bromwich, D. H., Werner, K., Casati, B., Powers, J. G., Gorodetskaya, I. V., Massonnet, F., Vitale, V., Heinrich, V. J., Liggett, D., Arndt, S., Barja, B., Bazile, E., Carpentier, S., Carrasco, J. F., Choi, T., Choi, Y., Colwell, S. R., Cordero, R. R., Gervasi, M., Haiden, T., Hirasawa, N., Inoue, J., Jung, T., Kalesse, H., Kim, S.-J., Lazzara, M. A., Manning, K. W., Norris, K., Park, S.-J., Reid, P., Rigor, I., Rowe, P. M., Schmithüsen, H., **Seifert, P.**, Sun, Q., Uttal, T., Zannoni, M. and Zou, X. 2020. The Year of Polar Prediction in the Southern Hemisphere (YOPP-SH). Bull. Amer. Meteor. Soc., **101**, E1653-E1676. https://doi.org/10.1175/BAMS-D-19-0255.1.

Brüggemann, M., Xu, R., **Tilgner, A.**, Kwong, K. C., **Mutzel, A.**, Poon, H. Y., **Otto, T.**, **Schaefer, T.**, **Poulain, L.**, Chan, M. N. and **Herrmann, H.** 2020. Organosulfates in ambient aerosol: State of knowledge and future research directions on formation, abundance, fate, and importance. Environ. Sci. Technol., **54**, 3767-3782. https://doi.org/10.1021/acs.est.9b06751.

Bühl, J., **Radenz, M.**, Schimmel, W., Vogl, T. and Lochmann, M. 2020. pyLARDA3 v0.1. Zenodo, http://doi.org/10.5281/zenodo.4271980.

Chen, Y., Cheng, Y., **Ma, N.**, Wei, C., Ran, L., **Wolke, R.**, **Größ, J.**, Wang, Q., Pozzer, A., Denier van der Gon, H. A. C., **Spindler, G.**, Lelieveld, J., **Tegen, I.**, Su, H. and **Wiedensohler, A.** 2020. Natural sea-salt emissions moderate the climate forcing of anthropogenic nitrate. Atmos. Chem. Phys., **20**, 771-786. https://doi.org/10.5194/acp-20-771-2020.

Clemen, H.-C., Schneider, J., Klimach, T., Helleis, F., Köllner, F., Hünig, A., Rubach, F., **Mertes, S.**, **Wex, H.**, **Stratmann, F.**, **Welti, A.**, Kohl, R., Frank, F. and Borrmann, S. 2020. Optimizing the detection, ablation, and ion extraction efficiency of a single-particle laser ablation mass spectrometer for application in environments with low aerosol particle concentrations. Atmos. Meas. Tech., **13**, 5923-5953. https://doi.org/10.5194/amt-13-5923-2020.

Coen, M. C., Andrews, E., Alastuey, A., Arsov, T. P., Backman, J., Brem, B. T., Bukowiecki, N., Couret, C., Eleftheriadis, K., Flentje, H., Fiebig, M., Gysel-Beer, M., Hand, J. L., Hoffer, A., Hooda, R., Hueglin, C.,

Joubert, W., Keywood, M., Kim, J. E., Kim, S. W., Labuschagne, C., Lin, N. H., Lin, Y., Myhre, C. L., Luoma, K., Lyamani, H., Marinoni, A., Mayol-Bracero, O. L., Mihalopoulos, N., Pandolfi, M., Prats, N., Prenni, A. J., Putaud, J. P., Ries, L., Reisen, F., Sellegri, K., Sharma, S., Sheridan, P., Sherman, J. P., Sun, J. Y., Titos, G., Torres, E., **Tuch, T.**, Weller, R., **Wiedensohler, A.**, Zieger, P. and Laj, P. 2020. Multidecadal trend analysis of in situ aerosol radiative properties around the world. Atmos. Chem. Phys., **20**, 8867-8908. https://doi.org/10.5194/acp-20-8867-2020.

Costa-Surós, M., Sourdeval, O., Acquistapace, C., **Baars, H.**, Henken, C. C., **Genz, C.**, Heseman, J., **Jimenez, C.**, **König, M.**, Kretzschmar, J., Madenach, N., Meyer, C. I., **Schrödner, R.**, **Seifert, P.**, **Senf, F.**, Brueck, M., Cioni, G., Engels, J. F., Fieg, K., Gorges, K., Heinze, R., Siligam, P. K., Burkhardt, U., Crewell, S., Hoose, C., Seifert, A., **Tegen, I.** and Quaas, J. 2020. Detection and attribution of aerosol-cloud interactions in large-domain large-eddy simulations with the ICOsahedral Non-hydrostatic model. Atmos. Chem. Phys., **20**, 5657-5678. https://doi.org/10.5194/acp-20-5657-2020.

Cox, R. A., Ammann, M., Crowley, J. N., **Herrmann, H.**, Jenkin, M. E., McNeill, V. F., Mellouki, A., Troe, J. and Wallington, T. J. 2020. Evaluated kinetic and photochemical data for atmospheric chemistry: Volume VII - Criegee intermediates. Atmos. Chem. Phys., **20**, 13497-13519. https://doi.org/10.5194/acp-20-13497-2020.

Donth, T., Jäkel, E., Ehrlich, A., **Heinold, B.**, **Schacht, J.**, Herber, A., Zanatta, M. and Wendisch, M. 2020. Combining atmospheric and snow radiative transfer models to assess the solar radiative effects of black carbon in the Arctic. Atmos. Chem. Phys., **20**, 8139-8156. https://doi.org/10.5194/acp-20-8139-2020.

Feistel, R. and **Hellmuth, O.** 2020. Zur Rolle des Wassers in der Energiebilanz des Klimasystems. *In: G. Pfaff, R. O. Greiling, and R. Pail (Eds.), Klimawandel - Anzeichen, Ursachen, Folgen : Kolloquium der Leibniz-Sozietät der Wissenschaften zu Berlin am 13.2.2020 in der Humboldt-Universität Berlin*. trafo Wissenschaftsverlag, Berlin, **144**, p. 51-139. (Sitzungsberichte Leibniz-Sozietät der Wissenschaften ; 144). https://leibnizsozietaet.de/wp-content/uploads/2020/12/Feistel-R-und-Hellmuth-O.pdf.

Felber, T., **Schaefer, T.** and **Herrmann, H.** 2020. Five-membered heterocycles as potential photosensitizers in the tropospheric aqueous phase: Photophysical properties of Imidazole-2-carboxaldehyde, 2-Furaldehyde, and 2-Acetylfuran. J. Phys. Chem. A, **124**, 10029-10039. https://doi.org/10.1021/acs.jpca.0c07028.

Filioglou, M., Giannakaki, E., Backman, J., Kesti, J., Hirsikko, A., **Engelmann, R.**, O'Connor, E., Leskinen, J. T. T., Shang, X. X., Korhonen, H., Lihavainen, H., Romakkaniemi, S. and Komppula, M. 2020. Optical and geometrical aerosol particle properties over the United Arab Emirates. Atmos. Chem. Phys., **20**, 8909-8922. https://doi.org/10.5194/acp-20-8909-2020.

Fomba, K. W., **Deabji, N.**, Barcha, S. E. I., Ouchen, I., Elbaramoussi, E. M., El Moursli, R. C., Harnafi, M., El Hajjaji, S., Mellouki, A. and **Herrmann, H.** 2020. Application of TXRF in monitoring trace metals in particulate matter and cloud water. Atmos. Meas. Tech., **13**, 4773-4790. https://doi.org/10.5194/amt-13-4773-2020.

Garmash, O., Rissanen, M. P., Pullinen, I., Schmitt, S., Kausiala, O., Tillmann, R., Percival, C., Bannan, T. J., Priestley, M., Hallquist, Å. M., Kleist, E., Kiendler-Scharr, A., Hallquist, M., **Berndt, T.**, McFiggans, G., Wildt, J., Mentel, T. and Ehn, M. 2020. Multi-generation OH oxidation as a source for highly oxygenated organic molecules from aromatics. Atmos. Chem. Phys., **20**, 515-537. https://doi.org/10.5194/acp-20-515-2020.

Gausa, M., Hanssen, I., Papayannis, A., Kokkalis, P., Mylonaki, M., Comeron, A., Muñoz-Porcar, C., Zenteno, A., García-Vizcaíno, D., Rocadenbosch, F., Pietruczuk, A., Szkop, A., Podgorski, J., Posyniak, M., Bortoli, D., Costa, M. J., Salgueiro, V., Pereira, S., Preissler, J., Kulkarni, P. S., Silva, A. M., Potes, M., Alados Arboledas, L., Granados Muñoz, M. J., Ortiz Amezcua, P., de Jerónimo Alvarez, J. A., Bravo Aranda, J. A., Guerrero Rascado, J. L., Guzman, F. N., Pantaleón, D. B., Jiménez Martín, M., Mattis, I., Mueller, G., Wagner, F., Nicolae, D., Belegante, L., Binietoglou, I., Nemuc, A., Talianu, C., Komppula, M., Filioglou, M., Giannakaki, E., Shang, X., **Baars, H.**, **Engelmann, R.**, **Althausen, D.**, **Basharova, E.**, **Floutsi, A.**, **Haarig, M.**, **Heese, B.**, **Jimenez, C.**, **Radenz, M.**, **Wandinger, U.**, Goloub, P., Podvin, T., Hu, Q., Chaikovsky, A., Haefele, A., Martucci, G., Navas, F., Brunamonti, S., Amodeo, A., Mona, L., Pappalardo, G., Giunta, A., Dema, C., D'Amico, G., Mytilinaios, M., Amato, F., Papagiannopoulos, N., Ciamprone, S., Freville, P., Sellegri, K., Chauvigne, A., Baray, J.-L., Montoux, N., Eswaran, K., Dionisi, D., Liberti, G. L., Cardillo, F., Collella, S., Di Paolantonio, M., Perrone, M. R., Quarta, G., Calcagnile, L., Romano, S., Burlizzi, P., De Tomasi, F., Maruccio, G., Stoyanov, D., Valkova, L., Grigorov, I., Dreischuh, T. N., Kolarov, G., Deleva, A., Balis, D., Michailidis, K., Siomos, N. and Voudouri, K. 2020. ACTRIS Aerosol Remote Sensing Data during the COVID-19 pandemic. *Data from: ACTRIS ARES Data Centre*, https://doi.org/10.21336/gen.w3w1-j222.

Gausa, M., Hanssen, I., Papayannis, A., Kokkalis, P., Mylonaki, M., Comeron, A., Muñoz-Porcar, C., Zenteno, A., García-Vizcaíno, D., Rocadenbosch, F., Pietruczuk, A., Szkop, A., Podgorski, J., Posyniak, M., Bortoli, D., Costa, M. J., Salgueiro, V., Pereira, S., Preissler, J., Kulkarni, P. S., Silva, A. M., Potes, M., Alados Arboledas,

L., Granados Muñoz, M. J., Ortiz Amezcua, P., de Jerónimo Alvarez, J. A., Bravo Aranda, J. A., Guerrero Rascado, J. L., Guzman, F. N., Pantaleón, D. B., Jiménez Martín, M., Mattis, I., Mueller, G., Wagner, F., Nicolae, D., Belegante, L., Binietoglou, I., Nemuc, A., Talianu, C., Komppula, M., Filioglou, M., Giannakaki, E., Shang, X., **Baars, H.**, **Engelmann, R.**, **Althausen, D.**, **Basharova, E.**, **Floutsi, A.**, **Haarig, M.**, **Heese, B.**, **Jimenez, C.**, **Radenz, M.**, **Wandinger, U.**, Goloub, P., Podvin, T., Hu, Q., Chaikovsky, A., Haefele, A., Martucci, G., Navas, F., Brunamonti, S., Amodeo, A., Mona, L., Pappalardo, G., Giunta, A., Dema, C., D'Amico, G., Mytilinaios, M., Amato, F., Papagiannopoulos, N., Ciamprone, S., Freville, P., Sellegri, K., Chauvigne, A., Baray, J.-L., Montoux, N., Eswaran, K., Dionisi, D., Liberti, G. L., Cardillo, F., Collella, S., Di Paolantonio, M., Perrone, M. R., Quarta, G., Calcagnile, L., Romano, S., Burlizzi, P., De Tomasi, F., Maruccio, G., Stoyanov, D., Valkova, L., Grigorov, I., Dreischuh, T. N., Kolarov, G., Deleva, A., Balis, D., Michailidis, K., Siomos, N. and Voudouri, K. 2020. ACTRIS Aerosol Remote Sensing COVID-19 campaign data of May 2020. *Data from: ACTRIS ARES Data Centre*, https://doi.org/10.21336/gen.xmbc-tj86.

Genz, C., **Schrödner, R.**, **Heinold, B.**, **Henning, S.**, **Baars, H.**, **Spindler, G.** and **Tegen, I.** 2020. Estimation of cloud condensation nuclei number concentrations and comparison to in situ and lidar observations during the HOPE experiments. Atmos. Chem. Phys., **20**, 8787-8806. https://doi.org/10.5194/acp-20-8787-2020.

Gerling, L., Löschau, G., **Wiedensohler, A.** and Weber, S. 2020. Statistical modelling of roadside and urban background ultrafine and accumulation mode particle number concentrations using generalized additive models. Sci. Total Environ., **703**, 134570. https://doi.org/10.1016/j.scitotenv.2019.134570.

Gialitaki, A., Tsekeri, A., Amiridis, V., Ceolato, R., Paulien, L., Kampouri, A., Gkikas, A., Solomos, S., Marinou, E., **Haarig, M.**, **Baars, H.**, **Ansmann, A.**, Lapyonok, T., Lopatin, A., Dubovik, O., Groß, S., Wirth, M., Tsichla, M., Tsikoudi, I. and Balis, D. 2020. Is the near-spherical shape the "new black" for smoke? Atmos. Chem. Phys., **20**, 14005-14021. https://doi.org/10.5194/acp-20-14005-2020.

Giannakaki, E., Kokkalis, P., Marinou, E., Bartsotas, N. S., Amiridis, V., **Ansmann, A.** and Komppula, M. 2020. The potential of elastic and polarization lidars to retrieve extinction profiles. Atmos. Meas. Tech., **13**, 893-905. https://doi.org/10.5194/amt-13-893-2020.

Glojek, K., Gregorič, A., Močnik, G., **Cuesta-Mosquera, A.**, **Wiedensohler, A.**, Drinovec, L. and Ogrin, M. 2020. Hidden black carbon air pollution in hilly rural areas — A case study of Dinaric depression. European Journal of Geography, **11**, 105-122. https://doi.org/10.48088/ejg.k.glo.11.2.105.122.

Goel, V., Mishra, S. K., **Ahlawat, A.**, Kumar, P., Senguttuvan, T. D., Sharma, C. and Reid, J. S. 2020. Insights into coarse particle optics based on field evidence of particle morphology, chemical composition and internal structure. Atmos. Environ., **232**, 117338. https://doi.org/10.1016/j.atmosenv.2020.117338.

Goel, V., Mishra, S. K., Pal, P., **Ahlawat, A.**, Vijayan, N., Jain, S. and Sharma, C. 2020. Influence of chemical aging on physico-chemical properties of mineral dust particles: A case study of 2016 dust storms over Delhi. Environ. Pollut., **267**, 115338. https://doi.org/10.1016/j.envpol.2020.115338.

Gong, X., **Wex, H.**, **van Pinxteren, M.**, **Triesch, N.**, **Fomba, K. W.**, **Lubitz, J.**, Stolle, C., Robinson, T.-B., **Müller, T.**, **Herrmann, H.** and **Stratmann, F.** 2020. Characterization of aerosol particles at Cabo Verde close to sea level and at the cloud level - Part 2: Ice-nucleating particles in air, cloud and seawater. Atmos. Chem. Phys., **20**, 1451-1468. https://doi.org/10.5194/acp-20-1451-2020.

Gong, X., **Wex, H.**, **Voigtländer, J.**, **Fomba, K. W.**, **Weinhold, K.**, **van Pinxteren, M.**, **Henning, S.**, **Müller, T.**, **Herrmann, H.** and **Stratmann, F.** 2020. Characterization of aerosol particles at Cape Verde close to sea and cloud level heights - Part 1: Particle number size distribution, cloud condensation nuclei and their origins. Atmos. Chem. Phys., **20**, 1431-1449. https://doi.org/10.5194/acp-20-1431-2020.

Griesche, H. J., **Seifert, P.**, **Ansmann, A.**, **Baars, H.**, **Barrientos Velasco, C.**, **Bühl, J.**, **Engelmann, R.**, **Radenz, M.** and **Zhenping, Y.** 2020. Application of the shipborne remote sensing supersite OCEANET for profiling of Arctic aerosols and clouds during *Polarstern* cruise PS106. Atmos. Meas. Tech., **13**, 5335-5358. https://doi.org/10.5194/amt-13-5335-2020.

Griessbach, S., Hoffmann, L., Spang, R., Achtert, P., von Hobe, M., Mateshvili, N., Müller, R., Riese, M., Rolf, C., **Seifert, P.** and Vernier, J.-P. 2020. Aerosol and cloud top height information of Envisat MIPAS measurements. Atmos. Meas. Tech., **13**, 1243-1271. https://doi.org/10.5194/amt-13-1243-2020.

Hartmann, M., Adachi, K., Eppers, O., Haas, C., Herber, A., Holzinger, R., **Hünerbein, A.**, Jäkel, E., **Jentzsch, C.**, **van Pinxteren, M.**, **Wex, H.**, Willmes, S. and **Stratmann, F.** 2020. Wintertime airborne measurements of ice nucleating particles in the high Arctic: A hint to a marine, biogenic source for ice nucleating particles. Geophys. Res. Lett., **47**, e2020GL087770 (11 pp.). https://doi.org/10.1029/2020GL087770.

He, L., Li, Y. P., Zhu, F. P., Sun, X. M., **Herrmann, H.**, **Schaefer, T.**, Zhang, Q. Z. and Wang, S. G. 2020. Insight into the mechanism of the OH-induced reaction of Ketoprofen: A combined DFT simulation and experimental

study. J. Environ. Inform., **35**, 128-137. http://www.jeionline.org/index.php?journal=mys&page=article&op=view&path%5B%5D=201900408.

Heintzenberg, J., Birmili, W., Hellack, B., **Spindler, G.**, **Tuch, T.** and **Wiedensohler, A.** 2020. Aerosol pollution maps and trends over Germany with hourly data at four rural background stations from 2009 to 2018. Atmos. Chem. Phys., **20**, 10967-10984. https://doi.org/10.5194/acp-20-10967-2020.

Hellmuth, O. and Feistel, R. 2020. Analytical determination of the nucleation-prone low-density fraction of subcooled water. Entropy, **22**, 933. https://doi.org/10.3390/e22090933.

Hellmuth, O., Schmelzer, J. W. P. and Feistel, R. 2020. Ice-crystal nucleation in water: Thermodynamic driving force and surface tension. Part I: Theretical foundation. Entropy, **22**, Art.-No. 50. https://doi.org/10.3390/e22010050.

Hengst, R., **Bayer, N.** and Doppler, L. 2020. Software package for processing of UV radiation data. Zenodo, http://doi.org/10.5281/zenodo.4322719.

Henning, S., Weller, R., Loftfield, J., Schumacher, M. and **Stratmann, F.** 2020. *VACCINE – Variation in Antarctic Cloud Condensation Nuclei (CCN) and Ice nucleating particle (INP) concentrations at NEumayer Station III*. T. Fromm, C. Oberdieck, T. Matz, and C. Wesche (Ed.), In: *Berichte zur Polar- und Meeresforschung - Reports on Polar and Marine Research, Expeditions to Antarctica: ANT-Land 2020/21 Neumayer Station III, Kohnen Station, Flight Operations and Field Campaigns*. Alfred-Wegener-Institut, Helmholtz-Zentrum für Polar- und Meeresforschung. Bremerhaven. **Berichte zur Polar- und Meeresforschung - Reports on Polar and Marine Research ; 745**. p. 118. https://doi.org/10.2312/BzPM_0745_2020.

Hodzic, A., Campuzano-Jost, P., Bian, H., Chin, M., Colarco, P. R., Day, D. A., Froyd, K. D., **Heinold, B.**, Jo, D. S., Katich, J. M., Kodros, J. K., Nault, B. A., Pierce, J. R., Ray, E., **Schacht, J.**, Schill, G. P., Schroder, J. C., Schwarz, J. P., Sueper, D. T., **Tegen, I.**, Tilmes, S., Tsigaridis, K., Yu, P. and Jimenez, J. L. 2020. Characterization of organic aerosol across the global remote troposphere: A comparison of ATom measurements and global chemistry models. Atmos. Chem. Phys., **20**, 4607-4635. https://doi.org/10.5194/acp-20-4607-2020.

Hofer, J., **Ansmann, A.**, **Althausen, D.**, **Engelmann, R.**, **Baars, H.**, Abdullaev, S. F. and Makhmudov, A. N. 2020. Long-term profiling of aerosol light extinction, particle mass, cloud condensation nuclei, and ice-nucleating particle concentration over Dushanbe, Tajikistan, in Central Asia. Atmos. Chem. Phys., **20**, 4695-4711. https://doi.org/10.5194/acp-20-4695-2020.

Hofer, J., **Ansmann, A.**, **Althausen, D.**, **Engelmann, R.**, **Baars, H.**, **Fomba, K. W.**, **Wandinger, U.**, Abdullaev, S. F. and Makhmudov, A. N. 2020. Optical properties of Central Asian aerosol relevant for spaceborne lidar applications and aerosol typing at 355 and 532 nm. Atmos. Chem. Phys., **20**, 9265-9280. https://doi.org/10.5194/acp-20-9265-2020.

Hoffmann, E. H., **Schrödner, R.**, **Tilgner, A.**, **Wolke, R.** and **Herrmann, H.** 2020. CAPRAM reduction towards an operational multiphase halogen and dimethyl sulfide chemistry treatment in the chemistry transport model COSMO-MUSCAT(5.04e). Geosci. Model Dev., **13**, 2587-2609. https://doi.org/10.5194/gmd-13-2587-2020.

Holanda, B. A., Pöhlker, M. L., Walter, D., Saturno, J., Sorgel, M., Ditas, J., Ditas, F., **Schulz, C.**, Franco, M. A., Wang, Q. Q., Donth, T., Artaxo, P., Barbosa, H. M. J., Borrmann, S., Braga, R., Brito, J., Cheng, Y. F., Dollner, M., Kaiser, J. W., Klimach, T., Knote, C., Krüger, O. O., Futterer, D., Lavric, J. V., Ma, N., Machado, L. A. T., Ming, J., Morais, F. G., Paulsen, H., Sauer, D., Schlager, H., Schneider, J., Su, H., Weinzierl, B., Walser, A., Wendisch, M., Ziereis, H., Zöger, M., Pöschl, U., Andreae, M. O. and Pöhlker, C. 2020. Influx of African biomass burning aerosol during the Amazonian dry season through layered transatlantic transport of black carbon-rich smoke. Atmos. Chem. Phys., **20**, 4757-4785. https://doi.org/10.5194/acp-20-4757-2020.

Janke, D., Caiazzo, A., Ahmed, N., Alia, N., **Knoth, O.**, Moreau, B., Wilbrandt, U., Willink, D., Amon, T. and John, V. 2020. On the feasibility of using open source solvers for the simulation of a turbulent air flow in a dairy barn. Comput. Electron. Agr., **175**, 105546 (16 pp.). https://doi.org/10.1016/j.compag.2020.105546.

Jimenez, C., **Ansmann, A.**, **Engelmann, R.**, Donovan, D., Malinka, A., Schmidt, J., **Seifert, P.** and **Wandinger, U.** 2020. The dual-field-of-view polarization lidar technique: A new concept in monitoring aerosol effects in liquid-water clouds – theoretical framework. Atmos. Chem. Phys., **20**, 15247-15263. https://doi.org/10.5194/acp-20-15247-2020.

Jimenez, C., **Ansmann, A.**, **Engelmann, R.**, Donovan, D., Malinka, A., **Seifert, P.**, **Wiesen, R.**, **Radenz, M.**, **Yin, Z.**, **Bühl, J.**, Schmidt, J., Barja, B. and **Wandinger, U.** 2020. The dual-field-of-view polarization lidar technique: A new concept in monitoring aerosol effects in liquid-water clouds – case studies. Atmos. Chem. Phys., **20**, 15265-15284. https://doi.org/10.5194/acp-20-15265-2020.

Kandler, K., Schneiders, K., Heuser, J., Waza, A., Aryasree, S., **Althausen, D.**, **Hofer, J.**, Abdullaev, S. F. and Makhmudov, A. N. 2020. Differences and similarities of Central Asian, African, and Arctic dust composition from a single particle perspective. Atmosphere, **11**, 269 (16 pp.). https://doi.org/10.3390/atmos11030269.

Khedidji, S., **Müller, K.**, Rabhi, L., **Spindler, G.**, **Fomba, K. W.**, **van Pinxteren, D.**, Yassaa, N. and **Herrmann, H.** 2020. Chemical Characterization of Marine Aerosols in a South Mediterranean Coastal Area Located in Bou Ismaïl, Algeria. Aerosol Air Qual. Res., **20**, 2448-2473. https://doi.org/10.4209/aaqr.2019.09.0458.

Kroflič, A., **Schaefer, T.**, Huš, M., **Le, H. P.**, **Otto, T.** and **Herrmann, H.** 2020. OH radicals reactivity towards phenol-related pollutants in water: Temperature dependence of the rate constants and novel insights into the [OH–phenol]˙ adduct formation. Phys. Chem. Chem. Phys., **22**, 1324-1332. https://pubs.rsc.org/en/content/articlelanding/2019/cp/c9cp05533a.

Laj, P., Bigi, A., Rose, C., Andrews, E., Myhre, C. L., Coen, M. C., Lin, Y., **Wiedensohler, A.**, Schulz, M., Ogren, J. A., Fiebig, M., Gliss, J., Mortier, A., Pandolfi, M., Petaja, T., Kim, S. W., Aas, W., Putaud, J. P., Mayol-Bracero, O., Keywood, M., Labrador, L., Aalto, P., Ahlberg, E., Arboledas, L. A., Alastuey, A., Andrade, M., Artinano, B., Ausmeel, S., Arsov, T., Asmi, E., Backman, J., Baltensperger, U., Bastian, S., Bath, O., Beukes, J. P., Brem, B. T., Bukowiecki, N., Conil, S., Couret, C., Day, D., Dayantolis, W., Degorska, A., Eleftheriadis, K., Fetfatzis, P., Favez, O., Flentje, H., Gini, M. I., Gregoric, A., Gysel-Beer, M., Hallar, A. G., Hand, J., Hoffer, A., Hueglin, C., Hooda, R. K., Hyvarinen, A., Kalapov, I., Kalivitis, N., Kasper-Giebl, A., Kim, J. E., Kouvarakis, G., Kranjc, I., Krejci, R., Kulmala, M., Labuschagne, C., Lee, H. J., Lihavainen, H., Lin, N. H., Loschau, G., Luoma, K., Marinoni, A., Dos Santos, S. M., Meinhardt, F., **Merkel, M.**, Metzger, J. M., Mihalopoulos, N., Nguyen, N. A., Ondracek, J., Perez, N., Perrone, M. R., Petit, J. E., Picard, D., Pichon, J. M., Pont, V., Prats, N., Prenni, A., Reisen, F., Romano, S., Sellegri, K., Sharma, S., Schauer, G., Sheridan, P., Sherman, J. P., Schutze, M., Schwerin, A., Sohmer, R., Sorribas, M., Steinbacher, M., Sun, J. Y., Titos, G., Toczko, B., **Tuch, T.**, Tulet, P., Tunved, P., Vakkari, V., Velarde, F., Velasquez, P., Villani, P., Vratolis, S., Wang, S. H., **Weinhold, K.**, Weller, R., Yela, M., Yus-Diez, J., Zdimal, V., Zieger, P. and Zikova, N. 2020. A global analysis of climate-relevant aerosol properties retrieved from the network of Global Atmosphere Watch (GAW) near-surface observatories. Atmos. Meas. Tech., **13**, 4353-4392. https://doi.org/10.5194/amt-13-4353-2020.

Lampert, A., Altstädter, B., Bärfuss, K., Bretschneider, L., Sandgaard, J., Michaelis, J., Lobitz, L., Asmussen, M., Damm, E., **Käthner, R.**, Krüger, T., Lüpkes, C., Nowak, S., Peuker, A., Rausch, T., Reiser, F., Scholtz, A., Sotomayor Zakharov, D., Gaus, D., Bansmer, S., **Wehner, B.** and Pätzold, F. 2020. Unmanned aerial systems for investigating the Polar atmospheric boundary layer—Technical challenges and examples of applications. Atmosphere, **11**, 416 (25 pp.). https://doi.org/10.3390/atmos11040416.

Lei, T., **Ma, N.**, Hong, J., **Tuch, T.**, Wang, X., Wang, Z., Pöhlker, M., Ge, M., Wang, W., Mikhailov, E., Hoffmann, T., Pöschl, U., Su, H., **Wiedensohler, A.** and Cheng, Y. 2020. Nano-hygroscopicity tandem differential mobility analyzer (nano-HTDMA) for investigating hygroscopic properties of sub-10nm aerosol nanoparticles. Atmos. Meas. Tech., **13**, 5551-5567. https://doi.org/10.5194/amt-13-5551-2020.

Li, J., Zhu, C., Chen, H., Fu, H., Xiao, H., Wang, X., **Herrmann, H.** and Chen, J. 2020. A more important role for the ozone-S(IV) oxidation pathway due to decreasing acidity in clouds. J. Geophys. Res. - Atmos., **125**, e2020JD033220. https://doi.org/10.1029/2020JD033220.

Li, J., Zhu, C., Chen, H., Zhao, D., Xue, L., Wang, X., Li, H., Liu, P., Liu, J., Zhang, C., Mu, Y., Zhang, W., Zhang, L., **Herrmann, H.**, Li, K., Liu, M. and Chen, J. 2020. The evolution of cloud and aerosol microphysics at the summit of Mt. Tai, China. Atmos. Chem. Phys., **20**, 13735-13751. https://doi.org/10.5194/acp-20-13735-2020.

Li, T., Wang, Z., Wang, Y., Wu, C., Liang, Y., Xia, M., Yu, C., Yun, H., Wang, W., Wang, Y., Guo, J., **Herrmann, H.** and Wang, T. 2020. Chemical characteristics of cloud water and the impacts on aerosol properties at a subtropical mountain site in Hong Kong SAR. Atmos. Chem. Phys., **20**, 391-407. https://doi.org/10.5194/acp-20-391-2020.

Lou, S. J., Shrivastava, M., Easter, R. C., Yang, Y., Ma, P. L., Wang, H. L., Cubison, M. J., Campuzano-Jost, P., Jimenez, J. L., Zhang, Q., Rasch, P. J., Shilling, J. E., Zelenyuk, A., Dubey, M., Cameron-Smith, P., Martin, S. T., Schneider, J. and **Schulz, C.** 2020. New SOA treatments within the energy exascale earth system model (E3SM): Strong production and sinks govern atmospheric SOA distributions and radiative forcing. J. Adv. Model. Earth Syst., **12**, e2020MS002266 (29 pp.). https://doi.org/10.1029/2020MS002266.

Macke, A. 2020. rt-crystal. Zenodo, http://doi.org/10.5281/zenodo.3965488.

Macke, A. 2020. rt-ellipsoid. Zenodo, http://doi.org/10.5281/zenodo.3965515.

Macke, A. 2020. rt-mc. Zenodo, http://doi.org/10.5281/zenodo.3965572.

Macke, A. 2020. rt-circcyl. Zenodo, http://doi.org/10.5281/zenodo.3965588.

Macke, A. 2020. rt-ellipsoidmc. Zenodo, http://doi.org/10.5281/zenodo.3965591.

Macke, A. 2020. mc-unik. Zenodo, http://doi.org/10.5281/zenodo.3965600.

Madueño, L., **Kecorius, S.**, Andrade, M. and **Wiedensohler, A.** 2020. Exposure and respiratory tract deposition dose of equivalent black carbon in high altitudes. Atmosphere, **11**, 598 (16 pp.). https://doi.org/10.3390/atmos11060598.

Mei, L., Rozanov, V., Ritter, C., **Heinold, B.**, Jiao, Z., Vountas, M. and Burrows, J. P. 2020. Retrieval of aerosol optical thickness in the Arctic snow-covered regions using passive remote sensing: Impact of aerosol typing and surface reflection model. IEEE T. Geosci. Remote, **58**, 5117-5131. https://ieeexplore.ieee.org/document/9007036/authors#authors.

Mekic, M., Zeng, J., Jiang, B., Li, X., Lazarou, Y. G., Brigante, M., **Herrmann, H.** and Gligorovski, S. 2020. Formation of toxic unsaturated multifunctional and organosulfur compounds from the photosensitized processing of fluorene and DMSO at the air-water interface. J. Geophys. Res. - Atmos., **125**, e2019JD031839 (15 pp.). https://doi.org/10.1029/2019JD031839.

Molleker, S., Helleis, F., Klimach, T., Appel, O., Clemen, H. C., Dragoneas, A., Gurk, C., Hünig, A., Köllner, F., **Rubach, F.**, **Schulz, C.**, Schneider, J. and Borrmann, S. 2020. Application of an O-ring pinch device as a constant-pressure inlet (CPI) for airborne sampling. Atmos. Meas. Tech., **13**, 3651-3660. https://doi.org/10.5194/amt-13-3651-2020.

Møller, K. H., **Berndt, T.** and Kjaergaard, H. G. 2020. Atmospheric autoxidation of amines. Environ. Sci. Technol., **54**, 11087-11099. https://doi.org/10.1021/acs.est.0c03937.

Mothes, F., **van Pinxteren, D.**, **Spindler, G.**, Löschau, G., Hausmann, A. and **Herrmann, H.** 2020. Partikuläre Emissionen aus der Holzverbrennung und ihr Beitrag zu PM. Gefahrst. Reinhalt. L., **80**, 305-317.

Niedermeier, D., **Voigtländer, J.**, **Schmalfuß, S.**, **Busch, D.**, Schumacher, J., Shaw, R. A. and **Stratmann, F.** 2020. Characterization and first results from LACIS-T: A moist-air wind tunnel to study aerosol-cloud-turbulence interactions. Atmos. Meas. Tech., **13**, 2015-2033. https://doi.org/10.5194/amt-13-2015-2020.

Ohneiser, K., **Ansmann, A.**, **Baars, H.**, **Seifert, P.**, Barja, B., **Jimenez, C.**, **Radenz, M.**, **Teisseire, A.**, **Floutsi, A.**, **Haarig, M.**, Foth, A., Chudnovsky, A., **Engelmann, R.**, Zamorano, F., **Bühl, J.** and **Wandinger, U.** 2020. Smoke of extreme Australian bushfires observed in the stratosphere over Punta Arenas, Chile, in January 2020: Optical thickness, lidar ratios, and depolarization ratios at 355 and 532 nm. Atmos. Chem. Phys., **20**, 8003-80015. https://doi.org/10.5194/acp-20-8003-2020.

Paglione, M., Gilardoni, S., Rinaldi, M., Decesari, S., Zanca, N., Sandrini, S., Giulianelli, L., Bacco, D., Ferrari, S., Poluzzi, V., Scotto, F., Trentini, A., **Poulain, L.**, **Herrmann, H.**, **Wiedensohler, A.**, Canonaco, F., Prévôt, A. S. H., Massoli, P., Carbone, C., Facchini, M. C. and Fuzzi, S. 2020. The impact of biomass burning and aqueous-phase processing on air quality: A multi-year source apportionment study in the Po Valley, Italy. Atmos. Chem. Phys., **20**, 1233-1254. https://doi.org/10.5194/acp-20-1233-2020.

Pandolfi, M., Mooibroek, D., Hopke, P., **van Pinxteren, D.**, Querol, X., **Herrmann, H.**, Alastuey, A., Favez, O., Hüglin, C., Perdrix, E., Riffault, V., Sauvage, S., van der Swaluw, E., Tarasova, O. and Colette, A. 2020. Long-range and local air pollution: What can we learn from chemical speciation of particulate matter at paired sites? Atmos. Chem. Phys., **20**, 409-429. https://doi.org/10.5194/acp-20-409-2020.

Papagiannopoulos, N., D'Amico, G., Gialitaki, A., Ajtai, N., Alados-Arboledas, L., Amodeo, A., Amiridis, V., **Baars, H.**, Balis, D., Binietoglou, I., Comerón, A., Dionisi, D., Falconieri, A., Fréville, P., Kampouri, A., Mattis, I., Mijić, Z., Molero, F., Papayannis, A., Pappalardo, G., Rodríguez-Gómez, A., Solomos, S. and Mona, L. 2020. An EARLINET early warning system for atmospheric aerosol aviation hazards. Atmos. Chem. Phys., **20**, 10775-10789. https://doi.org/10.5194/acp-20-10775-2020

Petäjä, T., Duplissy, E. M., Tabakova, K., Schmale, J., Altstädter, B., Ancellet, G., Arshinov, M., Balin, Y., Baltensperger, U., Bange, J., Beamish, A., Belan, B., Berchet, A., Bossi, R., Cairns, W. R. L., Ebinghaus, R., El Haddad, I., Ferreira-Araujo, B., Franck, A., Huang, L., Hyvärinen, A., Humbert, A., Kalogridis, A. C., Konstantinov, P., Lampert, A., MacLeod, M., Magand, O., Mahura, A., Marelle, L., Masloboev, V., Moisseev, D., Moschos, V., Neckel, N., Onishi, T., Osterwalder, S., Ovaska, A., Paasonen, P., Panchenko, M., Pankratov, F., Pernov, J. B., Platis, A., Popovicheva, O., Raut, J. C., Riandet, A., Sachs, T., Salvatori, R., Salzano, R., Schröder, L., Schön, M., Shevchenko, V., Skov, H., Sonke, J. E., Spolaor, A., Stathopoulos, V. K., Strahlendorff, M., Thomas, J. L., Vitale, V., Vratolis, S., Barbante, C., Chabrillat, S., Dommergue, A., Eleftheriadis, K., Heilimo, J., Law, K. S., Massling, A., Noe, S. M., Paris, J. D., Prévôt, A. S. H., Riipinen, I., **Wehner, B.**, Xie, Z. and Lappalainen, H. K. 2020. Overview: Integrative and Comprehensive Understanding on Polar Environments (iCUPE) – Concept and initial results. Atmos. Chem. Phys., **20**, 8551-8592. https://www.atmos-chem-phys.net/20/8551/2020/.

Pfeifer, S., **Müller, T.**, Freedman, A. and **Wiedensohler, A.** 2020. The influence of the baseline drift on the resulting extinction values of a cavity attenuated phase shift-based extinction monitor (CAPS PMex). Atmos. Meas. Tech., **13**, 2161-2167. https://doi.org/10.5194/amt-13-2161-2020.

Pfrommer, E., Dreier, C., Gabriel, G., Dallenga, T., Reimer, R., **Schepanski, K.**, Scherließ, R., Schaible, U. E. and Gutsmann, T. 2020. Enhanced tenacity of mycobacterial aerosols from necrotic neutrophils. Sci. Rep., **10**, 9159. https://doi.org/10.1038/s41598-020-65781-9.

Poulain, L., **Spindler, G.**, **Grüner, A.**, **Tuch, T.**, **Stieger, B.**, **van Pinxteren, D.**, Petit, J.-E., Favez, O., **Herrmann, H.** and **Wiedensohler, A.** 2020. Multi-year ACSM measurements at the central European research station Melpitz (Germany) - Part 1: Instrument robustness, quality assurance, and impact of upper size cutoff diameter. Atmos. Meas. Tech., **13**, 4973-4994. https://doi.org/10.5194/amt-13-4973-2020.

Pye, H. O. T., Nenes, A., Alexander, B., Ault, A. P., Barth, M. C., Clegg, S. L., Collett Jr., J. L., Fahey, K. M., Hennigan, C. J., **Herrmann, H.**, Kanakidou, M., Kelly, J. T., Ku, I.-T., McNeill, V. F., Riemer, N., **Schaefer, T.**, Shi, G., **Tilgner, A.**, Walker, J. T., Wang, T., Weber, R., Xing, J., Zaveri, R. A. and Zuend, A. 2020. The acidity of atmospheric particles and clouds. Atmos. Chem. Phys., **20**, 4809–4888. https://doi.org/10.5194/acp-20-4809-2020.

Quaas, J., Arola, A., Cairns, B., Christensen, M., **Deneke, H.**, Ekman, A. M. L., Feingold, G., Fridlind, A., Gryspeerdt, E., Hasekamp, O., Li, Z., Lipponen, A., Ma, P.-L., Mülmenstädt, J., Nenes, A., Penner, J. E., Rosenfeld, D., **Schrödner, R.**, Sinclair, K., Sourdeval, O., Stier, P., Tesche, M., van Diedenhoven, B. and Wendisch, M. 2020. Constraining the Twomey effect from satellite observations: Issues and perspectives. Atmos. Chem. Phys., **20**, 15079-15099. https://doi.org/10.5194/acp-20-15079-2020.

Radenz, M. 2020. martin-rdz/trace_airmass_source: trace version of aug2020 (Version v0.4). Zenodo, http://doi.org/10.5281/zenodo.4008383.

Regayre, L. A., Schmale, J., Johnson, J. S., **Tatzelt, C.**, Baccarini, A., **Henning, S.**, Yoshioka, M., **Stratmann, F.**, Gysel-Beer, M., Grosvenor, D. P. and Carslaw, K. S. 2020. The value of remote marine aerosol measurements for constraining radiative forcing uncertainty. Atmos. Chem. Phys., **20**, 10063-10072. https://doi.org/10.5194/acp-20-10063-2020.

Ren, Y., **Stieger, B.**, **Spindler, G.**, Grosselin, B., Mellouki, A., **Tuch, T.**, **Wiedensohler, A.** and **Herrmann, H.** 2020. Role of the dew water on the ground surface in HONO distribution: A case measurement in Melpitz. Atmos. Chem. Phys., **20**, 13069-13089. https://doi.org/10.5194/acp-20-13069-2020.

Righi, M., Hendricks, J., Lohmann, U., Beer, C. G., Hahn, V., **Heinold, B.**, Heller, R., Krämer, M., Ponater, M., Rolf, C., **Tegen, I.** and Voigt, C. 2020. Coupling aerosols to (cirrus) clouds in the global EMAC-MADE3 aerosol–climate model. Geosci. Model Dev., **13**, 1635-1661. https://doi.org/10.5194/gmd-13-1635-2020.

Riva, M., **Brüggemann, M.**, Li, D., Perrier, S., George, C., **Herrmann, H.** and **Berndt, T.** 2020. Capability of CI-Orbitrap for gas-phase analysis in atmospheric chemistry: A comparison with the CI-APi-TOF technique. Anal. Chem., **92**, 8142-8150. https://doi.org/10.1021/acs.analchem.0c00111.

Roudini, M., **Niedermeier, D.**, **Stratmann, F.** and Winkler, A. 2020. Droplet generation in Standing-Surface-Acoustic-Wave nebulization at controlled air humidity. Phys. Rev. Applied, **14**, 014071. https://doi.org/10.1103/PhysRevApplied.14.014071.

Rusumdar, A. J., **Tilgner, A.**, **Wolke, R.** and **Herrmann, H.** 2020. Treatment of non-ideality in the SPACCIM multiphase model - Part 2: Impacts on the multiphase chemical processing in deliquesced aerosol particles. Atmos. Chem. Phys., **20**, 10351-10377. https://doi.org/10.5194/acp-20-10351-2020.

Sakradzija, M., **Senf, F.**, Scheck, L., Ahlgrimm, M. and Klocke, D. 2020. Local impact of stochastic shallow convection on clouds and precipitation in the tropical Atlantic. Mon. Wea. Rev., **148**, 5041-5062. https://doi.org/10.1175/MWR-D-20-0107.1.

Sakradzija, M., **Senf, F.**, Scheck, L., Ahlgrimm, M. and Klocke, D. 2020. Local impact of stochastic shallow convection on clouds and precipitation in the tropical Atlantic. *Data from: World Data Center for Climate (WDCC) at DKRZ*, http://cera-www.dkrz.de/WDCC/ui/Compact.jsp?acronym=DKRZ_LTA_731_ds00001.

Schaefer, T., **Wen, L.**, Estelmann, A., Maak, J. and **Herrmann, H.** 2020. pH- and temperature-dependent kinetics of the oxidation reactions of OH with succinic and pimelic acid in aqueous solution. Atmosphere, **11**, 320. https://doi.org/10.3390/atmos11040320.

Schanze, J., Hornidge, A.-K., Hutter, G., **Macke, A.** and Osberghaus, D. 2020. Umweltkrisen. *In: F. Bösch, N. Deitelhoff, and S. Kroll (Eds.), Handbuch Krisenforschung*. Springer VS, Wiesbaden, p. 179-204.

Schepanski, K. and **Tegen, I.** 2020. *Schlussbericht PalMod-2-4-TP1*. Bundesministerium für Bildung und Forschung (BMBF). **FKZ 01LP15-08A**. p. 24.

Schubert, M., Knöller, K., **Tegen, I.** and Terzi, L. 2020. Variability of cosmogenic ^{35}S in rain – Resulting implications for the use of radiosulfur as natural groundwater residence time tracer. Water, **12**, 2953. https://doi.org/10.3390/w12102953.

Senf, F. 2020. NAWDEX Analysis Tools: Python Package for Analysis of CRE in the North Atlantic - Publication Release (Version v1.0.1). Zenodo, http://doi.org/10.5281/zenodo.4028394.

Senf, F. 2020. Jupyter Notebooks for Analysis of the Effects of Stochastic Convection Parameterization in (Sub-)Tropical Atlantic, 1st Revision of MWR Manuscript (Version v1.0.1). Zenodo, http://doi.org/10.5281/zenodo.3952525.

Senf, F. 2020. Jupyter Notebooks for Analysis of CRE in the North Atlantic, 1st Revision of JGR Manuscript (Version v1.0.1). Zenodo, http://doi.org/10.5281/zenodo.3952138.

Senf, F. 2020. Jupyter Notebooks for the ICON Semi-Direct Effect Paper 2020, Submission Release (Version v1.0). Zenodo, http://doi.org/10.5281/zenodo.4320924.

Senf, F. 2020. Jupyter Notebooks for the ICON Semi-Direct Effect Paper 2020, Revision 1 Release (v1.1). Zenodo, https://doi.org/10.5281/zenodo.5078285.

Senf, F. 2020. Post-Processed Simulation Data of ICON-LEM-DE Absorbing Aerosol Perturbation Experiments. *Data from: World Data Center for Climate (WDCC) at DKRZ*, http://cera-www.dkrz.de/WDCC/ui/Compact.jsp?acronym=DKRZ_LTA_1174_ds00001.

Senf, F. 2020. Metadata for ‚2016-2019_hdcp2-icon-lem-analysis-data-on-mistral.tgz'. *Data from: World Data Center for Climate (WDCC) at DKRZ*, http://cera-www.dkrz.de/WDCC/ui/Compact.jsp?acronym=DKRZ_LTA_834_ds00049.

Senf, F. 2020. Metadata for ‚2016-2019_hdcp2-icon-narval-analysis-data-on-mistral.tgz'. *Data from: World Data Center for Climate (WDCC) at DKRZ*, http://cera-www.dkrz.de/WDCC/ui/Compact.jsp?acronym=DKRZ_LTA_834_ds00050.

Senf, F. 2020. Metadata for ‚2016-2019_hdcp2-icon-synsat-data-on-mistral.tgz'. *Data from: World Data Center for Climate (WDCC) at DKRZ*, http://cera-www.dkrz.de/WDCC/ui/Compact.jsp?acronym=DKRZ_LTA_834_ds00051.

Senf, F. 2020. Metadata for ‚2020_data_cre-north-atlantic-paper.tgz'. *Data from: World Data Center for Climate (WDCC) at DKRZ*, http://cera-www.dkrz.de/WDCC/ui/Compact.jsp?acronym=DKRZ_LTA_834_ds00048.

Senf, F. 2020. NAWDEX Analysis Tools - Submission Release (v1.0.0-alpha). Zenodo, https://doi.org/10.5281/zenodo.3657387.

Senf, F., Voigt, A., Clerbaux, N., **Hünerbein, A.** and **Deneke, H.** 2020. Increasing resolution and resolving convection improve the simulation of cloud-radiative effects over the North Atlantic. J. Geophys. Res. - Atmos., **125**, e2020JD032667. https://doi.org/10.1029/2020JD032667.

Shaw, R. A., Cantrell, W., Chen, S., Chuang, P., Donahue, N., Feingold, G., Kollias, P., Korolev, A., Kreidenweis, S., Krueger, S., Mellado, J. P., **Niedermeier, D.** and Xue, L. 2020. Cloud–aerosol–turbulence interactions: Science priorities and concepts for a large-scale laboratory facility. Bull. Amer. Meteor. Soc., **101**, E1026-E1035. https://doi.org/10.1175/BAMS-D-20-0009.1.

Song, H., Chen, X., Lu, K., Zou, Q., Tan, Z., Fuchs, H., **Wiedensohler, A.**, Moon, D. R., Heard, D. E., Baeza-Romero, M.-T., Zheng, M., Wahner, A., Kiendler-Scharr, A. and Zhang, Y. 2020. Influence of aerosol copper on HO_2 uptake: A novel parameterized equation. Atmos. Chem. Phys., **20**, 15835-15850. https://doi.org/10.5194/acp-20-15835-2020.

Sporre, M. K., Blichner, S. M., **Schrödner, R.**, Karset, I. H. H., Berntsen, T. K., van Noije, T., Bergman, T., O'Donnell, D. and Makkonen, R. 2020. Large difference in aerosol radiative effects from BVOC-SOA treatment in three Earth system models. Atmos. Chem. Phys., **20**, 8953-8973. https://doi.org/10.5194/acp-20-8953-2020.

Spranger, T., **van Pinxteren, D.** and **Herrmann, H.** 2020. Atmospheric „HULIS" in different environments: Polarities, molecular sizes, and sources suggest more than 50% are not „humic-like". ACS Earth Space Chem., **4**, 272-282. https://doi.org/10.1021/acsearthspacechem.9b00299.

Stevens, B., Acquistapace, C., Hansen, A., Heinze, R., Klinger, C., Klocke, D., Rybka, H., Schubotz, W., Windmiller, J., Adamidis, P., Arka, I., **Barlakas, V.**, Biercamp, J., Brueck, M., Brune, S., Buehler, S. A., Burkhardt, U., Cioni, G., Costa-Surós, M., Crewell, S., Crüger, T., **Deneke, H.**, Friederichs, P., Henken, C. C., Hohenegger, C., Jacob, M., Jakub, F., Kalthoff, N., Köhler, M., van Laar, T. W., Li, P., Löhnert, U., **Macke, A.**, Madenach, N., Mayer, B., Nam, C., Naumann, A. K., Peters, K., Poll, S., Quaas, J., Röber, N., Rochetin, N., Scheck, L., Schemann, V., Schnitt, S., Seifert, A., **Senf, F.**, Shapkalijevski, M., Simmer, C., Singh, S.,

Sourdeval, O., Spickermann, D., Strandgren, J., Tessiot, O., Vercauteren, N., Vial, J., Voigt, A. and Zängl, G. 2020. The added value of large-eddy and storm-resolving models for simulating clouds and precipitation. J. Meteorol. Soc. Jpn. Ser. II, **98**, 395-435. https://doi.org/10.2151/jmsj.2020-021.

Stolle, C., Ribas-Ribas, M., Badewien, T. H., Barnes, J., Carpenter, L. J., Chance, R., Damgaard, L. R., Durán Quesada, A. M., Engel, A., Frka, S., Galgani, L., Gašparović, B., Gerriets, M., Hamizah Mustaffa, N. I., **Herrmann, H.**, Kallajoki, L., Pereira, R., Radach, F., Revsbech, N. P., Rickard, P., Saint, A., Salter, M., Striebel, M., **Triesch, N.**, Uher, G., Upstill-Goddard, R. C., **van Pinxteren, M.**, Zäncker, B., Zieger, P. and Wurl, O. 2020. The MILAN campaign: Studying diel light effects on the air-sea interface. Bull. Amer. Meteor. Soc., **101**, E146–E166. https://doi.org/10.1175/BAMS-D-17-0329.1.

Sun, J., **Birmili, W.**, **Hermann, M.**, **Tuch, T.**, **Weinhold, K.**, **Merkel, M.**, **Rasch, F.**, **Müller, T.**, Schladitz, A., Bastian, S., Löschau, G., Cyrys, J., Gu, J., Flentje, H., Briel, B., Asbach, C., Kaminski, H., Ries, L., Sohmer, R., Gerwig, H., Wirtz, K., Meinhardt, F., Schwerin, A., Bath, O., **Ma, N.** and **Wiedensohler, A.** 2020. Decreasing trends of particle number and black carbon mass concentrations at 16 observational sites in Germany from 2009 to 2018. Atmos. Chem. Phys., **20**, 7049-7068. https://doi.org/10.5194/acp-20-7049-2020.

Tan, Z., Hofzumahaus, A., Lu, K., Brown, S. S., Holland, F., Huey, L. G., Kiendler-Scharr, A., Li, X., Liu, X., **Ma, N.**, Min, K.-E., Rohrer, F., Shao, M., Wahner, A., Wang, Y., **Wiedensohler, A.**, Wu, Y., Wu, Z., Zeng, L., Zhang, Y. and Fuchs, H. 2020. No evidence for a significant impact of heterogeneous chemistry on radical concentrations in the North China plain in summer 2014. Environ. Sci. Technol., **54**, 5973-5979. https://dx.doi.org/10.1021/acs.est.0c00525.

Tao, J., Kuang, Y., **Ma, N.**, Zheng, Y., **Wiedensohler, A.** and Zhao, C. 2020. An improved parameterization scheme for size-resolved particle activation ratio and its application on comparison study of particle hygroscopicity measurements between HTDMA and DMA-CCNC. Atmos. Environ., **226**, 117403. https://doi.org/10.1016/j.atmosenv.2020.117403.

Teich, M., Schmidtpott, M., **van Pinxteren, D.**, Chen, J. and **Herrmann, H.** 2020. Separation and quantification of imidazoles in atmospheric particles using LC–Orbitrap-MS. J. Sep. Sci., **43**, 577-589. https://doi.org/10.1002/jssc.201900689.

Thiel, N., Münch, S., Behrens, W., Junker, V., **Faust, M.**, Biniasch, O., Kabelitz, T., Siller, P., Boedeker, C., Schumann, P., Roesler, U., Amon, T., **Schepanski, K.**, Funk, R. and Nübel, U. 2020. Airborne bacterial emission fluxes from manure-fertilized agricultural soil. Microbial Biotechnology, **13**, 1631-1647. https://doi.org/10.1111/1751-7915.13632.

Tõnisson, L., Kunz, Y., **Kecorius, S.**, **Madueño, L.**, Tamayo, E. G., Casanova, D. M., Zhao, Q., Schikowski, T., Hornidge, A.-K., **Wiedensohler, A.** and **Macke, A.** 2020. From transfer to knowledge co-production: A transdisciplinary research approach to reduce black carbon emissions in Metro Manila, Philippines. Sustainability, **12**, 10043. https://doi.org/10.3390/su122310043.

Valentini, S., Barnaba, F., Bernadoni, V., Calzolai, G., Costabile, F., Di Liberto, L., Forello, A. C., Gobbi, G. P., Gualtieri, M., Lucareli, F., Nava, S., Petralia, E., Valli, G., **Wiedensohler, A.** and Vecchi, R. 2020. Classifying aerosol particles through the combination of optical and physical-chemical properties: Results from a wintertime campaign in Rome (Italy). Atmos. Res., **235**, 104799. https://doi.org/10.1016/j.atmosres.2019.104799.

van Pinxteren, D., **Mothes, F.**, **Spindler, G.**, **Fomba, K. W.**, **Cuesta, A.**, **Tuch, T.**, **Müller, T.**, **Wiedensohler, A.** and **Herrmann, H.** 2020. *Zusatzbelastung aus Holzheizungen (Abschlussbericht)*. Landesamt für Umwelt, Landwirtschaft und Geologie. **Schriftenreihe des LfULG, Heft 12/2020**. p. 160. https://publikationen.sachsen.de/bdb/artikel/36106.

van Pinxteren, M., **Fomba, K. W.**, **Triesch, N.**, Stolle, C., Wurl, O., Bahlmann, E., **Gong, X.**, **Voigtländer, J.**, **Wex, H.**, Robinson, T.-B., **Barthel, S.**, **Zeppenfeld, S.**, **Hoffmann, E. H.**, Roveretto, M., Li, C., Grosselin, B., Daële, V., **Senf, F.**, **van Pinxteren, D.**, Manzi, M., Zabalegui, N., Frka, S., Gašparović, B., Pereira, R., Li, T., Wen, L., Li, J., Zhu, C., Chen, C., Chen, J., Fiedler, B., von Tümpling, W., Read, K. A., Punjabi, S., Lewis, A. C., Hopkins, J. R., Carpenter, L. J., Peeken, I., Rixen, T., Schulz-Bull, D., Monge, M. E., Mellouki, A., George, C., **Stratmann, F.** and **Herrmann, H.** 2020. Marine organic matter in the remote environment of the Cape Verde Islands – An introduction and overview to the MarParCloud campaign. Atmos. Chem. Phys., **20**, 6921-6951. https://doi.org/10.5194/acp-20-6921-2020.

Vandenbussche, S., Callewaert, S., **Schepanski, K.** and De Mazière, M. 2020. North African mineral dust sources: New insights from a combined analysis based on 3D dust aerosol distributions, surface winds and ancillary soil parameters. Atmos. Chem. Phys., **20**, 15127-15246. https://doi.org/10.5194/acp-20-15127-2020.

Villanueva, D., **Heinold, B.**, **Seifert, P.**, **Deneke, H.**, **Radenz, M.** and **Tegen, I.** 2020. The day-to-day co-variability between mineral dust and cloud glaciation: A proxy for heterogeneous freezing. Atmos. Chem. Phys., **20**, 2177-2199. https://doi.org/10.5194/acp-20-2177-2020.

Wang, D. X., Stachlewska, I. S., Song, X. Q., **Heese, B.** and Nemuc, A. 2020. Variability of the boundary layer over an urban continental site based on 10 years of active remote sensing observations in Warsaw. Remote Sens., **12**, 340 (33 pp.). https://doi.org/10.3390/rs12020340.

Wang, X., Hayeck, N., **Brüggemann, M.**, Abis, L., Riva, M., Lu, Y., Wang, B., Chen, J., George, C. and Wang, L. 2020. Chemical characteristics and brown carbon chromophores of atmospheric organic aerosols over the Yangtze River channel: A cruise campaign. J. Geophys. Res. - Atmos., **125**, e2020JD032497. https://doi.org/10.1029/2020JD032497.

Wang, Y., Chen, Y., Wu, Z., Shang, D., Bian, Y., Du, Z., Schmitt, S. H., Su, R., Gkatzelis, G. I., Schlag, P., Hohaus, T., Voliotis, A., Lu, K., Zeng, L., Zhao, C., Alfarra, M. R., McFiggans, G., **Wiedensohler, A.**, Kiendler-Scharr, A., Zhang, Y. and Hu, M. 2020. Mutual promotion between aerosol particle liquid water and particulate nitrate enhancement leads to severe nitrate-dominated particulate matter pollution and low visibility. Atmos. Chem. Phys., **20**, 2161-2175. https://doi.org/10.5194/acp-20-2161-2020.

Weber, J., Archer-Nicholls, S., Griffiths, P., **Berndt, T.**, Jenkin, M., Gordon, H., Knote, C. and Archibald, A. T. 2020. CRI-HOM: A novel chemical mechanism for simulating highly oxygenated organic molecules (HOMs) in global chemistry–aerosol–climate models. Atmos. Chem. Phys., **20**, 10889-10910. https://doi.org/10.5194/acp-20-10889-2020.

Weger, M., **Heinold, B.** and **Knoth, O.** 2020. CAIRDIO City-Scale Air Dispersion Model with Diffusive Obstacles (Version 1.0). Zenodo, http://doi.org/10.5281/zenodo.4159497.

Weger, M., **Heinold, B.** and **Knoth, O.** 2020. CAIRDIO City-Scale Air Dispersion Model with Diffusive Obstacles (Version 1.0). Zenodo, http://doi.org/10.5281/zenodo.4153462.

Weger, M., **Heinold, B.** and **Knoth, O.** 2020. CAIRDIO City-Scale Air Dispersion Model with Diffusive Obstacles (Version 1.0). Zenodo, http://doi.org/10.5281/zenodo.4088168.

Welti, A., Bigg, E. K., DeMott, P. J., **Gong, X.**, **Hartmann, M.**, Harvey, M., **Henning, S.**, **Herenz, P.**, Hill, T. C. J., Hornblow, B., Leck, C., **Löffler, M.**, McCluskey, C. S., Rauker, A. M., Schmale, J., **Tatzelt, C.**, **van Pinxteren, M.** and **Stratmann, F.** 2020. Ship-based measurements of ice nuclei concentrations over the Arctic, Atlantic, Pacific and Southern oceans. Atmos. Chem. Phys., **20**, 15191-15206. https://doi.org/10.5194/acp-20-15191-2020.

Werner, F. and **Deneke, H.** 2020. Increasing the spatial resolution of cloud property retrievals from Meteosat SEVIRI by use of its high–resolution visible channel: Evaluation of candidate approaches with MODIS observations. Atmos. Meas. Tech., **13**, 1089-1111. https://doi.org/10.5194/amt-13-1089-2020.

Witthuhn, J., **Deneke, H.** and **Macke, A.** 2020. Shipborne rotating shadowband radiometer data of spectral irradiance components and aerosol optical depth during Polarstern cruises PS83, PS95, PS98, PS102 and PS113. *Data from: Leibniz-Institut für Troposphärenforschung e.V., Leipzig, PANGAEA*, https://doi.org/10.1594/PANGAEA.910535.

Witthuhn, J., **Hünerbein, A.** and **Deneke, H.** 2020. Evaluation of satellite-based aerosol datasets and the CAMS reanalysis over the ocean utilizing shipborne reference observations. Atmos. Meas. Tech., **13**, 1387-1412. https://doi.org/10.5194/amt-13-1387-2020.

Wolke, R., **Chen, Y.**, **Schröder, W.**, **Spindler, G.** and **Wiedensohler, A.** 2020. A parameterization of heterogeneous hydrolysis of N_2O_5 for 3-D atmospheric modelling. *In: C. Mensink, W. Gong, and A. Hakami (Eds.), Air pollution modeling and its application XXVI : Proceedings of the 36th International Technical Meeting on Air Pollution Modelling and Its Application (Ottawa, Canada, 14-18 May 2018).* Springer International Publishing, Cham, Switzerland, p. 377-382 (Chapter 60). (Springer Proceedings in Complexity ; 26). https://www.springer.com/gp/book/9783030220549.

Zabalegui, N., Manzi, M., Depoorter, A., Hayeck, N., Roveretto, M., Li, C., **van Pinxteren, M.**, **Herrmann, H.**, George, C. and Monge, M. E. 2020. Seawater analysis by ambient mass spectrometry-based seaomics. Atmos. Chem. Phys., **20**, 6243-6257. https://doi.org/10.5194/acp-20-6243-2020.

Zeng, J., Yu, Z., Mekic, M., Liu, J., Li, S., Loisel, G., Gao, W., Gandolfo, A., Zhou, Z., Wang, X., **Herrmann, H.**, Gligorovski, S. and Li, X. 2020. Evolution of indoor cooking emissions captured by using secondary electrospray ionization high-resolution mass spectrometry. Environ. Sci. & Technol. Lett., **7**, 76-81. https://dx.doi.org/10.1021/acs.estlett.0c00044.

Zeppenfeld, S., **van Pinxteren, M.**, Engel, A. and **Herrmann, H.** 2020. A protocol for quantifying mono- and polysaccharides in seawater and related saline matrices by electro-dialysis (ED) – Combined with HPAEC-PAD. Ocean Sci. (OS), **16**, 817-830. https://doi.org/10.5194/os-16-817-2020.

Zhao, J., Birmili, W., **Wehner, B.**, Daniels, A., **Weinhold, K.**, Wang, L., **Merkel, M.**, **Kecorius, S.**, **Tuch, T.**, Franck, U., Hussein, T. and **Wiedensohler, A.** 2020. Particle mass concentrations and number size distributions in 40 homes in Germany: Indoor-to-outdoor relationships, diurnal and seasonal variation. Aerosol Air Qual. Res., **20**, 576-589. https://doi.org/10.4209/aaqr.2019.09.0444.

Zhu, C., Li, J., Chen, H., Cheng, T., **Wen, L.**, **Herrmann, H.**, Xiao, H. and Chen, J. 2020. Inorganic composition and occult deposition of frost collected under severe polluted area in winter in the North China Plain. Sci. Total Environ., **722**, 137911. https://doi.org/10.1016/j.scitotenv.2020.137911.

Zhu, Y., **Tilgner, A.**, **Hoffmann, E. H.**, **Herrmann, H.**, Kawamura, K., Yang, L., Xue, L. and Wang, W. 2020. Multiphase MCM-CAPRAM modeling of the formation and processing of secondary aerosol constituents observed during the Mt. Tai summer campaign in 2014. Atmos. Chem. Phys., **20**, 6725-6747. https://doi.org/10.5194/acp-20-6725-2020.

Zhu, Z., Zhang, J., Lv, G., George, C., **Herrmann, H.**, Fu, H., Li, D., Zhang, L., Sun, X., Sun, H., Guan, X., Li, Q., Dong, W., Li, X., Wang, X., Wang, L., Yang, X., Liu, Q., Chen, J. and Jiang, G. 2020. Complexation of Fe(III)/Catechols in atmospheric aqueous phase and the consequent cytotoxicity assessment in human bronchial epithelial cells (BEAS-2B). Ecotox. Environ. Safe, **202**, 110898. https://doi.org/10.1016/j.ecoenv.2020.110898.

2021

Alas, H. D., Stöcker, A., Umlauf, N., **Senaweera, O.**, **Pfeifer, S.**, Greven, S. and **Wiedensohler, A.** 2021. Pedestrian exposure to black carbon and $PM_{2.5}$ emissions in urban hot spots: New findings using mobile measurement techniques and flexible Bayesian regression models. J. Expo. Sci. Env. Epid., 11 p. https://doi.org/10.1038/s41370-021-00379-5.

Alpert, P. A., Dou, J., Corral Arroyo, P., Schneider, F., Xto, J., Luo, B., Peter, T., Huthwelker, T., Borca, C. N., Henzler, K. D., **Schaefer, T.**, **Herrmann, H.**, Raabe, J., Watts, B., Krieger, U. K. and Ammann, M. 2021. Photolytic radical persistence due to anoxia in viscous aerosol particles. Nat. Commun., **12**, 1769. https://doi.org/10.1038/s41467-021-21913-x.

Ansmann, A., **Ohneiser, K.**, Chudnovsky, A., **Baars, H.** and **Engelmann, R.** 2021. CALIPSO Aerosol-typing scheme misclassified stratospheric fire smoke: Case study from the 2019 Siberian wildfire season. Front. Environ. Sci., **9**, 769852. https://doi.org/10.3389/fenvs.2021.769852.

Ansmann, A., **Ohneiser, K.**, Mamouri, R.-E., Knopf, D. A., Veselovskii, I., **Baars, H.**, **Engelmann, R.**, Foth, A., **Jimenez, C.**, **Seifert, P.** and Barja, B. 2021. Tropospheric and stratospheric wildfire smoke profiling with lidar: Mass, surface area, CCN, and INP retrieval. Atmos. Chem. Phys., **21**, 9779-9807. https://doi.org/10.5194/acp-21-9779-2021.

Asmi, E., Backman, J., Servomaa, H., Virkkula, A., Gini, M. I., Eleftheriadis, K., **Müller, T.**, Ohata, S., Kondo, Y. and Hyvärinen, A. 2021. Absorption instruments inter-comparison campaign at the Arctic Pallas station. Atmos. Meas. Tech., **14**, 5397-5413. https://doi.org/10.5194/amt-14-5397-2021.

Baars, H., **Radenz, M.**, **Floutsi, A. A.**, **Engelmann, R.**, **Althausen, D.**, **Heese, B.**, **Ansmann, A.**, Flamant, T., Dabas, A., Trapon, D., Reitebuch, O., Bley, S. and **Wandinger, U.** 2021. Californian wildfire smoke over Europe: A first example of the aerosol observing capabilities of Aeolus compared to ground-based lidar. Geophys. Res. Lett., **48**, e2020GL092194. https://doi.org/10.1029/2020GL092194.

Baars, H., **Yin, Z.** and **Radenz, M.** 2021. PollyNET/Pollynet_Processing_Chain: Version 2.1. Zenodo, http://doi.org/10.5281/zenodo.4694451.

Baccarini, A., Dommen, J., Lehtipalo, K., **Henning, S.**, Modini, R. L., Gysel-Beer, M., Baltensperger, U. and Schmale, J. 2021. Low-volatility vapors and new particle formation over the Southern Ocean during the Antarctic Circumnavigation Expedition. J. Geophys. Res. - Atmos., **126**, e2021JD035126. https://doi.org/10.1029/2021JD035126.

Barry, K. R., Hill, T. C. J., **Jentzsch, C.**, Moffet, B. F., **Stratmann, F.** and DeMott, P. J. 2021. Pragmatic protocols for working cleanly when measuring ice nucleating particles. Atmos. Res., **250**, 105419. https://doi.org/10.1016/j.atmosres.2020.105419.

Barth, M. C., Ervens, B., **Herrmann, H.**, **Tilgner, A.**, McNeill, V. F., Tsui, W. G., Deguillaume, L., Chaumerliac, N., Carlton, A. and Lance, S. M. 2021. Box model intercomparison of cloud chemistry. J. Geophys. Res. - Atmos., **126**, e2021JD035486 (34 pp.). https://doi.org/10.1029/2021JD035486.

Bauer, T. P., Holtermann, P., **Heinold, B.**, Radtke, H., **Knoth, O.** and Klingbeil, K. 2021. ICONGETM v1.0 – Flexible NUOPC-driven two-way coupling via ESMF exchange grids between the unstructured-grid atmosphere model ICON and the structured-grid coastal ocean model GETM. Geosci. Model Dev., **14**, 4843-4863. https://doi.org/10.5194/gmd-14-4843-2021.

Bauer, T. P. and **Knoth, O.** 2021. Extended multirate infinitesimal step methods: Derivation of order conditions. J. Comput. Appl. Math., **387**, 112541. https://doi.org/10.1016/j.cam.2019.112541.

Berndt, T. 2021. Peroxy radical processes and product formation in the OH radical-initiated oxidation of α-pinene for near-atmospheric conditions. J. Phys. Chem. A, **125**, 9151-9160. https://doi.org/10.1021/acs.jpca.1c05576.

Berndt, T., Møller, K. H., Kjaergaard, H. G. and **Herrmann, H.** 2021. Trimethylamine outruns terpenes and aromatics in atmospheric autoxidation. J. Phys. Chem. A, **125**, 4454-4466. https://doi.org/10.1021/acs.jpca.1c02465.

Bousiotis, D., Brean, J., Pope, F. D., Dall'Osto, M., Querol, X., Alastuey, A., Perez, N., Petäjä, T., Massling, A., Nøjgaard, J., K., Nordstrøm, C., Kouvarakis, G., Vratolis, S., Eleftheriadis, K., Niemi, J. V., Portin, H., **Wiedensohler, A.**, **Weinhold, K.**, **Merkel, M.**, **Tuch, T.** and Harrison, R. M. 2021. The effect of meteorological conditions and atmospheric composition in the occurrence and development of new particle formation (NPF) events in Europe. Atmos. Chem. Phys., **21**, 3345-3370. https://doi.org/10.5194/acp-21-3345-2021.

Braga, R. C., Ervens, B., Rosenfeld, D., Andreae, M. O., Förster, J.-D., Fütterer, D., Hernández Pardo, L., Holanda, B. A., Jurkat-Witschas, T., Krüger, O. O., Lauer, O., Machado, L. A. T., Pöhlker, C., Sauer, D., Voigt, C., Walser, A., Wendisch, M., Pöschl, U. and **Pöhlker, M. L.** 2021. Cloud droplet formation at the base of tropical convective clouds: Closure between modeling and measurement results of ACRIDICON–CHUVA. Atmos. Chem. Phys., **21**, 17513-17528. https://doi.org/10.5194/acp-21-17513-2021.

Breitner, S., Su, C., Franck, U., **Wiedensohler, A.**, Cyrys, J., Pan, X., Wichmann, H.-E., Schneider, A. and Peters, A. 2021. The association between particulate air pollution and respiratory mortality in Beijing before, during, and after the 2008 Olympic and Paralympic Games. Front. Environ. Sci., **9**, 624180. https://doi.org/10.3389/fenvs.2021.624180.

Bressi, M., Cavalli, F., Putaud, J. P., Fröhlich, R., Petit, J. E., Aas, W., Äijälä, M., Alastuey, A., Allan, J. D., Aurela, M., Berico, M., Bougiatioti, A., Bukowiecki, N., Canonaco, F., Crenn, V., Dusanter, S., Ehn, M., Elsasser, M., Flentje, H., Graf, P., Green, D. C., Heikkinen, L., **Herrmann, H.**, Holzinger, R., Hueglin, C., Keernik, H., Kiendler-Scharr, A., Kubelová, L., Lunder, C., Maasikmets, M., Makeš, O., Malaguti, A., Mihalopoulos, N., Nicolas, J. B., O'Dowd, C., Ovadnevaite, J., Petralia, E., **Poulain, L.**, Priestman, M., Riffault, V., Ripoll, A., Schlag, P., Schwarz, J., Sciare, J., Slowik, J., Sosedova, Y., Stavroulas, I., Teinemaa, E., Via, M., Vodička, P., Williams, P. I., **Wiedensohler, A.**, Young, D. E., Zhang, S., Favez, O., Minguillón, M. C. and Prevot, A. S. H. 2021. A European aerosol phenomenology - 7: High-time resolution chemical characteristics of submicron particulate matter across Europe. Atmos. Environ.: X, **10**, 100108. https://doi.org/10.1016/j.aeaoa.2021.100108.

Brüggemann, M., Riva, M., Perrier, S., **Poulain, L.**, George, C. and **Herrmann, H.** 2021. Overestimation of monoterpene organosulfate abundance in aerosol particles by sampling in the presence of SO_2. Environ. Sci. & Technol. Lett., **8**, 206-211. https://dx.doi.org/10.1021/acs.estlett.0c00814.

Bulatovic, I., Igel, A. L., Leck, C., **Heintzenberg, J.**, Riipinen, I. and Ekman, A. M. L. 2021. The importance of Aitken mode aerosol particles for cloud sustenance in the summertime high Arctic - a simulation study supported by observational data. Atmos. Chem. Phys., **21**, 3871-3897. https://doi.org/10.5194/acp-21-3871-2021.

Chen, J., **Berndt, T.**, Møller, K. H., Lane, J. R. and Kjaergaard, H. G. 2021. Atmospheric fate of the CH_3SOO Radical from the $CH_3S + O_2$ equilibrium. J. Phys. Chem. A, **125**, 8933-8941. https://doi.org/10.1021/acs.jpca.1c06900.

Chen, J., Wu, Z. J., Zhao, X., Wang, Y. J., Chen, J. C., Qiu, Y. T., Zong, T. M., Chen, H. X., Wang, B. B., Lin, P., Liu, W., Guo, S., Yao, M. S., Zeng, L. M., **Wex, H.**, Liu, X., Hu, M. and Li, S. M. 2021. Atmospheric humic-like substances (HULIS) act as ice-nucleating particles. Geophys. Res. Lett., **48**, e2021GL092443. https://doi.org/10.1029/2021GL092443.

Córdoba-Jabonero, C., **Ansmann, A.**, **Jimenez, C.**, **Baars, H.**, López-Cayuela, M.-Á. and **Engelmann, R.** 2021. Experimental assessment of a micro-pulse lidar system in comparison with reference lidar measurements for aerosol optical properties retrieval. Atmos. Meas. Tech., **14**, 5225-5239. https://doi.org/10.5194/amt-14-5225-2021.

Cox, R. A., Ammann, M., Crowley, J. N., Griffiths, P. T., **Herrmann, H.**, **Hoffmann, E. H.**, Jenkin, M. E., McNeill, V. F., Mellouki, A., Penkett, C. J., **Tilgner, A.** and Wallington, T. J. 2021. Opinion: The germicidal effect of ambient air (open air factor) revisited. Atmos. Chem. Phys., **21**, 13011-13018. https://doi.org/10.5194/acp-21-13011-2021.

Cuesta-Mosquera, A., Močnik, G., Drinovec, L., **Müller, T.**, **Pfeifer, S.**, Minguillón, M. C., Briel, B., Buckley, P., Dudoitis, V., Fernández-García, J., Fernández-Amado, M., Ferreira De Brito, J., Riffault, V., Flentje, H., Heffernan, E., Kalivitis, N., Kalogridis, A. C., Keernik, H., Marmureanu, L., Luoma, K., Marinoni, A., Pikridas, M., Schauer, G., Serfozo, N., Servomaa, H., Titos, G., Yus-Díez, J., Zioła, N. and **Wiedensohler, A.** 2021. Intercomparison and characterization of 23 Aethalometers under laboratory and ambient air conditions: Procedures and unit-to-unit variabilities. Atmos. Meas. Tech., **14**, 3195-3216. https://doi.org/10.5194/amt-14-3195-2021.

Deabji, N., **Fomba, K. W.**, El Hajjaji, S., Mellouki, A., **Poulain, L.**, **Zeppenfeld, S.** and **Herrmann, H.** 2021. First insights into Northern Africa high-altitude background aerosol chemical composition and source influences. Atmos. Chem. Phys., **21**, 18147-18174. https://doi.org/10.5194/acp-21-18147-2021.

Deneke, H., **Barrientos-Velasco, C.**, Bley, S., **Hünerbein, A.**, **Lenk, S.**, **Macke, A.**, Meirink, J. F., Schroedter-Homscheidt, M., **Senf, F.**, Wang, P., Werner, F. and **Witthuhn, J.** 2021. Increasing the spatial resolution of cloud property retrievals from Meteosat SEVIRI by use of its high-resolution visible channel: Implementation and examples. Atmos. Meas. Tech., **14**, 5107-5126. https://doi.org/10.5194/amt-14-5107-2021.

Dinoi, A., **Weinhold, K.**, **Wiedensohler, A.** and Contini, D. 2021. Study of new particle formation events in southern Italy. Atmos. Environ., **244**, 117920. https://doi.org/10.1016/j.atmosenv.2020.117920.

Dou, J., Alpert, P. A., Corral Arroyo, P., Luo, B., Schneider, F., Xto, J., Huthwelker, T., Borca, C. N., Henzler, K. D., Raabe, J., Watts, B., **Herrmann, H.**, Peter, T., Ammann, M. and Krieger, U. K. 2021. Photochemical degradation of iron(III) citrate/citric acid aerosol quantified with the combination of three complementary experimental techniques and a kinetic process model. Atmos. Chem. Phys., **21**, 315-338. https://doi.org/10.5194/acp-21-315-2021.

Düsing, S., **Ansmann, A.**, **Baars, H.**, Corbin, J. C., **Denjean, C.**, Gysel-Beer, M., **Müller, T.**, **Poulain, L.**, **Siebert, H.**, **Spindler, G.**, **Tuch, T.**, **Wehner, B.** and **Wiedensohler, A.** 2021. Measurement report: Comparison of airborne, in situ measured, lidar-based, and modeled aerosol optical properties in the central European background – identifying sources of deviations. Atmos. Chem. Phys., **21**, 16745-16773. https://doi.org/10.5194/acp-21-16745-2021.

Egerer, U., Ehrlich, A., Gottschalk, M., **Griesche, H.**, Neggers, R. A. J., **Siebert, H.** and Wendisch, M. 2021. Case study of a humidity layer above Arctic stratocumulus and potential turbulent coupling with the cloud top. Atmos. Chem. Phys., **21**, 6347-6364. https://doi.org/10.5194/acp-21-6347-2021.

Engelmann, R., **Ansmann, A.**, **Ohneiser, K.**, **Griesche, H.**, **Radenz, M.**, **Hofer, J.**, **Althausen, D.**, Dahlke, S., Maturilli, M., Veselovskii, I., **Jimenez, C.**, **Wiesen, R.**, **Baars, H.**, **Bühl, J.**, **Gebauer, H.**, **Haarig, M.**, **Seifert, P.**, **Wandinger, U.** and **Macke, A.** 2021. Wildfire smoke, Arctic haze, and aerosol effects on mixed-phase and cirrus clouds over the North Pole region during MOSAiC: An introduction. Atmos. Chem. Phys., **21**, 13397-13423. https://doi.org/10.5194/acp-21-13397-2021.

Evangeliou, N., Platt, S. M., Eckhardt, S., Lund Myrhe, C., Laj, P., Alados-Arboledas, L., Backman, J., Brem, B. T., Fiebig, M., Flentje, H., Marinoni, A., Pandolfi, M., Yus-Dìez, J., Prats, N., Putaud, J. P., Sellegri, K., Sorribas, M., Eleftheriadis, K., Vratolis, S., **Wiedensohler, A.** and Stohl, A. 2021. Changes in black carbon emissions over Europe due to COVID-19 lockdowns. Atmos. Chem. Phys., **21**, 2675-2692. https://doi.org/10.5194/acp-21-2675-2021.

Fadnavis, S., Sabin, T. P., Rap, A., Müller, R., **Kubin, A.** and **Heinold, B.** 2021. The impact of COVID-19 lockdown measures on the Indian summer monsoon. Environ. Res. Lett., **16**, 074054. http://dx.doi.org/10.1088/1748-9326/ac109c.

Faust, M., **Wolke, R.**, Münch, S., Funk, R. and **Schepanski, K.** 2021. A new Lagrangian in-time particle simulation module (ltpas v1) for atmospheric particle dispersion. Geosci. Model Dev., **14**, 2205-2220. https://doi.org/10.5194/gmd-14-2205-2021.

Felber, T., **Schaefer, T.**, **He, L.** and **Herrmann, H.** 2021. Aromatic carbonyl and nitro compounds as photosensitizers and their photophysical properties in the tropospheric aqueous phase. J. Phys. Chem. A, **125**, 5078-5095. https://doi.org/10.1021/acs.jpca.1c03503.

Floutsi, A. A., **Baars, H.**, **Radenz, M.**, **Haarig, M.**, **Yin, Z.**, **Seifert, P.**, **Jimenez, C.**, **Ansmann, A.**, **Engelmann, R.**, Barja, B., Zamorano, F. and **Wandinger, U.** 2021. Advection of biomass burning aerosols towards the

southern hemispheric mid-latitude station of Punta Arenas as observed with multiwavelength polarization Raman lidar. Remote Sens., **13**, 138. https://doi.org/10.3390/rs13010138.

Foken, T., **Hellmuth, O.**, Huwe, B. and Sonntag, D. 2021. Physical quantities (Chapter 5). *In: T. Foken (Ed.) Springer handbook of atmospheric measurements*. Springer, Cham, p. 107-152. (Springer Handbooks). https://link.springer.com/book/10.1007/978-3-030-52171-4.

Fountoulakis, I., Kosmopoulos, P., Papachristopoulou, K., Raptis, I.-P., Mamouri, R.-E., Nisantzi, A., Gkikas, A., **Witthuhn, J.**, **Bley, S.**, Moustaka, A., **Buehl, J.**, **Seifert, P.**, Hadjimitsis, D. G., Kontoes, C. and Kazadzis, S. 2021. Effects of aerosols and clouds on the levels of surface solar radiation and solar energy in Cyprus. Remote Sens., **13**, 2319. https://doi.org/10.3390/rs13122319.

Galmarini, S., Makar, P., Clifton, O., Hogrefe, C., Bash, J., Bellasio, R., Bianconi, R., Bieser, J., Butler, T., Ducker, J., Flemming, J., Hozdic, A., Holmes, C., Kioutsioukis, I., Kranenburg, R., Lupascu, A., Perez-Camanyo, J. L., Pleim, J., Ryu, Y.-H., San Jose, R., Schwede, D., Silva, S. and **Wolke, R.** 2021. Technical Note: AQMEII4 Activity 1: Evaluation of wet and dry deposition schemes as an integral part of regional-scale air quality models. Atmos. Chem. Phys., **21**, 15663-15697. https://doi.org/10.5194/acp-21-15663-2021.

Gerling, L., **Wiedensohler, A.** and Weber, S. 2021. Statistical modelling of spatial and temporal variation in urban particle number size distribution at traffic and background sites. Atmos. Environ., **244**, 117925. https://doi.org/10.1016/j.atmosenv.2020.117925.

Görner, C., Franke, J., Kronenberg, R., **Hellmuth, O.** and Bernhofer, C. 2021. Multivariate non-parametric Euclidean distance model for hourly disaggregation of daily climate data. Theor. Appl. Climatol., **143**, 241-265. https://doi.org/10.1007/s00704-020-03426-7.

Gottschalk, M. and **Egerer, U.** 2021. Tethered balloon-borne measurements of turbulence and radiation during the Arctic field campaign Arctic Ocean 2018 in August/ September 2018. *Data from:* Arctic Amplification (AC3); Microbiology-Ocean-Cloud-Coupling in the High Arctic (MOCCHA). *PANGAEA*, https://doi.org/10.1594/PANGAEA.927100.

Griesche, H., **Ohneiser, K.**, **Seifert, P.**, **Radenz, M.**, **Engelmann, R.** and **Ansmann, A.** 2021. Contrasting ice formation in Arctic clouds: Surface-coupled vs. surface-decoupled clouds. Atmos. Chem. Phys., **21**, 10357-10374. https://doi.org/10.5194/acp-21-10357-2021.

Hamzeh, N. H., Karami, S., Kaskaoutis, D. G., **Tegen, I.**, Moradi, M. and Opp, C. 2021. Atmospheric dynamics and numerical simulations of six frontal dust storms in the Middle East region. Atmosphere, **12**, 125 (27 pp.). https://doi.org/10.3390/atmos12010125.

Han, R., Yu, C., Tang, X., Yu, S., Song, M., Shen, F., Fu, P., Hu, W., Du, L., Wang, X., **Herrmann, H.** and Wu, Y. 2021. Release of inhalable particles and viable microbes to the air during packaging peeling: Emission profiles and mechanisms. Environ. Pollut., **285**, 117338. https://doi.org/10.1016/j.envpol.2021.117338.

Hartmann, M., **Gong, X.**, **Kecorius, S.**, **van Pinxteren, M.**, **Vogl, T.**, **Welti, A.**, **Wex, H.**, **Zeppenfeld, S.**, **Herrmann, H.**, **Wiedensohler, A.** and **Stratmann, F.** 2021. Terrestrial or marine – indications towards the origin of ice-nucleating particles during melt season in the European Arctic up to 83.7° N. Atmos. Chem. Phys., **21**, 11613-11636. https://doi.org/10.5194/acp-21-11613-2021.

Heinold, B., **Baars, H.**, Barja, B., **Kubin, A.**, **Ohneiser, K.**, **Schepanski, K.**, **Senf, F.**, **Schrödner, R.**, **Villanueva, D.** and **Tegen, I.** 2021. Data for paper publication 'Extreme 2019-2020 Australian wildfires substantially perturbed Earth's radiation budget' (Version v1.0) [Data set]. *Data from: Zenodo*, http://doi.org/10.5281/zenodo.4550846.

Heinold, B., **Weger, M.**, **Knoth, O.**, **Schrödner, R.**, **Müller, T.** and **Tõnisson, L.** 2021. High-resolution air-quality modeling in urban areas – A case study for the City of Leipzig. *In: C. Mensink and V. Matthias (Eds.), Air pollution modeling and its application XXVII : Proceedings of the 37th International Technical Meeting on Air Pollution Modelling and Its Application (Hamburg, Germany, 23-27 September 2019)*. Springer International Publishing, Cham, Switzerland, p. 277-282. (Springer Proceedings in Complexity). https://link.springer.com/chapter/10.1007/978-3-662-63760-9_39.

Hellmuth, O., Feistel, R. and Foken, T. 2021. Intercomparison of different state-of-the-art formulations of the mass density of humid air. Bull. Atmos. Sci. Tech., **2**, 13. https://doi.org/10.1007/s42865-021-00036-7.

Hoffmann, E. H., **Heinold, B.**, **Kubin, A.**, **Tegen, I.** and **Herrmann, H.** 2021. The importance of the representation of DMS oxidation in global chemistry-climate simulations. Geophys. Res. Lett., **48**, e2021GL094068. https://doi.org/10.1029/2021GL094068.

Kabisch, N., Kraemer, R., Brenck, M. E., Haase, D., Lausch, A., **Luttkus, M. L.**, **Müller, T.**, Remmler, P., von Döhren, P., **Voigtländer, J.** and Bumberger, J. 2021. A methodological framework for the assessment of

regulating and recreational ecosystem services in urban parks under heat and drought conditions. Ecosyst. People, **17**, 464-475. https://doi.org/10.1080/26395916.2021.1958062.

Keeble, J., Hassler, B., Banerjee, A., Checa-Garcia, R., Chiodo, G., Davis, S., Eyring, V., Griffiths, P. T., Morgenstern, O., Nowack, P., Zeng, G., Zhang, J., Bodeker, G., Burrows, S., Cameron-Smith, P., Cugnet, D., Danek, C., Deushi, M., Horowitz, L. W., **Kubin, A.**, Li, L., Lohmann, G., Michou, M., Mills, M. J., Nabat, P., Olivié, D., Park, S., Seland, Ø., **Stoll, J.**, Wieners, K. H. and Wu, T. 2021. Evaluating stratospheric ozone and water vapour changes in CMIP6 models from 1850 to 2100. Atmos. Chem. Phys., **21**, 5015-5061. https://doi.org/10.5194/acp-21-5015-2021.

Kezoudi, M., Tesche, M., Smith, H., Tsekeri, A., **Baars, H.**, Dollner, M., Estellés, V., **Bühl, J.**, Weinzierl, B., Ulanowski, Z., Müller, D. and Amiridis, V. 2021. Measurement report: Balloon-borne in situ profiling of Saharan dust over Cyprus with the UCASS optical particle counter. Atmos. Chem. Phys., **21**, 6781-6797. https://doi.org/10.5194/acp-21-6781-2021.

Kroflič, A., **Anders, J.**, Drventić, I., **Mettke, P.**, **Böge, O.**, **Mutzel, A.**, Kleffmann, J. and **Herrmann, H.** 2021. Guaiacol nitration in a simulated atmospheric aerosol with an emphasis on atmospheric nitrophenol formation mechanisms. ACS Earth Space Chem., **5**, 1083-1093. https://doi.org/10.1021/acsearthspacechem.1c00014.

Kwiezinski, C., Weller, C., **van Pinxteren, D.**, **Brüggemann, M.**, **Mertes, S.**, **Stratmann, F.** and **Herrmann, H.** 2021. Determination of highly polar compounds in atmospheric aerosol particles at ultra-trace levels using ion chromatography Orbitrap mass spectrometry. J. Sep. Sci., **44**, 2343-2357. https://doi.org/10.1002/jssc.202001048.

Lacher, L., Clemen, H.-C., Shen, X., **Mertes, S.**, Gysel-Beer, M., Moallemi, A., Steinbacher, M., Henne, S., Saathoff, H., Möhler, O., Höhler, K., Schiebel, T., Weber, D., Schrod, J., Schneider, J. and Kanji, Z. A. 2021. Sources and nature of ice-nucleating particles in the free troposphere at Jungfraujoch in winter 2017. Atmospheric Chemistry and Physics **21**, 16925-16953. https://doi.org/10.5194/acp-21-16925-2021.

Liu, P., Ye, C., Zhang, C., He, G., Xue, C., Liu, J., Liu, C., Zhang, Y., Song, Y., Li, X., Wang, X., Chen, J., He, H., **Herrmann, H.** and Mu, Y. 2021. Photochemical aging of atmospheric fine particles as a potential source for gas-phase hydrogen peroxide. Environ. Sci. Technol., https://doi.org/10.1021/acs.est.1c04453.

Luttkus, M. L., **Wolke, R.**, **Heinold, B.**, **Tilgner, A.**, **Poulain, L.** and **Herrmann, H.** 2021. Biogenic emissions and urban air quality. *In: C. Mensink and V. Matthias (Eds.), Air pollution modeling and its application XXVII : Proceedings of the 37th International Technical Meeting on Air Pollution Modelling and Its Application (Hamburg, Germany, 23-27 September 2019)*. Springer International Publishing, Cham, Switzerland, p. 11-17. (Springer Proceedings in Complexity). https://link.springer.com/chapter/10.1007%2F978-3-662-63760-9_2.

Macke, A., **Tõnisson, L.**, **Voigtländer, J.**, **Assmann, D.**, **Heese, B.**, **Müller, T.**, **Heinold, B.**, **Knoth, O.**, **Käthner, R.** and **Arnhold, T.** 2021. *Abschlussbericht zum Verbundprojekt WTimpact – Kollaborative Wissensentwicklung als Transferinstrument: Vom Wissenstransfer zum Wissensaustausch*. Teilprojekt: „Luft Leipzig“ von “WTimpact“ – Citizen Science als Instrument für den Wissenstransfer (Förderkennzeichen: 01LE1903A). 32.

Marinou, E., Voudouri, K. A., Tsikoudi, I., Drakaki, E., Tsekeri, A., Rosoldi, M., Ene, D., **Baars, H.**, O'Connor, E., Amiridis, V. and Meleti, C. 2021. Geometrical and microphysical properties of clouds formed in the presence of dust above the Eastern Mediterranean. Remote Sens., **13**, 5001. https://doi.org/10.3390/rs13245001.

Meilinger, S., Herman-Czezuch, A., Kimiaie, N., Schirrmeister, C., Yousif, R., Geiss, S., Scheck, L., Weissmann, M., Gödde, F., Mayer, B., Zinner, T., Barry, J., Pfeilsticker, K., Kraiczy, M., Winter, K., Altayara, A., Reise, C., Rivera, M., **Deneke, H.**, **Witthuhn, J.**, Betcke, J., Schroedter-Homscheidt, M., Hofbauer, P. and Rindt, B. 2021. *Entwicklung innovativer satellitengestützter Methoden zur verbesserten PV-Ertragsvorhersage auf verschiedenen Zeitskalen für Anwendungen auf Verteilnetzebene : Schlussbericht*. Hochschule Bonn-Rhein-Sieg (Förderkennzeichen: 0350009A-G). Bonn. XVII, 180. https://doi.org/10.18418/opus-5955.

Mellouki, A., Ammann, M., Cox, R. A., Crowley, J. N., **Herrmann, H.**, Jenkin, M. E., McNeill, V. F., Troe, J. and Wallington, T. J. 2021. Evaluated kinetic and photochemical data for atmospheric chemistry: Volume VIII - gas-phase reactions of organic species with four, or more, carbon atoms (≥ C_4). Atmos. Chem. Phys., **21**, 4797-4808. https://doi.org/10.5194/acp-21-4797-2021.

Moallemi, A., Landwehr, S., Robinson, C. M., Simó, R., Zamanillo, M., Chen, G., Baccarini, A., Schnaiter, M., **Henning, S.**, Modini, R. L., Gysel-Beer, M. and Schmale, J. 2021. Sources, occurrence and characteristics of fluorescent biological aerosol particles measured over the pristine Southern Ocean. J. Geophys. Res. - Atmos., **126**, e2021JD034811. https://doi.org/10.1029/2021JD034811.

Modini, R. L., Corbin, J. C., Brem, B. T., Irwin, M., Bertò, M., Pileci, R. E., Fetfatzis, P., Eleftheriadis, K., Henzing, B., Moerman, M. M., Liu, F., **Müller, T.** and Gysel-Beer, M. 2021. Detailed characterization of the CAPS

single-scattering albedo monitor (CAPS PMssa) as a field-deployable instrument for measuring aerosol light absorption with the extinction-minus-scattering method. Atmos. Meas. Tech., **14**, 819-851. https://doi.org/10.5194/amt-14-819-2021.

Mutzel, A., **Zhang, Y.**, **Böge, O.**, **Rodigast, M.**, **Kolodziejczyk, A.**, Wang, X. and **Herrmann, H.** 2021. Importance of secondary organic aerosol formation of α-pinene, limonene and *m*-cresol comparing day- and nighttime radical chemistry. Atmos. Chem. Phys., **21**, 8479-8498. https://doi.org/10.5194/acp-21-8479-2021.

Mylonaki, M., Giannakaki, E., Papayannis, A., Papanikolaou, C.-A., Komppula, M., Nicolae, D., Papagiannopoulos, N., Amodeo, A., **Baars, H.** and Soupiona, O. 2021. Aerosol type classification analysis using EARLINET multiwavelength and depolarization lidar observations. Atmos. Chem. Phys., **21**, 2211-2227. https://doi.org/10.5194/acp-21-2211-2021.

Nowak, J. L., **Siebert, H.**, **Szodry, K.-E.** and Malinowski, S. P. 2021. Coupled and decoupled stratocumulus-topped boundary layers: Turbulence properties. Atmos. Chem. Phys., **21**, 10965-10991. https://doi.org/10.5194/acp-21-10965-2021.

Ohneiser, K., **Ansmann, A.**, Chudnovsky, A., **Engelmann, R.**, Ritter, C., Veselovskii, I., **Baars, H.**, **Gebauer, H.**, **Griesche, H.**, **Radenz, M.**, **Hofer, J.**, **Althausen, D.**, Dahlke, S. and Maturilli, M. 2021. The unexpected smoke layer in the High Arctic winter stratosphere during MOSAiC 2019–2020. Atmos. Chem. Phys., **21**, 15783-15808. https://doi.org/10.5194/acp-21-15783-2021.

Pileci, R. E., Modini, R. L., Bertò, M., Yuan, J., Corbin, J. C., Marinoni, A., Henzing, B., Moerman, M. M., Putaud, J. P., **Spindler, G.**, **Wehner, B.**, **Müller, T.**, **Tuch, T.**, Trentini, A., Zanatta, M., Baltensperger, U. and Gysel-Beer, M. 2021. Comparison of co-located refractory black carbon (rBC) and elemental carbon (EC) mass concentration measurements during field campaigns at several European sites. Atmos. Meas. Tech., **14**, 1379-1403. https://doi.org/10.5194/amt-14-1379-2021.

Poulain, L., **Fahlbusch, B.**, **Spindler, G.**, **Müller, K.**, **van Pinxteren, D.**, **Wu, Z.**, **Iinuma, Y.**, **Birmili, W.**, **Wiedensohler, A.** and **Herrmann, H.** 2021. Source apportionment and impact of long-range transport on carbonaceous aerosol particles in Central Germany during HCCT-2010. Atmos. Chem. Phys., **21**, 3667-3684. https://doi.org/10.5194/acp-21-3667-2021.

Radenz, M., **Bühl, J.**, **Seifert, P.**, **Baars, H.**, **Engelmann, R.**, Barja González, B., Mamouri, R.-E., Zamorano, F. and **Ansmann, A.** 2021. Hemispheric contrasts in ice formation in stratiform mixed-phase clouds: Disentangling the role of aerosol and dynamics with ground-based remote sensing. Atmos. Chem. Phys., **21**, 17969-17994. https://doi.org/10.5194/acp-21-17969-2021.

Radenz, M., **Seifert, P.**, **Baars, H.**, **Floutsi, A. A.**, **Yin, Z.** and **Bühl, J.** 2021. Automated time-height-resolved airmass source attribution for profiling remote sensing applications. Atmos. Chem. Phys., **21**, 3015-3033. https://doi.org/10.5194/acp-21-3015-2021.

Ramelli, F., Henneberger, J., David, R. O., **Bühl, J.**, **Radenz, M.**, **Seifert, P.**, Wieder, J., Lauber, A., Pasquier, J. T., **Engelmann, R.**, Mignani, C., Hervo, M. and Lohmann, U. 2021. Microphysical investigation of the seeder and feeder region of an Alpine mixed-phase cloud. Atmos. Chem. Phys., **21**, 6681-6706. https://doi.org/10.5194/acp-21-6681-2021.

Ramelli, F., Henneberger, J., David, R. O., Lauber, A., Pasquier, J. T., Wieder, J., **Bühl, J.**, **Seifert, P.**, **Engelmann, R.**, Hervo, M. and Lohmann, U. 2021. Influence of low-level blocking and turbulence on the microphysics of a mixed-phase cloud in an inner-Alpine valley. Atmos. Chem. Phys., **21**, 5151-5172. https://doi.org/10.5194/acp-21-5151-2021.

Rogozovsky, I., **Ansmann, A.**, **Althausen, D.**, **Heese, B.**, **Engelmann, R.**, **Hofer, J.**, **Baars, H.**, Schechner, Y., Lyapustin, A. and Chudnovsky, A. 2021. Impact of aerosol layering, complex aerosol mixing, and cloud coverage on high-resolution MAIAC aerosol optical depth measurements: Fusion of lidar, AERONET, satellite, and ground-based measurements. Atmos. Environ., **247**, 118163. https://doi.org/10.1016/j.atmosenv.2020.118163.

Romshoo, B., **Müller, T.**, **Pfeifer, S.**, Saturno, J., Nowak, A., Ciupek, K., Quincey, P. and **Wiedensohler, A.** 2021. Optical properties of coated black carbon aggregates: Numerical simulations, radiative forcing estimates, and size-resolved parameterization scheme. Atmos. Chem. Phys., **21**, 12989-13010. https://doi.org/10.5194/acp-21-12989-2021.

Rose, C., Collaud Coen, M., Andrews, E., Lin, Y., Bossert, I., Lund Myhre, C., **Tuch, T.**, **Wiedensohler, A.**, Fiebig, M., Aalto, P., Alastuey, A., Alonso-Blanco, E., Andrade, M., Artíñano, B., Arsov, T., Baltensperger, U., Bastian, S., Bath, O., Beukes, J. P., Brem, B. T., Bukowiecki, N., Casquero-Vera, J. A., Conil, S., Eleftheriadis, K., Favez, O., Flentje, H., Gini, M. I., Gómez-Moreno, F. J., Gysel-Beer, M., Hallar, A. G., Kalapov, I., Kalivitis, N., Kasper-Giebl, A., Keywood, M., Kim, J. E., Kim, S. W., Kristensson, A., Kulmala, M., Lihavainen, H.,

Lin, N. H., Lyamani, H., Marinoni, A., Martins Dos Santos, S., Mayol-Bracero, O. L., Meinhardt, F., **Merkel, M.**, Metzger, J. M., Mihalopoulos, N., Ondracek, J., Pandolfi, M., Pérez, N., Petäjä, T., Petit, J. E., Picard, D., Pichon, J. M., Pont, V., Putaud, J. P., Reisen, F., Sellegri, K., Sharma, S., Schauer, G., Sheridan, P., Sherman, J. P., Schwerin, A., Sohmer, R., Sorribas, M., Sun, J., Tulet, P., Vakkari, V., van Zyl, P. G., Velarde, F., Villani, P., Vratolis, S., Wagner, Z., Wang, S. H., **Weinhold, K.**, Weller, R., Yela, M., Zdimal, V. and Laj, P. 2021. Seasonality of the particle number concentration and size distribution: a global analysis retrieved from the network of Global Atmosphere Watch (GAW) near-surface observatories. Atmos. Chem. Phys., **21**, 17185-17223. https://doi.org/10.5194/acp-21-17185-2021.

Sarang, K., **Otto, T.**, Rudzinski, K., **Schaefer, T.**, Grgić, I., Nestorowicz, K., **Herrmann, H.** and Szmigielski, R. 2021. Reaction kinetics of Green Leaf Volatiles with sulfate, hydroxyl, and nitrate radicals in tropospheric aqueous phase. Environ. Sci. Technol., **55**, 13666-13676. https://doi.org/10.1021/acs.est.1c03276.

Schrödner, R., Genz, C., **Heinold, B.**, **Baars, H.** and **Wolke, R.** 2021. Estimating aerosol loads and aerosol-cloud-interaction in the 1980s and today. *In: C. Mensink and V. Matthias (Eds.), Air pollution modeling and its application XXVII : Proceedings of the 37th International Technical Meeting on Air Pollution Modelling and Its Application (Hamburg, Germany, 23-27 September 2019)*. Springer International Publishing, Cham, Switzerland, p. 25-30. (Springer Proceedings in Complexity). https://link.springer.com/chapter/10.1007/978-3-662-63760-9_4.

Seelig, T., **Deneke, H.**, Quaas, J. and Tesche, M. 2021. Life cycle of shallow marine cumulus clouds from geostationary satellite observations. J. Geophys. Res. - Atmos., **126**, e2021JD035577. https://doi.org/10.1029/2021JD035577.

Senf, F. 2021. Radar Precipitation Estimates (Radolan RW product) interpolated onto LfULG Stations Saxony [Data set]. Zenodo, https://doi.org/10.5281/zenodo.5113375.

Senf, F. 2021. Additional Data for Revision 1: Post-Processed Simulation Data of ICON-LEM-DE Absorbing Aerosol Perturbation Experiments. *Data from: World Data Center for Climate (WDCC) at DKRZ*, http://cera-www.dkrz.de/WDCC/ui/Compact.jsp?acronym=DKRZ_LTA_1174_ds00002.

Senf, F., **Heinold, B.**, **Tegen, I.** and **Villanueva, D.** 2021. Course Material for "ComputerLab - Atmospheric models: Scales and Parameterizations", University Leipzig. Zenodo, https://doi.org/10.5281/zenodo.5533794.

Senf, F., Quaas, J. and **Tegen, I.** 2021. Absorbing aerosol decreases cloud cover in cloud-resolving simulations over Germany. Q. J. Roy. Meteor. Soc., **147**, 4083-4100. https://doi.org/10.1002/qj.4169.

Siebert, H., **Szodry, K.-E.**, **Egerer, U.**, **Wehner, B.**, **Henning, S.**, **Chevalier, K.**, **Lückerath, J.**, **Welz, O.**, **Weinhold, K.**, Lauermann, F., Gottschalk, M., Ehrlich, A., Wendisch, M., Fialho, P., Roberts, G., Allwayin, N., Schum, S., Shaw, R. A., Mazzoleni, C., Mazzoleni, L., Nowak, J. L., Malinowski, S., Karpinska, K., Kumala, W., Czyzewska, D., Luke, E. P., Kollias, P., Wood, R. and Mellado, J. P. 2021. Observations of aerosol, cloud, turbulence and radiation properties at the top of the marine boundary layer over the Eastern North Atlantic Ocean: The ACORES campaign. Bull. Amer. Meteor. Soc., **102**, E123-E147. https://doi.org/10.1175/BAMS-D-19-0191.1.

Sonntag, D., Foken, T., Vömel, H. and **Hellmuth, O.** 2021. Humidity sensors (Chapter 8). *In: T. Foken (Ed.) Springer handbook of atmospheric measurements*. Springer, Cham, p. 209-241. (Springer Handbooks). https://link.springer.com/book/10.1007/978-3-030-52171-4.

Stevens, B., Bony, S., Farrell, D., Ament, F., Blyth, A., Fairall, C., Karstensen, J., Quinn, P. K., Speich, S., Acquistapace, C., Aemisegger, F., Albright, A. L., Bellenger, H., Bodenschatz, E., Caesar, K. A., Chewitt-Lucas, R., de Boer, G., Delanoë, J., Denby, L., Ewald, F., Fildier, B., Forde, M., George, G., Gross, S., Hagen, M., Hausold, A., Heywood, K. J., Hirsch, L., Jacob, M., Jansen, F., Kinne, S., Klocke, D., Kölling, T., Konow, H., Lothon, M., Mohr, W., Naumann, A. K., Nuijens, L., Olivier, L., Pincus, R., Pöhlker, M., Reverdin, G., Roberts, G., Schnitt, S., Schulz, H., Siebesma, A. P., Stephan, C. C., Sullivan, P., Touzé-Peiffer, L., Vial, J., Vogel, R., Zuidema, P., Alexander, N., Alves, L., Arixi, S., Asmath, H., Bagheri, G., Baier, K., Bailey, A., Baranowski, D., Baron, A., Barrau, S., Barrett, P. A., Batier, F., Behrendt, A., Bendinger, A., Beucher, F., Bigorre, S., Blades, E., Blossey, P., Bock, O., Böing, S., Bosser, P., Bourras, D., Bouruet-Aubertot, P., Bower, K., Branellec, P., Branger, H., Brennek, M., Brewer, A., Brilouet, P. E., Brügmann, B., Buehler, S. A., Burke, E., Burton, R., Calmer, R., Canonici, J. C., Carton, X., Cato Jr, G., Charles, J. A., Chazette, P., Chen, Y., Chilinski, M. T., Choularton, T., Chuang, P., Clarke, S., Coe, H., Cornet, C., Coutris, P., Couvreux, F., Crewell, S., Cronin, T., Cui, Z., Cuypers, Y., Daley, A., Damerell, G. M., Dauhut, T., **Deneke, H.**, Desbios, J. P., Dörner, S., Donner, S., Douet, V., Drushka, K., Dütsch, M., Ehrlich, A., Emanuel, K., Emmanouilidis, A., Etienne, J. C., Etienne-Leblanc, S., Faure, G., Feingold, G., Ferrero, L., Fix, A., Flamant, C., Flatau, P. J., Foltz, G. R., Forster, L., Furtuna, I., Gadian, A., Galewsky, J., Gallagher, M., Gallimore, P., Gaston, C., Gentemann,

C., Geyskens, N., Giez, A., Gollop, J., Gouirand, I., Gourbeyre, C., de Graaf, D., de Groot, G. E., Grosz, R., Güttler, J., Gutleben, M., Hall, K., Harris, G., Helfer, K. C., Henze, D., Herbert, C., Holanda, B., Ibanez-Landeta, A., Intrieri, J., Iyer, S., Julien, F., Kalesse, H., Kazil, J., Kellman, A., Kidane, A. T., Kirchner, U., Klingebiel, M., Körner, M., Kremper, L. A., Kretzschmar, J., Krüger, O., Kumala, W., Kurz, A., L'Hégaret, P., Labaste, M., Lachlan-Cope, T., Laing, A., Landschützer, P., Lang, T., Lange, D., Lange, I., Laplace, C., Lavik, G., Laxenaire, R., Le Bihan, C., Leandro, M., Lefevre, N., Lena, M., Lenschow, D., Li, Q., Lloyd, G., Los, S., Losi, N., Lovell, O., Luneau, C., Makuch, P., Malinowski, S., Manta, G., Marinou, E., Marsden, N., Masson, S., Maury, N., Mayer, B., Mayers-Als, M., Mazel, C., McGeary, W., McWilliams, J. C., Mech, M., Mehlmann, M., Meroni, A. N., Mieslinger, T., Minikin, A., Minnett, P., Möller, G., Morfa Avalos, Y., Muller, C., Musat, I., Napoli, A., Neuberger, A., Noisel, C., Noone, D., Nordsiek, F., Nowak, J. L., Oswald, L., Parker, D. J., Peck, C., Person, R., Philippi, M., Plueddemann, A., Pöhlker, C., Pörtge, V., Pöschl, U., Pologne, L., Posyniak, M., Prange, M., Quiñones Meléndez, E., Radtke, J., Ramage, K., Reimann, J., Renault, L., Reus, K., Reyes, A., Ribbe, J., Ringel, M., Ritschel, M., Rocha, C. B., Rochetin, N., Röttenbacher, J., Rollo, C., Royer, H., Sadoulet, P., Saffin, L., Sandiford, S., Sandu, I., Schäfer, M., Schemann, V., Schirmacher, I., Schlenczek, O., Schmidt, J., Schröder, M., Schwarzenboeck, A., Sealy, A., Senff, C. J., Serikov, I., Shohan, S., Siddle, E., Smirnov, A., Späth, F., Spooner, B., Stolla, M. K., Szkółka, W., de Szoeke, S. P., Tarot, S., Tetoni, E., Thompson, E., Thomson, J., Tomassini, L., Totems, J., Ubele, A. A., Villiger, L., von Arx, J., Wagner, T., Walther, A., Webber, B., Wendisch, M., Whitehall, S., Wiltshire, A., Wing, A. A., Wirth, M., Wiskandt, J., Wolf, K., Worbes, L., Wright, E., Wulfmeyer, V., Young, S., Zhang, C., Zhang, D., Ziemen, F., Zinner, T. and Zöger, M. 2021. EUREC^{4}A. Earth Syst. Sci. Data, **13**, 4067-4119. https://doi.org/10.5194/essd-13-4067-2021.

Stieger, B., **van Pinxteren, D.**, **Tilgner, A.**, **Spindler, G.**, **Poulain, L.**, **Grüner, A.**, Wallasch, M. and **Herrmann, H.** 2021. Strong deviations from thermodynamically expected phase partitioning of low-molecular-weight organic acids during one year of rural measurements. ACS Earth Space Chem., **5**, 500-515. https://doi.org/10.1021/acsearthspacechem.0c00297.

Sun, J., **Hermann, M.**, Yuan, Y., **Birmili, W.**, Coen, M. C., **Weinhold, K.**, **Madueño, L.**, **Poulain, L.**, **Tuch, T.**, Ries, L., Sohmer, R., Couret, C., Frank, G., Brem, B. T., Gysel-Beer, M., **Ma, N.** and **Wiedensohler, A.** 2021. Long-term trends of black carbon and particle number concentration in the lower free troposphere in Central Europe. Environ. Sci. Eur., **33**, 47. https://doi.org/10.1186/s12302-021-00488-w.

Tilgner, A., **Schaefer, T.**, Alexander, B., Barth, M., Collett Jr., J. L., Fahey, K. M., Nenes, A., Pye, H. O. T., **Herrmann, H.** and McNeill, V. F. 2021. Acidity and the multiphase chemistry of atmospheric aqueous particles and clouds. Atmos. Chem. Phys., **21**, 13483-13536. https://doi.org/10.5194/acp-21-13483-2021.

Tõnisson, L., **Voigtländer, J.**, **Weger, M.**, **Assmann, D.**, **Käthner, R.**, **Heinold, B.** and **Macke, A.** 2021. Knowledge transfer with citizen science: Luft-Leipzig case study Sustainability, **13**, 7855. https://doi.org/10.3390/su13147855.

Triesch, N., **van Pinxteren, M.**, Engel, A. and **Herrmann, H.** 2021. Concerted measurements of free amino acids at the Cabo Verde islands: High enrichments in submicron sea spray aerosol particles and cloud droplets. Atmos. Chem. Phys., **21**, 163-181. https://doi.org/10.5194/acp-21-163-2021.

Triesch, N., **van Pinxteren, M.**, Frka, S., Stolle, C., **Spranger, T.**, **Hoffmann, E. H.**, **Gong, X.**, **Wex, H.**, Schulz-Bull, D., Gašparović, B. and **Herrmann, H.** 2021. Concerted measurements of lipids in seawater and on submicrometer aerosol particles at the Cabo Verde Islands: Biogenic sources, selective transfer and high enrichments. Atmos. Chem. Phys., **21**, 4267-4283. https://doi.org/10.5194/acp-21-4267-2021.

Triesch, N., **van Pinxteren, M.**, Salter, M., Stolle, C., Pereira, R., Zieger, P. and **Herrmann, H.** 2021. Sea spray aerosol chamber study on selective transfer and enrichment of free and combined amino acids. ACS Earth Space Chem., **5**, 1564-1574. https://doi.org/10.1021/acsearthspacechem.1c00080.

Ungeheuer, F., **van Pinxteren, D.** and Vogel, A. L. 2021. Identification and source attribution of organic compounds in ultrafine particles near Frankfurt International Airport. Atmos. Chem. Phys., **21**, 3763-3775. https://doi.org/10.5194/acp-21-3763-2021.

Vakkari, V., **Baars, H.**, Bohlmann, S., **Bühl, J.**, Komppula, M., Mamouri, R.-E. and O'Connor, E. J. 2021. Aerosol particle depolarization ratio at 1565 nm measured with a Halo Doppler lidar. Atmos. Chem. Phys., **21**, 5807-5820. https://doi.org/10.5194/acp-21-5807-2021.

van Noije, T., Bergman, T., Le Sager, P., O'Donnell, D., Makkonen, R., Gonçalves-Ageitos, M., Döscher, R., Fladrich, U., von Hardenberg, J., Keskinen, J.-P., Korhonen, H., Laakso, A., Myriokefalitakis, S., Ollinaho, P., Pérez García-Pando, C., Reerink, T., **Schrödner, R.**, Wyser, K. and Yang, S. 2021. EC-Earth3-AerChem: A global climate model with interactive aerosols and atmospheric chemistry participating in CMIP6. Geosci. Model Dev., **14**, 5637-5668. https://doi.org/10.5194/gmd-14-5637-2021.

Appendices: Publications

Villanueva, D., Neubauer, D., Gasparini, B., Ickes, L. and **Tegen, I.** 2021. Constraining the impact of dust-driven droplet freezing on climate using cloud-top-phase observations. Geophys. Res. Lett., **48**, e2021GL092687. https://doi.org/10.1029/2021GL092687.

Villanueva, D., **Senf, F.** and **Tegen, I.** 2021. Hemispheric and seasonal contrast in cloud thermodynamic phase from A-Train spaceborne instruments. J. Geophys. Res. - Atmos., **126**, e2020JD034322. https://doi.org/10.1029/2020JD034322.

von Schoenberg, P., Tunved, P., Grahn, H., **Wiedensohler, A.**, Krejci, R. and Brännström, N. 2021. Aerosol dynamics and dispersion of radioactive particles. Atmos. Chem. Phys., **21**, 5173–5193. https://doi.org/10.5194/acp-21-5173-2021.

Wagner, R., Schepanski, K. and Klose, M. 2021. The dust emission potential of agricultural-like fires—Theoretical estimates from two conceptually different dust emission parameterizations. J. Geophys. Res. - Atmos., **126**, e2020JD034355. https://doi.org/10.1029/2020JD034355.

Wang, K., Huang, R.-J., **Brüggemann, M.**, Zhang, Y., Yang, L., Ni, H., Guo, J., Wang, M., Han, J., Bilde, M., Glasius, M. and Hoffmann, T. 2021. Urban organic aerosol composition in Eastern China differs from north to south: Molecular insight from a liquid chromatography-mass spectrometry (Orbitrap) study. Atmos. Chem. Phys., **21**, 9089-9104. https://doi.org/10.5194/acp-21-9089-2021.

Wang, N., **He, L.**, Lv, G. and Sun, X. 2021. Potential environmental fate and risk based on the hydroxyl radical-initiated transformation of atmospheric 1,2-dibromo-4-(1,2dibromoethyl) cyclohexane stereoisomers. J. Hazard. Mater., **417**, 126031. https://doi.org/10.1016/j.jhazmat.2021.126031.

Wang, N., Lv, G., **He, L.** and Sun, X. 2021. New insight into photodegradation mechanisms, kinetics and health effects of p-nitrophenol by ozonation in polluted water. J. Hazard. Mater., **403**, 123805. https://doi.org/10.1016/j.jhazmat.2020.123805.

Wang, Y., **He, L.**, Lv, G. and Sun, X. 2021. Experimental and theoretical insights into the RCS-Involved electrocatalytic transformation of 4-nitrophenol. Chemosphere, **262**, 128015. https://doi.org/10.1016/j.chemosphere.2020.128015.

Wang, Z., Ehn, M., Rissanen, M. P., Garmash, O., Quéléver, L., Xing, L., Monge-Palacios, M., Rantala, P., Donahue, N. M., **Berndt, T.** and Sarathy, S. M. 2021. Efficient alkane oxidation under combustion engine and atmospheric conditions. Communications Chemistry, **4**, 18. https://doi.org/10.1038/s42004-020-00445-3.

Weger, M., **Heinold, B.** and **Knoth, O.** 2021. CAIRDIO City-Scale Air Dispersion Model with Diffusive Obstacles (Version 1.0). Zenodo, http://doi.org/10.5281/zenodo.4486984.

Weger, M., **Knoth, O.** and **Heinold, B.** 2021. An urban large-eddy-simulated-based dispersion model for marginal grid resolutions: CAIRDIO v1.0. Geosci. Model Dev., **14**, 1469-1492. https://doi.org/10.5194/gmd-14-1469-2021.

Wen, L., **Schaefer, T.**, **He, L.**, Zhang, Y., Sun, X., **Ventura, O. N.** and **Herrmann, H.** 2021. T- and pH-dependent kinetics of the reactions of $\cdot OH_{(aq)}$ with glutaric and adipic acid for atmospheric aqueous-phase chemistry. ACS Earth Space Chem., **5**, 1854-1864. https://doi.org/10.1021/acsearthspacechem.1c00163.

Wiedenhaus, H., Ehrsperger, L., Klemm, O. and Strauss, H. 2021. Stable ^{15}N isotopes in fine and coarse urban particulate matter. Aerosol Sci. Technol., **55**, 859-870. https://doi.org/10.1080/02786826.2021.1905150.

Wiesner, A., **Pfeifer, S.**, **Merkel, M.**, **Tuch, T.**, **Weinhold, K.** and **Wiedensohler, A.** 2021. Real world vehicle emission factors for black carbon derived from longterm in-situ measurements and inverse modelling. Atmosphere, **12**, 31 (19 pp.). https://doi.org/10.3390/atmos12010031.

Witthuhn, J. 2021. jonas-witthuhn/Aerosol-REari-Germany-2015: Source code for the publication: "Aerosol properties and aerosol-radiation interactions in clear sky conditions over Germany" (v1.1). Zenodo, http://doi.org/10.5281/zenodo.5347706.

Witthuhn, J. 2021. jonas-witthuhn/shrad-pro: v0.1.0-alpha: calibration, cosine error correction, and misalignment correction (v0.1.0-alpha). Zenodo, http://doi.org/10.5281/zenodo.5562282.

Witthuhn, J., **Hünerbein, A.**, Filipitsch, F., Wacker, S., Meilinger, S. and **Deneke, H.** 2021. Aerosol properties and aerosol–radiation interactions in clear-sky conditions over Germany. Atmos. Chem. Phys., **21**, 14591-14630. https://doi.org/10.5194/acp-21-14591-2021.

Witthuhn, J., **Hünerbein, A.**, Filipitsch, F., Wacker, S., Meilinger, S. and **Deneke, H.** 2021. Dataset for the publication: "Aerosol properties and aerosol-radiation interactions in clear sky conditions over Germany" [Data set]. *Data from: Zenodo*, https://doi.org/10.5281/zenodo.4892730.

Ye, C., Chen, H., **Hoffmann, E. H.**, **Mettke, P.**, **Tilgner, A.**, **He, L.**, **Mutzel, A.**, **Brüggemann, M.**, **Poulain, L.**, **Schaefer, T.**, **Heinold, B.**, Ma, Z., Liu, P., Xue, C., Zhao, X., Zhang, C., Zhang, F., Sun, H., Li, Q., Wang, L., Yang, X., Wang, J., Liu, C., Xing, C., Mu, Y., Chen, J. and **Herrmann, H.** 2021. Particle-phase

photoreactions of HULIS and TMIs establish a strong source of H_2O_2 and particulate sulfate in the Winter North China Plain. Environ. Sci. Technol., **55**, 7818-7830. https://doi.org/10.1021/acs.est.1c00561.

Yuan, J., Modini, R. L., Zanatta, M., Herber, A. B., **Müller, T.**, **Wehner, B.**, **Poulain, L.**, **Tuch, T.**, Baltensperger, U. and Gysel-Beer, M. 2021. Variability in the mass absorption cross section of black carbon (BC) aerosols is driven by BC internal mixing state at a central European background site (Melpitz, Germany) in winter. Atmos. Chem. Phys., **21**, 635-655. https://doi.org/10.5194/acp-21-635-2021.

Zeppenfeld, S., **van Pinxteren, M.**, **van Pinxteren, D.**, **Wex, H.**, Berdalet, E., Vaqué, D., Dall'Osto, M. and **Herrmann, H.** 2021. Aerosol marine primary carbohydrates and atmospheric transformation in the Western Antarctic Peninsula. ACS Earth Space Chem., **5**, 1032-1047. https://doi.org/10.1021/acsearthspacechem.0c00351.

Zhang, C., Bu, L., Fan, F., **Ma, N.**, Wang, Y., Yang, Y., **Größ, J.**, Yan, J. and **Wiedensohler, A.** 2021. Surfactant effect on the hygroscopicity of aerosol particles at relative humidity ranging from 80% to 99.5%: Internally mixed adipic acid-ammonium sulfate particles. Atmos. Environ., **266**, 118725. https://doi.org/10.1016/j.atmosenv.2021.118725.

Zhang, C., **Ma, N.**, Fan, F., Yang, Y., **Größ, J.**, Yan, J., Bu, L., Wang, Y. and **Wiedensohler, A.** 2021. Hygroscopic growth of aerosol particles consisted of oxalic acid and its internal mixture with ammonium sulfate for the relative humidity ranging from 80% to 99.5%. Atmos. Environ., **252**, 118318. https://doi.org/10.1016/j.atmosenv.2021.118318.

Zhao, J., Birmili, W., Hussein, T., **Wehner, B.** and **Wiedensohler, A.** 2021. Particle number emission rates of aerosol sources in 40 German households and their contributions to ultrafine and fine particle exposure. Indoor Air, **31**, 818-831. https://doi.org/10.1111/ina.12773.

University courses

Lecturer	Course	WS 2019/ 2020	SS 2020	WS 2020/ 2021	SS 2021	WS 2021/ 2022
Ansmann, A. Althausen, D. Baars, H. Engelmann, R. Seifert, P.	Lidar Remote Sensing of the Atmosphere (2sh)	x		*		x
Ansmann, A. Althausen,D. Baars, H. Engelmann, R.	Seminar Lidar Remote Sensing of the Atmosphere (2 sh)	x				x
Brüggemann, M. van Pinxteren, D.	Advanced studies: Analytics and Spektroscopy (Atmospheric Chemistry)		x		x	
Hartmann, S. Henning, S. Wex, H.	LIM Meteorological Seminar			x		
Herrmann, H.	Basic Atmospheric Chemistry + Exercises (3 sh)		x		x	
	Atmospheric Chemistry, the Multiphase System + exercises (3 sh)	x		x		x
	Atmospheric Chemistry Seminar (1 sh)	x	x	x	x	x
	Atmospheric Chemistry Lab Course (1 sh)	x	x	x		
	Course of Atmospheric Chemistry, Shanding University			x		
	Organiser of the MARSU Summer School	x				
Macke, A.	Atmospheric Radiation (1 sh)		x		x	
Macke, A. Deneke, H. (SS20/21) Hünerbein, A. (SS20/21) Bley, S. (SS21)	Satellite Remote Sensing + Exercises (2 sh)		x		x	
Macke, A. Stratmann, F. Niedermeier, D.	Cloud Physics + Exercises (3 sh)		*		x	
Schepanski, K.	Dust in the Atmosphere (2sh)	x				
	Dust in the Atmosphere Seminar (1sh)	x				
Seifert, P.	Microwave remote sensing	x		x		x

Lecturer	Course	WS 2019/ 2020	SS 2020	WS 2020/ 2021	SS 2021	WS 2021/ 2022
Tegen, I.	Modeling of Atmospheric Trace Substances (2 sh)	*		x		x
	Seminar Modeling of Atmospheric Trace Substances (1 sh)			x		x
	Modelling of the Atmosphere (2sh)		x			
	Basics of Mesoscale Model Simulations + Exercises (3 sh)		x		x	
	Contribution to modul SQ15 "Energy and Environment", University of Leipzig: "Transport of Atmospheric Pollutants"	x		x		
Tegen, I. Senf, F. Heinold, B.	Atmospheric Models: Scales and Parameterizations + Exercises (3 sh)		*		x	
	Contribution to modul SQ15 "Energy and Environment", University of Leipzig: "Transport of Atmospheric Pollutants"	x		x		x
Wandinger, U.	Scattering and Atmospheric Optics (2 sh)	x		x		x
	Seminar Applied Scattering Theory (1 sh)	x		x		x
Stratmann, F. Müller, T. Pöhlker, M. Wiedensohler, A.	Atmospheric Aerosols (2 sh) Master	x				x
	Seminar Atmospheric Aerosols (1 sh)					x
van Pinxteren, M.	Guest lecture: Analysis and Spectroscopy: Gas Chromatography, Lecture in an one week course	x		x		
	Lecturer at the Sino-European Summer School on Atmospheric Chemistry (SESAC 4)	x				

** did not take place, but was offered*

Academic degrees

Completed academic qualifications 2020/2021

Academic degree*	Name	Title	Faculty	Year
Ph. D.	Egerer, U.	A new set of tethered balloon-borne instrument payloads for collocated turbulence and radiation measurements in the cloudy Arctic boundary layer: First applications	University of Leipzig, Faculty of Physics and Earth Sciences	2021
	Felber, T.	Photochemical and kinetic studies and time-resolved laser spectroscopy of imidazoles and other photosensitizers in the tropospheric aqueous phase	University of Leipzig, Faculty of Chemistry and Mineralogy	2021
	Feuerstein, S.	Alluvial dust sources and their implementation in a dust-emission model	University of Leipzig, Faculty of Physics and Earth Sciences	2020
	Gong, X.	Cloud condensation nuclei and ice-nucleating particles over tropical and subtropical regions in the northern hemisphere	University of Leipzig, Faculty of Physics and Earth Sciences	2020
	Hartmann, M.	Ice nucleating particles in the Arctic : A story of their abundance, properties and possible origin from the Little Ice Age to the current age of unpreceded Arctic warming	University of Leipzig, Faculty of Physics and Earth Sciences	2021
	Hofer, J.	Aerosol characterization over a Central Asian site: Long-term lidar profiling at Dushanbe, Tajikistan (March 2015 - August 2016)	University of Leipzig, Faculty of Physics and Earth Sciences	2020
	Hoffmann, E.	CAPRAM mechanism and model developments for investigating marine multiphase chemistry effects linked to air quality and climate: From process to regional scale modelling	University of Leipzig, Faculty of Physics and Earth Sciences	2020
	Jimenez, C.	Observations of aerosol and liquid-water clouds with Dual-Field-of-View Polarization Lidar	University of Leipzig, Faculty of Physics and Earth Sciences	2021
	Otto, T.	Kinetic and mechanistic studies of the oxidatzion of biogenic oxygenated organic compounds in the atmospheric aqueous phase	University of Leipzig, Faculty of Chemistry and Mineralogy	2020
	Radenz, M.	Hemispheric contrasts of ice formation in stratiform supercooled liquid louds: Long-term observations with the ground-based remote-sensing supersite LACROS	University of Leipzig, Faculty of Physics and Earth Sciences	2021
	Schacht, J.	Black carbon aerosol in the Arctic: Ageing, transport and radiative effects	University of Leipzig, Faculty of Physics and Earth Sciences	2021

Academic degree*	Name	Title	Faculty	Year
Ph. D.	Spranger, T.	2D liquid chromatographic fractionation of humic-likesubstances in atmospheric aerosol particles	University of Leipzig, Faculty of Chemistry and Mineralogy	2020
	Stieger, B.	Highly time-resolved and long-time quantification of inorganics and low-molecular-weight organic acids in the gas and particle phases at the research station Melpitz	University of Leipzig, Faculty of Chemistry and Mineralogy	2021
	Triesch, N.	Sources, transfer and enrichments of amino acids and lipids on aerosol particles in the marine environment	University of Leipzig, Faculty of Chemistry and Mineralogy	2021
	Villanueva, D.	A story of dust and ice - constraining dust-driven immersion freezing in climate models using spaceborne retrievals	University of Leipzig, Faculty of Physics and Earth Sciences	2021
	Wagner, R.	Dust emissions driven by pyro-convection - A model perspective	University of Leipzig, Faculty of Physics and Earth Sciences	2020
	Zeppenfeld, S.	Carbohydrates in the Arctic and the Southern Ocean - Chemical analysis, transfer from the sea to the atmosphere and potential relevance for cloud formation	University of Leipzig, Faculty of Chemistry and Mineralogy	2021
	Zhao, J.	Particle exposure in German dwellings: Particle number and mass size distributions, indoor particle dynamics, and source apoortionment	University of Leipzig, Faculty of Physics and Earth Sciences	2021
M.Sc.	Nguyen, D. H.	Automatisierte Aggregatzustandsdetektion von atmosphärischen Eiskeimproben im Rahmen des INDA (Ice Nucleation Droplet Array) - Projektes des Leibniz-Instituts für Troposphärenforschung	Leipzig University of Applied Sciences, Faculty of Computer Science and Media	2021
	Ort, L.	The relative importance of turbulent fluctuations compared to the variability in aerosol particle properties on the formation and growth of cloud droplets	University of Leipzig, Faculty of Physics and Earth Sciences	2020
	Wiesen, R.	Implementation and test of the dual-field-of-view depolarization method into PollyXT	University of Leipzig, Faculty of Physics and Earth Sciences	2020
B.Sc.	Bayer, N.	Observation and radiative transfer modelling of spectrally resolved UV radiation in Melpitz, Germany	University of Leipzig, Faculty of Physics and Earth Sciences	2020
	Bischay, J.	Analyse von Wolkenprodukten aus passiven Messungen anhand simulierter EarthCARE-Daten	University of Leipzig, Faculty of Physics and Earth Sciences	2021
	Clauß, C.	Untersuchung des photoinduzierten Reaktions-verhaltens von Furfural in wässriger Lösung	University of Leipzig, Faculty of Physics and Earth Sciences	2020

Appendices: Academic degrees

Academic degree*	Name	Title	Faculty	Year
B.Sc.	Estelmann, A.	Untersuchung der Kinetik von OH-Radikalen und Triplettzuständen in wässriger Lösung	University of Leipzig, Faculty of Chemistry and Mineralogy	2020
	Hoffmann, R.	Bestimmung der chemischen Zusammensetzung des Aerosols an der städtischen Messstation Eisenbahnstraße des TROPOS mit Hilfe eines Aerosol-Massenspektrometers (AMS)	University of Leipzig, Faculty of Physics and Earth Sciences	2020
	Lehmicke, L.	Untersuchungen zur direkten Messung von Kinetik des Hydroxylradikals in wässriger Lösung	University of Leipzig, Faculty of Chemistry and Mineralogy	2020
	Paul, S.	Einfluss absorbierender Aerosole auf die Bewölkung über Deutschland - Sensitivitätsstudie mit ICON	University of Leipzig, Faculty of Physics and Earth Sciences	2021
	Rug, L.	Solving the linearized Boussinesq equation using triangular and compound finite elements	Leipzig University of Applied Sciences, Faculty of Computer Science, Mathematics and Natural Sciences	2020
	Vogel, D.	Solving the shallow water equation on the cubed sphere using the finite element method	Leipzig University of Applied Sciences, Faculty of Computer Science, Mathematics and Natural Sciences	2020
	Wenzel, B.	Untersuchung zur Bestimmung der Konzentration, Eigenschaften und Quellen arktischer Eiskeime	University of Leipzig, Faculty of Physics and Earth Sciences	2021

** Habil.: Habilitation, Ph. D.: Doctoral theses, Dipl.: Diploma, M.Sc.: Master of Science, B.Sc.: Bachelor of Science*

Summary of completed academic qualifications

Academical degrees	Number		Total
	2020	2021	
Habilitation	0	0	0
Doctoral theses	7	11	18
Master of Science	2	1	3
Bachelor of science	7	3	10

Editorships

Name	Journal
Deneke, H.	Section Editor "Atmospheric Remote Sensing", Remote Sensing
Frey, W.	Associate Editor "Atmospheric Measurement Techniques"
Heinold, B.	Guest Editor "Frontiers Environmental Science"
	Associate Editor "Atmosphere - MDPI"
Herrmann, H.	Associate Editor "Atmospheric Measurement Techniques"
	Editorial Board Member "Atmospheric Pollution Research"
	"Atmospheric Chemistry and Physics", Special Issue Editor (HCCT-2010)
	Editorial Board Member "Aerosol and Air Quality Research" (AAQR)
	"Science of the Total Environment" (STOTEN) - Special Issue Editor)
	"Atmospheric Chemistry and Physics" (ACP) - EUROCHAMP-2020 Special Issue Editor
	"Journal of Geophysical Research" (JGR) Atmospheres - Associate Editor
	International Advisory Board "Environmental Science and Technology"
Macke, A.	Member of the Advisory Board "Meteorologische Zeitschrift"
	Associate Editor „Atmospheric Measurement Techniques"
	Member of Editing Committee "promet"
Schepanski, K.	Associate Editor "Aeolian Research"
	Review Editor "Satellite Missions", Frontiers in Remote Sensing
Seifert, P.	Guest Editor for an Atmospheric Chemistry and Physics and Atmospheric Measurement Techniques Special Issue (PROM)
Tegen, I.	Associate Editor "Journal of Geophysical Research"
Wandinger, U.	Editorial Board Member "Atmospheric Measurement Techniques"
Wiedensohler, A.	Editorial Board Member "Atmospheric Measurement Techniques"
	Chief Editor "Atmospheric Environment"
van Pinxteren, D.	Scientific Advisory Board of the Journal "Gefahrstoffe, Reinhaltung der Luft"
van Pinxteren, M.	"Atmospheric Chemistry and Physics", Special Issue Editor (MarParCloud)

Appendices: Awards / Memberships

Awards

Name	Prize	Awarding institution	Comments/Description
Romshoo, B.	Best Poster Award	(European Aerosol Assembly) EAA	title: “Optical properties of laboratory generated soot: Application for modelling validation”
Herrmann, H.	Double-Hundred Talent Plan of the Shandong Province	Shandong University	

Memberships

Name	Board
Althausen, D.	Commission on Air Pollution Prevention of VDI and DIN - Standards Committee KRdL NA 134-02-01-22 UA “Ground-based remote sensing of meteorological parameters”, Department II Environmental Meteorology
Baars, H.	Member of the Aeolus Science and Data Quality Group (Aeolus SAG)
Deneke, H.	Member of the Steering Committee of the BMWi Research Network MetPVNet
	Member of the International Radiation Comission
	Member of the Convection Working Group
	Member of the International Cloud Working Group (ICWG)
Heinold, B.	HAMMOZ Steering Comittee member
Hellmuth, O.	Membership in the International Association for the Properties of Water and Steam (IAPWS), Working Group Thermophysical Properties of Water and Steam (TPWS)
	Member of Leibniz-Sozietät der Wissenschaften zu Berlin e. V.
Henning, S.	Co-chair EAA Working Group: Atmospheric Aerosol Studies (AAS) for Aerosol-cloud-interaction in warm, mixed-phase and ice clouds
Hermann, M.	HALO Scientific Steering Committee (WLA)
	Member of the HALO Board of Trusties
Herrmann, H.	Chairman of the working group “Atmospheric Chemistry” in the GDCh-division “Environmental Chemistry and Ecotoxicology (AKAC)”
	DECHEMA/GDCh/ (Bunsen Society); Community Committee “Chemistry of the Atmosphere”
	DECHEMA/GDCh/KRdL Division Particulate Matter - Co-Chair
	IUPAC Task Group on Atmospheric Chemical Kinetic Data Evaluation

Name	Board
Herrmann, H.	Advisory Board Member of ProcessNet-Fachgemeinschaft (Specialist Community) SuPER
	Fellow of International Union of Pure and Applied Chemistry (IUPAC)
	National Co-Representative “International Surface Ocean - Lower Atmosphere Study” (SOLAS)
	Membership of the American Chemical Society (AMC)
	Member of the Second International Indian Ocean Expedition (IIOE-2)
	Distinguished Visiting Professor for Environmental Sciences and Engineering at Shandong University, Quingdao, China
	Professor for Environmental Sciences and Engineering at Fudan University, Shanghai, China
	Member of the Evaluation Commission of the Czech Academy of Sciences
Macke, A.	Member of the DFG Senate Commission Oceanography
	Member of the EU Steering Committee of the Leibniz Association
	Member of the DFG Topical Board 313 “Atmosphere and Ocean Research”
	Deputy Chair of Section E of the Leibniz Society
	Member of the Steering Committee of the Leibniz-Research Network “Crisis in a globalized World”
Mertes, S.	Member of the Science Team of CIRRUS-HL: The airborne experiment on CIRRUS in High Latitudes with the highaltitude long-range research aircraft HALO
	Ordinary member of the DFG collaborative research center TR 172 “Arctic Amplification”
Müller, Ke.	Member of the “German Library Association (dbv)”
	Member of the “Professional Association Information Library (BIB)”
Müller T.	VDI-Comission “Assesment of dust pollution on solar energy systems”
Poulain, L.	Management Committee Member for COST-COLOSSAL
	VDI and DIN - Standards Committee KRdL, member of the working group “Measurement of aerosol particles in the outdoor air”
Schepanski, K.	Member of Executive Commitee Leibniz Research Alliance “INFECTIONS‘21”
	Board member of the International Society for Aeolian Research (ISAR)
	Steering Commitee member of the Leibniz Research Alliance “INFECTIONS‘21”
	Steering Commitee AEROCLO-sA
	Management Committee Substitute member for EU COSTaction InDust

Appendices: Memberships

Name	Board
Seifert, P.	Ordinary member of the DFG collaborative research center TR 172 "Arctic Amplification"
Spindler, G.	VDI and DIN - Standards Committee KRdL, member of the working group "Measurement of aerosol particles in the outdoor air"
	Member of the KRdL working group "Spiegelgremium zu CEN/TC 264/WG 35 EC/ OC in PM"
Stratmann, F.	Member of the Science Team of CIRRUS-HL: The airborne experiment on CIRRUS in High Latitudes with the highaltitude long-range research aircraft HALO
Tegen, I.	"SDS-WAS" (WMO Sand and Dust Storm Warning Advisory and Assessment System), Member of Steering Committee
	Member of Scientific Advisory Committee, Science Europe
	HAMMOZ Steering Comittee member
	Member of Management Committee für EU COSTaction 16202 InDust
	Member of the Steering Committee Collaborative Research Cluster TR 172 "Arctic Amplification"
	Steering Commitee member of the Leibniz Research Alliance "INFECTIONS'21"
Tilgner, A.	Member of the working group NA 134 VDI/DIN-Kommission Reinhaltung der Luft (KRdL) - Normenausschuss NA 134-02-01-08 UA Unterausschuss Umwelmetereologie - Depositionsparameter
van Pinxteren, D.	Member of the European working group CEN/TC 264/WG 44 "Source apportionment"
	Member of the KRdl National Mirror Committee of CEN/TC 264/WG 44 "Source apportionment"
Wandinger, U.	Member of the ESA-JAXA EarthCARE Joint Mission Advisory Group
	Member of the EARLINET Council
	Member of the "Research Infrastructure Committee" von ACTRIS
	Member of the ICOS Evaluation Committee
Wehner, B.	Member of VDI/DIN Commission "Clean Air" (KRdL) - subgroup Meteorological Measurements
	Speaker of the Working Group Chairs within the EAA (European Aerosol Assembly)
	Secretary General of GAeF (Gesellschaft für Aerosolforschung)
Wex, H.	Vice President of the International Comission on Clouds and Precipitation (ICCP)
Wiedensohler, A.	Scientific Advisory Group for aerosols within the "Global Atmosphere Watch" program of the "Meteorological Organization"
	Head of the World Calibration Center WMO-GAW

Name	Board
Wiedensohler, A.	Head of the European Center for Aerosol Calibration (ECAC)
	Member of the Comité Européen de Normalisation, working group “CEN/TC 264/WG 32 Air quality - Determination of the particle number concentration”
	Member of the International Organization for Standardization (ISO), working group “ISO/TC 24/SC 4 particle characterization”
	Member of the International Advisory Board of the Institute of Chemical Process Fundamentals of the Czech Academy of Science and the Academy Council of the Czech Academy of Science

Meetings

Meetings	Date	national/ international	number of participants
Arctic Amplification (AC)^3, Kick off Meeting Phase II	08. - 09.10.2020	national	ca. 100
MesSBAR Project Meeting	30. - 31.1.2020	national	22
ACTRIS-D Meeting	30.11. / 08.12.2020	national	45
GUAN Consortium	10. - 11.03.2020	national/ international	35
ACTRIS Data QA & Submission Workshop	15. - 17.09.2020	national/ international	60
ACTRIS-D-Projekcts, Kick-Off Meeting	16. - 17.09.2021	national	61
2nd ESA EarthCARE Validation Workshop	25. - 28.05.2021	international	>100
DACAPO-PESO Workshop	06. - 07.09.2021	international	20
Arctic Amplification (AC)^3 Science Meeting	12. - 27.10.2021	national	ca. 100

Reviews

Reviews	Number	
	2020	2021
Journals	218	167
Projects	25	11
Statements, position papers	3	0
Others	15	19
Total	261	197

Guest scientists

Name	Period of stay	Institution
Ellouzi, I.	01.12.19 - 31.01.20	Mohammed V University of Rabat, Morocco
Das, A.	01.01.20 - 30.06.21	Indian Institute of Science Education and Research, Bhopal, India
He, L.	01.01.20 - 31.12.21	Shandong University, Quingdao, China
Kroflic, A.	06.01. - 17.01.20	National Institute of Chemistry Ljubljana, Slowenia
Drventic, I.	06.01. - 31.01.20	National Institute of Chemistry Ljubljana, Slowenia
Im, U.	15.01. - 16.01.20	Aarhuus University, The Netherlands
Yagni, S. R.	01.02. - 31.12.20	Pandit Deendayal Petroleum University, Raisan, India
Riva, M.	03.02. - 14.02.20	Universität Lyon, France
Haas, R.	05.02. - 20.02.20	Universität Florianopolis, Brazil
Kienle, A.	13.02. - 13.02.20	Universität Ulm, Germany
Hölling, M.	18.02. - 19.02.20	Universität Oldenburg, Germany
Lippold, M.	18.02. - 19.02.20	Ingenieurbüro Mathias Lippold, Friedland, Germany
Lorenz-Meyer, W.	18.02. - 19.02.20	Ingenieurbüro Dr. Ing. W. Lorenz-Meyer, Göttingen, Germany
Hennigan, C.	24.02. - 20.03.20	University of Maryland, Baltimor Country, USA
George, C.	27.02. - 28.02.20	University Lyon, France
Pereira, R.	11.03. - 13.03.20	Heriot Watt University, Edinburgh, UK
Velarde Apaza, F.	13.03. - 18.03.20	Universidad Mayor de San Andres, La Paz, Bolivia
Quinones, V.	20.04. - 30.06.20	Venezuelan Institute für Scientific Research, Miranda, Venezuela
Das, A.	25.07. - 31.12.20	Indian Institute of Science Education and Research, Bhopal, India
Sarang, K.	17.08. - 16.10.20	Institytut Chemii Fizycznej PAN, Warszawa, Poland
Dong, Y.	15.09.20 - 28.02.21	Shandong University, Quingdao, China
Yang, D.	21.10.20 - 20.02.21	Shandong University, Shandong Provinced, China
Quinones, V.	21.10.20 - 30.06.21	Venezuelan Institute für Scientific Research, Caracas, Venezuela
Li, H. P.	01.11.20 - 31.12.22	Shandong University, Quingdao, China
Bravo Aranda, J. A.	23.11.20 - 19.02.21	University of Granada, Spain
Jiang, Y.	10.12.20 - 09.12.21	Shandong University, Quingdao, China

Name	Period of stay	Institution
Iezzi, L.	01.10.21 - 30.11.21	Paul-Scherrer Institut, Villingen, Switzerland
Wagner, R.	01.05.21 - 31.12.22	FU Berlin, Institute for Meteorology, Germany
Urbanneck, C.	01.06.21 - 31.12.22	FU Berlin, Institute for Meteorology, Germany
Kolawole, O. T.	01.06. - 01.07.21	Osun state University, Osogbo, Nigeria
D'Aronco, S.	28.06. - 09.07.21	University of Cambrigde, UK
Kjaergaard, E.	12.07. - 23.07.21	University of Copenhagen, Denmark
Keinert, A.	19.07. - 30.07.21	Karlsruhe Institute of Tecnology, Eggenstein-Leopoldshafen, Germany
Kiselev, A.	19.07. - 30.07.21	Karlsruhe Institute of Tecnology, Eggenstein-Leopoldshafen, Germany
Haiyan, Y.	21.07. - 31.10.21	Helmholtz-Zentrum für Umweltforschung, Leipzig, Germany
Zeising, M.	26.07. - 30.07.21	Alfred Wegener Institute, Helmholtz Center for Polar and marine Research, Bremerhafen, Germany
Hantschke, L.	23.08. - 27.08.21	Forschungszentrum Jülich GmbH, Germany
Hölling, M.	27.08. - 28.08.21	The University of Oldenburg, Germany
Hölling, A.	27.08. - 28.08.21	The University of Oldenburg, Germany
Jiang, Y.	01.11. - 31.12.21	Shandong University, Shandong Provinced, China
Huo, Y.	08.11.21 - 15.02.22	Shandong University, Shandong Provinced, China
Zhou, B.	08.11.21 - 15.02.23	Shandong University, Shandong Provinced, China
Spindler, R.	15.11. - 19.11.21	Eidgenössische Technische Hochschule Zürich, Switzerland

Visits of TROPOS scientists

Name	Period of stay	Institution
Fomba, K. W.	01.02. - 10.02.2020	University of Cabo Verde, Praia, Santiago
Engelmann, R.	23.06. - 03.07.2020	Atmospheric Research Centre of Eastern Finland, Kuopio
Engelmann, R.	21.10. - 31.10.2020	Cyprus University of Technology, Limassol
Engelmann, R.	24.10. - 30.10.2021	Tajik Academy of Sciences, Dushanbe
Engelmann, R.	13.11. - 19.11.2021	Tel Aviv University, Israel
Radenz, M.	24.11. - 04.12.2021	University of Magallanes, Punta Arenas, Chile
Seifert, P:	24.11. - 04.12.2021	University of Magallanes, Punta Arenas, Chile

International and national field campaigns

Campaign	Project partner
Aerosol measurements at the Atlas mountains, Ifrane, Morocco TROPOS: ACD**	Mohammed V University in Rabat, Morocco; ICARE, IRCELYON, France
ALADINA Ny-Alesund Identification and characterization of new particle formation events in the Arctic boundary layer in Ny-Alesund TROPOS: ExAWoMp*	Technical University Braunschweig, University Tübingen, Alfred-Wegener-Institute for Polar and Marine Research, Germany; National Research Council Italy; University Stockholm, Sweden; University Helsinki, Finland
BC Berlin TROPOS: ExAWoMp, ACD	Federal Environmental Ageny, Berlin; Senate Administration, Germany; Netherlands Organisation for Applied Scientific Research
BELUGA@AWIPEV Tethered-balloon profiling of the cloudy Arctic boundary layer over Svalbard TROPOS: ExAWoMp	Alfred-Wegener Institute, Bremerhaven, Germany; Institute for Meteorology, University of Leipzig, Germany
CIRRUS-HL The HALO mission on cirrus in high latitudes: Physical and chemical properties of cloud particle residuals and ice nucleating particles related to high latitude clouds from mixed phase to cirrus level TROPOS: ExAWoMp	Max Planck Insitute for Chemistry, Mainz, Karlsruhe Institute of Technology, DLR-Institute of Atmspheric Physics , Research Center Juelich, University of Mainz, Ludwig-Maximilians-University Munich, Leipzig Institute for Meteorology, Germany
CLOUDNET (permanent experiment) Cloud Measurement Network Leipzig, Germany TROPOS: Remote Sensing Dept.	CLOUDNET Consortium
DACAPO-PESO (Dynamics, Aerosol, Cloud and Precipitation Observations in the Pristine Environment of the Southern Ocean) TROPOS: Remote Sensing Dept., ExAWoMP	University de Magallanes, Chile; Leipzig Institute for Meteorology, Germany
EARLINET (permanent experiment) European Aerosol Research Lidar Network Leipzig, Germany TROPOS: Remote Sensing Dept.	EARLINET Consortium
Formation and Properties of highly oxidized multifunctional compounds TROPOS: ACD	Weizmann Institute Rehevot, Israel
Fri/Sat-evening effect Mobile Measurements to characterize the Friday/ Saturday evening effect in Dresden and Leipzig TROPOS: ACD, ExAWoMp	State Office for Environment and Geology, Dresden, Germany

Campaign	Project partner
GUAN German Ultrafine Aerosol Network TROPOS: ExAWoMp, ACD	German Federal Environmental Agency Langen, German Research Center for Environmental Health, Munich, Saxon State Ministry of the Environment and Agriculture, Dresden; Institute of Energy and Environmental Technology e.V., Duisburg; DWD Hohenpeißenberg, Germany; ISSEP, Liège, Belgium
Hera4Halo PamArcMip-campaign March/April 2018: Testing of the sampler concerning the physical and chemical characterization of ice nucleating aerosol particles with HALO TROPOS: ExAWoMp, ACD	HALO Consortium, Alfred Wegener Institute, Germany; Aarhus University, Denmark
HiLDA, Iceland TROPOS: Modelling Dept.	Technical University Darmstadt, Germany
IAGOS-CARIBIC (monthly intercontinental measurement flights) Civil Aircraft for Remote Sensing and In situ measurement in Tropospheric and Lower Stratosphere based on the Instrumentation Container Concept TROPOS: ExAWoMp	CARIBIC Consortium
IDEFIX-I Studying Secondary Ice Particle Production during riming TROPOS: ExAWoMp	Karlsruhe Institute of Technology, Germany
JATAC Joint Aeolus Tropical Atlantic Campaign. Measruements at Cabo Verde for the validation of Aeolus. TROPOS: Remote Sensing Dept.	European Space Agency, France; The German Aerospace Center; US National Aeronautics and Space Administration, Météo-France, Laboratoire atmosphères, milieux, observations spatiales, France; National Observatory of Athens, Greece; University of Nova Gorica, Slowenia; National Institute for Research and Development for Optoelectronics, Romania; Ocean Science Centre Mindelo, Cape Verde; GEOMAR, Germany
La Paz and El Alto mobile air quality measurement campaign Bolivia TROPOS: ExAWoMp	Universidad Mayor de San Andrés, La Paz, Bolivia
MARSU Marine Atmospheric Sciences Unravel Remote vs. Urban pollution TROPOS: ACD	CNRS, ICARE, ICELYON, France; Mohamed V University of Rabat, Morocco; University of Fudan, China; Max Planck Insitute for Chemistry, Germany
MetPVNet Development of innovative satellite based methods for improved forecasts of PV-yields, 2nd field campaign TROPOS: Remote Sensing Dept.	10 national partner

Appendices: International and national field campaigns

Campaign	Project partner
MOSAiC Multidisciplinary drifting Observatory for the Study of Arctic Climate TROPOS: all departments	Alfred-Wegener Institute, Bremerhaven, Germany
PARAMOUNT Laboratory studies for the production of aerosol particle organic matter in clouds at the CESAM cloud chamber in Paris TROPOS: ACD, ExaWomp	Laboratoire Interuniversitaire des Systèmes Atmosphériques Paris, Laboratoire de Chimie de l'Environnement Marseille, France
PHOSDMAP Phosphorus speciation in dust and marine aerosol particles TROPOS: ACD	GOBABEB, Namibia; Instituto Nacional de Meteorologia e Geofísica, Cabo Verde
ProAerosol and Gas Ex Aerosole over the Baltic Sea TROPOS: ACD	Leibniz Institute for Baltic Sea Research, Germany; University Stockholm, Sweden
PollyNet (permanent experiment) Network of institutions with a PollyXT TROPOS: Remote Sensing Dept.	PollyNet Consortium
Pollution from domestic wood burning Melpitz research station and Melpitz village TROPOS: ACD, ExaWomp	State Office for Environment and Geology, Germany
TAME-BC Clean Air for a Sustainable Future: A Transdisciplinary Approach to Mitigate Emissions of Black Carbon in Metro Manila, Philippines (TAME-BC) Metro Manila TROPOS: ExaWomp	CleanAirAsia, RescueAir, Leibniz Institute for Environment-medical Research, Germany, DIE, Metro Manila, Philippines
TRACE Transport und Transformation von atmosphärischem Aerosol in Mitteleuropa mit Fokus auf anthropogene Quellen TROPOS: all departments	Institute of Chemical Process Fundamentals of the CAS, Czech Republic
VACCINE Variation of Antarctic Cloud Condensation (CCN) and ice nucleating particle concentrations (INP) at Neumayer Station TROPOS: ExaWomp	Alfred-Wegener Institute (AWI), Bremerhaven, Germany

* *Atmospheric Chemistry Department*

** *Experimental Aerosol and Cloud Microphysics Department*

Cooperations

International cooperations

Research project	Cooperation partners
ACD-C Atmospheric Chemistry Chamber	University of British Columbia, Dept. of Chemistry, Canada; University College Cork, Ireland; Institute of Chemistry, Slovenia
ACLOUD Arctic CLoud Observations Using airborne measurements during polar Day	Max Planck Institute for Chemistry, Mainz; Alfred Wegener Institute, Bremerhaven; Karlsruhe Institute for Technology; University of Mainz, Germany; University of Clermont-Ferrand, France
A-CARE Technical Assistance for EarthCARE related research activities in combination with the A-LIFE field experiment	German Aerospace Center; University Vienna, Austria; National Observatory of Athens, Greece; European Space Research and Technology Center (ESTEC), The Netherlands
ACCLIMATE Aerosol-radiation and aerosol-cloud effects on the West African Monsoon system in a changing climate	Department of Meteorology and Climate Science, Federal University of Technology (FUTA), Akure, Nigeria
ACORES Project about clouds, aerosols, and radiation at the Azores	Michigan Tech. University; ARM Facilities of DOE, USA; Storm Peak Laboratory, DRI, USA; Max Planck Institute for Chemistry, Mainz; TU-Berlin, Germany; University Warsaw, Poland; Universitat Politécnica de Catalunya, Barcelona, Spain
ACTRIS Aerosol, Clouds and Trace Gases Research Infrastructure	more than 100 partners from 21 European countries
ACTRIS-CAMS Aerosol, Clouds and Trace Gases Research Infrastructure - Copernicus Atmosphere Monitoring Service	Norwegian Institute for Air Research, Kjeller, Norway; Centre National de la Recherche Scientifique, Paris, Verneuil-en-Halatte, France
ACTRIS measurement station Melpitz Cooperation partners involved in research projects at the TROPOS Research Station Melpitz	Norway, UK, Italy, Switzerland, Czech Republic, Hungary, Ireland, Finland, Austria, Sweden, Bulgaria, Belgium, France, Greece, The Netherlands, Spain, Denmark, Latvia, Poland, Portugal
Aeolus DISC (Data, Innovation, and Science Cluster) - ESA's data quality framework to support the Aeolus mission	German Aerosopace Center, DoRIT, Centre National de la Recherche Scientifique (CNRS), European Centre for Medium-Range Weather Forecasts (ECMWF), Royal Netherlands Meteorological Institute (KNMI), ASEA Brown Boveri (ABB)
AerChemMip - Contribution of MPI-ESM-LR-HAM2	ETH Zurich, Switzerland; University Oxford, UK, Deutsches Klimarecherchezentrum, Hamburg, Germany

Appendices: Cooperations

Research project	Cooperation partners
Aerosolized fungi and eukaryotic microbes as ice-nucleating particles above the Arctic Ocean	University of Tromsoe, Norway
AIE Atmospheric Environmental Impacts of Aerosol in East Asia	30 partners
A-Life	University Vienna, Austria, Ludwig Maximilians University München, Germany
AMBIEnCE Impact of atmospheric multi-stressors to coastal marine systems in a changing climate scenario	University of Cape Verde, Cabo Verde; University of Aveiro, Portugal
Analysis of DYAMOND simulations	DLR Oberpfaffenhofen, Germany
Anthropogenic influence of Asian aerosol on tropical cirrus clouds	National Center for Atmospheric Research (NCAR), Boulder, Colorado, USA
APRIL Atmospheric Products from Imager and Lidar	Royal Netherlands Meteorological Institute (KNMI), The Netherlands; Institute for Space Science, Free University of Berlin (FUB), Germany
AQMEII Air Quality Model Evaluation International Initiative	Austria, Australia, Belgium, Canada, Switzerland, Cyprus, Germany, Denmark, Finland, France, Greece, Italy, Luxembourg, Malta, The Netherlands, Norway, Poland, Portugal, Sweden, UK, USA
BBComp Biomass burning organic aerosol in Europe and Asia: Molecular composition and impact on air quality	Chubu University, Japan
CARDINAL Clouds, Aerosol, Radiation – Development of INtegrated ALgorithms	9 partners from The Netherlands, Germany, Belgium, Canada, Spain, UK, France
COST Action COLOSSAL Chemical On-Line cOmpoSition and Source Apportionment of fine aerosoL	partners from 24 European countries, USA
Central European Air Quality Cooperation - Harmonization of aerosol sampling and measurement; exchange of measurement data; comparison of PM transport models	Poland, Czech Republic
CLOUD – motion Cosmics leaving OUtdoor Droplets - International Training Network	Germany, Switzerland, Finland, Austria, UK
CLOUD Cosmics Leaving OUtdoor Droplets	16 partners from Germany, Switzerland, Finland, Austria, Portugal, Russia, UK, USA

Research project	Cooperation partners
CLIMB How do aerosol-cloud interactions influence the surface mass balance in East Antarctica?	Royal Meteorological Institute of Belgium (RMI); Catholic University of Leuven Belgium; Royal Belgian Institute for Space Aeronomy (BIRA); Ghent University, Belgium
COST Chemistry transport model intercomparison	Germany, Denmark, Finland, France, Bulgaria, Estonia, Italy, Malta, Spain, The Netherlands, Norway, Poland, Switzerland, UK, Greece, Israel
DACAPO-PESO Dynamics, Aerosol, Cloud and Precipitation Observations in the Pristine Environment of the Southern Ocean	University de Magallanes, Chile; Leipzig Institute for Meteorology, Germany
DUSTRISK A risk index for health effects of mineral dust and associated microbes	The University of Cape Verde, The National Institute of Meteorology of Cape Verde, The National Directorate of Environment, The Instituto Nacional de Saúde Pública, Dr. Baptist de Sousa Hospital, and Dr. Agostinho Neto Hospital Praia, Cabo Verde
EARLINET European Aerosol Research Network	Germany, Italy, Spain, Greece, Switzerland, Sweden, Portugal, Poland, Belarus, France, Bulgaria, Romania, Norway, The Netherlands, Finland, Ireland, Cyprus
EMPIR-BC European Metrology Programme for Innovation and Research - Black Carbon	Germany, France, UK, Finland, Greece, Switzerland
E-PROFILE EUMETNET Profiling Programme: automatic lidars and ceilometers (ALC)	EUMETNET members
ESA-Aeolus European Space Agency, Atmospheric Dynamics Mission	European Space Research and Technology Center, The Netherlands, ESA Centre for Earth Observation (ESRIN), Italy
ESA-EarthCARE European Space Agency, Earth Clouds, Aerosol and Radiation Explorer	European Space Research and Technology Center (ESTEC), The Netherlands; Japan Aerospace Exploration Agency
EUROCHAMP-2020 Integration of European Simulation Chambers for Investigating Atmospheric Processes – Towards 2020 and beyond	Germany, France, Switzerland, Spain, Ireland, Finland, Greece, Italy, Romania, UK
EXCELSIOR ERATOSTHENES: EXcellence Research Centre for Earth SurveiLlance and Space-Based MonItoring Of the EnviRonment	Cyprus, Germany, Greece
Generalized Definition of Relative Humidity	Saxon State Agency for Environment, Agriculture and Geology, Dresden, Germany

Appendices: Cooperations

Research project	Cooperation partners
HAMMOZ hosting	ETH Zürich; C2SM Zürich, Switzerland; Univ. Oxford, UK; Finish Meteorological Institute; GEOMAR, Max Planck Institute Hamburg, Leipzig Institute for Meteorology, Leipzig University, Germany
Heterogeneous ice and salt crystallisation in aqueous electrolyte and polymeric solutions	State University St. Petersburg, Russia; University Rostock; IOW Warnemünde, Germany; Institute of Thermomechanics AS, Prague, Czech Republic; University of Odessa; Kharkov Institute of Technology, Ukraine
IAGOS-CARIBIC In-service Aircraft for a Global Observing System - Civil Aircraft for Remote Sensing and In situ measurement in Tropospheric and Lower Stratosphere based on the Instrumentation Container Concept	Germany, UK, France, The Netherlands, Sweden
ICON Cloud Issues Bewertung von Bewölkungsvorhersagen mit dem Modell ICON	German Weather Service, Israel Meteorological Service, Karlsruhe Institute of Technology
ICON-HAMMOZ Development Model development	Max Planck Institute for Meteorology, Germany, ETH Zurich, Institute for Atmospheric and Climate Science, Switzerland, Oxford University, UK; University of Leipzig, Germany
Impact of the COVID-19 lockdown on the Asian summer monsoon	Indian Institute of Tropical Meteorology
InDust Cost Action International Network to Encourage the Use of Monitoring and Forecasting Dust Products	29 Cost countries
Intercomparison of Satellite Derived Wind Observations	EUMETSAT, Darmstadt, Germany
Laboratory investigations in the field of liquid phase chemistry	National Institute of Chemistry Ljubljana, Slovenia; Université de Lyon; Université de Marseilles, France; Semenov Institute of Chemical Physics, Moscow, Russia
LACIS-T Turbulent Leipzig Aerosol Cloud Interaction Simulator	Leibniz Institute for Solid State and Materials Research Dresden; University of Ilmenau, Germany, Michigan Technological University; University of Utah, USA; University of Warsaw, Poland
LOSTECCA Lidar Observations of SpatioTEmporal Contrasts in Clouds and Aerosols	National Institute of Water & Atmospheric Research (NIWA, Lauder Atmospheric Research station), Lauder, New Zealand
MACE Manila Aerosol Characterization Experiment	De La Salle University, Manila, Philippines

Research project	Cooperation partners
MARSU Marine Atmospheric Science Unravelled: Analytical and Mass Spectrometric Techniques Development and Application	8 partners from Marocco, Kap Verde, France, Austria, Argentina, China
Mobile Seestation Autonomous measurement platform for the determination of the material and energy exchanges between ocean and atmosphere	Helmholtz Centre for Ocean Research, Kiel; Alfred Wegener Institute für Polar and Marine Research, Bremerhaven; Institute for Meteorology, University Leipzig; Max Planck Institute for Meteorology, Hamburg; University Hamburg, Germany; National Observatory Athens, Greece
MOSARICS Combining MOSAIC and satellite observations for radiative closure and climate implications	Leipzig University; University of Cologne, Germany; Langley Research Center, NASA, USA; Laboratoire de Météorologie Dynamique, France
Multirate Methods in CLIMA	California Institute of Technology CalTech, Pasadena; Masachusetts Institute of Technology, Cambridge; NavyMil Monterey, USA
Ocean Science Center Mindelo (OSCM)	Instituto Nacional de Desenvolvimento das Pescas, Mindelo, S. Vicente, Republic of Cape Verde; GEOMAR Helmholtz Centre for Ozean Research Kiel, Germany
PARAMOUNT Production of Aerosol paRticle orgAnic Matter in ClOUds: chamber and laboratory studies, mechanisms, modelling and iNTegration	University Paris-Est Créteil Val de Marne; Institut Pierre Simon Laplace; Laboratoire Inter-universitaire des Systèmes Atmosphériques; Aix-Marseille Université; Laboratoire de Chemie de l'Environnement, France
PHOSDMAP, Phosphorspeziation in Staub und marinen Aerosolpartikeln	GOBABEB, Namibia, Institute for Meteorology and Geophysics, Mindelo, S. Vicente, Cabo Verde
PMO3 ozone and PM air pollution in China	Fudan University, China
PollyNet Development and application of Polly systems	8 partners from Finland, Sweden, Poland, Portugal, Korea, Greece, Israel, Tajikistan
Properties and impacts of Secondary Organic Aerosols composed of highly oxidized multifunctional organic compounds (HOMs SOA)	Weizmann Institute, Rehovot, Israel
RACLETS Role of Aerosols and CLouds Enhanced by Topography on Snow	Eidgenössische Technische Hochschule, Zürich; Meteoswiss, Zürich, Switzerland
RI-URBANS Research Infrastructures Services Reinforcing Air Quality Monitoring Capacities in European Urban & Industrial Areas	Spain, Finland, France, Germany, Italy, Netherlands, United Kingdom, Greece, Switzerland, Belgium, Norway, Romania, Poland, Russia

Appendices: Cooperations

Research project	Cooperation partners
Theory of Ice and Salt Crystallization in Aqueous Electrolyte and Polymeric Solutions	Georgia Institute of Technology, Atlanta, Georgia, USA; IAWPS International Association for the Properties of Water and Steam; Institute for Thermal Physics, Ekaterinburg, Russia; Joint Institute for Nuclear Research Dubna; St. Petersburg State University, Saint Petersburg, Russia; SUNY at Buffalo, Buffalo, NY, USA
Tobac Development of an Open-Source-Python Software for Tracking and Object-based Analysis of Clouds in Observations and Simulations	University of Oxford, UK; Colorado State University, USA; Texas Tech University, USA; Argonne National Laboratory, USA
TRACE Transport and transformation of atmospheric aerosol across Central Europe with emphasis on anthropogenic sources	Institute of Chemical Process Fundamentals of the CAS (ICPF-CAS)
TWAS DFG Characterization of trace metals in atmospheric aerosols in urban and non-urban areas of Praia, Cabo Verde	University of Cape Verde, Cabo Verde
WCCAP World Calibration Center for Aerosol Physics	Anmyeon, Republic of Korea; Malaysian Meteorological Service, Danum Valley, Malaysia; Bulgarian Academy of Sciences, BEO-Moussala, Bulgaria

National cooperations

Research project	cooperation partners
Absorption efficiency of Black Carbon: determining representative atmospheric values and implications for radiative transfer	Max Planck Institute for Chemistry, Mainz
$(AC)^3$ projekt A-01 DFG-SFB/Transregio 172 Arctic aerosol, cloud, and radiation characteristics from ground–based observations and modelling	Leipzig Institute for Meteorology, University Leipzig; Alfred Wegener Institute, Bremerhaven & Potsdam
$(AC)^3$ projekt A-01 DFG-SFB/Transregio 172 Radiative closure studies and cloud radiative effects	Leipzig Institute for Meteorology, University Leipzig; University of Cologne
$(AC)^3$ project D-02 DFG-SFB/Transregio 172 Modelling marine organic aerosol and its impact on clouds in the Arctic	Leipzig Institute for Meteorology, University Leipzig; University Bremen; Alfred Wegener Institute, Bremerhaven & Potsdam

Research project	cooperation partners
(AC)³ project A-02 DFG-SFB/Transregio 172 Tethered balloon-borne energy budget measurements in the cloudy central Arctic	Leipzig Institute for Meteorology, University Leipzig; Alfred Wegener Institute, Bremerhaven & Potsdam
(AC)³ project B-03 DFG-CRC/Transregio 172 Characterization of Arctic mixed-phase clouds by airborne in-situ measurements and remote sensing	Leipzig Institute for Meteorology, University Leipzig; University of Cologne
(AC)³ project B-04 DFG-SFB/Transregio 172 Properties and sources of Arctic ice nucleating particles and cloud condensation nuclei by ship-based in-situ measurements	Leipzig Institute for Meteorology, University Leipzig; Alfred Wegener Institute, Bremerhaven & Potsdam
ACTRIS-D Aerosol, Clouds and Trace Gases Research Infrastructure - Deutschland	10 project partners
ALADINA Investigating the Small-Scale Vertical and Horizontal Variability of the Atmospheric Boundary Layer Aerosol using Unmanned Aerial Vehicles	Technical University Baunschweig; University Tübingen
Aging of the emissions in a smog chamber	Helmholtz Zentrum München; German Research Center for Environmental Health (GmbH), Cooperation Group of Comprehensive Molecular Analytics
BC Berlin Orientierende Erfassung von Black Carbon in Deutschland und Identifikation relevanter Quellen mit Chemie-Transport-Modellen	Max Planck Institute for Chemistry, Mainz; Goethe University Frankfurt am Main; Technical University Darmstadt; University Mainz; University Bielefeld; KIT Karlsruhe
CARIBIC-AMS An Automated Aerosol Mass Spectrometer for the Regular Chemical Characterization of Aerosol Particles in the Upper Troposphere and Lowermost Stratosphere	Max Planck Institute for Chemistry, Mainz
ChemTAL Chemical transformationsin the plant-related dispersion calculation according to TA Luft	Federal Environmental Agency, Dessau-Roßlau; Janicke Consulting, Überlingen; Lohmeyer Consulting, Dresden
CIRRUS-HL The HALO mission on cirrus in high latitudes	7 partners
CLOUD-16	Goethe University Frankfurt Main
Colrawi Combined Observations with Lidar RAdar and WInd profiler	German Weather Service (DWD), Lindenberg

Appendices: Cooperations

Research project	cooperation partners
DUSTRISK A risk index for health effects of mineral dust and associated microbes	Leibniz Institute DSMZ (German Collection of Microorganisms and Cell Cultures, Braunschweig; Leibniz Research Institute for Environmental Medicine, Düsseldorf; Leibniz Lung Center, Borstel
EVAA Experimental Validation and Assimilation of Aeolus observations: Validation of aerosol and wind products with ground-based instruments of TROPOS	German Weather Service, Ludwig-Maximilians-Universität Munich
Extramural Research Programme Improved Nowcasting of Convective Initiation with METEOSAT SEVIRI (INCITES)	German Weather Service, Offenbach
GUAN German Ultrafine Aerosol Network	Federal Environmental Agency, Dessau-Roßlau, Langen, Garmisch-Partenkirchen, Hofsgrund; German Weather Service, Hohenpeißenberg; IUTA Duisburg e. V.; Helmholtz Zentrum München, University Augsburg
HuCAR Classification of HULIS carbon from different atmospheric environments via a 2-D-Off-line chromatography (HuCar)	Helmholtz Centre for Environmental Research Leipzig
IAGOS-D In-situ Aircraft for a Global Observing System	Research Center Jülich; Karlsruhe Institute of Technology; Max Planck Institutes for Chemistry and Biogeochemistry, Jena; German Aerospace Center, University of Heidelberg
Isotope analysis of stable oxdiation products induced by radical reactions in the aqueous phase	Helmholtz Centre for Environmental Research Leipzig
Leibniz Research Alliance „Crisis in a Globalized World“	22 partners
MMS Leibniz Network “Mathematical Modeling and SImulation (MMS)”	24 partners
MARGA Physico-chemical characterization of the dynamic behaviour of ammonium salt in particulate matter aerosol particles - testing a new high-resolutions measurement method at EMEP-Level 3-Station Melpitz	Federal Environmental Agency, Dessau-Roßlau
MARSU Marine Atmospheric Science Unravelled: Analytical and Mass Spectrometric Techniques Development and Application	8 partners
Measurements of ozone VOC precursors in Saxony	Saxon State Agency for Environment, Agriculture and Geology, Dresden

Research project	cooperation partners
Measurements of ammonia in Saxony	Saxon State Agency for Environment, Agriculture and Geology, Dresden
MOSS TREE A new urban green infrastructure to actively reduce air pollution in urban hotspots	Green City Solutions GmbH, Institut für Luft- und Kältetechnik gGmbH
PICNICC Polarimetry Influenced by CCN aNd INP in Cyprus and Chile	Leipzig Institute for Meteorology, Leipzig University
PM-OST Source appointment of PM10 and estimation of contribution from trans-boundary air pollution	Senate Department for Urban Development and Housing, Berlin; Saxon State Agency for Environment, Agriculture and Geology; Ministry of Rural Development, Environment and Agriculture of the Federal State of Brandenburg; Ministry of Rural Development, Protection of Nature and Geology, State of Mecklenburg-Western Pomerania
Prototype Doppler Lidar (design phase)	ABACUS-Laser Göttingen; Licel Berlin
Influence of soot on air quality and climate (pilot study)	Saxon State Agency for Environment, Agriculture and Geology, Dresden
HiLDA Iceland as a model for high-latitude dust sources - a combined experimental and modeling approach for characterization of dust emission and transport processes	Technical University Darmstadt
SOARiAL Spread of Antibiotic Resistance in an Agrarian Landscape	Leibniz Institute DSMZ - German Collection of Microorganisms and Cell Cultures Braunschweig; Leibniz Centre for Agricultural Landscape Research Müncheberg; Leibniz Institute for Agriculture and Bioeconomy Potsdam, FU Berlin
SPOCC Spectrally Resolved Observation and Computation of Clouds	Meteorologisches Observatorium Hohenpeißenberg, DWD, Hohenpeißenberg
Statistical modelling of aerosol particle size distribution in urban and rural environment	TU Braunschweig, Section of Climatology and Environmental Meteorology
STEP Solving The Entrainment Puzzle (Marie Skłodowska-Curie Action)	Leipzig Institute for Meteorology, University Leipzig; Max Planck Institute for Meteorology, Hamburg
Theory of ice and salt crystallisation in aqueous electrolyte and polymeric solutions	Polymer Physics, University Rostock; Leibnitz Institute for Baltic Sea Research, Warnemünde
Low Emission Zone Deep analysis to verify the effectiveness of the Leipzig Low Emission Zone	Saxon State Agency for Environment, Agriculture and Geology, Dresden
UV monitoring network Deutschlandweites Netzwerk zur Beobachtung der UV-Strahlung und Vorhersage des UV-Index	Federal Office for Radiation Protection, German Weather Service, Federal Environmental Agency

Appendices: Cooperations / Boards

Research project	cooperation partners
Improvement of data quality for the measurement of ultrafine particles in the outdoor air	Saxon State Agency for Environment, Agriculture and Geology, Dresden
Trends, causative factors and effects of ozone pollution in Saxony	Saxon State Agency for Environment, Agriculture and Geology, Dresden
Quantification of the secondary ice production mechanisms: droplet shattering on freezing vs. droplet-ice collision	Institute of Meteorology and Climate Research, Karlsruhe Institute of Technology
VACCINE Variation of Antarctic Cloud Condensation (CCN) and ice nucleating particle concentrations (INP) at Neumayer Station	Alfred Wegener Institute, Helmholtz Centre for Polar and Marine Research
WTimpact Citizen Science as Transfer Instrument	Leibniz Institute for Zoo and Wildlife Research, Berlin; Leibniz Institute for Science and Mathematics Education, Kiel; Leibniz-Institute for Media Research, Hamburg

Boards

Boards of trustees

Name	Institution
V. Stercken	Federal Ministry of Education and Research
RORin C. Liebner	Saxon State Ministry for Science, Culture and Tourism
Prof. Dr. A. Wahner	Forschungszentrum Jülich GmbH, Institute for Energy and Climate Research, IEK-8: Troposphere

Scientific advisory board

Name	Institution
Dr. F. Beyrich	Meteorological Observatory Lindenberg
Prof. Dr. A. Engel	GEOMAR Helmholtz Centre for Ocean Research Kiel
Dr. C. Fittschen	University of Lille, PhysicoChemistry of Combustion Processes and Atmosphere
Prof. Dr. C. Hoose	Karlsruhe Institute of Technology (KIT), Institute of Meteorology and Climate Research

Name	Institution
Prof. Dr. T. Koop	Bielefeld University, Faculty of Chemistry
Prof. Dr. M. Lawrence	IASS Potsdam, Institute for Advanced Sustainability Studies e.V.
Prof. Dr. T. Koop	Bielefeld University, Faculty of Chemistry
Prof. Dr. H. Pawlowska	University of Warsaw, Faculty of Physics / Institute of Geophysics
Prof. Dr. J. Quaas	University Leipzig, Leipzig Institute for Meteorology (LIM)
Prof. Dr. M. Rapp **(Chairman)**	German Aerospace Center, Institute of Atmospheric Physics
Prof. Dr. Bernadett Weinzierl	University Vienna, Faculty of Physics

Members of the TROPOS association

Name	Institution
Prof. Dr. C. Jacobi **(Chairman)**	Leipzig University, Leipzig Institute for Meteorology (LIM)
RORin C. Liebner	Saxon State Ministry for Science, Culture and Tourism
V. Stercken	Federal Ministry of Education and Research
Prof. Dr. B. Abel	Leibniz Institute of Surface Engineering (IOM)
Prof. Dr. B. Brümmer	University of Hamburg, Meteorological Institute
Prof. Dr. W. Engewald	Leipzig University, Faculty for Chemistry and Mineralogy
Prof. Dr. J. Quaas	Leipzig University, Leipzig Institute for Meteorology (LIM)
Dr. H.-H. Richnow	Helmholtz Centre for Environmental Research (UFZ)
Prof. Dr. C. Simmer	Rhineland Friedrich Wilhelm University Bonn, Institute for Meteorology
Prof. Dr. E. Renner, honorary member	Professor emeritus
Prof. Dr. J. Heintzenberg, honorary member	Professor emeritus

Appendices: Organigram

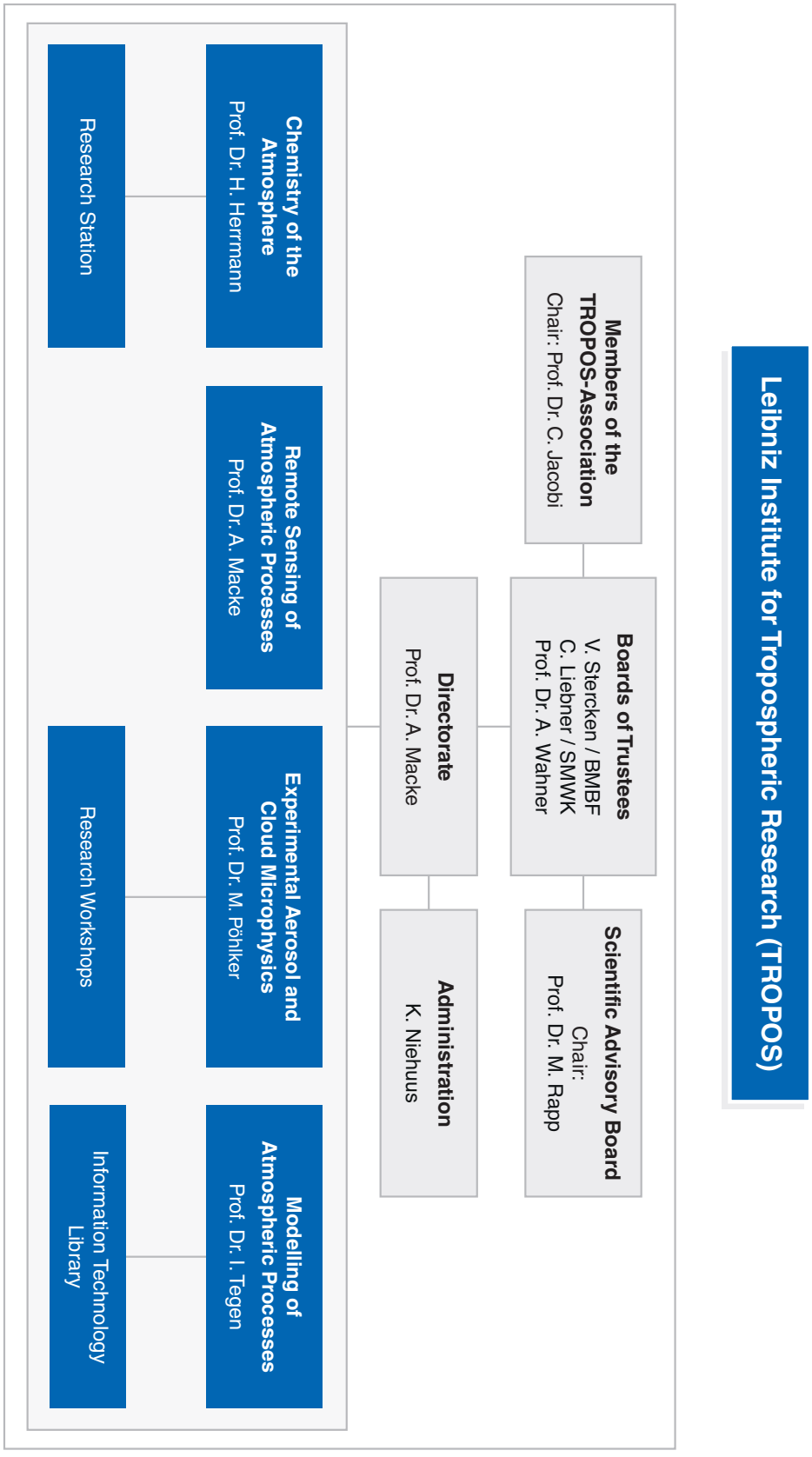

TROPOS

Leibniz Institute for Tropospheric Research
Leibniz-Institut für Troposphärenforschung e.V. Leipzig
Member of the Leibniz Association

Permoserstraße 15
04318 Leipzig
Germany

Phone: ++49 (341) 2717-7060
Fax: ++49 (341) 2717-99-7060
Email: info@tropos.de
Internet: www.tropos.de